Institut für Geodäsie und Geoinformation der Universität Bonn

Astronomische, Physikalische und Mathematische Geodäsie

The Use of Topographic-Isostatic Mass Information in Geodetic Applications

Inaugural–Dissertation zur
Erlangung des akademischen Grades
Doktor–Ingenieur (Dr.–Ing.)
der Hohen Landwirtschaftlichen Fakultät
der Rheinischen Friedrich–Wilhelms–Universität
zu Bonn

vorgelegt am 5. Februar 2007 von

M.Sc. Atef Abd–Elhakeem Makhloof

aus El Minia, Ägypten

D 98

Referent:	Prof. Dr.–Ing. K. H. Ilk
Korreferent:	Prof. Dr.–Ing. B. Witte
Tag der mündlichen Prüfung:	13.04.2007
Gedruckt bei:	Diese Dissertation ist auf dem Hochschulschriften-server der ULB Bonn http://hss.ulb.uni-bonn.de/diss_online elektronisch publiziert.

Zusammenfassung

Die Gravitationsfeldeffekte der topographisch-isostatischen Massen stellen eine wichtige Information des hochfrequenten Anteils des Gravitationsfeldes dar. In dieser Arbeit werden die physikalisch-mathematischen Grundlagen der klassischen topographisch-isostatischen Modelle dargestellt. Es werden die verschiedenen isostatischen Modelle mathematisch formuliert, wobei auf der Modellbildungsseite der Schwerpunkt auf der sphärischen Approximation liegt und von den Anwendungen die Beobachtungstypen der Flugzeuggravimetrie und der modernen Satellitenmethoden im Vordergrund stehen. Neben der Darstellung der topographisch-isostatischen Masseneffekte durch sphärische Volumenintegrale, diskretisiert durch sphärische Volumenelemente, werden die Reihendarstellungen nach Kugelflächenfunktionen und nach ortslokalisierenden Basisfunktionen zugrunde gelegt. Detaillierte Formeln werden für den direkten bzw. den sekundären indirekten topographischen Effekt in den Schwerewerten und den primären indirekten Effekt in den Geoidhöhen für die verschiedenen Darstellungen angegeben. Schliesslich werden Formeln für die Berechnung der Fernzoneneffekte der topographisch-isostatischen Massen angegeben. Hierzu wird eine von Molodenskii angegebene Methode angewendet, die auf der Kugelfunktionsentwicklung der topographisch-isostatischen Massen beruht. Umfangreiche Rechenbeispiele vermitteln einen Eindruck von der Grösse und der Verteilung der verschiedenen Effekte, basierend auf unterschiedlich aufgelösten regionalen und globalen Testgebieten.

Summary

The gravity field effects of the topographic-isostatic masses represent an important information of the high-frequent part of the gravity field. In this work the physical-mathematical basics of the classical topographic-isostatic models are presented. These models are formulated mathematically with the emphasis on a spherical approximation from the modelling point of view and on the observables of airborne gravimetry but also of the modern satellite techniques from the application point of view. Besides the representation of the topographic-isostatic mass effects by volume integrals, discretized by spherical volume elements, the representations by series of spherical harmonics and space localizing base functions are considered. Detailed formulae are presented for the direct and secondary indirect topographical effect as well as for the primary indirect topographical effect in the geoid heights for the different representations. Finally, extended test computations give an impression of the size and distribution of the various effects for regional and global test areas with different resolutions of the topography.

Table of Contents

1. Introduction

The topographic masses represent an important source of gravity field information especially in the high-frequency band of the gravity field spectrum, even if the detailed density function inside the topographic masses is only approximately known. The gravity field effect of the visible topography is partially reduced by isostatic compensation mechanisms – the net effect of both are nevertheless significant larger and of more pronounced high-frequent character than the effects of the inhomogeneities inside the crust of the Earth. With the global detailed digital elevation models of the topography at the continents and of the bathymetry at the oceans, accessible nowadays, a very important source of gravity field information is available. In this research, only geodetically relevant aspects are treated, but many of the topics discussed in this work are important also in structural and exploration geophysics or in geological applications.

In geodesy, the topographic-isostatic masses can be used in a threefold way: (1) the solution of the Laplace equation within the frame of the geodetic boundary value problem of Stokes requires a mass-free space outside the boundary surface, the (co-)geoid. This is the reason that the topographic masses have to be removed or shifted inside the geoid; the effects of this process have to be restored after the solution to reconstitute the original situation. But also in case of the geodetic boundary value problem according to Molodenskii the numerical results can be achieved in a simpler and more accurate way by making use of the topographic information than without it. (2) A rough topography causes strong oscillations in the gravity field functionals, e.g., gravity anomalies and disturbances, deflections of the vertical or the second derivatives of the gravity potential. If these functionals can be filtered by the topographic-isostatic masses then the filtered functionals can be interpolated or extrapolated much easier and more precise than by using the unfiltered quantities. Because of the fact that the various geodetic applications of gravity require the knowledge of the gravity field functionals at locations different from the measurement locations the prediction is a frequently applied procedure. These principle ideas are behind the so-called remove-restore procedure, where the observational functionals of the gravity field are reduced by the known global gravity field information, based on precise global gravity field models and the high frequent effects of the topographic-isostatic masses. The resulting residual gravity field functionals are considerably smoother than before and can be represented by generalized approximation/prediction techniques such as Least Squares Collocation. (3) The determination of the gravity field from observations at a certain altitude above sea level, especially at aircraft or satellite altitudes, is an improperly posed problem in the sense that small changes in the observations at flight level produce large effects in the gravity field parameters on the Earth's surface or geoid level. This holds especially for the high-frequency constituents of the observation spectrum. To prevent the results from unrealistic oscillations in the parameters, regularization techniques are usually applied in very poorly conditioned cases. Most of the regularization methods represent a filtering procedure and the filtering property can be controlled by a regularization parameter. This is critical in those cases where the signal shows similar spectral characteristics as the observation noise. The topographic-isostatic masses represent a gravity field information, especially in the high frequency band of the gravity field spectrum, which can be superposed with the measurement noise in aircraft or satellite altitude. Therefore, it is helpful, if those signal parts are reduced before the downward continuation and restored afterwards. In this case, it can be assumed that the high-frequency part in the observations is mainly caused by the observation noise, which can be filtered without loosing gravity field information.

Because of the local effects of the topographic masses in the gravity field functionals the planar approximation was frequently applied in the past. In global applications, this approximation cannot be used anymore (see Novák el al. 2001). Therefore, the very efficient fast Fourier transformation (FFT) techniques will not be applied for large-scale computations as demonstrated by Schwarz et al. (1990) in case of applications in airborne gravimetry in this investigation. This holds especially for large-scale regional or even global applications in case of the processing of observables of the new gravity satellite missions. There are two principal possibilities for calculating the effects of the topographic-isostatic masses on gravitational functionals in spherical approximation: the representation of the topographic masses by any spherical discretisation in form of spherical compartments (e.g. defined by spherical coordinate lines) and a subsequent integration (Abd-Elmotaal 1995b, Smith et al. 2001; Tenzer et al. 2003; Heck 2003) or the representation of Newton's

integral by a spherical harmonic expansion (e.g., Sünkel 1985; Rummel et al. 1988; Tsoulis 1999a, 2001). Sjöberg (1998a) implemented the formulae for the exterior Airy-Heiskanen topographic-isostatic gravity potential and the corresponding gravity anomalies. Surface spherical harmonics are base functions with global support and they are tailored to global computations. This is the reason that usually the gravity potential is modelled by a spherical harmonic expansion. Nevertheless, the heterogeneity of the gravity field cannot be properly taken into account with the help of spherical harmonics as base functions with global support. The maximum degree must be adapted to the roughest gravity field features which are concentrated especially in the regions with very high mountains. In most of the regions the maximum degree could be much smaller. The representation of gravity field functionals by spherical harmonics is very efficient but limited to an upper spherical harmonic degree of about 2700 which corresponds to a 4 arc-minute resolution. Beyond this degree numerical computation problems concerning the stability of the recursive computation of Legendre's polynomials occur (see, e.g., Holmes and Featherstone 2002) and increasing of the computational time. It is preferable to model the gravity field only up to a moderate spherical harmonic degree to represent properly most of the regions of the Earth; the specific detailed features tailored to the individual gravity field characteristics in areas of rough gravity field signal can be modelled additionally by space localizing base functions such as spherical spline functions (Freeden et al. 1998) or spherical wavelets (Freeden and Windheuser 1996). These more sophisticated base functions are applied for the modelling of topographic-isostatic effects for the first time.

There is a huge list of publications related to the modelling of topographic-isostatic mass effects and the various computation procedures. The investigations performed thus far are limited to the determination of the potential or its first derivatives. The effects of the topographic-isostatic masses on the second derivatives of the gravitational potential of the topographic-isostatic masses, necessary for Satellite Gravity Gradiometry (SGG) are not treated for the general case. Only the topographic-isostatic effects on the radial component of the gravitational tensor have been studied by Wild and Heck (2004a) and Heck and Wild (2005). The effects of topographic-isostatic masses on Satellite-to-Satellite Tracking (SST) data and SGG functionals based on spherical harmonic series are investigated by Makhloof and Ilk (2004).

In the present research the modelling of topographic-isostatic masses based on different isostatic or compensation models is reviewed and enhanced with respect to different details, then the various computation techniques are recapitulated and improved with respect to accuracy and additional features. The procedures are applied to various geodetically important functionals with specific emphasis to the observables of the new satellite gravity field missions such as GRACE and GOCE. The outcome of this investigation is demonstrated with numerous examples, based on different test regions with varying resolutions of the digital elevation models.

The ***second chapter*** reviews some basic facts important to understand the use of gravity field effects of topographic-isostatic masses. Newton's law of universal gravity is recapitulated with extensions to a set of mass points and to the gravity field of an extended body. Then the concept of the gravitational potential is reviewed as well as the potentials of a solid body and of a single mass layer. Furthermore, the boundary value problems of Stokes and Molodenskii are shortly characterized and the computation formulae reviewed. The different topographic-isostatic effects in Stokes' problem are specified and the use of topographic-isostatic effects in the computation of the telluroid or the quasi-geoid, respectively, is summarized. Then the use of topographic-isostatic effects in airborne gravimetry is sketched as well as applications referring to the observables of Satellite-to-Satellite Tracking (SST) and Satellite Gravity Gradiometry (SGG).

The ***third chapter*** reviews the mass models of the topography of the Earth. The chapter is introduced by some remarks on the digital terrain and density models. It follows the presentation of the classical isostatic models by Airy-Heiskanen, Pratt-Hayford, a combined model of both of them and the Vening-Meinesz model. Additionally, Helmert's models of mass condensation are reviewed.

The ***fourth chapter*** is dedicated to modelling aspects of the topographic-isostatic masses. It is subdivided in three sections. A first section is dedicated to the *direct integration method* with subsections related to the planar approximation, the spherical approximations specified for the topographic masses and the isostatic compensation and condensation masses. A second section treats the representation of the topographic-isostatic mass effects by series of *surface spherical harmonics*. In a first subsection the effects of topographic

masses in the observational functionals of satellite geodesy are outlined as well as the effects of the isostatic masses for the different isostasy models. It follows a subsection about the effects of the condensation masses in the sense of Helmert's condensation methods. Another important application of spherical harmonic series of the topography is the determination of so-called far-zone effects. They are important in those cases where the integration of the global mass effects shall be restricted to certain caps around the computation point. Formulae are derived for the direct topographical effects on gravity, the primary indirect topographical effect on geoid heights and the secondary indirect topographical effect on gravity. In the third section, formulae are derived for the representation of the topographical effects, based on *space localizing base functions* – in the specific case spherical spline functions. In a first subsection, the direct and secondary indirect topographical effects on gravity are investigated and in a second one the primary indirect topographical effect.

In the ***fifth chapter*** various numerical aspects of the determination of the topographic-isostatic mass effects are investigated. Different test areas are selected such that typical features of these computations can be demonstrated properly. An important part of this chapter is the investigation of computational aspects such as the investigation of discretization effects, the investigation of numerical aspects of the expansion of the topography by spherical harmonics as well as the near and far-zone effects of the topographic-isostatic masses. Then - as a main part of this dissertation - the effects of the topographic-isostatic masses for various geodetic functionals at the surface of the Earth and at aeroplane altitudes are investigated as well as the gravitational effects in satellite applications.

The results of the test computations are reviewed and discussed in the ***sixth chapter***. The new developments in this work are summarized and its relevance for airborne gravimetry and gradiometry as well as for the analysis of the observations of the new gravity satellite missions is outlined. An outlook to further investigations conclude this chapter.

In the ***appendix*** the formulae for the truncation coefficients for the direct terrain effects based on spherical harmonics are derived for Helmert's methods of condensation and for the Airy-Heiskanen model.

Remark:Because of the large number of different quantities used in this work, the notation may vary in the different chapters and sections.

2. Topographic masses and the gravity field of the Earth

This chapter summarizes some basic facts of the Earth's gravity field and the role of the topographic-isostatic masses for the determination of the gravity field of the Earth according to the boundary value problems of Stokes and Molodenskii. The regularizing effect of topographic-isostatic masses is outlined, especially for the interpolation of gravity values and for the downward continuation of observables at airborne and satellite altitudes. The role of topographic-isostatic masses in the observables of the Satellite-to-Satellite Tracking (SST) technique and the Satellite Gravity Gradiometry (SGG) is reviewed. Throughout this chapter, the Earth is regarded as a rigid body whenever necessary.

2.1 The gravity potential and its derivatives

In this section, we will shortly review Newton's law of gravitation for two point masses and for an extended body consisting either of a multiple of point masses or composed by mass elements described by an arbitrary density function. Then the gravitational potential is introduced from which the force field function of the gravitational field of a gravitating body can be derived by building the gradient of the gravitational potential. Besides the source representation of the gravitational potential the representation by a series in terms of spherical harmonics is given. Apart from the gravitational potential itself the important second derivatives of the gravitational potential as well as *Laplace's equation* are reviewed. Then the basic formulae for the topographic masses and its isostatic compensation masses are presented. Finally, the gravitational potential of a single mass layer and its derivatives are summarized, including its jump relations at the layer.

2.1.1 Newton's law of gravitation

Newton's law of universal gravitation describes the mutual attraction of gravitating mass points. Due to this law the attraction force of point mass m_1 acting onto point mass m_2 reads (Fig. 2.1),

$$\mathbf{F}_{21} = -G\, m_1\, m_2 \frac{\mathbf{r}_2 - \mathbf{r}_1}{|\,\mathbf{r}_2 - \mathbf{r}_1|^3}, \tag{2.1}$$

where the vectors $\mathbf{r}_1$ and $\mathbf{r}_2$ describe the positions of the two point masses m_1 and m_2. The constant G with the value $G = (6672 \pm 4)\ 10^{-14} m^3 s^{-2} kg^{-1}$ is the universal gravitational constant. Because of the mutual character of the gravitational force it can be written as well in the form,

$$\mathbf{F}_{12} = -G\, m_1\, m_2 \frac{\mathbf{r}_1 - \mathbf{r}_2}{|\,\mathbf{r}_1 - \mathbf{r}_2|^3}. \tag{2.2}$$

The role of the attracting point mass and the attracted one is exchangeable. Newton's law of universal gravitation can be formulated also with the help of a force function, describing the force field of the respective attracting point mass. In this case, we consider the attracting point mass as a source point, written as m_Q, so that it holds,

$$\mathbf{a}_Q(\mathbf{r}) = -G\, m_Q \frac{\mathbf{r} - \mathbf{r}_Q}{|\,\mathbf{r} - \mathbf{r}_Q|^3}. \tag{2.3}$$

The attraction force acting on point mass m located at the position $\mathbf{r}$ can be expressed as

$$\mathbf{F}_Q(\mathbf{r}) = m\, \mathbf{a}_Q(\mathbf{r}), \tag{2.4}$$

with the gravitational field strength $\mathbf{a}_Q(\mathbf{r})$ of the gravitational field of mass m_Q.

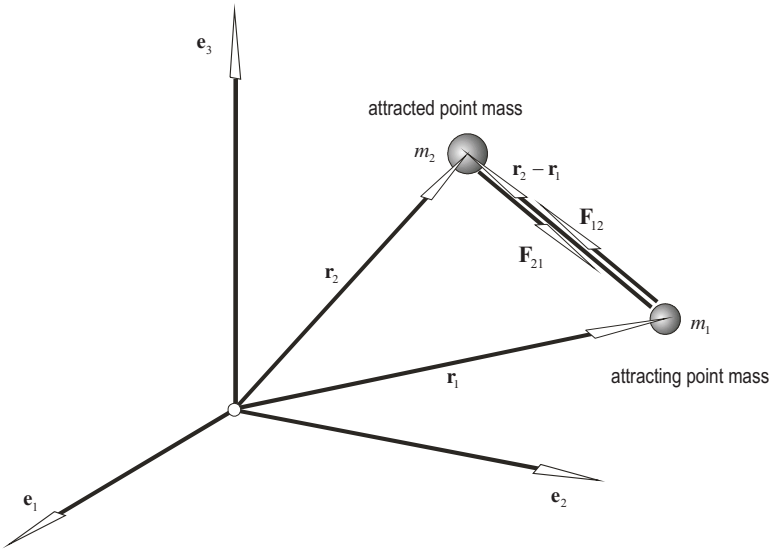

Fig. 2.1: Newton's universal law of gravitation, here point mass m_1 considered as attracting mass and m_2 as attracted one

2.1.2 The gravitational field of a solid body

Because of the fact that the force function of a single point point is a vector, the gravitational fields of more than one point mass can be superimposed by simply adding the individual components,

$$\mathbf{a}\left(\mathbf{r}\right) = \sum_i \mathbf{a}_i\left(\mathbf{r}\right). \tag{2.5}$$

Analogously, the gravitational force field function of an extended mass, distributed in a volume described by a certain density function $\rho\left(\mathbf{r}_Q\right)$ can be derived. The contribution of a mass element dm_Q to the force function reads (Fig. 2.2),

$$d\mathbf{a}\left(\mathbf{r}\right) = -G\, dm_Q \frac{\mathbf{r}-\mathbf{r}_Q}{\left|\,\mathbf{r}-\mathbf{r}_Q\right|^3} =: -G\, dm_Q \frac{\mathbf{l}}{\left|\,\mathbf{l}\right|^3}. \tag{2.6}$$

The force function of the gravitational field of the total mass distribution can be derived as integral over the total volume with $dm_Q = \rho\left(\mathbf{r}_Q\right) dv$,

$$\mathbf{a}\left(\mathbf{r}\right) = -G \iiint\limits_v \rho\left(\mathbf{r}_Q\right) \frac{\mathbf{l}}{\left|\,\mathbf{l}\right|^3} dv. \tag{2.7}$$

The gravitational force is a conservative force and the gravity field strength can be determined by the gradient of a scalar function,

$$\mathbf{a}(\mathbf{r}) = \nabla V(\mathbf{r}), \tag{2.8}$$

the gravitational potential,

$$V\left(\mathbf{r}\right) = G \iiint\limits_v \rho\left(\mathbf{r}_Q\right) \frac{1}{\left|\,\mathbf{r}-\mathbf{r}_Q\right|} dv = G \iiint\limits_v \rho\left(\mathbf{r}_Q\right) \frac{1}{l} dv. \tag{2.9}$$

With the relation,

$$\nabla l^{-1} = \nabla\left(\left|\,\mathbf{r}-\mathbf{r}_Q\right|\right)^{-1} = -\frac{\mathbf{r}-\mathbf{r}_Q}{\left|\,\mathbf{r}-\mathbf{r}_Q\right|^3} = -\frac{\mathbf{l}}{l^3}, \tag{2.10}$$

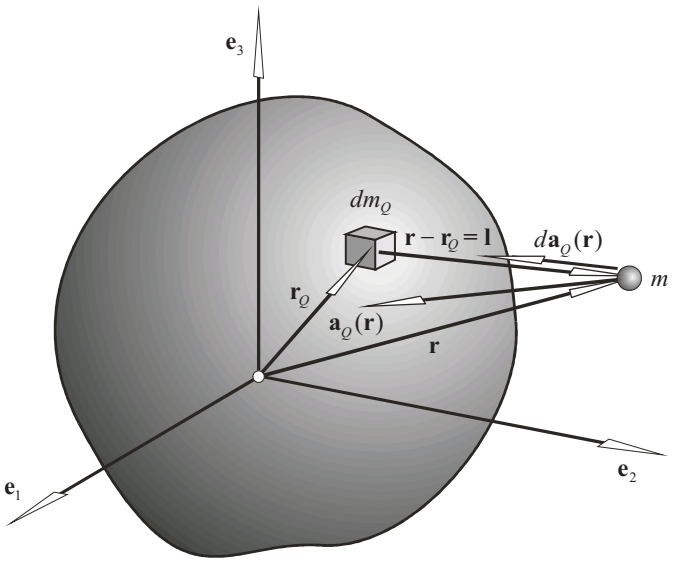

Fig. 2.2: The gravitational field of an extended mass body

we arrive at the formula for the gravitational force. It should be pointed out that the gravitational potential can be determined only up to a constant V_0. This constant is set to zero to guarantee regularity at infinity,

$$\lim_{l\to\infty} V(\mathbf{r}) = 0. \tag{2.11}$$

The gravitational potential of a solid body can be differentiated arbitrarily often outside the masses. If the *Laplace operator* $\Delta = \nabla \cdot \nabla$ is applied onto the potential function,

$$\Delta V = \nabla \cdot (\nabla V) = G \iiint_v \rho(\mathbf{r}_Q)\ \Delta(1/l)\ dv, \tag{2.12}$$

then it follows *Laplace's equation* because of $\Delta(1/l) = 0$ for the space outside the masses. *Laplace's equation* reads, written in orthogonal Cartesian coordinates x,y and z,

$$\Delta V = \frac{\partial^2 V}{\partial x^2} + \frac{\partial^2 V}{\partial y^2} + \frac{\partial^2 V}{\partial z^2} = 0. \tag{2.13}$$

It should be pointed out that the sum of the partials vanish but not the single components, as e.g. in case of x,

$$\frac{\partial^2 V}{\partial x^2} = G \iiint_v \rho\ (\mathbf{r}_Q)\ \frac{\partial^2 (1/l)}{\partial x^2}\ dv = G \iiint_v \rho(\mathbf{r}_Q)\ \left(-\frac{1}{l^3} + \frac{3x^2}{l^5}\right) dv. \tag{2.14}$$

Corresponding expressions can be derived for the other coordinates y and z. Inside the masses *Poisson's equation* holds instead of the *Laplace's equation*,

$$\Delta V(\mathbf{r}) = \frac{\partial^2 V}{\partial x^2} + \frac{\partial^2 V}{\partial y^2} + \frac{\partial^2 V}{\partial z^2} = -4\pi G\rho(\mathbf{r}). \tag{2.15}$$

By introducing spherical coordinates φ, λ, r for the computation point and φ', λ', r' (see Fig. 2.3) for the source point (location of a mass element) a solution of *Laplace's equation* expressed in spherical harmonics reads,

$$V(\mathbf{r}) = \frac{GM}{r} \sum_{n=0}^{\infty} \left(\frac{R}{r}\right)^n Y_n(\varphi, \lambda), \tag{2.16}$$

with *Laplace' surface spherical harmonics of degree n*,

$$Y_n(\varphi,\lambda) = \frac{1}{M}\iiint_v \left(\frac{r'}{R}\right)^n P_n(\cos\psi)\ \rho(\mathbf{r}')\ dv \quad = \sum_{m=0}^{n} ((c_{nm}\cos m\lambda + s_{nm}\sin m\lambda)\, P_{nm}(\sin\varphi)). \tag{2.17}$$

The functions $P_{nm}(\sin\varphi)$ are the *fully normalized Legendre functions* of degree n and order m. The co-

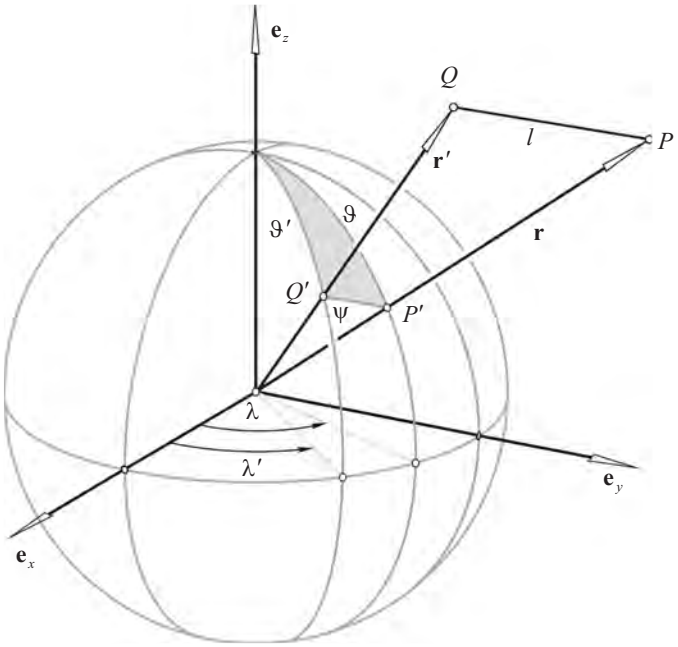

Fig. 2.3: Spherical coordinates for computation and source point

efficients c_{nm}, s_{nm} represent the fully normalized spherical harmonic coefficients. M is the total mass of the Earth and R the mean radius of the Earth. If the density function inside the Earth is known, then the potential coefficients c_{nm}, s_{nm} can be determined also by the following integrals (with the *Kronecker symbol* δ_{0m}),

$$\begin{aligned} c_{nm} &= \frac{(2-\delta_{0m})}{M}\frac{(n-m)!}{(n+m)!}\iiint_v \left(\frac{r'}{a}\right)^n C_{nm}(\varphi',\lambda')\ \rho(\mathbf{r}')\ dv, \\ s_{nm} &= \frac{2\,(1-\delta_{0m})}{M}\frac{(n-m)!}{(n+m)!}\iiint_v \left(\frac{r'}{a}\right)^n S_{nm}(\varphi',\lambda')\ \rho(\mathbf{r}')\ dv. \end{aligned} \tag{2.18}$$

2.1.3 The potential of the topographical and compensating masses

Let us start with the gravitational potential induced by the topographic masses above the geoid (Martinec 1998),

$$V^t(\mathbf{r})\big|_{\mathbf{r}=\mathbf{r}_P} = G\iint_\sigma \int_{\xi=r_g(Q)}^{r_g(Q)+H(Q)} \frac{\rho^t(\varphi_Q,\lambda_Q,\xi)}{l(r,\xi,\psi)}\bigg|_{\mathbf{r}=\mathbf{r}_P} \xi^2 d\xi d\sigma, \tag{2.19}$$

with

$$l := \sqrt{r_P^2+\xi^2-2r_P\xi\cos\psi}, \tag{2.20}$$

and the three dimensional (3-D) density function of the topographic masses, $\rho^t(\varphi_Q, \lambda_Q, \xi)$. The quantity ξ is the geocentric radius of the mass element and $d\sigma = \cos\varphi_Q d\varphi_Q d\lambda_Q$ the surface element in spherical coordinates. The geocentric angle ψ is the spherical distance between the radius vectors of the computation point $\mathbf{r}_P(r_P, \varphi, \lambda)$ and the integration point $\mathbf{r}_Q(r_Q, \varphi_Q, \lambda_Q)$. It is given by

$$\cos\psi = \sin\varphi \sin\varphi_Q + \cos\varphi \cos\varphi_Q \cos(\lambda_Q - \lambda). \tag{2.21}$$

The integration in Eq. (2.19) is performed over the topographic masses bounded by the radius of the geoid r_g and the Earth surface $r_g + H$, where H stands for the topographic (orthometric) heights. It is a well-known fact that the topographical masses generate a rough gravitational field with an equipotential surface undulating by hundreds of meters with respect to the level ellipsoid. Since the undulations of the geoid are significantly smaller, compensation mechanisms of the topographical masses must exist which reduce the gravitational effects of the topographic masses. These mechanisms are most probably connected with lateral mass heterogeneities of the crust but also with deep dynamic processes (Matyska 1994). Frequently applied are more or less idealized compensation models which are described in chapter 3.

The gravitational potential of the compensation masses can be given also by Newton's integral as follows:

$$V^c(\mathbf{r})|_{\mathbf{r}=\mathbf{r}_P} = G \iint_\sigma \int_{\xi=r_1}^{r_2} \frac{\Delta\rho^t(\varphi_Q, \lambda_Q, \xi)}{l(r, \xi, \psi)}\Big|_{\mathbf{r}=\mathbf{r}_P} \xi^2 d\xi d\sigma, \tag{2.22}$$

where the integration is performed over all masses for the actual compensation model with the (3-D) density function $\Delta\rho^t(\varphi_Q, \lambda_Q, \xi)$, which indicates the difference between a mean density and the actual density. The radial integration limits r_1, r_2 indicate the lower and upper bounds of the actual compensation masses and depend on the applied compensation model (see chapter 3).

2.1.4 The gravitational field of a single mass layer

If the attracting masses are assumed to form a layer, or a coating on a certain closed surface σ, with a thickness approaching to zero, then the surface density reads (Fig. 2.4),

$$k_Q := k(\mathbf{r}_Q) = \frac{dm_Q}{d\sigma}, \tag{2.23}$$

where $d\sigma$ is the surface element and k_Q the single layer density. The potential of this surface of masses at a certain computation point P is given by

$$V(\mathbf{r}) = G \iint_\sigma k_Q \frac{1}{l} d\sigma, \tag{2.24}$$

where l is the distance between the surface element $d\sigma$ and the computation point under consideration.

On the surface σ the potential V is continuous, but there are discontinuities of the first derivatives depending on the derivation direction e. The limit of the first derivative approaching from an external point P_a to a point P_σ at the surface σ is called the *external derivative* (Fig. 2.4),

$$\lim_{P_a \to P_\sigma} \frac{dV}{de} = -\lim_{P_a \to P_\sigma} G \iint_\sigma k_Q \frac{\mathbf{e} \cdot \mathbf{e}_l}{l_a^2} d\sigma =: \frac{dV_a}{de}, \tag{2.25}$$

and from an internal point P_i to a point P_σ at the surface σ the *internal derivative*,

$$\lim_{P_i \to P_\sigma} \frac{dV}{de} = -\lim_{P_i \to P_\sigma} G \iint_\sigma k_Q \frac{\mathbf{e} \cdot \mathbf{e}_l}{l_i^2} d\sigma =: \frac{dV_i}{de}. \tag{2.26}$$

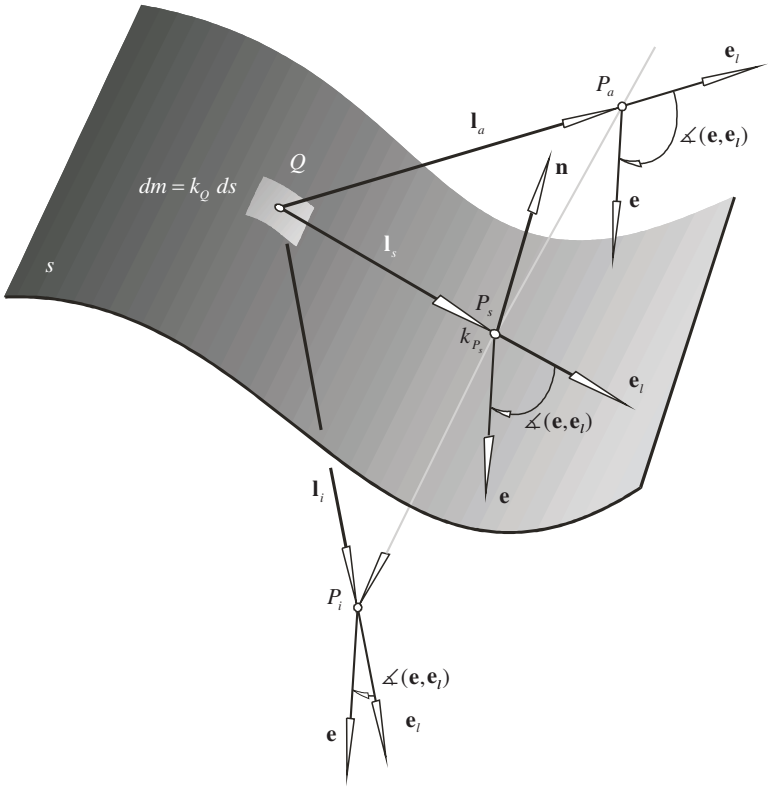

Fig. 2.4: Potential of a material surface

The derivative at a point P_σ at the surface σ is called the *direct derivative*,

$$\left.\frac{dV}{de}\right|_\sigma = G \iint\limits_\sigma k_Q \frac{d(1/l_\sigma)}{de} d\sigma = -\, G \iint\limits_\sigma k_Q \frac{\mathbf{e}\cdot\mathbf{e}_l}{l_\sigma^2} d\sigma =: \frac{dV_\sigma}{de}. \tag{2.27}$$

If the vector $\mathbf{n}$ is the outer normal of the surface σ at point P_σ with the surface density $k_\sigma := k_{P_\sigma}$ in this point, the *external derivative* can be written in the form

$$\frac{dV_a}{de} = -\, G \iint\limits_\sigma k_Q \frac{\mathbf{e}\cdot\mathbf{e}_l}{l_\sigma^2} d\sigma - 2\pi G\, k_\sigma \mathbf{n}\cdot\mathbf{e}, \tag{2.28}$$

and the *internal derivative*, respectively,

$$\frac{dV_i}{de} = -\, G \iint\limits_\sigma k_Q \frac{\mathbf{e}\cdot\mathbf{e}_l}{l_\sigma^2} d\sigma + 2\pi G\, k_\sigma \mathbf{n}\cdot\mathbf{e}. \tag{2.29}$$

The direction derivative of a single layer shows a jump at the layer in the size of

$$\frac{dV_a}{de} - \frac{dV_i}{de} \;=\; -\, 4\pi G\, k_\sigma \mathbf{n}\cdot\mathbf{e}, \tag{2.30}$$

and the *direct derivative* is the arithmetic mean between external and internal derivatives,

$$\frac{dV_\sigma}{de} = \frac{1}{2}\left(\frac{dV_a}{de} \;+\; \frac{dV_i}{de}\right) \;=\; -G \iint\limits_\sigma k_Q \frac{\mathbf{n}\cdot\mathbf{e}}{l_\sigma^2} d\sigma. \tag{2.31}$$

The potential V of a single layer is regular at infinity,

$$\lim_{l\to\infty} V(\mathbf{r}) = 0, \tag{2.32}$$

satisfies everywhere *Laplace's equation*,

$$\Delta V(\mathbf{r}) = 0, \tag{2.33}$$

except on σ itself, and is continuous everywhere together with all its derivatives.

2.2 The geodetic boundary value problems

2.2.1 Gravitational field and gravity field

The force acting on a test mass at the Earth's surface is the resultant of the gravitational force and the centrifugal force of the Earth. The centrifugal force acting on a mass m can be determined as follows:

$$\mathbf{C} = m\omega^2\mathbf{p}, \tag{2.34}$$

with the vector $\mathbf{p} = (x, y, 0)$ and the Earth's angular velocity ω. Then the total force is given by

$$\mathbf{G}(\mathbf{r}) = \mathbf{F}(\mathbf{r}) + \mathbf{C}(\mathbf{r}). \tag{2.35}$$

The first term of Eq. (2.35) is the gravitational force and the second term the centrifugal force which can be written as follows:

$$\mathbf{C}(\mathbf{r}) = m\mathbf{c}(\mathbf{r}), \tag{2.36}$$

where $\mathbf{c}(\mathbf{r})$ is the centrifugal field strength. It is given by

$$\mathbf{c}(\mathbf{r}) = \mathbf{C}(\mathbf{r})/m = \omega^2\mathbf{p}. \tag{2.37}$$

The resultant of the gravitational field strength and the centrifugal field strength is the gravity acceleration or simply the gravity vector,

$$\mathbf{g}(\mathbf{r}) = \mathbf{a}(\mathbf{r}) + \mathbf{c}(\mathbf{r}). \tag{2.38}$$

The gravity potential is the sum of the gravitational potential and the centrifugal potential,

$$W(\mathbf{r}) = V(\mathbf{r}) + Z(\mathbf{r}) = G\iiint_v \frac{\rho}{l}dv + \frac{1}{2}\omega^2(x^2 + y^2). \tag{2.39}$$

Since Z is an analytic function, the discontinuities of W are those of V: the second derivatives have jumps at discontinuities of the density function. Any linear function of the gravity potential can be calculated by applying the linear operator L as follows:

$$L(W(\mathbf{r})) = G\iiint_v L\left(\frac{\rho}{l}\right)dv + L\left(\frac{1}{2}\omega^2(x^2 + y^2)\right). \tag{2.40}$$

An example of such an operator is the *Nabla operator* ∇. When applied to Eq. (2.40) it gives the gravity $\mathbf{g}$:

$$\mathbf{g}(\mathbf{r}) = \nabla W = G\iiint_v \nabla\left(\frac{\rho}{l}\right)dv + \nabla\left(\frac{1}{2}\omega^2(x^2 + y^2)\right). \tag{2.41}$$

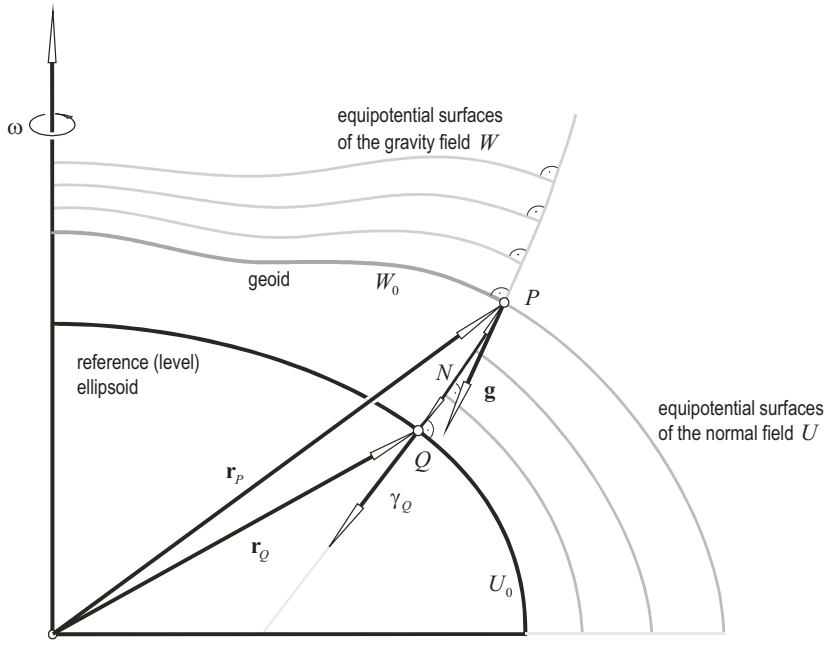

Fig. 2.5: Gravity field and normal field

The magnitude g of the vector $\mathbf{g}$ is frequently called gravity in the narrower sense.

Again, the potential of the Earth can be introduced using a spherical harmonic expansion as follows (Heiskanen and Moritz 1967):

$$W(\mathbf{r}) = \frac{GM}{r}\left(1 + \sum_{n=2}^{\infty}\left(\frac{R}{r}\right)^n \sum_{m=0}^{n}\left(c_{nm}\cos m\lambda + s_{nm}\sin m\lambda\right) P_{nm}(\sin\varphi)\right) + \frac{\omega^2 r^2}{3}\left(1 - P_2(sin\varphi)\right), \quad (2.42)$$

with the mass of the Earth M and the mean radius R. The coefficients c_{nm}, s_{nm} are defined in Eq. (2.18).

Applying the *Laplace operator* to the gravity potential results in,

$$\Delta W(\mathbf{r}) = -4\pi G\rho + 2\omega^2, \quad (2.43)$$

which is the well-known *Poisson's differential equation*. For the space outside the masses it reads,

$$\Delta W(\mathbf{r}) = 2\omega^2. \quad (2.44)$$

2.2.2 Normal figure and normal field

For linearization tasks the actual gravity field can be approximated by a model gravity field generated by a level ellipsoid. This ellipsoid serves as a reference and is also an approximation of the mathematical figure of the Earth, the geoid or the quasi-geoid. The reference ellipsoid has the same mass M as the actual Earth. Its center coincides with the center of the Earth and it rotates with the same angular velocity ω as the real Earth. The gravity field generated by this model is fully described by four parameters a, GM, J_2, ω, the defining parameters of a Geodetic Reference System (GRS). Its gravity potential can be expressed as follows:

$$U(\mathbf{r}) = \frac{GM}{r}\left(1 - \sum_{n=1}^{\infty}\left(\frac{a}{r}\right)^n \sum_{m=0}^{n}\left(c'_{nm}\cos m\lambda + s'_{nm}\sin m\lambda\right) P_{nm}(\sin\varphi)\right) + \frac{\omega^2 r^2}{3}\left(1 - P_2(sin\varphi)\right), \quad (2.45)$$

where c'_{nm} and s'_{nm} are the fully normalized coefficients of the reference ellipsoid and a its equatorial radius of the reference ellipsoid. It is sufficient to calculate these coefficients up to degree six or eight as the values

of higher degree tend to zero (Rapp 1982). Because of its symmetries, the normal potential is described only by an even degree zonal harmonic expansion. The zonal coefficients can be determined through,

$$c'_{n0} = -\frac{J_n}{\sqrt{2n+1}}, \tag{2.46}$$

with the coefficients

$$J_2 = \frac{2}{3}\left[f\left(1-\frac{1}{2}f\right) - \frac{1}{2}m\left(1-\frac{2}{7}f+\frac{11}{49}f^2\right)\right], \tag{2.47}$$

$$J_4 = -\frac{4}{35}f\left(1-\frac{1}{2}f\right)\left[7f\left(\left(1-\frac{1}{2}f\right) - 5m\left(1-\frac{2}{7}f\right)\right)\right], \tag{2.48}$$

$$J_6 = \frac{4}{21}f^2(6f-5m), \tag{2.49}$$

and the flattening f of the reference ellipsoid and the parameter m, defined by

$$m = \frac{\omega^2 a^3(1-f)}{GM}. \tag{2.50}$$

Applying the *Nabla operator* to the normal gravity potential leads to the normal gravity vector,

$$\nabla U(\mathbf{r}) = \gamma(\mathbf{r}). \tag{2.51}$$

The application of the *Laplace operator* yields

$$\Delta U(\mathbf{r}) = 2\omega^2. \tag{2.52}$$

Eq. (2.52) represents Poisson's differential equation for the normal gravity potential in mass free space.

2.2.3 The boundary value problem of Stokes

In case of *Stokes' boundary value problem* the equipotential surface of the gravity field in sea level, the geoid, is selected as boundary surface. The points at the geoid are projected onto the reference (level) ellipsoid along the ellipsoidal normals (Fig. 2.5). The ellipsoidal coordinates, latitude and longitude, of the geoid points are considered to be known. The vertical distance between two points, the geoid height or undulation N, is unknown and has to be determined as solution of *Stokes' problem*. The reference ellipsoid is a level ellipsoid, that means, the ellipsoidal surface is an equipotential surface of the normal field as explained in the last section. The normal figure (ellipsoidal surface) and the normal field are approximations of the geoid and the gravity field, respectively. The disturbing gravity potential T is defined as the difference between the gravity potential and the normal potential,

$$T(\mathbf{r}) = W(\mathbf{r}) - U(\mathbf{r}). \tag{2.53}$$

The disturbing potential and the geoid height are the unknowns of the boundary value problem of Stokes while the (scalar) gravity values at the geoid, $g = g(P)$, are considered to be the known (measured) quantities. The disturbing potential T is regular at infinity and has to be harmonic outside the boundary surface to fulfil the *Laplace equation*,

$$\Delta T(\mathbf{r}) = 0. \tag{2.54}$$

This will be achieved by removing all masses outside the geoid; the changes have to be corrected properly as explained in the following chapters. A linear relation in spherical approximation between the gravity values at the geoid, g_P, and the disturbing potential T, the so-called *Fundamental equation of Physical Geodesy* (Fig. 2.6),

$$\Delta g = g_P - \gamma_Q = -\left.\frac{\partial T}{\partial r}\right|_Q - \frac{2}{r}T_Q, \tag{2.55}$$

with the gravity anomalies Δg. The linearization provides also a relation between the geoid height and the disturbing potential (*Theorem of Bruns*),

$$N = \frac{T_Q}{\gamma}, \tag{2.56}$$

with a mean normal value γ (Somigliana 1929).

The solution of the *Laplace equation* (2.54) with the boundary condition (2.55) is the *Stokes formula*,

$$T(r,\varphi,\lambda) = T_0(r,\varphi,\lambda) + T_1(r,\varphi,\lambda) + \frac{R}{4\pi}\iint_s \Delta g'(\varphi',\lambda')\, S(r,\psi)\, ds, \tag{2.57}$$

with the terms,

$$T_0(r,\varphi,\lambda) = -\frac{R^2}{r}\langle \Delta g'(\varphi,\lambda)\rangle, \tag{2.58}$$

and

$$T_1(r,\varphi,\lambda) = \frac{GM}{r^2} R X_1(\varphi,\lambda), \tag{2.59}$$

as well as the *Stokes-Pizzetti function* $S(r,\psi)$. The quantity $\langle \Delta g'\rangle$ is the mean value of the gravity anomalies over the Earth,

$$\langle \Delta g'\rangle := \frac{1}{4\pi}\iint_s \Delta g'(r,\varphi',\lambda')\, ds, \tag{2.60}$$

and $X_1(\varphi,\lambda)$ is the *Laplace surface spherical harmonic of degree* $n = 1$,

$$X_1(\varphi,\lambda) = c_{10}C_{10}(\varphi,\lambda) + c_{11}C_{11}(\varphi,\lambda) + s_{11}S_{11}(\varphi,\lambda). \tag{2.61}$$

The *Stokes formula* reads at the boundary surface, the geoid, in spherical approximation by setting $r \to R$:

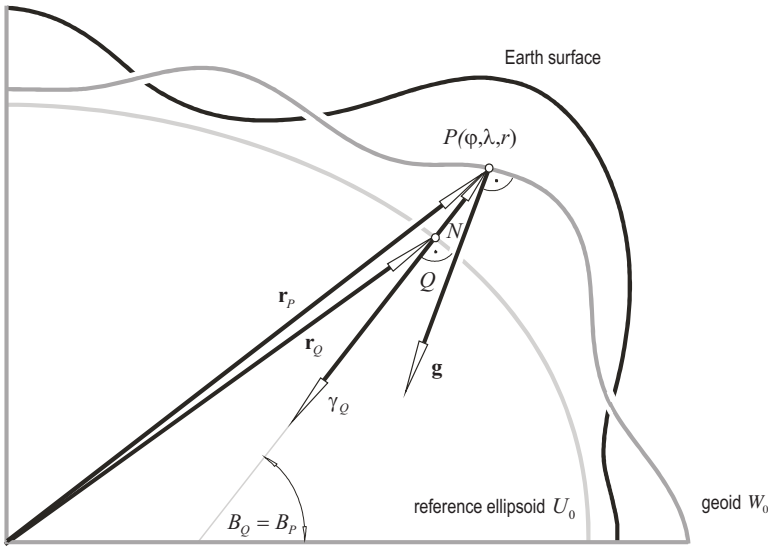

Fig. 2.6: Relation between the surface of the Earth, the geoid and the reference ellipsoid

$$T(\varphi,\lambda) = T(R,\varphi,\lambda) = T_0(\varphi,\lambda) + T_1(\varphi,\lambda) + \frac{R}{4\pi}\iint_s \Delta g(\varphi',\lambda')\, S(\psi(\varphi,\lambda;\varphi',\lambda'))\, ds, \tag{2.62}$$

with

$$T_0(\varphi,\lambda) = \frac{G\delta M}{R} = -R\left\langle \Delta g(\varphi,\lambda)\right\rangle, \tag{2.63}$$

and

$$T_1(\varphi,\lambda) = \frac{GM}{R^2}\left(\cos\varphi\cos\lambda\ \mathbf{e}_x + \cos\varphi\sin\lambda\ \mathbf{e}_y + \sin\varphi\ \mathbf{e}_z\right)\cdot\mathbf{r}_{CM}, \tag{2.64}$$

where the *Stokes-Pizzetti function* $S(r,\psi)$ becomes the *Stokes function* $S(\psi)$. For the geoid height it follows according to the *Theorem of Bruns*,

$$N(\varphi,\lambda) = \frac{T(\varphi,\lambda)}{\gamma} = N_0(\varphi,\lambda) + N_1(\varphi,\lambda) + \frac{R}{4\pi\gamma}\iint_\sigma \Delta g'(\varphi',\lambda')\ S(\psi(\varphi,\lambda;\varphi',\lambda'))\ d\sigma. \tag{2.65}$$

Because of the fact that the masses outside the geoid have to be removed or shifted inside the boundary surface these geoid heights are the heights of a preliminary boundary surface, the co-geoid.

2.2.4 Topographic isostatic effects in Stokes' boundary value problem

The solution of the *boundary value problem of Stokes* by solving the Laplace equation requires that the gravity potential outside the geoid is harmonic. As pointed out already, it is necessary to remove the topographic masses or shift them inside the boundary surface. Then it is possible to solve the boundary value problem based on *Laplace's equation*. Obviously, the solution has to be corrected afterwards to restore the original situation, that means, the determination of the geoid inside the masses. Therefore, the reduction and correction steps require a detailed knowledge of the topographic masses.

The effects of the topographic and the isostatic or condensed masses on the geoid heights are evaluated as three separate contributions: the *direct topographic effect on the gravity*, the *primary indirect topographic effect on the geoid* and the *secondary indirect topographic effect on the gravity* (e.g., Novàk et al. 2001) in case of the gravity at the surface of the Earth. For airborne gravimetry where gravity disturbances at flight level are considered as observations, only the direct and the secondary indirect topographic effects have to be considered. The harmonized disturbing potential can be determined for any point in space by (Martinec et al. 1993),

$$\begin{aligned} T^h(\mathbf{r}) &= T(\mathbf{r}) - \delta V(\mathbf{r}),\\ T^h(r,\varphi,\lambda) &= T(r,\varphi,\lambda) - \delta V(r,\varphi,\lambda), \end{aligned} \tag{2.66}$$

with the disturbing potential T of the Earth's gravity field, and the direct topographic-isostatic effect on the gravitational potential $\delta V(r,\varphi,\lambda)$. The latter one is the difference between the gravitational potential of the topography $V^t(r,\varphi,\lambda)$ and the gravitational potential of the isostatic or condensed masses $V^c(r,\varphi,\lambda)$,

$$\delta V(r,\varphi,\lambda) = V^t(r,\varphi,\lambda) - V^c(r,\varphi,\lambda). \tag{2.67}$$

The spherical coordinates r,φ and λ of the computation point at the surface of the Earth or at airborne altitude refer to a geocentric coordinate system.

The geoid heights of the *co-geoid* can be derived by *Bruns' theorem* from the harmonized disturbing potential as solution of the geodetic boundary value problem and a correction term on the co-geoid height, the *primary indirect topographic-isostatic effect* $PITE(R,\varphi,\lambda)$,

$$N(\varphi,\lambda) = \frac{T(R,\varphi,\lambda)}{\gamma_0(\varphi)} = \frac{T^h(R,\varphi,\lambda)}{\gamma_0(\varphi)} + \frac{\delta V(R,\varphi,\lambda)}{\gamma_0(\varphi)} =: \frac{T^h(R,\varphi,\lambda)}{\gamma_0(\varphi)} + PITE(R,\varphi,\lambda), \tag{2.68}$$

with the normal gravity $\gamma_0(\varphi)$ at the level ellipsoid.

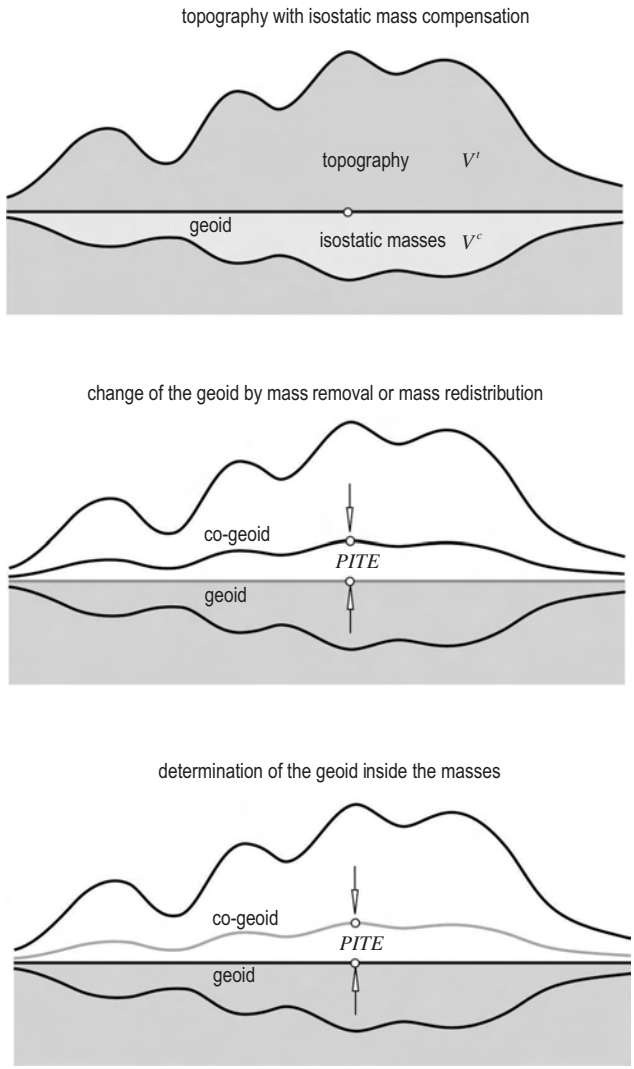

Measurement

- gravity values at the Earth surface: g^σ

Determination of the surface gravity anomalies

$$\Delta g = g^\sigma - \left(\gamma + \frac{\partial \gamma}{\partial h} H + \ldots\right)$$

Determination of topographic-isostatic effects on the gravity anomalies

- direct topographic-isostatic mass effects on the gravity potential $\delta V = V^t - V^c$
- direct topographic-isostatic mass effect on the gravity: $\partial \delta V / \partial r = DTE$
- secondary indirect topographic-isostatic mass effect on the gravity: $2\delta V / r = SITE$

$$\Delta g^h = \Delta g + DTE + SITE$$

Downward continuation of surface gravity anomalies from the Earth surface down to the geoid

$$\Delta g^h \rightarrow \Delta g^h_c$$

Determination of the co-geoid

- Stokes formula:

$$N^h = \frac{R}{4\pi\gamma} \iint_\sigma \Delta g^h S(\psi)\, d\sigma$$

Determination of the geoid

- topographic-isostatic mass effects on the geoid height (primary indirect topographic-isostatic effect)

$$N = N^h + PITE$$

Fig. 2.7: Flow chart of the geoid determination procedure considering the various topographic-isostatic effects

By applying the negative radial derivative to Eq. (2.66), the corresponding topographical effect on gravity can be obtained as follows:

$$\delta g^h(r,\varphi,\lambda) = -\frac{\partial T^h(r,\varphi,\lambda)}{\partial r} = -\frac{\partial T(r,\varphi,\lambda)}{\partial r} + \frac{\partial \delta V(r,\varphi,\lambda)}{\partial r} =: \delta g(r,\varphi,\lambda) + DTE(r,\varphi,\lambda), \tag{2.69}$$

where δg and δg^h are the gravity disturbances of the real gravity field and the harmonized gravity field, respectively, and $DTE(r,\varphi,\lambda)$ is the *direct topographic-isostatic effect on gravity*. The direct and primary indirect topographic-isostatic effects given in Eq. (2.68) and Eq. (2.69), respectively, represent the effect of the topographic and isostatic masses for geoid determinations based on airborne gravity measurements. Since the gravity disturbances δg differ from the gravity anomalies Δg only by the vertical change of normal gravity along the separation between the actual equipotential surface and the corresponding normal equipotential surface, the following expression can be obtained for points at the surface of the Earth:

$$\begin{aligned} \Delta g^h(r,\varphi,\lambda) &= \Delta g(r,\varphi,\lambda) + \frac{\partial \delta V(r,\varphi,\lambda)}{\partial r(\varphi,\lambda)} + \frac{2}{r}\delta V(r,\varphi,\lambda) \\ &=: \Delta g(r,\varphi,\lambda) + DTE(r,\varphi,\lambda) + SITE(r,\varphi,\lambda). \end{aligned} \tag{2.70}$$

The second term at the right hand side of Eq. (2.71) represents the *direct topographic-isostatic effect on gravity*, $DTE(r, \varphi, \lambda)$, and the third term the *secondary indirect topographic effect on gravity*, $SITE(r, \varphi, \lambda)$.

To determine the geoid, the downward continuation of the gravity anomalies, defined in Eq. (2.71), from the topography to the geoid has to be performed according to (Novàk 2000):

$$\Delta g_c^h(R, \varphi, \lambda) = \Delta g^h(r, \varphi, \lambda) + D\Delta g^h(\varphi, \lambda), \tag{2.71}$$

where $D\Delta g^h(\varphi, \lambda)$ is the downward continuation term. The geoid can be determined by Eq. (2.65). If the masses of the reference ellipsoid and the Earth are identical and the origin of the terrestrial reference frame is located at the center of mass of the Earth then the first two terms become zero and the solution reads as follows,

$$N^h = N_0 = \frac{R}{4\pi\gamma} \iint_s \Delta g_c^h(R, \varphi, \lambda) S(\psi) ds, \tag{2.72}$$

here N_0 is the harmonized undulation of the co-geoid referred to the reference ellipsoid and $S(\psi)$ the Stokes' function given by:

$$S(\psi) = \frac{1}{\sin(\psi/2)} - 6\sin(\psi/2) + 1 - 5\cos\psi - 3\cos\psi \ln\left(\sin(\psi/2) + \sin^2(\psi/2)\right). \tag{2.73}$$

Finally, the geoid heights can be restored by the formula:

$$N = N^h + PITE = N^h + \delta N. \tag{2.74}$$

The computation steps are shown in the flow chart of Fig. 2.7.

2.2.5 The role of topography in Molodenskii's boundary value problem

With the solution of Stokes' problem the surface of the Earth can be described mathematically. The geoid, on the one hand, is determined by the geoid heights referring to the reference ellipsoid and the surface of the Earth, on the other hand, by the orthometric heights referring to the geoid. But both quantities, geoid heights and orthometric heights, cannot be determined without hypothesis:

- the gravity values measured at the Earth's surface have to be reduced down to the geoid which is the boundary surface of *Stokes' problem*. Furthermore the masses outside the geoid, the topographic masses, have to be removed – otherwise *Laplace equation* does not hold. To perform these steps rigorously the density function of the masses must be known which is usually not the case. Therefore, hypotheses of the density structure of the external masses are necessary.
- to derive orthometric heights of the Earth surface mean values of the gravity along the plumb lines from the geoid to the Earth's surface are necessary. Because of the fact that these values cannot be measured they have to be derived indirectly based on hypotheses of the density structure of the masses along the plumb lines.

It should be pointed out that the surface of the Earth is described correctly without hypothesis as the sum of geoid heights and orthometric heights, but the geoid heights and the orthometric heights themselves depend on the hypothesis about the density function of the topographic masses.

An alternative way to solve this problem is to use the surface of the Earth directly as boundary surface for the geodetic boundary value problem. This solution has been proposed in the years 1940 to 1950 by the Russian scientist M.S. Molodenskii. The first English publication appeared in 1962, together with V.F. Eremeev and M.I. Yurkina (Molodenskii et al. 1962). The advantage of this idea is to avoid any hypothesis in deriving a solution to the geodetic boundary value problem. The disadvantage is that this solution strategy

causes much more mathematical problems than in case of the Stokes' problem. The first obvious difference is that the boundary surface of Molodenskii's problem is not an equipotential surface with normals directed to the gravity vector. Instead the boundary surface is an arbitrary not even continuous function. It is also a non-linear problem similar to Stokes' problem, but the linearization causes much more problems because of the fact that the geoid deviates from the reference ellipsoid only by a maximum of 100 m, while the surface of the Earth shows ellipsoidal heights of up to approximately 9000 m. Furthermore, Molodenskii's problem is not only a free boundary value problem but also a so-called oblique boundary value problem because of the fact that the gravity vector is usually not orthogonal to the boundary surface.

A consequence of the large deviations of the surface of the Earth (considered as boundary surface) from the reference ellipsoid is that an approximation of the boundary surface has to be introduced which is closer to the boundary surface. This approximation is the *telluroid*, which is referred to the reference ellipsoid by a type of heights which can be determined without hypothesis, the so-called *normal heights*. The deviations of the surface of the Earth and the *telluroid*, the *height anomalies*, are in the size of the geoid heights. If the points of the surface of the Earth are referred to a vertical reference surface by the normal heights – similar to the geoid in case of orthometric heights – then one arrives at the quasi geoid which coincides approximately with the geoid (Fig. 2.10). In the following, we will only give the solution of *Molodenskii's*

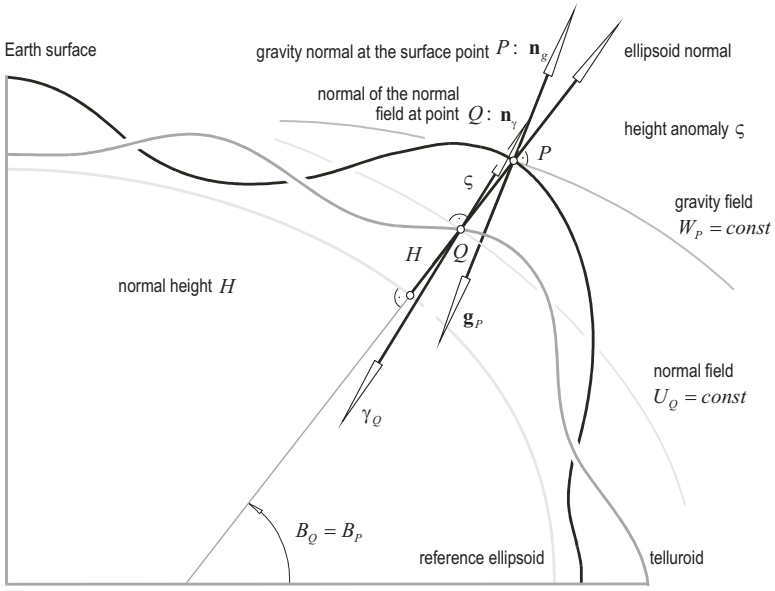

Fig. 2.8: Relation between the surface of the Earth, the telluroid and the reference ellipsoid

boundary value problem in form of the so-called *Molodenskii series* where the first approximation is identical with the solution of Stokes problem with a slightly different definition of the gravity anomalies used in the solutions (Heiskanen and Moritz 1967; Klees 1992; Lehmann 1994),

$$T = \sum_{n=0}^{\infty} T_n, \tag{2.75}$$

with

$$T_n = \frac{R}{4\pi} \iint_\sigma G_n S(\psi)\, d\sigma \quad \text{for} \quad n = 0, 1. \tag{2.76}$$

and

$$T_n = \frac{R}{4\pi} \iint_\sigma G_0\, S(\psi)\; d\sigma - \frac{R^2}{4\mu} \iint_\sigma \frac{(h - h_P)^2}{l_0^3}\, G_{n-2} d\sigma \quad \text{for} \quad n \geq 2. \tag{2.77}$$

The functions G_n can be determined by the following formulae,

$$G_0 = \Delta g, \tag{2.78}$$

with the surface gravity anomalies $\Delta g = g_P - \gamma_Q$ and

$$G_1 = \frac{R^2}{2\pi} \iint\limits_{\sigma} \frac{h - h_P}{l_0^3} G_0 d\sigma, \tag{2.79}$$

$$G_2 = \frac{R^2}{2\pi} \iint\limits_{\sigma} \frac{h - h_P}{l_0^3} G_1 d\sigma + G_0 \tan^2 \beta, \tag{2.80}$$

$$G_3 = \frac{R^2}{2\pi} \iint\limits_{\sigma} \frac{h - h_P}{l_0^3} G_2 d\sigma + G_1 \tan^2 \beta - \frac{3R^2}{4\pi} \iint\limits_{\sigma} \frac{(h - h_P)^3}{l_0^5} G_0 d\sigma, \tag{2.81}$$

where β is the maximum inclination of the terrain, h_P the ellipsoidal height of the computation point and h the ellipsoidal height of the integration point (for the notation refer also to Moritz 1965, 1980).

The height anomalies can be derived subsequently by applying Bruns' theorem

$$\zeta = \frac{T}{\gamma}. \tag{2.82}$$

The first two terms of the series Eq. (2.75) represent an approximation of the solution of Molodenskii's problem which is sufficient for many applications. The disturbance potential reads,

$$T \approx T_0 + T_1 = \frac{R}{4\pi} \iint\limits_{\sigma} (\Delta g + G_1)\ S(\psi)\ d\sigma, \tag{2.83}$$

which can be used to derive the height anomalies again by Bruns' theorem,

$$\zeta \approx \zeta_0 + \zeta_1 = \frac{R}{4\pi\gamma} \iint\limits_{\sigma} \Delta g\, S(\psi)\ d\sigma + \frac{R}{4\pi\gamma} \iint\limits_{\sigma} G_1\, S(\psi)\ d\sigma. \tag{2.84}$$

The term G_1 can be considered as terrain correction with constant density (Moritz 1968),

$$G_1 = \frac{1}{2} G\rho R^2 \iint\limits_{\sigma} \frac{(h - h_P)^2}{l_0^3}\, d\sigma. \tag{2.85}$$

The solution of the boundary value problem of Molodenskii does not need any assumptions about the density of the topography and the crust as it depends on the free-air anomalies at the surface of the Earth. But it is known that the free-air anomalies are small and strongly dependent on the roughness of the topography, so that their interpolation is very inaccurate (Heiskanen and Moritz 1967). Therefore, it is preferable also in case of Molodenskii's boundary value problem to make use of the well-known advantages of the Bouguer and isostatic anomalies. These anomalies are smoother and more representative than the free air anomalies and can be interpolated more easily and more accurately.

To take the effect of the topographic-isostatic masses into account, we start with Eq. (2.66) as it represents the disturbing potential by removing the topographic-isotatic masses as follows:

$$T^r(r_P, \varphi, \lambda) = T(r_P, \varphi, \lambda) - \delta V(r_P, \varphi, \lambda). \tag{2.86}$$

With these reductions the disturbing potential will be smoother than the original one; therefore we call it *regularized disturbance potential* T^r. In this case, the physical surface of the Earth will remain unchanged, but the *telluroid* will change, because its points Q are defined by $U_Q = W_P$, and the potential W at any point P will be affected by the removing of the topographic masses. The height anomaly difference $\delta\zeta$ between

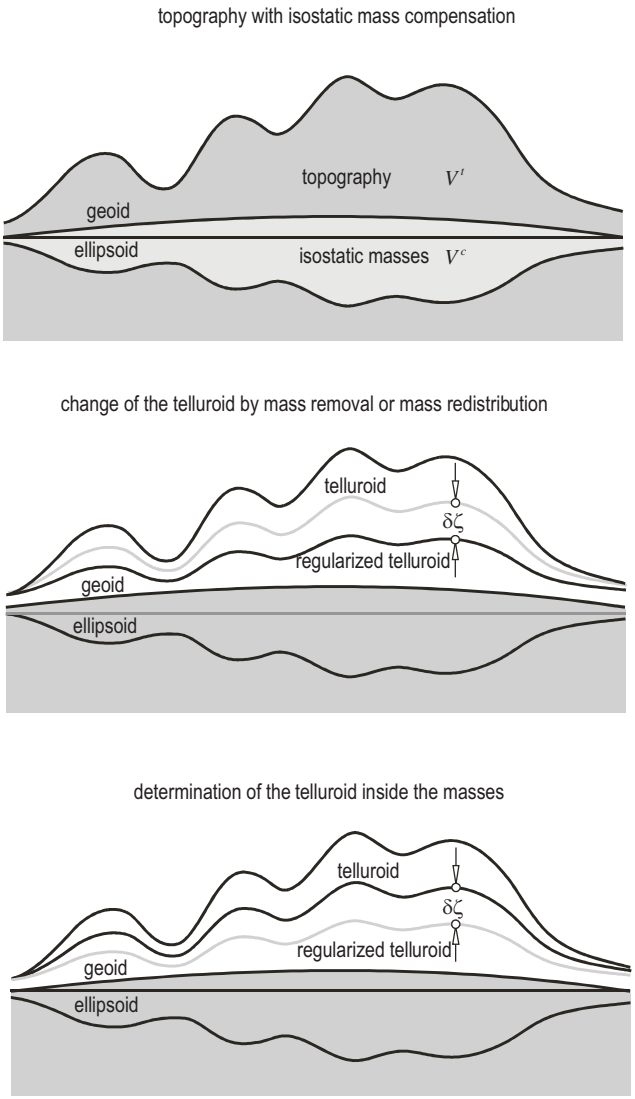

Measurement

- gravity values at the Earth surface: g^σ

Determination of topographic-isostatic effects on gravity anomalies

- direct topographic-isostatic mass effects on the gravity potential: $\delta V = V^t - V^c$
- direct topographic-isostatic mass effect on the gravity: $\partial\delta V/\partial r = DTE$
- secondary indirect topographic-isostatic mass effect on the gravity: $2\delta V/r = SITE$

Determination of the regularized surface gravity anomalies

- regularized gravity anomaly:

$$\Delta g^r = \Delta g + DTE + SITE$$

$$\Delta g = g - \gamma$$

Determination of the regularized telluroid

- Molodenskii series:

$$\zeta^r \approx \frac{R}{4\pi\gamma}\iint_\sigma \Delta g^r\, S(\psi)\, d\sigma +$$

$$+\frac{R}{4\pi\gamma}\iint_\sigma G_1\, S(\psi)\, d\sigma$$

Determination of the telluroid

- topographic-isostatic mass effects on the height anomalies

$$\zeta = \zeta^r + \delta\zeta$$

Fig. 2.9: Flow chart of the telluroid determination procedure considering the various topographic-isostatic effects

the original *telluroid* and the *regularized telluroid* according to Bruns' theorem is given by (Heiskanen and Moritz 1967),

$$\delta\zeta = \zeta - \zeta^r = \frac{\delta V}{\gamma}, \tag{2.87}$$

where γ is the normal gravity on the *telluroid*. In this case the regularized gravity anomalies at the surface of the Earth will be given by:

$$\Delta g^r = \Delta g - \delta g - \frac{\partial\gamma}{\partial h}\delta V = \Delta g + DTE + SITE. \tag{2.88}$$

The second term in the right hand side of Eq. (2.88) represents the *direct topographical effect on gravity* and the third term the *secondary indirect topographical effect on gravity*, both analogously to Eq. (2.70). After

that the regularized height anomalies ζ^r are computed from the regularized gravity anomalies Δg^r by the solution of Molodenskii's problem according to Eq. (2.82) or approximately by Eq. (2.84),

$$\zeta^r \approx \frac{R}{4\pi\gamma} \iint_\sigma \Delta g^r \, S(\psi) \, d\sigma + \frac{R}{4\pi\gamma} \iint_\sigma G_1 \, S(\psi) \, d\sigma. \tag{2.89}$$

Finally, the original height anomalies ζ are obtained by considering the indirect effect by inserting $\delta\zeta$ according to Eq. (2.87):

$$\zeta = \zeta^r + \delta\zeta. \tag{2.90}$$

The computation steps are shown in the flow chart of Fig. 2.9.

If the geoid heights are required, instead of height anomalies, the following equation can be used (Heiskanen and Moritz 1967),

$$N = \zeta + \frac{\bar{g} - \bar{\gamma}}{\bar{\gamma}} \overset{O}{H}, \tag{2.91}$$

where $\bar{g}$ is the mean gravity along the plumb line between the geoid and the ground and $\bar{\gamma}$ the mean normal gravity along the normal plumb line between the ellipsoid and the telluroid and the orthometric height H^O. The term $\bar{g} - \bar{\gamma}$ is approximately equal to the Bouguer anomaly, and Eq. (2.91) can be transformed to the following equation:

$$N_{\text{in meters}} = \zeta + \Delta g_{B\,\text{in Gals}} H^O_{\text{in km}}. \tag{2.92}$$

But it is shown that using only the Bouguer anomalies brings some errors in calculating the geoid heights, because the value of the mean gravity $\bar{g}$ depends on the density of the topographic masses and maybe also on the density of the crust, mantle and core of the Earth (see, e.g., Tenzer et al. 2005).

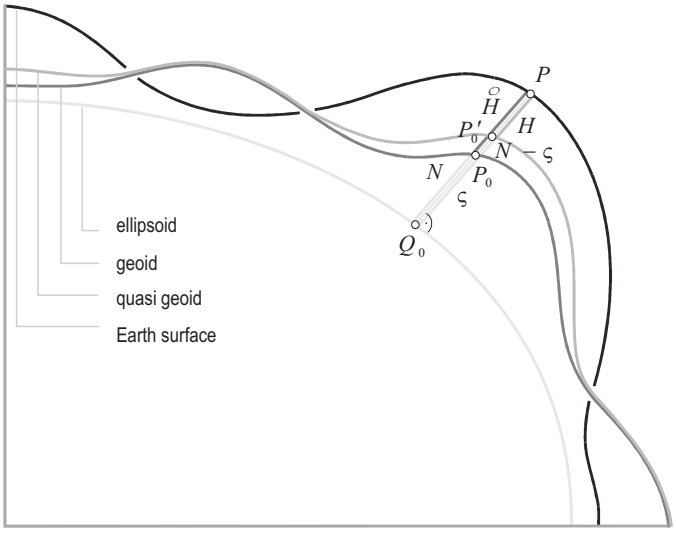

Fig. 2.10: Telluroid before and after the reduction of the topographic masses

2.3 Topographic-isostatic effects in airborne gravimetry

Airborne gravimetry is a fast and accurate gravity measurement technique to derive high resolution geoids in not easily accessible regions. Under optimal conditions the measurement accuracy varies around 1 to

2 mGal for a spatial resolution of approximately 2 km. The downward continuation of these observations requires a filtering of the observables to reduce the intrinsic instabilities. To ease the downward continuation of filtered data from aircraft altitude down to sea level, it is helpful to additionally apply a remove-restore technique (Forsberg and Tscherning 1997) based on gravity field information provided by the topographic-isostatic masses. The effects of the topographic-isostatic masses on the geoid heights from airborne gravity are evaluated as two separate contributions: the direct topographical effect on the gravity (DTE) and the (primary) indirect topographical effect on the geoid ($PITE$) (Novàk et al. 2001).

The observables of airborne gravimetry are gravity disturbances at aircraft altitude. They are defined as differences between the actual gravity and the normal gravity at the same point. If the gravity disturbances on the reference ellipsoid are given and the disturbing potential is required in the space outside the masses, then we have to solve a *geodetic boundary value problem of the second kind* or a so-called *Neumann problem*. In this case, the *Laplace equation* for the disturbing potential,

$$\Delta T = 0, \tag{2.93}$$

has to be solved, satisfying the following boundary condition (defined on the reference ellipsoid),

$$\delta g = g_p - \gamma_P = -\frac{\partial T}{\partial n}, \tag{2.94}$$

where n is the ellipsoidal normal and g_p and γ_P the actual and normal gravity at the boundary surface. In case of a spherical approximation Eq. (2.94) can be simplified as

$$\delta g = g_p - \gamma_P = -\frac{\partial T}{\partial r}. \tag{2.95}$$

The solution of the *Neumann problem* in this case is given by (e.g., Hotine 1969; Novàk et al. 2000):

$$T(\varphi, \lambda) = \frac{R + h_f}{4\pi} \iint_{\sigma} \delta g \, H(\psi) \, d\psi, \tag{2.96}$$

where $H(\psi)$ is the *Hotine function* and h_f is the height of the aircraft. It can be given as a closed formula as follows (Hotine 1969):

$$H(\psi) = \sum_{n=0}^{\infty} \frac{(2n+1)}{(n+1)} P_n(\cos\psi) = \operatorname{cosec}(1/2\psi) + \ln\left(1 + \operatorname{cosec}(1/2\psi)\right). \tag{2.97}$$

This equation includes the zero and the first order terms of the spherical harmonic expansion of the disturbing potential. If the mass of the Earth is assumed to be equal to the mass of the reference ellipsoid and the center of the Earth is assumed to coincide with the origin of the reference system, then *Hotine's function* can be simplified as following:

$$H(\psi) = \sum_{n=2}^{\infty} \frac{(2n+1)}{(n+1)} P_n(\cos\psi) = \operatorname{cosec}(1/2\psi) + \ln\left(1 + \operatorname{cosec}(1/2\psi)\right) - 1 - (3/2)\cos\psi. \tag{2.98}$$

If we want to remove the topographic-isostatic masses then we have to follow, in principle, the procedure described in Fig. 2.7. The observations δg have to be corrected by the DTE at aircraft altitude to get the harmonized gravity disturbance at aircraft altitude,

$$\delta g^h = \delta g - DTE\,(R + D, \varphi, \lambda) \tag{2.99}$$

with

$$\delta g^h = \frac{\partial T^h(R + D, \varphi, \lambda)}{\partial r}, \tag{2.100}$$

$$\delta g = \frac{\partial T(R + D, \varphi, \lambda)}{\partial r}, \tag{2.101}$$

$$DTE\,(R+D,\varphi,\lambda) := \left.\frac{\partial \delta V(r,\varphi,\lambda)}{\partial r}\right|_{r=R+D} = \frac{\partial V^t}{\partial r} - \frac{\partial V^c}{\partial r}, \tag{2.102}$$

where $\delta V\,(r,\varphi,\lambda)$ is the difference between the gravitational potential of the topography V^t and the gravitational potential of the isostatic or condensed topographic masses, V^c. In the following step, the harmonized gravity disturbances at aircraft altitude have to be downward continued to the boundary surface,

$$\delta g^h \quad \rightarrow \quad \delta g_c^h. \tag{2.103}$$

Then the *Hotine integral* is applied to give the co-geoid as follows:

$$N^h(\varphi,\lambda) = \frac{R}{4\pi} \iint\limits_{\sigma} \delta g_c^h H(\psi) d\psi. \tag{2.104}$$

Finally, the *primary indirect topographical effects* are added to give the geoid heights,

$$N(\varphi,\lambda) = N^h(\varphi,\lambda) + PITE, \tag{2.105}$$

with

$$PITE = \frac{\delta V}{\gamma}. \tag{2.106}$$

2.4 Topographic-isostatic mass effects in satellite application

The dedicated satellite gravity missions CHAMP (Reigber et al. 1999) and GRACE (Tapley et al. 2004) as well as ESA's GOCE mission, to be launched in 2007, (ESA 1999) will improve our knowledge of the Earth's gravity field in the long, medium and short wavelength ranges. The novel measurement techniques are Satellite-to-Satellite Tracking (SST) either in the high-low, the low-low or the Precise Orbit Determination (POD) mode and Satellite Gravity Gradiometry (SGG), respectively. After an operational period of only a few months after its launch in July 2000, a global gravity field model has been generated from the CHAMP GPS-SST data, which recovers the long- to medium-wavelength part of the gravity field by one order of magnitude more accurate than during the last decades of classical satellite geodesy (Reigber et al. 2002). As a result of ultra-precise ranging between satellites, a further breakthrough in accuracy and resolution has been achieved with the gravity field models derived from data generated by the twin-satellite mission GRACE, launched in 2002 (Mayer-Gürr et al. 2006). Meanwhile, monthly snapshots of the gravity field have been computed, allowing for the first time the resolution of temporal variations over a wide spatial and temporal spectrum.

The innovative character of these missions consists in the more or less complete coverage with observations by the Global Positioning System (GPS) and the continuous very precise line-of-sight range-rate measurements by GRACE, as well as the measurement of the gravity gradients by a three-dimensional gravity gradiometer without interruption in the case of GOCE. To prevent the observations from non-gravitational constituents, the surface forces are either measured and considered in a pre-processing step or will be compensated by a drag-free control system directly, as in case of GOCE.

2.4.1 Improperly posed problems in satellite geodesy

A critical point of the determination of gravity field parameters from observations at satellite altitude is the downward continuation of the high-precise SST data and the SGG observations. It is well-known that these gravity field recovery problems are improperly posed problems, that means, small changes in the observations produce large effects in the solutions. These problems usually require a proper regularization to receive stable recovery results. The basic principle behind regularization, e.g., in case of Tichnov's regularization method, is a balancing procedure between observation noise and unknowns. Regularization of unstable problems is

especially critical in those cases where the noise is intermingled with the signal content in the observations. Some contributions of the gravity signal are well known a-priori. Therefore, it is advantageous if those signal parts are reduced prior to the downward continuation and restored after the recovery procedure. In this case, we can anticipate that the high frequent part in the observations is mainly caused by the observation noise which can be filtered without loosing gravity field signals.

One important source of high frequent signal constituents in the satellite observations is caused by the topographical masses and its isostatic compensation. Nowadays, very precise digital elevation models (DEM) of land and sea (bathymetry) are available. The effects of the topographic-isostatic masses on the gravity field determinations from the new in-situ satellite gravity missions are evaluated also in this case as two separate contributions: the direct topographical effect on the gravity (DTE) and the (primary) indirect topographical effect on the geoid ($PITE$). The application of the direct topographic-isostatic effects on the observables at satellite altitude acts as a smoothing of the observations which simplifies the downward continuation procedure. Here we give only some basic information of the recovery models – the numerical effects in satellite altitude will be discussed later.

2.4.2 The use of topographic-isostatic mass effects in the Satellite -to- Satellite Tracking technique

The mathematical models for global as well as regional gravity field recovery from precise kinematical orbits, high-low and low-low Satellite-to-Satellite Tracking data is based on the formulation of *Newton's equation of motion*,

$$\ddot{\mathbf{r}}(t) = \mathbf{a}(t; \mathbf{r}, \dot{\mathbf{r}}; \mathbf{x}), \tag{2.107}$$

as a boundary value problem,

$$\mathbf{r}(t) = (1-\tau)\,\mathbf{r}_A + \tau \mathbf{r}_B - T^2 \int_{\tau'=0}^{1} K(\tau, \tau')\, \mathbf{a}(t; \mathbf{r}, \dot{\mathbf{r}}, \mathbf{x})\, d\tau' \tag{2.108}$$

with the integral kernel,

$$K(\tau, \tau') = \begin{cases} \tau\,(1-\tau'), & \tau \le \tau', \\ \tau'\,(1-\tau), & \tau' \le \tau, \end{cases} \tag{2.109}$$

the normalized time variable,

$$\tau = \frac{t - t_A}{T} \text{ with } T = t_B - t_A,\ t \in [t_A, t_B], \tag{2.110}$$

and the boundary values

$$\mathbf{r}_A := \mathbf{r}(t_A), \quad \mathbf{r}_B := \mathbf{r}(t_B), \quad t_A < t_B. \tag{2.111}$$

The specific force function in Eq. (2.108) with the unknown parameters $\mathbf{x}$ can be separated as follows,

$$\mathbf{a}(t; \mathbf{r}, \dot{\mathbf{r}}; \mathbf{x}) = \mathbf{a}_d(t; \mathbf{r}, \dot{\mathbf{r}}) + \nabla V(t; \mathbf{r}; \mathbf{x}_0) + \nabla T(t; \mathbf{r}; \Delta\mathbf{x}). \tag{2.112}$$

The quantity $\mathbf{a}_d$ is a disturbance part, which represents the non-conservative disturbing forces, ∇V is a reference part, representing the long wavelength gravity field features $\mathbf{x}_0$ and ∇T is an anomalous part, modelling the high frequent refinements $\Delta\mathbf{x}$ to the low frequent gravity field parameters $\mathbf{x}_0$ of the global model.

In case of the analysis of precisely determined kinematical orbits according to the POD technique the Eq. (2.108) together with Eq. (2.112) represents the physical model. It has to be supplied by a properly selected

stochastic model, where both models together build the mathematical model to determine corrections to the field parameters. This model has been successfully applied for the determination of the gravity field model ITG-Champ01 (details can be found in Mayer-Gürr et al. 2005).

If precise intersatellite functionals such as line-of-sight measurements between two satellites, following each other on the same orbit are available, as in case of the GRACE mission, the mathematical model for range observations can be derived by projecting the relative vector to the line-of-sight connection,

$$\rho(\tau) = \mathbf{e}_{12}(\tau) \cdot (\mathbf{r}_2(\tau) - \mathbf{r}_1(\tau)) \,. \tag{2.113}$$

Analog formulae can be derived for range-rates and range accelerations. The quantity $\mathbf{e}_{12}$ is the unit vector of the line-of-sight direction of the two GRACE satellites with the positions $\mathbf{r}_1(\tau)$ and $\mathbf{r}_2(\tau)$. This vector is known with high accuracy, assuming that the satellite positions are measured with an accuracy of a few cm and taking into account the distance of approximately $200km$ between the two satellites. Nevertheless, this accuracy is not adequate to the extremely high accuracy of the range measurements in the size of some μm. Therefore, a model refinement is necessary which improves implicitly also the relative orbit. The arcs of the satellites are fitted to the observables such that the unknown gravity field parameters are solved for while the quadratic norm of the observation residuals is minimized. To end up with a stable solution, a regularized solver of Tichnov type has to be applied, where the regularization parameter is preferably computed according to the variance component estimation procedure due to Koch and Kusche (2003). Further details to the physical model of the gravity field recovery technique based on GRACE low-low SST data can be found also in Mayer-Gürr (2006) and in Mayer-Gürr et al. (2006).

2.4.3 The use of topographic-isostatic mass effects in Satellite Gravity Gradiometry

GOCE (Gravity Field and Steady-State Ocean Circulation Explorer) has the potential of deriving the global gravity field with unprecedented accuracy in the high resolution spectral part. The usual way is to model the gravity field by spherical harmonics. A disadvantage of this kind of gravity field representation is the lack of flexibility in modelling the inhomogeneous gravity field features in specific regions. An alternative approach is to determine a global gravity field solution, based on GRACE SST observations up to a moderate degree and improve this global solution in selected regions by an adapted regional recovery procedure. The individual gravity field features in these regions can be modelled by space localizing base functions such as spherical spline functions. The advantage of this method is the possibility of adjusting the spline representation and the recovery procedure according to the regional gravity field structures and the specific data distribution. In the present case, the consideration of topographic-isostatic effects as discussed above is even more important than in case of SST because of the higher satellite altitudes of the latter one.

The observations of the GOCE gradiometer are the second derivatives of the gravitational potential $\nabla\nabla V(P)$. They are observed along the satellite orbit at a regular sampling rate. Every observation constitutes an observation equation if the gravity field is parameterized, adapted to the specific task. The parameterization of the potential is performed in terms of spherical harmonics for the global solution, in case of a regional gravity field recovery the potential has to be parameterized by space localizing base functions. It can be modelled as a sum of base functions as follows:

$$V(\mathbf{r}_P) = \sum_{i=1}^{I} a_i \, \varphi(\mathbf{r}_P, \mathbf{r}_{Q_i}) \tag{2.114}$$

with the field parameters a_i arranged in a column matrix and the base functions,

$$\varphi(\mathbf{r}_P, \mathbf{r}_{Q_i}) = \sum_{n=0}^{\infty} k_n \left(\frac{R}{r}\right)^{n+1} P_n(\mathbf{r}_P, \mathbf{r}_{Q_i}). \tag{2.115}$$

The coefficients k_n are the degree variances of the gravity field spectrum to be determined,

$$k_n = \sum_{m=0}^{M} \left(\Delta c_{nm}^2 + \Delta s_{nm}^2\right). \tag{2.116}$$

R is the mean equator radius of the Earth, r the distance of a field point from the geocenter and $P_n(\mathbf{r}_P, \mathbf{r}_{Q_i})$ are the Legendre's polynomials depending on the spherical distance between a field point P and the nodal points Q_i of the set of base functions. With this definition the base functions can be interpreted as isotropic and homogeneous harmonic spline functions (Freeden et al. 1998). The nodal points are generated on a grid by a uniform subdivision of an icosahedron of twenty equal-area spherical triangles. In this way the global pattern of the spline nodal points Q_i shows approximately uniform nodal point distribution (details can be found in Eicker et al. 2004).

The observation equation for gradiometer measurements is obtained by differentiating the potential twice:

$$\nabla\nabla V(P) = \sum_{i=1}^{I} a_i \, \nabla\nabla\varphi(\mathbf{r}_P, \mathbf{r}_Q). \tag{2.117}$$

The observation equations are established for short arcs over the selected regional recovery area, while the coverage with short arcs should be slightly larger than the recovery region itself to prevent the solution from geographical truncation effects. Every short arc builds a partial normal equation. To consider different accuracies of the short arcs these normal equations are combined by estimating a variance factor for every arc by means of a variance component estimation such as described by Koch and Kusche (2003). In those cases where a regularization is required, the regularization factor can be determined within the variance component estimation procedure as well.

3. Mass models of the Earth's topography

In chapter 2, various geodetic applications are presented which demonstrate the need or at least the usefulness of considering the effects of topographic-isostatic masses. For this reason, the mass of the Earth must be modeled in a satisfying way. The topographic-isostatic models with mass density information from geological and geophysical investigations and orthometric heights from digital terrain models can be used for geodetic applications. These models have more or less a geophysical meaning. Other models, such as Helmert's methods of condensation can be used as purely mathematical approaches to remove the masses outside the geoid and shift it inside the boundary surface. In this chapter a review of the various topographic-isostatic models and the different data sets is given which can be used for the geodetic applications of topographic-isostatic masses as mentioned in chapter 2:

1. digital terrain models (DTM) for modelling the shape of the topography,
2. digital density models (DDM) for modelling the spatial distribution of density in the topography and deeper masses,
3. isostatic models for analytically modelling the Earth's outer masses,
4. Helmert's method of condensation as a simple model to fulfill the assumption of Stokes' theory.

3.1 Digital terrain model

A digital terrain model (DTM) is a digital representation of the topography of the Earth, that is, by horizontal coordinates and a numerical description of the topography heights. A large variety of digital terrain models is currently available. Some DTM's only contain height information of the solid Earth surface (i.e. land heights and ocean depths), whereas others also contain information on, for instance, thicknesses of glaciers and oceanic ice shelves, or lake depths. In this investigation the digital terrain model ETOPO5 with a resolution of five arc-minutes is used for the satellite applications. ETOPO5 (Earth Topography 5-minute) is a gridded elevation (land) and bathymetry (sea floor) data set for the entire Earth at a grid spacing of 5 minutes (1/12 of a degree or 300 arcseconds). The entire data set consists of a single file which has 4320 columns and 2160 rows. This data set was compiled using data from many different sources by the National Geophysical Data Center (NGDC), which is part of the National Oceanic and Atmospheric Administration (NOAA). Most of the data set dates back to 1988, except for a small area in Canada that was re-gridded in 1990. Elevation values are stored in a flat binary file (row major, no header) as signed 2-byte integers, and are available with both the LSB (least significant byte first) and MSB (most significant byte first) byte orders. The elevation units are meters. This data set provides global coverage and can be obtained free of charge from NGDC/NOAA. A version with a resolution of two arc-minutes (3.6 km) was published in 2001. Five major data sources were assembled into the ETOPO2 data base: data derived from GLOBE DEM (Sandwell and Smith 1997), bathymetric data from the Digital Bathymetric Data Base (DBDB), from the International Bathymetric Chart of the Arctic Ocean (IBCAO) and the Digital Bathymetric Data Base with a 5 arc-minutes resolution (DBDB5) filling any gaps (Kiamehr and Söjberg 2005). For more information see: www.ngdc.noaa.gov/mgg/fliers/01mgg04.html. In this investigation, for Earth surface and airborne applications the numerical tests are based on the high-resolution DTM GEBCO with one arc-minute resolution (www.ngdc.noaa.gov/mgg/gebco). The GEBCO Digital Atlas project is carried out under the auspices of the Intergovernmental Oceanographic Commission (IOC) and the International Hydrographic Organization (IHO). It has been reviewed by the Joint IOC/IHO Guiding Committee for GEBCO; a technical guidance is provided by the GEBCO Sub-Committee on Digital Bathymetry.

3.2 Digital density models

So far, the actual density of the Earth crust is not known; occasionally density models describe only the surface densities, derived from geological maps. Therefore, many of the investigations performed in the past depend on a constant density for the Earth crust. Since the actual density of the topographic masses may differ by more than 10% from a constant density (Martinec 1993; Tziavos et al. 1996; Pagiatakis and Armenakis 1998; Kuhn 2000a, b; Huang et al. 2001), the resulting geoid models will contain significant errors. Therefore, a 3-D digital density model (3-DDM) would be required to give a better modelling of the topographic masses. But in practice, it is very difficult – if not impossible – to provide such models on a global scale. On the other hand, 2-DDM are sufficient for many geodetic applications. Nowadays, a 2-DDM is available for some regions such as for Canada (see, e.g., Pagiatikis and Armenakis 1998). In general, any reasonable density model will give an improvement by using more realistic gravity reductions for the geoid determination.

3.3 Isostatic models

One of the first ideas about the equilibrium of the Earth's outer layers originate from Leonardo da Vinci (1452-1519). He expressed interesting speculations how the Earth might response to loads on its surface. Much later, Bouguer in 1749 gave the first experimental proof for the isostasy theory during the expedition to Quito (South America) in the year 1735 to measure the length of the meridian at the equator to derive the eccentricity of the ellipsoidal figure of the Earth. He discovered that the attraction effects of the Andes are by far smaller than it would have been expected because of the huge visible masses. For the explanation of this phenomena Bouguer and Boscovich (1755) speculated that the mass excess of the mountains might be compensated in some way by a mass deficiency at depth (Watts 2001). Some decades later, Everest carried out geodetic measurements in India in the years 1840 to 1859. As part of these measurements he computed the geodetic position at a number of locations where he had already measured astronomic positions. He found that for the cities Kaliana and Kalianpur in the Ganges plain the latitude differences between the positions computed geodetically was 5.24 arc-seconds smaller than those determined astronomically. Everest concluded that this discrepancy was not caused by the astronomical measurements; they could only be caused by the geodetic determination of the positions. But Pratt in 1854 and Airy in 1859 disagreed; they explained these significant differences by their isostatic models that they proposed before. Both came to the conclusion that the visible topographic masses of the Himalaya must be compensated in some way. This idea was the same which has been expressed much earlier by Leonardo da Vinci. He had stated that the visible masses must be in equilibrium with more deep-seated masses (Heiskanen and Vening-Meinesz 1958). The first who used the term "isostasy" was the American geologist C.E. Dutton (1889) in his article "On Some of the Greater Problems of Physical Geology".

For the determination of the gravity field, the following considerations of a compensation mechanism in the crust by the Bouguer anomalies are important (Heiskanen and Moritz 1967): "One might be inclined to assume that the topographic masses are simply superposed on an essentially homogeneous crust. If this were the case, the Bouguer reduction would remove the main irregularities of the gravity field, so that the Bouguer anomalies would be very small and would fluctuate randomly around zero. However, just the opposite is true. Bouguer anomalies in mountain areas are systematically negative and may attain large values, increasing in magnitude on the average by 100 mGals per 1000 meters of elevation. The only explanation possible is that there is some kind of mass deficiency under the mountains". This means that the topographic masses are compensated in some way which has consequences for the roughness of the functionals of the gravity field, such as gravity anomalies and gravity disturbances as well as deflections of the vertical.

The idea of isostasy consists of the assumption that the topographic masses above the geoid are compensated by more deep-seated mass distributions. There are two principle concepts, which differ substantially. In the first concept, which was developed by Pratt, the mountains have risen from the underground somewhat like a fermenting dough. In the second concept according to Airy, the mountains are floating on a fluid

lava of higher density, so that the higher the mountains are, the deeper they sinks. In both concepts the pressure produced by the topographic masses on the compensation surface must be equal to the buoyant forces produced by the isostatic masses.

Now the question arises which model should preferably be used for the isostatic compensation, especially for the determination of the gravity field. There are regions in which the concept of Pratt and others in which the concept of Airy meets the reality better. But there are also areas, in which the simple isostatic equilibrium as discussed before is disturbed and the isostatic compensation is much more complicated than in these simplified cases. This can only be decided after a careful analysis of the specific gravity field features within the various geographical regions of the Earth. Important for the determination of gravity field models is the fact that the gravity functionals should be smoothed by consideration of the topographic-isostatic reductions. It shall be pointed out that this demand might be different from the demands of different other applications. In the following subsections different isostatic models will be discussed.

3.3.1 Airy-Heiskanen model

In 1855 the English astronomer G.B. Airy published his hypothesis of the compensation mechanism of topographic masses. He assumed that the Earth's crust in regions with substantial topographic masses such as mountain chains in the scale of the Himalayas must sink with individual depth into the mantle. The weight of the topographic masses must be compensated by buoyant forces from below. According to his hypothesis, these forces result from the immersion of the lighter crust material into the denser mantle. Airy came already to the conclusion that the compensation can not be purely local and a certain part of the topography is carried by the resistance of the crust. This idea was enhanced later by Vening Meinesz in his regional compensation model. The model of Airy was mathematically described in 1924 and 1938 by W.A. Heiskanen and after that used for the computation of different isostatic corrections. From that time the isostatic model was called the Airy-Heiskanen Model. It can be applied under the following assumptions:

1. the isostatic compensation takes place completely and locally, i.e. the compensation mass is directly under the regarded topographic mass and there is no regional emanating effect,
2. the density of the crust is assumed to be 2670 kg/m^3. The difference in the density between the crust and mantle is taken to be 600 kg/m^3.

The choice of the depth of the crust for the entire Earth, T, is extremely difficult (Fig. 3.2, left), since the crust thickness within the continents varies strongly; Heiskanen suggested a mean value of T=30 km. The mathematical treatment of this model can be performed by dividing the topographic masses into individual compartments, for which the hydrostatic balance condition is applied. This means that the pressure exerted by the weight of the topographic masses must be equal to the pressure produced by the lift forces of the isostatic masses. Also, the mass equality condition can be used for estimating the roots with thickness t under mountains or anti-roots with thickness t' under oceans. In the following, the spherical and planar approximation will be studied.

Spherical approximation In the following, the geoid used as reference surface for the heights given by the DTMs is approximated by a geocentric mean sphere of radius R =6371 km (Fig. 3.1). The geocentric radii of the computation and the integration points are given by adding the DTM heights, interpreted here as orthometric heights of these points, to the radius of the geocentric sphere, so that the ellipsoidal shape of the Earth is neglected. The error of this simplification is very small and in the size of approximately one percent of the total effect (cf. Novák and Grafarend 2005). In spherical approximation, a mass element of the topographic or compensation masses is called *tesseroid*. The ideal situation of the Earth can be defined as follow: below R the density equals the density of the crust ρ_{cr}, above R the density equals 0.0 and below $(R-T)$ the density equals the density of the mantle ρ_m. The mass of the topography in this case is defined as the sum of all mass deviations (with respect to the ideal situation). The mass of a layered topography can

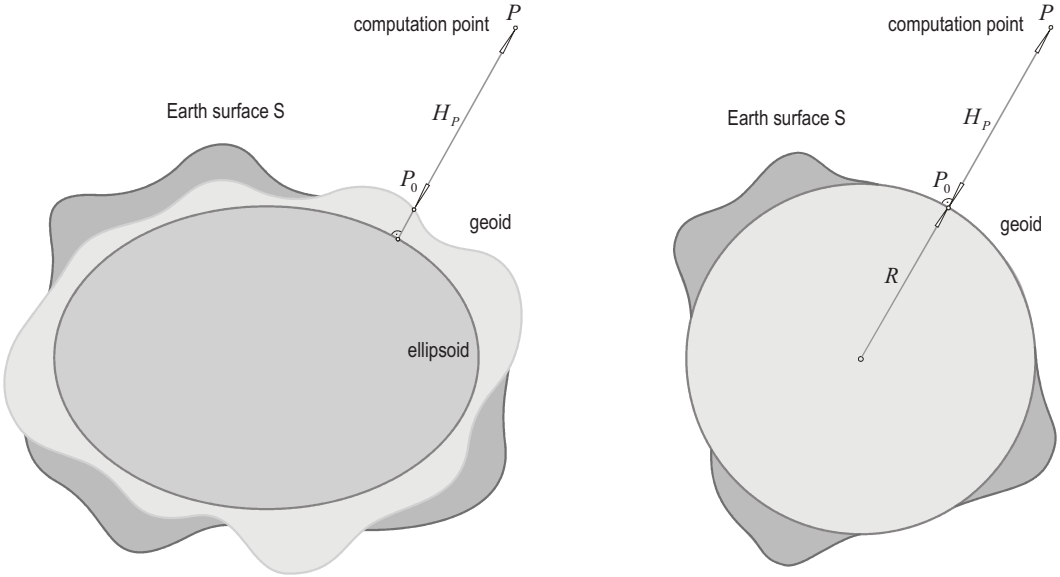

Fig. 3.1: Approximation of the geoid by an ellipsoid (left) and a sphere (right)

be defined as the sum of all mass deviations with respect to ρ_{cr}. Thus, assuming that a column consists of several layers with constant densities, the differences of the masses of these layers and the masses with ρ_{cr} give the topographic mass of this column (Fig. 3.2, left). The mass of the topography column can be given by (Classens 2003):

$$M_S^T = \sum_{i=0}^{i=l} \iint_{\sigma} \int_{R}^{R+H_i} (\rho_i - \rho_{i+1}) \xi^2 d\xi d\sigma, \tag{3.1}$$

with

$$\rho_0 = \begin{cases} 0 & \text{for } H_0 \geq 0 \\ \rho_{cr} & \text{for } H_0 \leq 0 \end{cases} \qquad \text{and} \qquad \rho_{l+1} = \begin{cases} 0 & \text{for } H_l > 0 \\ \rho_{cr} & \text{for } H_l < 0 \end{cases}. \tag{3.2}$$

Also, the mass of the root with thickness t or of the anti-root with thickness t' is given in spherical approximation by

$$M_S^C = \iint_{\sigma} \int_{R-T-t}^{R-T} \Delta\rho r^2 dr d\sigma, \tag{3.3}$$

where $\Delta\rho$ is the difference between the density of the mantle ρ_m and the density of the crust ρ_{cr}.

The condition of the "equilibrium of masses" between an element of mass at the surface of the Earth and a mass element at a depth T reads in spherical approximation

$$M_S^T = M_S^C, \tag{3.4}$$

or

$$\sum_{i=0}^{i=l} \iint_{\sigma} \int_{R}^{R+H_i} (\rho_i - \rho_{i+1}) \xi^2 d\xi d\sigma = \iint_{\sigma} \int_{R-T-t}^{R-T} \Delta\rho \xi^2 d\xi d\sigma. \tag{3.5}$$

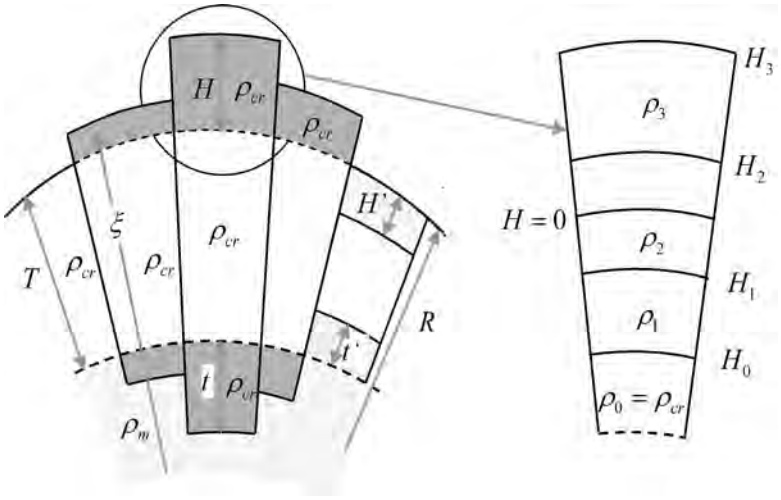

Fig. 3.2: Airy-Heiskanen model, left with constant density; several layers right

If the area elements $d\sigma$ are assumed to be equal, Eq. (3.5) can be integrated with respected to r to give the following equation:

$$\sum_{i=0}^{l} \frac{(\rho_i - \rho_{i+1})}{3} \left[(R + H_i)^3 - R^3\right] = \frac{\Delta\rho}{3} \left[(R - T)^3 - (R - T - t)^3\right]. \tag{3.6}$$

This equation can be solved for the root columns t to give

$$t = (R - T) \left[1 - \sqrt[3]{1 - \frac{\sum_{i=0}^{l} \left[(R + H_i)^3 - R^3\right](\rho_i - \rho_{i+1})}{(R - T)^3 \Delta\rho}}\right]. \tag{3.7}$$

If the density of the topographic masses is assumed to be constant and identical to the density of the crust, Eq. (3.7) can be simplified for the roots as follows,

$$t = (R - T) \left[1 - \sqrt[3]{1 - \frac{\left[(R + H)^3 - R^3\right]\rho_{cr}}{(R - T)^3 \Delta\rho}}\right], \tag{3.8}$$

and for the anti-roots

$$t' = (R - T) \left[\sqrt[3]{1 + \frac{\left[R^3 - (R - H')^3\right]}{(R - T)^3} \frac{(\rho_{cr} - \rho_w)}{\Delta\rho}} - 1\right], \tag{3.9}$$

where ρ_w is the density of the water.

Eq. (3.8) can be rearranged to give

$$t = (R - T) \left[1 - \sqrt[3]{1 - \eta \left[\left(1 + \frac{H}{R}\right)^3 - 1\right]}\right], \tag{3.10}$$

with

$$\eta := \frac{R^3}{(R - T)^3} \frac{\rho_{cr}}{\Delta\rho} \tag{3.11}$$

Expanding the term inside the root of Eq. (3.10) into a binomial series,

$$\eta\left[\left(1+\frac{H}{R}\right)^3-1\right]=\eta\left(\frac{3H}{R}+\frac{3H^2}{R^2}+\frac{H^3}{R^3}\ldots\right)=:\zeta, \tag{3.12}$$

Eq. (3.10) can be written as

$$t=(R-T)\left[1-(1-\zeta)^{1/3}\right]. \tag{3.13}$$

Also, expanding the term $(1-\zeta)^{1/3}$ in Eq. (3.13) in a binomial series and restricting the series to the quadratic term gives after some rearrangements

$$t=\left(\frac{R}{R-T}\right)^2\frac{\rho_{cr}}{\Delta\rho}H\left[1+\frac{H}{R}\left(\left(\frac{R}{R-T}\right)^3\frac{\rho_{cr}}{\Delta\rho}+1\right)\right]+O\left(\frac{H}{R}\right)^3. \tag{3.14}$$

Applying an analogous procedure for the anti-roots, Eq. (3.9) can be approximated as

$$t'=\left(\frac{R}{R-T}\right)^2\frac{(\rho_{cr}-\rho_w)}{\Delta\rho}H'\left[1+\frac{H'}{R}\left(\left(\frac{R}{R-T}\right)^3\frac{(\rho_{cr}-\rho_w)}{\Delta\rho}-1\right)\right]+O\left(\frac{H'}{R}\right)^3. \tag{3.15}$$

The roots and anti-roots in spherical approximation with constant topographic densities have been derived also by Heiskanen and Vening Meinesz (1958), Rummel et al. (1988) and Abd-Elmotaal (1991).

A frequently used concept to reduce the several topographic layers to only one layer for reducing CPU time is the concept of "equivalent rock topography". In this approach, all layers consisting of material with different densities are replaced by an equivalent rock layer with the density of the crust ρ_{cr} and a certain thickness. The thickness of the equivalent layer H_{eq} is determined by assuming the condition that the mass of a column of equivalent rock layer should be equal to the mass of the original layers in the same column so that it holds (see Fig. 3.3):

$$M_S^T=\sum_{i=0}^{l}\frac{(\rho_i-\rho_{i+1})}{3R^2}\left[(R+H_i)^3-R^3\right]d\sigma=\frac{\rho_{cr}}{3R^2}\left[(R+H_{eq})^3-R^3\right]d\sigma. \tag{3.16}$$

Eq. (3.16) can be solved for the quantity H_{eq} (rock equivalent topography):

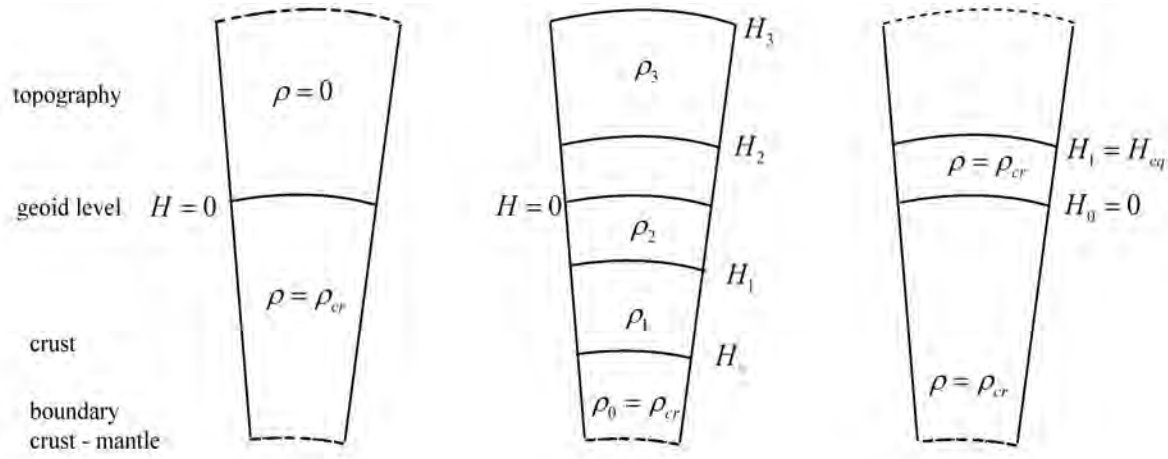

Fig. 3.3: Ideal situation of the topography (left), three layers of topography (middle) and rock equivalent topography (right)

$$H_{eq}=\left[R^3+\frac{3R^2}{\rho_{cr}}M_S^T\right]^{\frac{1}{3}}-R. \tag{3.17}$$

If the equivalent rock topography is used, the roots can be given in spherical approximation by inserting the rock equivalent topography in Eq. (3.14):

$$t_{eq} = \left(\frac{R}{R-T}\right)^2 \frac{\rho_{cr}}{\Delta\rho} H_{eq} \left[1 + \frac{H_{eq}}{R}\left(\left(\frac{R}{R-T}\right)^3 \frac{\rho_{cr}}{\Delta\rho} + 1\right)\right] + O\left(\frac{H_{eq}}{R}\right)^3. \tag{3.18}$$

Planar approximation In case of the planar approximation, the mass of the topography and the compensating masses are given by (Fig. 3.4),

$$M_P^T = \sum_{i=0}^{l} (\rho_l - \rho_{l+1}) H_i d\sigma \tag{3.19}$$

and

$$M_P^C = \Delta\rho t d\sigma, \tag{3.20}$$

respectively. Therefore, the root or anti-root is given by

$$t = \frac{1}{\Delta\rho} \sum_{i=0}^{l} (\rho_l - \rho_{l+1}) H_i. \tag{3.21}$$

The formulae for the roots and anti-roots in planar approximation and by assuming constant density can

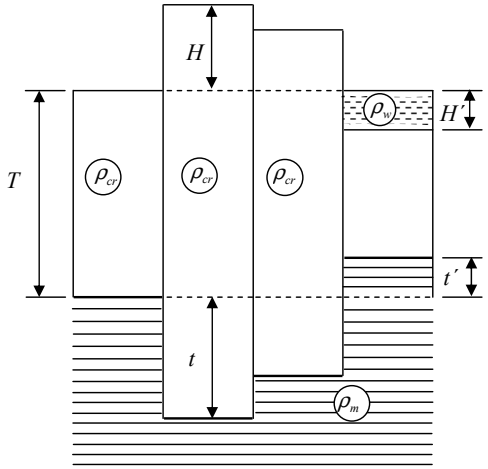

Fig. 3.4: Airy-Heiskanen isostatic model in planar approximation

be given as the limits of the functions in Eq. (3.14) and Eq. (3.15) with $R \to \infty$:

$$t = \lim_{R\to\infty} \left(\left(\frac{R}{R-T}\right)^2 \frac{\rho_{cr}}{\Delta\rho} H \left[1 + \frac{H}{R}\left(\left(\frac{R}{R-T}\right)^3 \frac{\rho_{cr}}{\Delta\rho} + 1\right)\right] + \mathrm{O}\left(\frac{H}{R}\right)^3\right) = \frac{\rho_{cr}}{\Delta\rho} H \tag{3.22}$$

$$\begin{aligned} t' &= \lim_{R\to\infty} \left(\left(\frac{R}{R-T}\right)^2 \frac{(\rho_{cr} - \rho_w)}{\Delta\rho} H' \left[1 + \frac{H'}{R}\left(\left(\frac{R}{R-T}\right)^3 \frac{(\rho_{cr} - \rho_w)}{\Delta\rho} - 1\right)\right]\right) \\ &= \frac{(\rho_{cr} - \rho_w)}{\Delta\rho} H'. \end{aligned} \tag{3.23}$$

Also the rock equivalent topography in planar approximation is given by:

$$M_P^T = \sum_{i=0}^{l} (\rho_i - \rho_{i+1}) H_i d\sigma = \rho_{cr} H_{eq} d\sigma, \tag{3.24}$$

which follows (assuming also the areas of the elements to be equal):

$$H_{eq} = \frac{\sum_{i=0}^{l} (\rho_i - \rho_{i+1}) H_i}{\rho_{cr}}. \tag{3.25}$$

If the topography has a constant density ρ_{cr} (one layer topography), the rock equivalent topography can be derived by

$$H_{eq} = \left\{ \begin{array}{l} \text{land: } H_{eq} = H \\ \text{ocean: } H_{eq} = \dfrac{\rho_{cr} - \rho_w}{\rho_{cr}} H' \end{array} \right\}. \tag{3.26}$$

In this case the roots or anti-roots are given by

$$t_{eq} = \frac{\rho_{cr}}{\Delta\rho} H_{eq}. \tag{3.27}$$

3.3.2 Pratt-Hayford model

In 1854 J.H. Pratt developed his hypothesis to explain the significant differences in the deflections of the vertical, computed from the attraction of the topographic masses of the mountains and obtained by astro-geodetic measurements. In 1859 he published the theory that the topographic masses of the mountains (mass surplus) are compensated by a mass deficit within the Earth's crust under the mountains. The mass deficit extends down to a constant depth into the Earth's crust. Pratt assumed that the density of the topography depends on the height above the geoid, so that the density under the mountains is smaller than under the ocean. Pratt proposed a compensation depth of 100 km for the Himalayan area so that the difference between the astro-geodetically observed deflections of the vertical and those derived from the topographic-isostatic masses becomes nearly zero. The depth of the compensation surface coincides approximately with the thickness of the lithosphere of approximately 100 km in the global mean (Kertz 1969). In 1909/1910 Hayford formulated Pratt's model mathematically. This isostatic model of the Earth's crust is well-known afterwards as the model of Pratt-Hayford. Usually it is applied assuming that

1. the isostatic equilibrium is realized everywhere in the same way, so that the density under the mountains is smaller than under the flat regions or under the oceans,

2. the compensation masses with laterally varying densities are located below the sea level and reach down to a depth D (compensation depth) until hydrostatic equilibrium is reached,

3. Hayford modified this model and proposed that the condensation depth D is reckoned from the Earth's surface instead from the sea level to end up with simpler computation formulae.

The general mathematical description of the model is based on the principle of hydrostatic equilibrium, which is reached in a depth D. For the determination of the lateral density variations, the topographic and isostatic masses are divided also into individual compartments (rock columns). The principle of hydrostatic balance or the condition of mass equality has the consequence that the pressure exerted on the compensation surface is identical for every rock column. The density distributions in the different topography columns, ρ_L, can be determined based on the density of the crust ρ_{cr}. In the following the model densities for the rock columns are derived from the mass equality condition. This condition means that the mass of a column with a topographic height zero (and therefore a thickness D) is identical to the masses of a column consisting of the crust column and the layered topography. The gravity forces are assumed identical in each column. This holds for the spherical as well as for the planar approximation.

Spherical approximation In the following, the density of the oceans is assumed to be constant. The density under the geoid at the continental areas can be derived based on the mass equality condition as follows:

$$\iint_{\sigma}\int_{R-D}^{R}\rho_{cr}\xi^2 d\xi d\sigma = \iint_{\sigma}\int_{R-D}^{R}\rho_L\xi^2 d\xi d\sigma + \sum_{i=0}^{i=l}\iint_{\sigma}\int_{R}^{R+H_i}(\rho_i-\rho_{i+1})\xi^2 d\xi d\sigma, \tag{3.28}$$

where D is the Pratt-Hayford compensation depth which is taken to be constant and equal to 100 km (Heiskanen and Moritz 1967), and ρ_L is the density under continental areas. The densities ρ_0 and ρ_{l+1} are defined in Eq. (3.2). In this case the *topographic density is assumed to be known* above the geoid and the density ρ_L will be calculated for the mass column between the geoid and the compensating surface. After definite integration of Eq. (3.28) it reads:

$$\rho_{cr}\left[(R)^3-(R-D)^3\right] = \left[R^3-(R-D)^3\right]\rho_L + \sum_{i=0}^{l}\frac{(\rho_i-\rho_{i+1})}{3}\left[(R+H_i)^3-R^3\right]. \tag{3.29}$$

The density function for the continental areas can be determined by the formulae as follows:

$$\rho_L = \frac{\left[R^3-(R-D)^3\right]\rho_{cr} - \sum_{i=0}^{l}\frac{(\rho_i-\rho_{i+1})}{3}\left[(R+H_i)^3-R^3\right]}{(R)^3-(R-D)^3}. \tag{3.30}$$

If the *density of the topography and the crust under the mountains are assumed to be unknown*, the condition of mass equality leads to the formula (Fig. 3.5):

$$\iint_{\sigma}\int_{R-D}^{R}\rho_{cr}\xi^2 d\xi d\sigma = \iint_{\sigma}\int_{R-D}^{R+H}\rho_{land}\xi^2 d\xi d\sigma. \tag{3.31}$$

In this case the density ρ_{land} is calculated for the mass element reaching from the surface of the Earth down

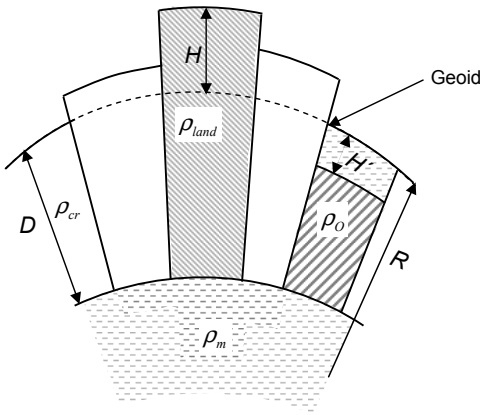

Fig. 3.5: Pratt-Hayford compensating model in spherical approximation with constant density

to the compensation depth resulting in

$$\rho_{land} = \frac{R^3-(R-D)^3}{(R+H)^3-(R-D)^3}\rho_{cr}. \tag{3.32}$$

Eq. (3.32) can be reformulated to give

$$\begin{aligned}\rho_{land} &= \frac{R^3(1-(1-D/R)^3}{R^3\left[(1+H/R)^3-(1-D/R)^3\right]}\rho_{cr}\\ &= \frac{D}{(H+D)}\left[\frac{3R^2-3DR+D^2}{3R^2+3RH-3RD+H^2-HD+D^2}\right]\rho_{cr}.\end{aligned} \tag{3.33}$$

By simplification of the term in brackets Eq. (3.33) can be written in the following form (Kuhn 2000a):

$$\rho_{land} = \frac{D}{D+H}\left[1 - \frac{H}{R} + \frac{2}{3}\frac{H(H-D)}{R^2}\right]\rho_{cr}. \tag{3.34}$$

If the topographic masses are considered with lateral variable density ρ_t only (Fig. 3.6), the density for the column between the geoid and the compensation depth can be determined as follows:

$$\iint\limits_{\sigma}\int\limits_{R-D}^{R} \rho_{cr} r^2 dr d\sigma = \iint\limits_{\sigma}\int\limits_{R-D}^{R} \rho_L r^2 dr d\sigma + \iint\limits_{\sigma}\int\limits_{R}^{R+H} \rho_t r^2 dr d\sigma. \tag{3.35}$$

After definite integration Eq. (3.35) can be rearranged as

$$\rho_L = \frac{\left[R^3 - (R-D)^3\right]\rho_{cr} - \left[(R+H)^3 - R^3\right]\rho_t}{\left[R^3 - (R-D)^3\right]}. \tag{3.36}$$

Eq. (3.36) can be reformulated analogously to Eq. (3.32) to give (Kuhn 2000a),

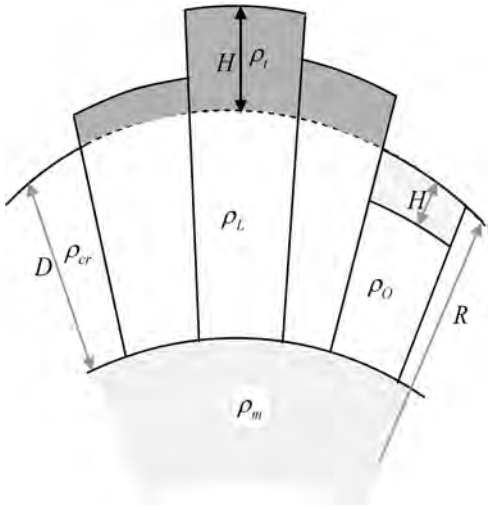

Fig. 3.6: Pratt-Hayford compensating model in spherical approximation with laterally variable density

$$\rho_L = \rho_{cr} - \frac{H}{D}\left[1 + \frac{H+D}{R} + \frac{(H+D)(H+2D)}{3R^2}\right]\rho_t. \tag{3.37}$$

The density in ocean areas ρ_O can be found assuming a constant water density ρ_w by the formula

$$\int\limits_{R-D}^{R} \rho_{cr}\xi^2 d\xi d\sigma = \int\limits_{R-D}^{R-H'} \rho_O \xi^2 d\xi d\sigma + \int\limits_{R-H'}^{R} \rho_w \xi^2 d\xi d\sigma, \tag{3.38}$$

or after definitive integration

$$\left[R^3 - (R-D)^3\right]\rho_{cr} = \rho_w\left[R^3 - (R-H')^3\right] + \rho_O\left[(R-H')^3 - (R-D)^3\right], \tag{3.39}$$

which leads to a formula for the column density of the ocean areas

$$\rho_O = \frac{\left[R^3 - (R-D)^3\right]\rho_{cr} - \rho_w\left[R^3 - (R-H')^3\right]}{\left[(R-H')^3 - (R-D)^3\right]}. \tag{3.40}$$

Eq. (3.40) can be reformulated analogously to Eq. (3.32) to give (Kuhn 2000a):

$$\rho_O = \frac{D\rho_{cr} - H'\rho_w}{D-H'}\left[1 + \frac{DH'}{D\rho_{cr} - H'\rho_w}\frac{(\rho_{cr}-\rho_w)}{R} + \frac{2}{3}\frac{DH'(D-H')}{(D\rho_{cr} - H')}\frac{(\rho_{cr}-\rho_w)}{R^2}\right]. \tag{3.41}$$

Planar approximation The principle of hydrostatic equilibrium and of the condition of mass preservation leads analogously to Eq. (3.28) to the formula:

$$d\sigma\,(D\rho_{cr}) = d\sigma\,(D\rho_L) + \sum_{i=0}^{i=l}(\rho_i - \rho_{i+1})H_i d\sigma. \tag{3.42}$$

Then the column density in continental areas is given by:

$$\rho_L = \frac{D\rho_{cr} - \sum\limits_{i=0}^{i=l}(\rho_i - \rho_{i+1})H_i}{D}. \tag{3.43}$$

If the density of the topographic masses and the crust are assumed to be unknown (Fig. 3.7), then ρ_L will

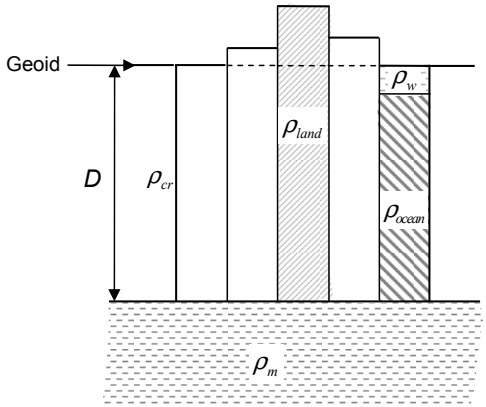

Fig. 3.7: Pratt-Hayford compensating model (constant density) in planar approximation

be determined by

$$\rho_{land} = \frac{D}{D+H}\rho_{cr}, \tag{3.44}$$

which follows from the mass equality condition, too. Again, if the density of the topographic masses is assumed to be laterally variable only, then Eq. (3.43) reads

$$\rho_L = \frac{D\rho_{cr} - H\rho_t}{D}. \tag{3.45}$$

In Pratt's original formulation which was defined only over continental areas, the topographic masses are considered with the same constant density ρ_{cr} (constant crust density). The density in the continental areas can be given by (Kuhn 2000a):

$$\rho_L = \frac{D-H}{D}\rho_{cr}. \tag{3.46}$$

Finally the density under the ocean areas can be determined based on the mass equality condition as follows:

$$\rho_O = \frac{D\rho_{cr} - H'\rho_w}{D-H'}. \tag{3.47}$$

It is preferable in the Pratt-Hayford model to adapt the topographic heights and bathymetric depths from the DTM directly as absolute values. This means that the concepts of the rock equivalent topography will not be applied in this investigation (see Tsoulis 1999a; 2001).

3.3.3 Combined Airy-Pratt model

A disadvantage of the original Airy-Heiskanen model is the fact that the anti-roots in the ocean areas can attain values which are larger than the thickness of the crust. Obviously, the anti-roots can never extend the thickness of the crust, i.e. t' in Eq. (3.15) can never be larger than $T - H'$. This means that H' must be not larger than approximately 8000 m for the realistic values $\rho = 2670 kg/m^3$, $\rho_w = 1027 kg/m^3$, $\rho_m = 3270 kg/m^3$, R=6371 km and T =30 km. In reality, several deep-sea trenches exceed this value. This example demonstrates that the Airy-Heiskanen model cannot be correct in these cases. As a way out of this problem, the anti-roots can either be restricted to the crust boundary or the normal crust thickness T has to be changed. In our study T will not be changed to enable comparability on the one hand; on the other hand, the restriction of the anti-roots to the crust boundary causes some errors in computing the isostatic effects. Therefore, a combined Airy-Pratt model is applied as a combination of the Airy-Heiskanen model and the Pratt-Hayford model (Wild and Heck 2004a, b). In this model, the Airy-Heiskanen model is applied in the land areas and the Pratt-Hayford model in the ocean areas.

3.3.4 Vening-Meinesz model

The well known compensation principle of Airy-Heiskanen postulates an isostatic compensation within each mass column; there is no dependency between neighbouring columns. This is not true in reality due to the elasticity of the Earth. Vening-Meinesz modified the Airy floating theory to include also these features (Vening Meinesz 1931, Vening Meinesz 1939). In his approach, each topographic column of infinitely small cross section is considered to be compensated by a mass equal to the local compensation of this element but spreads horizontally according to the curved deformation of the Earth's crust (Fig. 3.8). He assumed the crust as a homogenous elastic plate floating on a viscous material. Its deformation can be represented by the deformation of an infinitely thin plate according to the laws developed within the frame of the elasticity theory. The bending of the crust plate is described based on elasticity theory (Heiskanen and Moritz 1967; Landau and Lifshitz 1959; Grüninger 1990; Abd-Elmotaal 1995a; Watts 2001). The equation of equilibrium

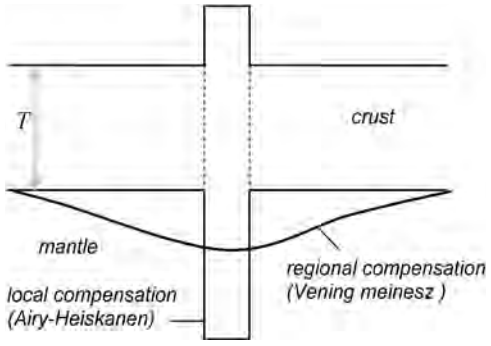

Fig. 3.8: Local and regional compensation

for a free plate of constant thickness T bent by an external force F acting on a point P can be written as (Courant and Hilbert 1953; Landau and Lifshitz 1959),

$$D\Delta^2 z = \mathrm{F}, \tag{3.48}$$

with the two-dimensional Laplace operator Δ,

$$\Delta = \frac{\partial^2}{\partial x^2} + \frac{\partial^2}{\partial y^2}. \tag{3.49}$$

and the downward displacement z. The flexural rigidity of the plate D can be determined by (see, e.g., Jeffreys 1976; Banks et al. 1977; Abd-Elmotaal 1995a; Watts 2001)

$$D = \frac{ET^3}{12(1-\chi^2)}, \tag{3.50}$$

where E is Young's modulus and χ Poisson's ratio.

The bent plate is considered to be floating on a liquid layer (substratum) of higher density ρ_m (Fig. 3.9). In this case, a hydrostatic uplift force per unit area equal to $gz\rho_m$ will act opposite to the external force F and must be subtracted from it. Thus, the equation of equilibrium for a floating bent plate will be given by:

$$D\Delta^2 z = \mathrm{F} - gz\rho_m. \tag{3.51}$$

This equation was treated for the first time in Hertz (1884) and was also used without derivation in Jeffreys (1976). To get a horizontal upper surface of the plate, the upper concave surface appearing in Fig. 3.10 must

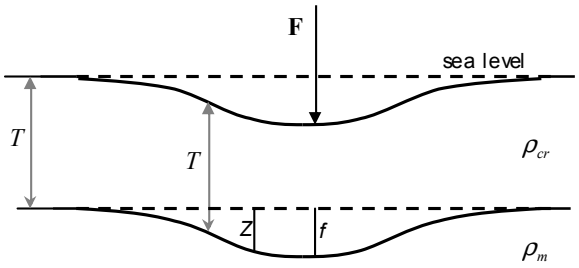

Fig. 3.9: Bending of a floating plate

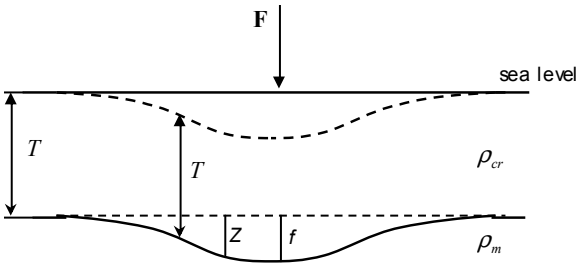

Fig. 3.10: The indirect effect

be filled with mass; this represents the indirect effect (do not mix it up with the indirect effect in case of the geoid computation). This depression can be considered to be filled up with the same material as the plate. Then this filling produces a force equal to $gz\rho_{cr}$ per unit area, acting in the same direction as the external force. Finally, the equation of equilibrium for a floating bent plate will be given by (Abd-Elmotaal 1995a):

$$D\Delta^2 z = \mathrm{F} - gz\rho_m + g\rho_{cr} z = \mathrm{F} - gz(\rho_m - \rho_{cr}). \tag{3.52}$$

The solution of Eq. (3.52) can be determined with the help of the Thomson function $kei(x)$ (Márkus 1978, Grüninger 1990) as follow:

$$z = -\frac{\mathrm{F}}{2\pi l^2 \Delta\rho} kei(x), \tag{3.53}$$

with

$$x = \frac{r}{l} \qquad \text{and} \qquad \Delta\rho = \rho_m - \rho_{cr}. \tag{3.54}$$

To simplify the computations, Vening Meinesz (1939) introduced a polynomial function $Z(x)$ in order to describe the vertical component of the bending by two different polynomials of the form

$$Z(x) = Z_1(x) + Z_2(x), \tag{3.55}$$

with

$$Z_1(x) = f\left[c_1x^6 + c_2x^4 + c_3x^2 + c_4\right]; \qquad 0 \le x \le 2 \tag{3.56}$$

$$Z_1(x) = f\left[c_5x^4 + c_6x^2 + c_7\right]; \qquad 0 \le x \le r_{\max} \tag{3.57}$$

and

$$f = \frac{m_p}{8\Delta\rho l^2}; \qquad l = \sqrt[4]{\frac{D}{g\Delta\rho}}; \qquad x = \frac{r}{l}, \tag{3.58}$$

where l is the degree of regionality which describes the mechanical stiffness of the plate using the flexural rigidity D (Jeffreys 1976; Banks et al. 1977), f is the maximum downward displacement (Vening Meinesz 1939, P. 5), r_{max} is the maximum extension of the regional compensation for one single load/relief (Vening Meinesz 139, p. 713) and m_p is the load generated by the topographic masses. In ocean area, m_p denotes the relief generated by the ocean water mass deficiencies with the density difference $(\rho_{cr} - \rho_w)$. The coefficient $(c_i, i = 1, \ldots..., 7)$ can be found, for example, in Heiskanen and Vening Meinesz (1958), Abd-Elmotaal (1991) and Abd-Elmotaal (1995a) as shown in Table 3.1.

Table 3.1: Polynomial coefficients of the bended curve

Coefficients	Vening Meinesz (r_{max}=2.905l)	Abd-Elmotaal (r_{max}=2.914l)
c_1	-0.00913	-0.00925
c_2	0.09906	0.09922
c_3	-0.35434	-0.34969
c_4	0.41660	0.40336
c_5	0.00275	0.00320
c_6	-0.09234	-0.09748
c_7	0.58340	0.59664

The difference between the exact solution, given by the elasticity theory, and the approximate solution, given by Eqs. (3.56) and (3.57), can be neglected in all practical cases (Grüninger 1990, Abd-Elmotaal 1995a).

For the determining the Vening-Meinesz compensation depths, the mass of the point load m_p due to a vertical column of topography of density ρ_{cr}, height H and infinity small cross sectional area ds, can be written as:

$$m_p = \rho_{cr} H ds. \tag{3.59}$$

Thus the bending due to this topographic column will be

$$Zm_p = f(r)\rho_{cr} H ds. \tag{3.60}$$

The total bending t due to the entire topographic masses can be given by (Abd-Elmotaal 1995a):

$$t(x, y) = \iint_s \rho_{cr} H(x', y') f(r) ds, \tag{3.61}$$

with

$$f(r) = z, \tag{3.62}$$

where ds can be expressed in Cartesian or spherical coordinates as follows:

$$ds = dxdy, \qquad ds = R^2 \cos\varphi d\varphi d\lambda, \tag{3.63}$$

and R is the radius of the mean Earth, $d\varphi$ and $d\lambda$ represent the dimensions of the topographic column in the latitude and the longitude directions, respectively. The total bending t is closely related to the Moho depth

$$H_m = T + t, \tag{3.64}$$

where T is the crustal thickness for a topography with zero heights.

3.4 Helmert's models of condensation

Helmert proposed the condensation method to remove the topographic masses outside the geoid and condense them onto a surface as a single layer within the masses. One alternative is to condense the topographic masses on a surface parallel to the geoid located at a depth of 21 km below the geoid (Helmert 1884). This depth, corresponding to the difference in the lengths of the equatorial and the minor semi-axes of the Earth ellipsoid, was chosen in order to shift the topographical masses below a sphere situated completely within the geoid. This proposal is the so-called *Helmert's first method of condensation*. In a second method, the condensation surface is the geoid itself. There is a large number of publications referred to Helmerts condensation models, see, e.g., Wichiencharoen (1982); Heck (1992); Martinec et al. (1993); Sjöberg (1994), (1995), (1996a), b; Martinec and Vaníček (1994a, b); Vaníček et al. (1999); Sjöberg and Nahavandchi (1999); Kuhn (2000a), b; Kuhn (2002); Kuhn (2003). Although *Helmert's second method of condensation* cannot adequately describe the density distribution within the Earth's crust, it has been applied for practical determination of the geoid. Its advantage is the very small indirect effect even in case of very high mountains. It is well-known from the analysis of gravity observations (Kuhn 2000a) that the true gravity field of the Earth contains significant short wavelengths. These short wavelength constituents are generated by the topographical masses and show approximately a linear dependency with the topographical heights. Therefore, gravity anomalies computed from Helmert's second method of condensation are as rough as free-air anomalies. This is the reason that the downward continuation of the gravity from the surface of the Earth to the geoid in a rough gravity field may become dubious. Since the short wave-length components cannot be eliminated by the reduction procedure of Helmert's second method of condensation, it is obvious that the reduction model implied by this method cannot work in a satisfaying way in high-resolution applications (Heck 2003). Although some authors (e.g., Martinec 1995; Kuhn 2000a) have pointed out that the gravity anomalies related to Helmert's second method are strongly correlated with the topographical heights, this model is still widely used in the determination of the geoid due to their small indirect effect.

In case of Helmert's first method of condensation, the reduced gravity is rather smooth (Kuhn 2000a), showing strong similarities to the reduction results by classical isostatic models such as discussed before (Heck 2003). This model approximates the geophysical reality better than Helmert's second model. With a proper selection of Helmert's condensation depth D_1 the condensation method can be adjusted to a more realistic topographic-isostatic reality. This modification of Helmert's condensation method has been proposed by Heck (2003) and can be defined as generalized Helmert method of condensation. In the following the single layer density for spherical and planar approximation will be discussed.

Spherical approximation In Helmert's methods of condensation, the single-layer density k is a function of the topographical heights. Using the mass conservation principle, the local single-layer density can be given in spherical approximation as follows (Fig. 4.8):

$$kR_C^2 d\sigma = M_S^T, \tag{3.65}$$

which follows

$$k = \frac{1}{R_C^2} \sum_{i=0}^{i=l} \int_R^{R+H_i} (\rho_i - \rho_{i+1}) \xi^2 d\xi, \tag{3.66}$$

where ρ_0, ρ_{l+1} are defined in Eq. (3.2), $R_C = R$ for Helmert's second method of condensation and $R_C = R - D_1$ in case of Helmert's first or generalized method of condensation with Helmert's condensation depth D_1.

After integration and applying a binomial series expansion, the single-layer density can be given by:

$$k = \sum_{i=0}^{l} (\rho_i - \rho_{i+1}) \left[\frac{(R+H)_i^3 - R^3}{3R_c^2} \right] = \sum_{i=0}^{l} \frac{(\rho_i - \rho_{i+1})}{R_c^2} R^3 \left[\left(\frac{H_i}{R} \right) + \left(\frac{H_i}{R} \right)^2 + \frac{1}{3} \left(\frac{H_i}{R} \right)^3 \right]. \tag{3.67}$$

If the topographic masses have a constant density (one layer with density ρ_{cr}), Eq. (3.67) can be simplified to

$$k = \frac{\rho_{cr}}{R_c^2} R^3 \left[\left(\frac{H}{R} \right) + \left(\frac{H}{R} \right)^2 + \frac{1}{3} \left(\frac{H}{R} \right)^3 \right]. \tag{3.68}$$

From the above formulae and from the formulae which will be given in chapter 4 it is shown that the respective formulae for the generalized Helmert's model of condensation are much simpler than the isostatic models (for example the Airy-Heiskanen model). Therefore this model can be considered as a proper method for downward continuation and related tasks within the frame of geoid determination (Heck 2003).

The only disadvantage of this generalized method of Helmert is that the indirect effect, primarily due to non-vanishing components proportional to the topographical height, will be larger than those of Helmert's second method of condensation. It has the same order of magnitude as the indirect effects related to the classical isostatic models (Kuhn 2002).

Planar approximation In case of the planar approximation, the single layer density is given by using Eq. (3.19) as follows:

$$\begin{aligned} d\sigma k &= \sum_{i=0}^{l} (\rho_i - \rho_{i+1}) H_i d\sigma \\ k &= \sum_{i=0}^{l} (\rho_i - \rho_{i+1}) H_i, \end{aligned} \tag{3.69}$$

and for a constant density or the rock equivalent topographic procedures it follows analogously to Eq. (3.24)

$$k = \rho_{cr} H_{eq}. \tag{3.70}$$

4. Computation of the gravitational effects of the topographic-isostatic masses

The effects of the topographic-isostatic masses can be calculated using analytical, numerical and combination methods. The numerical and combination methods are preferable in the case of more than one computation point, especially when the goal is the computation of these effects at the points of a regular grid. The latter may coincide with the outer boundary of the topographic masses as described by the surface relief or may be located at a given flight altitude above the terrain for airborne gravimetry. The different demands of the numerical evaluations depend on the nature of the problem and on the required accuracy level. The efficiency of the computation methods can be increased by introducing spectral techniques which permit a fast evaluation of the respective quantities (Tsoulis and Tziavos 2003).

There are various computation methods which are used for calculating the topographic-isostatic effects:

1. direct integration method,
2. Fast Fourier Transform (FFT),
3. spherical harmonic expansion,
4. spline function,
5. combined method.

The FFT method is restricted first of all to planar applications and has been extensively discussed in the past. In the present applications the focus is on spherical approximations and will, therefore, not be treated here. Details can be found in various publications (see, e.g., Bracewell 1978; Forsberg 1985; Sideris 1985; Schwarz et al. 1990; Parker 1995, 1996; Kirby and Featherstone 1999; Smith 2002; Bracewell 1978; Harrison and Dickinson 1989; Li and Sideris 1994). The singularity at the computation point in the numerical calculation of FFT was studied by e.g. Martinec et al. (1996), Kirby and Featherstone (1999), Nagy et al. (2000). The weak singularities in the terrain correction kernel can be avoided using the procedures derived by Nagy et al. (2000), Tsoulis (1999b) and Klose and Ilk (1993). In the following, the direct integration technique, the spherical harmonic expansion method as well as the space localizing base function technique will be discussed in detail. Finally, the combinations of these techniques are proposed, including methods which allow the determination of the topographic-isostatic far-zone effects using also spherical harmonic expansion.

4.1 Direct integration method

In a flat Earth approximation the integration compartments can be represented by rectangular prisms which is admissible for small areas only. Nevertheless, this approximation is useful for model studies (Nagy et al. 2000). The use of spherical models requires extensive computational efforts if tesseroids are used or spherical harmonic series (Papp and Wang 1996). For instance, in order to resolve 1 x 1 km topography information in spherical geometry, a spherical harmonic expansion up to degree and order 36 000 would be necessary. Spherical harmonic expansions up to this high degree can not be calculated because of the instability of the determination of the associated Legendre functions. Therefore, a spherical harmonic expansion of the topography may not be selected for a very detailed local modeling.

4.1.1 Gravitational potential and its derivatives modelled by prisms

4.1.1.1 Effect of the topographic and isostatic masses

The determination of the potential as well as its first and second derivatives by using the integration method based on rectangular prisms has been studied by many authors (e.g., Mader 1951; Nagy 1966; Forsberg 1984). Formulae for the calculation of the derivatives of the potential up to the third order are given by Mader (1951). Here we give only a short review of the gravitational potential, represented by rectangular prisms, as well as of its various derivatives. The gravitational potential of a rectangular prism of homogeneous mass-density ρ is described by Newton's integral (e.g., Heiskanen and Moritz 1967):

$$V_t|_{\mathbf{r}=\mathbf{r}_P} = G \iiint_v \rho(Q) \left. \frac{1}{l(\mathbf{r},\mathbf{r}_Q)} \right|_{\mathbf{r}=\mathbf{r}_P} dv_Q, \tag{4.1}$$

where $\rho(Q)$ is the density of the topographic masses or the density contrast of the topographic masses and the water masses of the oceans. Because of lack of more detailed knowledge, the density of the topographic masses is assumed to be constant (see, e.g., Vaníček and Kleusberg 1987; Featherstone 1992; Forsberg and Sideris 1993; Abd-Elmotaal 1999; Smith and Milbert 1999; Featherstone et al. 2001). However, the real density distribution can differ from this value by 10% or more (see, e.g., Martinec 1993; Tziavos el al. 1996; Pagiatakis and Armenakis 1998; Kuhn 2000a, b; Huang et al. 2001).

The point P in Eq.(4.1) is the computation point with the Cartesian coordinates x_P, y_P, z_P and Q (the center of the prism) represents the source point with the coordinates x', y' and z' referring to the same Cartesian coordinate system (Fig. 4.1). The quantity $l(\mathbf{r},\mathbf{r}_Q)$ is the distance between the computation point and the source point. It is given by the well-known formula,

$$l(\mathbf{r},\mathbf{r}_Q)|_{\mathbf{r}=\mathbf{r}_P} = \left. \sqrt{(x-x')^2+(y-y')^2+(z-z')^2} \right|_{\mathbf{r}=\mathbf{r}_P}. \tag{4.2}$$

Insertion of Eq. (4.2) into Eq. (4.1) gives

$$V_t|_{\mathbf{r}=\mathbf{r}_P} = G \int_{x_1}^{x_2}\int_{y_1}^{y_2}\int_{z_1}^{z_2} \rho(Q) \left. \frac{1}{\sqrt{(x-x')^2+(y-y')^2+(z-z')^2}} \right|_{\mathbf{r}=\mathbf{r}_P} dx'dy'dz'. \tag{4.3}$$

If the density of the prism for simplicity is assumed to be homogeneous and constant (ρ_{cr}), the integral of

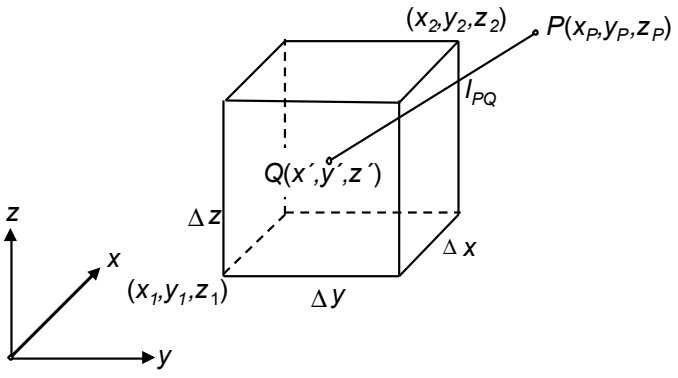

Fig. 4.1: Notation used for the definition of a prism

the Eq. (4.3) takes the form (Nagy 1966; Nagy et al. 2000):

$$\begin{aligned} V =& G\rho_{cr}\Bigg|\Bigg|\Big|(x-x')(y-y')\ln((z-z')+l(\mathbf{r},\mathbf{r}_Q))+(x-x')(z-z')\ln((y-y')+l(\mathbf{r},\mathbf{r}_Q))+\\ &+(y-y')(z-z')\ln((x-x')+l(\mathbf{r},\mathbf{r}_Q))-\frac{(x-x')^2}{2}\arctan\frac{(y-y')(z-z')}{(x-x')l(\mathbf{r},\mathbf{r}_Q)}-\\ &-\frac{(y-y')^2}{2}\arctan\frac{(x-x')(z-z')}{(y-y')l(\mathbf{r},\mathbf{r}_Q)}-\frac{(z-z')^2}{2}\arctan\frac{(x-x')(y-y')}{(z-z')l(\mathbf{r},\mathbf{r}_Q)}\Big|_{\mathbf{r}=\mathbf{r}_P}\Bigg|_{x_1}^{x_2}\Bigg|_{y_1}^{y_2}\Bigg|_{z_1}^{z_2}. \end{aligned} \tag{4.4}$$

The first derivatives of the potential with respected to z are given by (Nagy 1966):

$$\frac{\partial V}{\partial z} = -G\rho_{cr}\int_{x_1}^{x_2}\int_{y_1}^{y_2}\int_{z_1}^{z_2}\frac{(z-z')}{l(\mathbf{r},\mathbf{r}_Q)^{3/2}}\Big|_{\mathbf{r}=\mathbf{r}_P}dx'dy'dz', \tag{4.5}$$

$$\begin{aligned} \frac{\partial V}{\partial z} =& G\rho_{cr}\Bigg|\Bigg|\Big|(x-x')\ln((y-y')+l(\mathbf{r},\mathbf{r}_Q))+(y-y')\ln((x-x')+l(\mathbf{r},\mathbf{r}_Q))\\ &-(z-z')\tan\left[(x-x')(y-y')/((z-z')l(\mathbf{r},\mathbf{r}_Q))\right]\Big|_{x_1}^{x_2}\Big|_{y_1}^{y_2}\Big|_{z_1}^{z_2}. \end{aligned} \tag{4.6}$$

The other two partial derivatives of the potential with respect to x, y can be obtained from Eq. (4.6) by cyclic permutation

$$\begin{aligned} \frac{\partial V}{\partial x} =& G\rho_{cr}\Bigg|\Bigg|\Big|(y-y')\ln((z-z')+l(\mathbf{r},\mathbf{r}_Q))+(z-z')\ln((y-y')+l(\mathbf{r},\mathbf{r}_Q))-\\ &-(x-x')\tan\left[(y-y')(z-z')/((x-x')l(\mathbf{r},\mathbf{r}_Q))\right]\Big|_{x_1}^{x_2}\Big|_{y_1}^{y_2}\Big|_{z_1}^{z_2}, \end{aligned} \tag{4.7}$$

$$\begin{aligned} \frac{\partial V}{\partial y} =& G\rho_{cr}\Bigg|\Bigg|\Big|(z-z')\ln((x-x')+l(\mathbf{r},\mathbf{r}_Q))+(x-x')\ln((y-y')+l(\mathbf{r},\mathbf{r}_Q))-\\ &-(y-y')\tan\left[(x-x')(z-z')/\left((y-y')l(\mathbf{r},\mathbf{r}_Q)\right)\right]\Big|_{x_1}^{x_2}\Big|_{y_1}^{y_2}\Big|_{z_1}^{z_2}. \end{aligned} \tag{4.8}$$

The second derivatives of the potential are given by (ibid.)

$$\frac{\partial^2 V}{\partial x^2} = G\rho_{cr}\Bigg|\Bigg|-\arctan\frac{(y-y')(z-z')}{(x-x')l(\mathbf{r},\mathbf{r}_Q)}\Big|_{x_1}^{x_2}\Big|_{y_1}^{y_2}\Big|_{z_1}^{z_2}, \tag{4.9}$$

$$\frac{\partial^2 V}{\partial y^2} = G\rho_{cr}\Bigg|\Bigg|-\arctan\frac{(x-x')(z-z')}{(y-y')l(\mathbf{r},\mathbf{r}_Q)}\Big|_{x_1}^{x_2}\Big|_{y_1}^{y_2}\Big|_{z_1}^{z_2}, \tag{4.10}$$

$$\frac{\partial^2 V}{\partial z^2} = G\rho_{cr}\Bigg|\Bigg|-\arctan\frac{(x-x')(y-y')}{(z-z')l(\mathbf{r},\mathbf{r}_Q)}\Big|_{x_1}^{x_2}\Big|_{y_1}^{y_2}\Big|_{z_1}^{z_2}, \tag{4.11}$$

$$\frac{\partial^2 V}{\partial x\partial y} = G\rho_{cr}\Bigg|\Bigg|\ln((z-z')+l(\mathbf{r},\mathbf{r}_Q))\Big|_{x_1}^{x_2}\Big|_{y_1}^{y_2}\Big|_{z_1}^{z_2}, \tag{4.12}$$

$$\frac{\partial^2 V}{\partial x\partial z} = G\rho_{cr}\Bigg|\Bigg|\ln((y-y')+l(\mathbf{r},\mathbf{r}_Q))\Big|_{x_1}^{x_2}\Big|_{y_1}^{y_2}\Big|_{z_1}^{z_2}, \tag{4.13}$$

$$\frac{\partial^2 V}{\partial y \partial z} = G\rho_{cr} \left| \left| \ln((x - x') + l(\mathbf{r}, \mathbf{r}_Q)) \right|_{x_1}^{x_2} \right|_{y_1}^{y_2} \Bigg|_{z_1}^{z_2}. \tag{4.14}$$

From Eqs. (4.4) to (4.14), it is easy to realize that these formulae show singularities for special locations of P (e.g., if P coincides with a prism's corner or is situated on an edge of the prism); the respective limit values have been derived by Nagy et al. (2000, 2002). The above relations can be used for calculating the potential and its first and second derivatives of the topographic masses on or above the surface of the Earth. Since the prism matches the concept of the DTM, the TC software (Forsberg 1984) for prismatic topographic elements situated in an intermediate zone can be used after modifying it for calculating different topographic-isostatic models.

Due to the decrease of the gravitational effects with increasing distance, the complex formula (4.4) can be substituted by a simpler one for prisms which are located at a large distance from the computation point. This simpler formula can be derived based on a Taylor expansion of the integration kernel in Eq. (4.1). The Taylor expansion is fixed at the geometrical centre of the prism. The gravitational potential of the rectangular prism neglecting terms of order four and higher is given by MacMillan's (1930) formula (also see Anderson 1976; Forsberg 1984; Heck and Seitz 2006):

$$V = G\rho_{cr}\Delta x \Delta y \Delta z \left[\frac{1}{l_0} + \frac{3\left(x_0 - x\right)^2 - l_0^2}{24 l_0^5}\Delta x^2 + \frac{3\left(y_0 - y\right)^2 - l_0^2}{24 l_0^5}\Delta y^2 + \frac{3\left(z_0 - z\right)^2 - l_0^2}{24 l_0^5}\Delta z^2 + ... \right], \tag{4.15}$$

where

$$\begin{aligned} x_o &= (x_1 + x_2)/2, \\ y_o &= (y_1 + y_2)/2, \\ z_o &= (z_1 + z_2)/2. \end{aligned} \tag{4.16}$$

and l_0 denotes the Euclidean distance between the computation point P and the geometrical center (x_0, y_0, z_0) of the computation prism with $\Delta x = x_2 - x_1$, $\Delta y = y_2 - y_1$ and $\Delta z = z_2 - z_1$. The first and higher order derivatives of the potential can be simply found by differentiation of Eq. (4.15) with respect to x, y and z. Near the computation point (Eqs. 4.4 to 4.14), the flat-topped approximation of the topographic prism is assumed. This approximation produces some errors for the computation of the gravitational functions. A better approximation can be supplied by a prism topped by an inclined plane (Koch 1965) or by a bilinear surface (Smith 2000; Tsoulis et al. 2003). This procedure can be transformed to polyhedral bodies which can easily be determined by numerical methods (Talwani and Ewing 1960; Paul 1974; Petrović 1996).

For prisms which are far from the computation point, the curvature of the Earth must be taken into account. These prisms are inclined with respect to the local vertical and shifted with respect to the horizontal plane at the computation point, due to the (approximate) sphericity of the Earth. These effects have to be taken into account for distant prismatic elements (Grüninger 1990; Kuhn 2000a; Smith 2000, 2002). Also, due to the curvature of the Earth, the topocentric Cartesian coordinate systems, according to the direction of the vertical at the computation point and the edges of the prismatic topographic element, are not parallel. The transformation between the two systems is visualized in Fig.4.2 where (X, Y, Z) denote the Cartesian coordinates related to a global terrestrial reference frame and (x, y, z) and (x^*, y^*, z^*) the local Cartesian coordinates related to the edge system of the prism and the local vertical reference frame at the computation point P, respectively. The transformation of the first derivatives of the potential known in the edge system into the local coordinate system at P is given by the respective basis transformation with respect to the global equatorial system (Heck and Seitz 2006). The direction of the plumbline at the computation point is defined by the geodetic latitude φ and the geodetic longitude λ of the point P. The direction of the z-axis of the edge system is defined by φ' and λ'. The relations between the orthonormal base vectors are given by (Grüninger 1990; Kuhn 2000a; Heck and Seitz 2006)

$$\left(\mathbf{e_x}, \mathbf{e_y}, \mathbf{e_z}\right)^T = \mathbf{P_1} \cdot \mathbf{R_2}\left(\frac{\pi}{2} - \varphi'\right) \cdot \mathbf{R_3}\left(\lambda'\right) \cdot \left(\mathbf{e_X}, \mathbf{e_Y}, \mathbf{e_Z}\right)^T, \tag{4.17}$$

$$\left(\mathbf{e_x^*}, \mathbf{e_y^*}, \mathbf{e_z^*}\right)^T = \mathbf{P_1} \cdot \mathbf{R_2}\left(\frac{\pi}{2} - \varphi\right) \cdot \mathbf{R_3}\left(\lambda\right) \cdot \left(\mathbf{e_X}, \mathbf{e_Y}, \mathbf{e_Z}\right)^T, \tag{4.18}$$

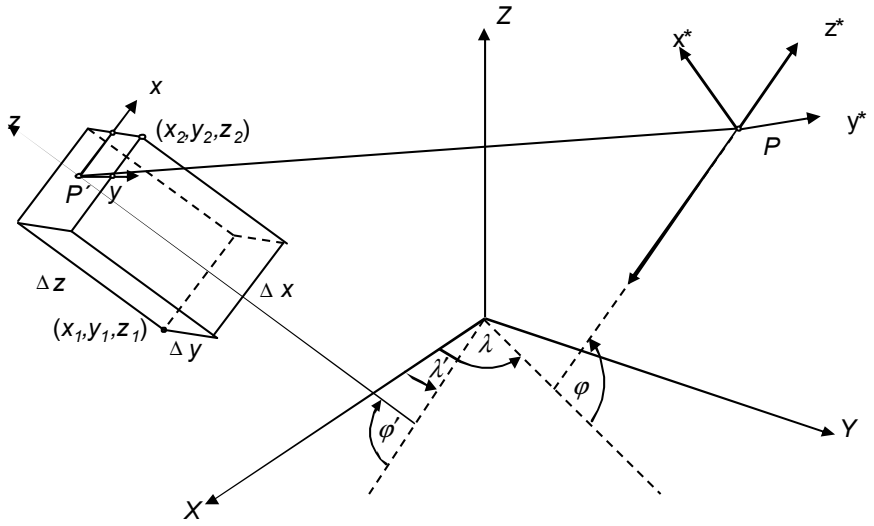

Fig. 4.2: Transformation between the edge system of the prism and the local vertical system at the computation point

where $\mathbf{R_2}$ and $\mathbf{R_3}$ are the rotation matrices for rotations about the y- and z-axis, respectively, while the reflection matrix $\mathbf{P_1}$ has to be introduced for the transition between the right-handed global system and the left-handed local system. In numerical applications, the geodetic latitudes φ, φ' may be replaced by the geocentric latitudes. From Eqs. (4.17) and (4.18) the formula for the transformation between the edge system of the prism and the local vertical system at the computation point is given by (Kuhn 2000a):

$$(v_x^*, v_y^*, v_z^*)^T = \mathbf{R}(\varphi, \lambda, \varphi', \lambda') \cdot (v_x, v_y, v_z)^T, \tag{4.19}$$

where (v_x^*, v_y^*, v_z^*) and (v_x, v_y, v_z) are the first derivatives of the potential in the edge system and in the local vertical system at P, respectively. The transformation matrix $\mathbf{R}(\varphi, \lambda, \varphi', \lambda')$ is given by (ibid.)

$$\mathbf{R}(\varphi, \lambda, \varphi', \lambda') = \begin{pmatrix} s_1 s_1'(c_2 c_2' + s_2 s_2') + c_1 c_1' & s_1(-c_2 s_2' - s_2 c_2') & -s_1 c_1'(c_2 c_2' + s_2 s_2') + c_1 c_1' \\ s_1'(s_2 c_2' + c_2 s_2') & s_2 s_2' + c_2 c_2' & c_1'(-s_2 c_2' + c_2 s_2') \\ -c_1 s_1'(c_2 c_2' + s_2 s_2') + s_1 c_1' & c_1(-c_2 s_2' + s_2 c_2') & c_1 c_1'(c_2 c_2' + s_2 s_2') + s_1 s_1' \end{pmatrix} \tag{4.20}$$

with

$$\begin{array}{llll} s_1 = \sin\varphi, & s_2 = \sin\lambda, & c_1 = \cos\varphi, & c_2 = \cos\lambda, \\ s_1' = \sin\varphi', & s_2' = \sin\lambda', & c_1' = \cos\varphi', & c_2' = \cos\lambda'. \end{array} \tag{4.21}$$

This transformation is carried out for every single prism situated at a large distance from the computation point P. Also, the second derivatives of the potential can be transformed using the same transformation matrix given in Eq. (4.20).

The dimensions of the prism have to be derived from the dimensions of a tesseroid. These dimensions can be determined based on the mass conservation as follows:

$$m_{tesseroid} = m_{prism}, \tag{4.22}$$

which follows

$$\begin{aligned} \Delta z &= \Delta r, \\ \Delta x &= R\Delta\varphi, \\ \Delta y &= R\cos\varphi\Delta\lambda. \end{aligned} \tag{4.23}$$

For calculating the effects of the topographic masses, the height of the prismatic element is taken to be equal to the orthometric height of the topography of this element with ρ equals the density of the masses in case of land areas. In case of ocean regions the density is taken to be

$$\rho(x_Q, y_Q, z_Q) = \rho_w - \rho_{cr}, \tag{4.24}$$

where ρ_{cr} is the density of the crust and ρ_w the density of the water. For calculating the effects of the isostatic masses in case of Airy-Heiskanen and Vening Meinesz models, the height of the prismatic element is taken to be equal to the roots or antiroots of the isostatic masses with density contrast $\Delta\rho = \rho_m - \rho_{cr}$. In case of the Pratt-Hayford model, the height of the prismatic element is taken to be equal to the height of the orthometric height of the topography in addition to the Pratt-Hayford compensation depth with the density contrast as determined in chapter 3 for land and ocean areas.

4.1.1.2 Effect of the condensation masses

For calculating the effect of the condensation masses in the case of *Helmert's methods of condensation* using the prism integration method, Eq. (4.1) will be transformed to the following equation (Smith et al. 2001):

$$V_c|_{\mathbf{r}=\mathbf{r}_P} = G \iint\limits_{\sigma} \frac{k_Q}{l^*(\mathbf{r}, \mathbf{r}_Q)}\bigg|_{\mathbf{r}=\mathbf{r}_P} dx'dy', \tag{4.25}$$

with the surface element $d\sigma = dx_Q\, dy_Q$ and the single layer density k_Q, which depends on the height and density of the topography (see chapter 3). If the density of the prism is taken to be constant (ρ_{cr}), the potential, the first and the second derivatives can be determined as follows (see Fig. 4.3):

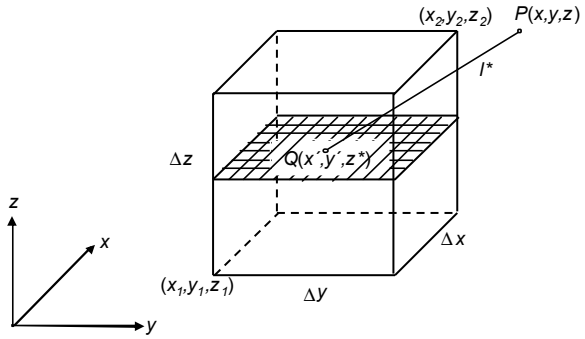

Fig. 4.3: Notation used for the definition of a condensed prism

$$\begin{aligned} V_c|_{\mathbf{r}=\mathbf{r}_P} =& G\rho_{cr}\Delta z \Bigg| \Big|(x-x')\ln((y-y') + l^*(\mathbf{r},\mathbf{r}_Q)) + (y-y')\ln((x-x') + l^*(\mathbf{r},\mathbf{r}_Q)) - \\ & - z\arctan\left[(x-x')(y-y')/((z-z^*)l^*(\mathbf{r},\mathbf{r}_Q))\right]\Big|_{\mathbf{r}=\mathbf{r}_P}\Bigg|_{x_1}^{x_2}\Bigg|_{y_1}^{y_2}, \end{aligned} \tag{4.26}$$

$$\frac{\partial V_c}{\partial z} = G\rho_{cr}\Delta z \Bigg| \Big| - \arctan\left[(x-x')(y-y')/((z-z^*)l^*(\mathbf{r},\mathbf{r}_Q))\right]\Big|_{x_1}^{x_2}\Bigg|_{y_1}^{y_2}, \tag{4.27}$$

$$\frac{\partial V_c}{\partial x} = G\rho_{cr}\Delta z \Bigg| \Big|\ln((y-y') + l^*(\mathbf{r},\mathbf{r}_Q))\Big|_{x_1}^{x_2}\Bigg|_{y_1}^{y_2}, \tag{4.28}$$

$$\frac{\partial V_c}{\partial y} = G\rho_{cr}\Delta z \Bigg| \Big|\ln((x-x') + l^*(\mathbf{r},\mathbf{r}_Q))\Big|_{x_1}^{x_2}\Bigg|_{y_1}^{y_2}, \tag{4.29}$$

$$\frac{\partial^2 V_c}{\partial z^2} = G\rho_{cr}\Delta z \left| \left| \frac{(x-x')(y-y')}{l^*(\mathbf{r},\mathbf{r}_Q)} \left(\frac{1}{(x-x')^2+(z-z^*)^2} + \frac{1}{(y-y')^2+(z-z^*)^2} \right) \right|_{x'=x_1}^{x_2} \right|_{y'=y_1}^{y_2}, \quad (4.30)$$

$$\frac{\partial^2 V_c}{\partial x^2} = G\rho_{cr}\Delta z \left| \left| \frac{(x-x')}{l^*(\mathbf{r},\mathbf{r}_Q)((y-y')+l^*(\mathbf{r},\mathbf{r}_Q))} \right|_{x_1}^{x_2} \right|_{y_1}^{y_2}, \quad (4.31)$$

$$\frac{\partial^2 V_c}{\partial y^2} = G\rho_{cr}\Delta z \left| \left| \frac{(y-y')}{l^*(\mathbf{r},\mathbf{r}_Q)((x-x')+l^*(\mathbf{r},\mathbf{r}_Q))} \right|_{x_1}^{x_2} \right|_{y_1}^{y_2}, \quad (4.32)$$

$$\frac{\partial^2 V_c}{\partial x \partial y} = G\rho_{cr}\Delta z \left| \left| \frac{1}{l^*(\mathbf{r},\mathbf{r}_Q)} \right|_{x_1}^{x_2} \right|_{y_1}^{y_2}, \quad (4.33)$$

$$\frac{\partial^2 V_c}{\partial x \partial z} = G\rho_{cr}\Delta z \left| \left| \frac{(z-z^*)}{l^*(\mathbf{r},\mathbf{r}_Q)((y-y')+l^*(\mathbf{r},\mathbf{r}_Q))} \right|_{x_1}^{x_2} \right|_{y_1}^{y_2}, \quad (4.34)$$

$$\frac{\partial^2 V_c}{\partial y \partial z} = G\rho_{cr}\Delta z \left| \left| \frac{(z-z^*)}{l^*(\mathbf{r},\mathbf{r}_Q)((x-x')+l^*(\mathbf{r},\mathbf{r}_Q))} \right|_{x_1}^{x_2} \right|_{y_1}^{y_2}, \quad (4.35)$$

where

$$l^*(\mathbf{r},\mathbf{r}_Q) = \left((x-x')^2+(y-y')^2+(z-z^*)^2\right)^{1/2}. \quad (4.36)$$

In our case $\Delta z = z_2 - z_1$ is equal to the orthometric height of the prismatic element and z^* the vertical coordinate of the geometrical center of the condensed integration element.

4.1.2 Gravitational potential and its derivatives modelled by tesseroids (using the analytic vertical integration)

Taking the curvature of the Earth into account, a much better level of approximation in the calculation of the topographic mass effects is obtained. In this case the geoid can be modelled by a sphere of radius R, coinciding with the mean radius of the Earth. There are two principal possibilities: a representation of the topography by any spherical discretisation and a subsequent integration (Smith et al. 2001; Tenzer et al. 2003; Heck 2003) or a representation of the topography by a spherical harmonic expansion (see, e.g., Sünkel 1985, 1986; Rummel et al. 1988; Tsoulis 1999a, 2001). In the case of the direct integration method, the weak singularities are solved numerically by separating the topographic masses in spherical approximation in two terms: the spherical Bouguer shell and a spherical terrain correction (see, e.g., Novák et al. 2001; Vaníček et al. 2001; Heck 2003). The effects of the spherical shell on the potential and its first and second derivatives are studied in many previous investigations such as Wichiencharoen (1982), Blakely (1995), Vaníček et al. (2001), Tenzer et al. (2003), Vajda et al. (2004a), (2004b) and Vaníček et al. (2004).

4.1.2.1 Effect of the topographic masses

The potential of the topographic masses between the topographic surface S and the sphere of radius R at the computation point P is given by Newton's integral in spherical coordinates as follows (Fig. 4.4):

$$V_t|_{\mathbf{r}=\mathbf{r}_P} = G \iint_\sigma \left[\int_R^{r_Q} \rho(Q) \frac{\xi^2}{l} \Big|_{\mathbf{r}=\mathbf{r}_P} d\xi \right] d\sigma, \quad (4.37)$$

with

$$l := \sqrt{r^2+\xi^2-2r\xi\cos\psi}, \quad (4.38)$$

the density of the topography $\rho(Q)$, $r_Q = R + H_Q$, and the surface element in spherical coordinates $d\sigma = \cos\varphi_Q d\varphi_Q d\lambda_Q$. $\rho(Q)$ is the density of the spherical integration element; it reads in case of the ocean

area $\rho(Q) = \rho_{cr} - \rho_w$. The geocentric angle ψ is the spherical distance between the radius vectors of the computation point $\mathbf{r}_P(r, \varphi, \lambda)$ and the integration point $\mathbf{r}_Q(r_Q, \varphi_Q, \lambda_Q)$:

$$\cos\psi = \sin\varphi \sin\varphi_Q + \cos\varphi\cos\varphi_Q \cos(\lambda_Q - \lambda), \tag{4.39}$$

where φ and λ are the geodetic latitude and longitude of the computation point, respectively. Additional quantities are shown in Fig. 4.4. If the column of topography consists of several layers with different densities (Fig. 3.2, left), the potential of the topographic masses is given by:

$$V_t|_{\mathbf{r}=\mathbf{r}_P} = G \iint\limits_{\sigma} \left[\int\limits_{R}^{R+H_i} \sum_{i=0}^{i=l} (\rho_i - \rho_{i+1}) \frac{\xi^2}{l}\Big|_{\mathbf{r}=\mathbf{r}_P} d\xi \right] d\sigma, \tag{4.40}$$

where ρ_0, ρ_{l+1} are defined in Eq. (3.2). If the rock equivalent representation is used, Eq. (4.37) is transformed to

$$V_t|_{\mathbf{r}=\mathbf{r}_P} = G\rho_{cr} \iint\limits_{\sigma} \left[\int\limits_{R}^{r_Q} \frac{\xi^2}{l}\Big|_{\mathbf{r}=\mathbf{r}_P} d\xi \right] d\sigma. \tag{4.41}$$

The inner integral of Eq. (4.37) can be evaluated by using (Gradshteyn and Ryzhik 1980):

$$V_t|_{\mathbf{r}=\mathbf{r}_P} = \frac{1}{2} G\rho_{cr} \iint\limits_{\sigma} \left[F_0(r, \psi, \xi)|_{\mathbf{r}=\mathbf{r}_P} \right]_{\xi=R}^{r_Q} d\sigma, \tag{4.42}$$

with

$$F_0(r, \psi, \xi) = (\xi + 3r\cos\psi) l(r, \psi, \xi) + r^2(3cos^2\psi - 1) \ln(l(r, \psi, \xi) + \xi - r\cos\psi) \tag{4.43}$$

and $\mathbf{r}_P = (R + H_P, \varphi, \lambda)$. The integration interval in Eq. (4.42) can be separated into two parts, $(R,\ r_{P'})$ and $(r_{p'},\ r_Q)$. The quantity $r_{P'} = R + H_{p'}$ denotes the geocentric radius of the surface point $P' \in S$ which is located under the computation point P (Fig. 4.4). Then the integral of Eq. (4.3) can be given by (Heck 2003):

$$\begin{aligned} V_t|_{\mathbf{r}=\mathbf{r}_P} = \frac{2\pi G\rho_{cr}}{r_P} \begin{Bmatrix} \frac{2}{3}(r_{P'}^3 - R^3) & \forall r_P \geq r_{P'} \\ r_P(r_{P'}^2 - R^2) & \forall r_P \leq r_{P'} \end{Bmatrix} + \frac{1}{2} G\rho_{cr} \iint\limits_{\sigma} \big[r_Q \bar{l}' - r_{P'}\bar{l} + \\ + 3r_P\cos\psi(\bar{l}' - \bar{l}) + r_P^2(3\cos^2\psi - 1) \ln \left| \frac{\bar{l}' + r_Q - r_P\cos\psi}{\bar{l} + r_{P'} - r_P\cos\psi} \right| \Big] d\sigma, \end{aligned} \tag{4.44}$$

with the Euclidean distances as shown in Fig. 4.4 and defined by:

$$\bar{l} := \sqrt{r_P^2 + r_{P'}^2 - 2r_P r_{P'}\cos\psi}, \tag{4.45}$$

$$\bar{l}' := \sqrt{r_P^2 + r_Q^2 - 2r_P r_Q \cos\psi}. \tag{4.46}$$

The first term in Eq. (4.44) is due to the mass of a homogenous spherical shell of thickness $H_{P'} = r_{P'} - R$ acting on the gravitational potential at the computation point P. Two cases have to be distinguished: the point is located either on or outside the topography of the Earth ($r_P \geq r_{P'}$) or the point is located below or on the geoid ($r_P \leq r_{P'}$). The integral term in Eq. (4.44) denotes the influence of the varying terrain due to $r_Q \neq r_{P'}$(terrain correction). The first case ($r_P \geq r_{P'}$) will be used to determine the effect of the topographic-isostatic masses at the surface of the Earth or outside at aeroplane or satellite altitude. The second case of Eq. (4.44) is necessary only for the calculation of the primary indirect topographical effect on the geoidal height.

The first and second derivatives of the potential of the topographic masses are determined in a tangential coordinate system. This tangential coordinate system is defined with the x-axis oriented to north, the z-axis

coinciding with the radius vector and the y-axis oriented to east, completing a left-hand-system (see Fig. 4.5). The first derivatives of the potential of the topographic masses with respect to z can be calculated using the following formula (Novák et al. 2001):

$$\frac{\partial V_t}{\partial z} = \frac{\partial V_t}{\partial r}, \tag{4.47}$$

$$\left.\frac{\partial V_t}{\partial r}\right|_{\mathbf{r}=\mathbf{r}_P} = -\left.\frac{4\pi G\rho_{cr}}{3r^2}(r_{p'}^3 - R^3)\right|_{\mathbf{r}=\mathbf{r}_P} + G\rho_{cr}\iint_\sigma \left[F_1(r,\psi,\xi|_{\mathbf{r}=\mathbf{r}_P})\right]_{\xi=r_{P'}}^{r_Q} d\sigma, \tag{4.48}$$

$$\begin{aligned} F_1(r,\psi,\xi) = \big(\big[(\xi^2+3r^2)\cos\psi + \xi r(1-6\cos^2\psi)\big]\ /l(r,\psi,\xi) + \\ + r(3\cos^2\psi - 1)\ln|\xi - r\cos\psi + l(r,\psi,\xi)|\big)\,. \end{aligned} \tag{4.49}$$

The first derivative of the potential of the topographic masses with respect to x can be calculated as follows (Tscherning 1976):

$$\left.\frac{\partial V_t}{\partial x}\right|_{\mathbf{r}=\mathbf{r}_P} = \left.\frac{1}{r}\frac{\partial V_t}{\partial \varphi}\right|_{\mathbf{r}=\mathbf{r}_P} = \left.\frac{1}{r}\frac{\partial \psi}{\partial \varphi}\ \frac{\partial V_t}{\partial \psi}\right|_{\mathbf{r}=\mathbf{r}_P}, \tag{4.50}$$

It follows from Eq. (4.37) with Eq. (4.38) according to Fig. 4.5,

$$\left.\frac{\partial V_t}{\partial \psi}\right|_{\mathbf{r}=\mathbf{r}_P} = G\rho_{cr}\iint_\sigma \left[\left.\frac{\partial F_0}{\partial \psi}\right|_{\mathbf{r}=\mathbf{r}_P}\right]_R^{r_Q} d\sigma, \tag{4.51}$$

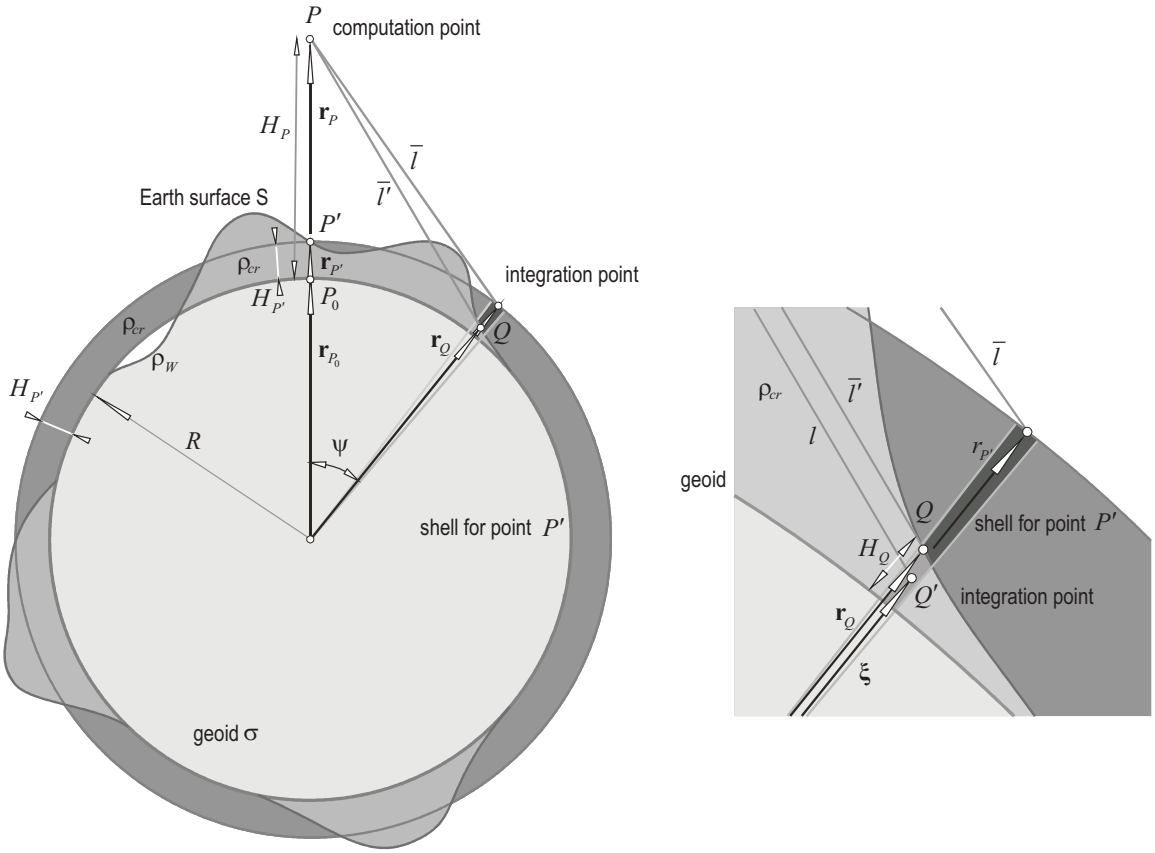

Fig. 4.4: Geometry of the topography in spherical approximation

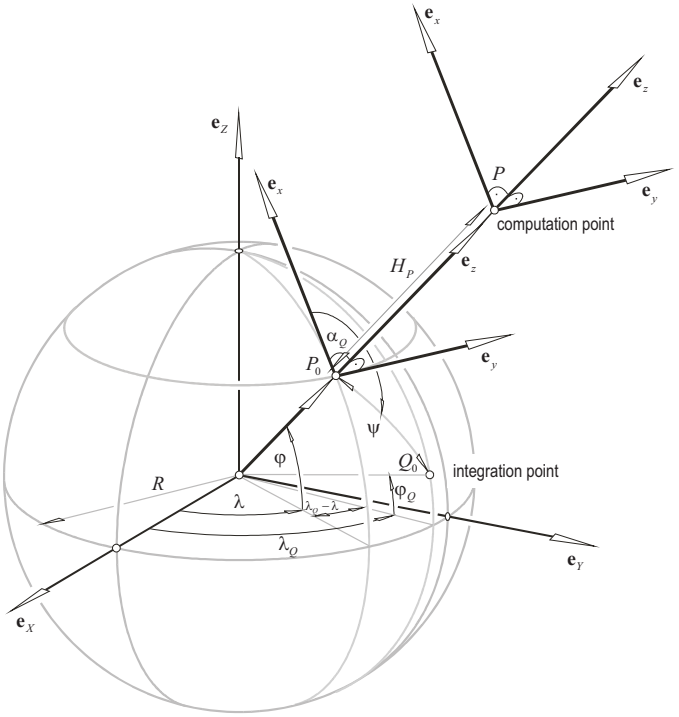

Fig. 4.5: Local coordinate system

with

$$\left.\frac{\partial F_0}{\partial \psi}\right|_{\mathbf{r}=\mathbf{r}_P} =: F_2(r,\psi,\xi)|_{\mathbf{r}=\mathbf{r}_P}\,, \tag{4.52}$$

and according to Heiskanen and Moritz (1967),

$$\frac{\partial \psi}{\partial \varphi} = -\cos\alpha_Q, \tag{4.53}$$

with the spherical azimuth α_Q as given by e.g. Heiskanen and Moritz (1967, Eq. 2-212):

$$\tan\alpha_Q = \frac{\cos\varphi_Q \sin(\lambda_Q-\lambda)}{\sin\varphi_Q\cos\varphi - \cos\varphi_Q\sin\varphi\cos(\lambda_Q-\lambda)}. \tag{4.54}$$

The integration interval in Eq. (4.51) is again separated into two parts, $(R,\ r_{P'})$ and $(r_{p'},\ r_Q)$. The first part represents the effect of the spherical Bouguer shell and is zero for the first derivatives in x and y directions. Then the second part can be given by:

$$\left.\frac{\partial V_t}{\partial \psi}\right|_{\mathbf{r}=\mathbf{r}_P} = G\rho_{cr}\iint\limits_{\sigma}\left[F_2(r,\psi,\xi)|_{\mathbf{r}=\mathbf{r}_P}\right]_{r_{P'}}^{r_Q} d\sigma, \tag{4.55}$$

with

$$\begin{aligned} F_2(r,\psi,\xi) = \big[&-\left(r\xi^2\sin\psi - r^2\xi\cos\psi(5-6\cos^2\psi)/\sin\psi + r^3(2-3\cos^2\psi)/\sin\psi\right)/ \\ &- l(r,\psi,\xi) - \left(r^2(3/2\sin 2\psi)\ln|\xi - r\cos\psi + l(r,\psi,\xi)|\right)\big]. \end{aligned} \tag{4.56}$$

The first derivative of the potential of the topographic masses with respect to y can be determined analogously to Eq. (4.50) resulting in the formula,

$$\left.\frac{\partial V_t}{\partial y}\right|_{\mathbf{r}=\mathbf{r}_P} = \frac{1}{r\cos\varphi}\left.\frac{\partial V_t}{\partial \lambda}\right|_{\mathbf{r}=\mathbf{r}_P} = \frac{1}{r\cos\varphi}\frac{\partial\psi}{\partial\lambda}\left.\frac{\partial V_t}{\partial\psi}\right|_{\mathbf{r}=\mathbf{r}_P}, \tag{4.57}$$

where $\partial V_t/\partial\psi|_{\mathbf{r}=\mathbf{r}_P}$ is given by Eq. (4.55) and

$$\frac{\partial\psi}{\partial\lambda} = -\cos\varphi\sin\alpha_Q, \tag{4.58}$$

based on the Eq. (4.39) and Eq. (4.54). Eqs. (4.48), (4.50) and (4.57) can be used to study the effects of the topographic masses on Satellite-to-Satellite Tracking (SST) observations as shown in Makhloof and Ilk (2004).

The second derivatives of the potential of the topographic masses are important for airborne or Satellite Gravity Gradiometry. It holds for the radial component, starting from Eq. (4.48):

$$\left.\frac{\partial^2 V_t}{\partial z^2}\right|_{\mathbf{r}=\mathbf{r_P}} = \left.\frac{\partial^2 V_t}{\partial r^2}\right|_{\mathbf{r}=\mathbf{r}_P}, \tag{4.59}$$

with

$$\left.\frac{\partial^2 V_t}{\partial r^2}\right|_{\mathbf{r}=\mathbf{r}_P} = \left.\frac{8\pi G\rho_{cr}}{3r^3}(r_{P'}^3 - R^3)\right|_{\mathbf{r}=\mathbf{r}_P} + G\rho_{cr}\iint\limits_{\sigma}\left[\left.\frac{\partial F_1(r,\psi,\xi)}{\partial r}\right|_{\mathbf{r}=\mathbf{r}_P}\right]_{\xi=r_{P'}}^{r_Q} d\sigma, \tag{4.60}$$

and

$$\left.\frac{\partial F_1(r,\psi,\xi)}{\partial r}\right|_{\mathbf{r}=\mathbf{r}_P} =: \left.F_3(r,\psi,\xi)\right|_{\mathbf{r}=\mathbf{r}_P}, \tag{4.61}$$

where $F_3(r,\psi,\xi)$ can be given after some algebraic operations by:

$$\begin{aligned} F_3(r,\psi,\xi) = \big(\big[(\xi\cos\psi - r)\left((\xi^2+3r^2)\cos\psi + r\xi(1-6\cos^2\psi)\right)\big]\, l^{-3}(r,\psi,\xi) \\ + (3\cos^2\psi - 1)\ln|\xi - r\cos\psi + l(r,\psi,\xi)| + \\ + \left[2\xi + 6r\cos\psi - 9\xi\cos^2\psi\right] l^{-1}(r,\psi,\xi)\big). \end{aligned} \tag{4.62}$$

The second derivative of the potential of the topographic masses with respect to x can be given by the relation (Tscherning 1976),

$$\left.\frac{\partial^2 V_t}{\partial x^2}\right|_{\mathbf{r}=\mathbf{r_P}} = \left.\frac{1}{r}\frac{\partial V_t}{\partial r}\right|_{\mathbf{r}=\mathbf{r_P}} + \left.\frac{1}{r^2}\frac{\partial^2 V_t}{\partial\varphi^2}\right|_{\mathbf{r}=\mathbf{r_P}}. \tag{4.63}$$

The first term is given by Eq. (4.48) and the second term can be derived starting from Eq. (4.50):

$$\left.\frac{1}{r^2}\frac{\partial^2 V_t}{\partial\varphi^2}\right|_{\mathbf{r}=\mathbf{r}_P} = \left.\frac{1}{r^2}\left[\frac{\partial^2 V_t}{\partial\psi^2}\left(\frac{\partial\psi}{\partial\varphi}\right)^2 + \frac{\partial V_t}{\partial\psi}\frac{\partial^2\psi}{\partial\varphi^2}\right]\right|_{\mathbf{r}=\mathbf{r}_P}, \tag{4.64}$$

with

$$\frac{\partial^2\psi}{\partial\varphi^2} = \sin^2\alpha_Q\cot\psi, \tag{4.65}$$

by considering Eqs. (4.53), (4.39) and (4.54). The term

$$\left.\frac{\partial^2 V_t}{\partial\psi^2}\right|_{\mathbf{r}=\mathbf{r_P}} = G\rho_{cr}\iint\limits_{\sigma}\left[\left.\frac{F_2(r,\psi,\xi)}{\partial\psi}\right|_{\mathbf{r}=\mathbf{r}_P}\right]_{r_{P'}}^{r_Q} d\sigma \tag{4.66}$$

follows from Eq. (4.51) with Eq. (4.52) with the relation

$$\left.\frac{F_2(r,\psi,\xi)}{\partial\psi}\right|_{\mathbf{r}=\mathbf{r}_P} =: \left.F_4(r,\psi,\xi)\right|_{\mathbf{r}=\mathbf{r}_P}, \tag{4.67}$$

where $F_4(r,\psi,\xi)$ can be expressed after some algebraic operations by:

$$\begin{aligned} F_4(r,\psi,\xi) = &- \left[3r^2(\cos 2\psi)\ln|\xi - r\cos\psi + l(r,\psi,\xi)|\right] + \\ &+ \left[r\xi\left(r\xi^2\sin^2\psi - r^2\xi\cos\psi(5-6\cos^2\psi) + r^3(2-3\cos^2\psi)\right)/l^3(r,\psi,\xi)\right] + \\ &+ \left[\left(-r\xi^2\cos\psi + 15r^2\xi\cos^2\psi - r^2\xi(5-6\cos^2\psi)/\sin^2\psi - \right.\right. \\ &\left.\left. -9r^3\cos\psi + r^3\cos\psi(2-3\cos^2\psi)/\sin^2\psi\right)/l(r,\psi,\xi)\right]. \end{aligned} \tag{4.68}$$

The second derivative of the potential of the topographic masses with respect to y, $(V_t)_{yy}$, reads as follows (Tscherning 1976):

$$\left.\frac{\partial^2 V_t}{\partial y^2}\right|_{\mathbf{r}=\mathbf{r}_P} = \left.\frac{1}{r}\frac{\partial V_t}{\partial r}\right|_{\mathbf{r}=\mathbf{r}_P} + \left.\frac{1}{r^2\cos^2\varphi}\frac{\partial^2 V_t}{\partial\lambda^2}\right|_{\mathbf{r}=\mathbf{r}_P} - \left.\frac{\tan\varphi}{r^2}\frac{\partial V_t}{\partial\varphi}\right|_{\mathbf{r}=\mathbf{r}_P}. \tag{4.69}$$

The first term of Eq. (4.69) coincides with the first term of Eq. (4.63) and is given by Eq. (4.48) corresponding to Eq. (4.50) and the second term can be calculated starting from

$$\left.\frac{1}{r^2\cos^2\varphi}\frac{\partial^2 V_t}{\partial\lambda^2}\right|_{\mathbf{r}=\mathbf{r}_P} = \left.\frac{1}{r^2\cos^2\varphi}\left[\frac{\partial^2 V_t}{\partial\psi^2}\left(\frac{\partial\psi}{\partial\lambda}\right)^2 + \frac{\partial V_t}{\partial\psi}\frac{\partial^2\psi}{\partial\lambda^2}\right]\right|_{\mathbf{r}=\mathbf{r}_P}, \tag{4.70}$$

with the first derivative as given in Eq. (4.58) and the second derivative

$$\frac{\partial^2\psi}{\partial\lambda^2} = \cos^2\alpha_Q\cos^2\phi\cot\psi - \frac{1}{2}\sin 2\phi\cos\alpha_Q, \tag{4.71}$$

again based on Eq. (4.39) and Eq. (4.54).

The derivatives $\partial V_t/\partial\psi$ and $\partial^2 V_t/\partial\psi^2$ are given by Eq. (4.55) and Eq. (4.66), respectively. The mixed second derivatives $(V_t)_{xz}$ and $(V_t)_{yz}$ read according to Tscherning (1976):

$$\left.\frac{\partial^2 V_t}{\partial x\partial z}\right|_{\mathbf{r}=\mathbf{r}_P} = -\left.\frac{1}{r^2}\frac{\partial V_t}{\partial\varphi}\right|_{\mathbf{r}=\mathbf{r}_P} + \left.\frac{1}{r}\frac{\partial^2 V_t}{\partial\varphi\partial r}\right|_{\mathbf{r}=\mathbf{r}_P}, \tag{4.72}$$

$$\left.\frac{\partial^2 V_t}{\partial y\partial z}\right|_{\mathbf{r}=\mathbf{r}_P} = -\left.\frac{1}{r^2\cos\varphi}\frac{\partial V_t}{\partial\lambda}\right|_{\mathbf{r}=\mathbf{r}_P} + \left.\frac{1}{r\cos\varphi}\frac{\partial^2 V_t}{\partial r\partial\lambda}\right|_{\mathbf{r}=\mathbf{r}_P}. \tag{4.73}$$

The first term of Eq. (4.72) is given by Eq. (4.50) and the second term can be determined from the following formula:

$$\left.\frac{1}{r}\frac{\partial^2 V_t}{\partial\varphi\partial r}\right|_{\mathbf{r}=\mathbf{r}_P} = \left.\frac{1}{r}\frac{\partial^2 V_t}{\partial r\partial\psi}\right|_{\mathbf{r}=\mathbf{r}_P}\frac{\partial\psi}{\partial\varphi} = -\left.\frac{1}{r}\frac{\partial^2 V_t}{\partial r\partial\psi}\cos\alpha_Q\right|_{\mathbf{r}=\mathbf{r}_P}, \tag{4.74}$$

with

$$\left.\frac{\partial^2 V_t}{\partial r\partial\psi}\right|_{\mathbf{r}=\mathbf{r}_P} = G\rho_{cr}\iint\limits_{\sigma}\left[\left.\frac{\partial F_2(r,\psi,\xi)}{\partial r}\right|_{\mathbf{r}=\mathbf{r}_P}\right]_{r_{P'}}^{r_Q} d\sigma, \tag{4.75}$$

where

$$\left.\frac{\partial F_2(r,\psi,\xi)}{\partial r}\right|_{\mathbf{r}=\mathbf{r}_P} =: \left.F_5(r,\psi,\xi)\right|_{\mathbf{r}=\mathbf{r}_P}. \tag{4.76}$$

$F_5(r,\psi,\xi)$ can be derived from Eq. (4.56) by differentiating with respect to r and after some rearrangements:

$$\begin{aligned} F_5(r,\psi,\xi) = &\left[-r\xi\sin\psi(\cos\psi(\xi^2+3r^2) + r\xi(1-6\cos^2\psi))l^{-3}(r,\psi,\xi) + \right. \\ &+ \left(6r\xi\sin 2\psi - \sin\psi(\xi^2+3r^2)\right)l^{-1}(r,\psi,\xi) - \\ &- 3r\sin 2\psi\ln|\xi + l(r,\psi,\xi) - r\cos\psi| \\ &\left. + \frac{r\sin\psi(l(r,\psi,\xi)+\xi)}{l(r,\psi,\xi)(l(r,\psi,\xi)+\xi-r\cos\psi)}\,r(3\cos^2\psi - 1)\right]. \end{aligned} \tag{4.77}$$

The first term of the mixed derivatives $(V_t)_{yz}$ (see Eq. 4.73) reads as shown in Eq. (4.57) and the second term can be determined as follows:

$$\frac{1}{r\cos\varphi}\frac{\partial^2 V_t}{\partial r\partial\lambda}\bigg|_{\mathbf{r}=\mathbf{r}_P} = \frac{1}{r\cos\varphi}\frac{\partial^2 V}{\partial r\partial\psi}\bigg|_{\mathbf{r}=\mathbf{r}_P}\frac{\partial\psi}{\partial\lambda} = -\frac{1}{r}\frac{\partial^2 V_t}{\partial r\partial\psi}\sin\alpha_Q\bigg|_{\mathbf{r}=\mathbf{r}_P}, \tag{4.78}$$

with $\partial^2 V_t/\partial r\partial\psi\big|_{\mathbf{r}=\mathbf{r}_P}$ as given by Eq. (4.75).

Finally, the mixed second derivative in $(V_t)_{xy}$ can be derived based on the formula (Tscherning 1976):

$$\begin{aligned}\frac{\partial^2 V_t}{\partial x\partial y}\bigg|_{\mathbf{r}=\mathbf{r}_P} &= -\frac{\tan\varphi}{r^2\cos\varphi}\frac{\partial V_t}{\partial\lambda}\bigg|_{\mathbf{r}=\mathbf{r}_P} + \frac{1}{r^2\cos\varphi}\frac{\partial^2 V_t}{\partial\varphi\partial\lambda}\bigg|_{\mathbf{r}=\mathbf{r}_P}\\ &= -\frac{\tan\varphi}{r}\frac{\partial V_t}{\partial y}\bigg|_{\mathbf{r}=\mathbf{r}_P} + \frac{1}{r^2\cos\varphi}\frac{\partial V_t}{\partial\varphi\partial\lambda}\bigg|_{\mathbf{r}=\mathbf{r}_P}.\end{aligned} \tag{4.79}$$

The first term at the right hand side of Eq. (4.79) is given by Eq. (4.57) and the second term reads:

$$\frac{1}{r^2\cos\varphi}\frac{\partial^2 V_t}{\partial\varphi\partial\lambda}\bigg|_{\mathbf{r}=\mathbf{r}_P} = \frac{1}{r_P^2\cos\varphi}\left[\frac{\partial^2 V_t}{\partial\psi^2}\frac{\partial\psi}{\partial\varphi}\frac{\partial\psi}{\partial\lambda}\bigg|_{\mathbf{r}=\mathbf{r}_P} + \frac{\partial^2\psi}{\partial\varphi\partial\lambda}\frac{\partial V_t}{\partial\psi}\bigg|_{\mathbf{r}=\mathbf{r}_P}\right], \tag{4.80}$$

where

$$\frac{\partial^2\psi}{\partial\varphi\partial\lambda} = \sin\alpha_Q(\sin\varphi - \cos\varphi\cos\alpha_Q\cot\psi). \tag{4.81}$$

$\partial V_t/\partial\psi$ as well as $\partial^2 V_t/\partial\psi^2$ can be determined using Eq. (4.55) and Eq. (4.66), respectively.

4.1.2.2 Effect of the isostatic masses

In the previous section, the effect of the uncompensated topographic masses has been studied. In the following, the contributions of the isostatic compensating masses due to different models will be investigated.

Airy-Heiskanen model The topography of height $H = 0$ corresponds to the normal thickness T of the Earth's crust with the density equal to the density of the topography ρ. The higher the mountains are, the deeper they sink (see Fig. 4.6). Thus the thickness of a root column under a mountain column with height H can be determined by the formulae as given in chapter 3. The potential of the isostatic masses at the computation point P can be determined in the same way as the potential of the topographic masses, see Eq. 4.37

$$V_I\big|_{\mathbf{r}=\mathbf{r}_P} = G\Delta\rho\iint\limits_{\sigma}\left[\int\limits_{R-T-t_Q}^{R-T}\frac{\xi^2}{l}\bigg|_{\mathbf{r}=\mathbf{r}_P}d\xi\right]d\sigma, \tag{4.82}$$

with the spherical surface element $d\sigma$ of a sphere with radius R and the integration variable ξ and l due to

$$l := \sqrt{r^2+\xi^2-2r\xi\cos\psi}. \tag{4.83}$$

The integration interval $(R-T-t_Q,\ R-T)$ can be decomposed again into two parts, the terrain correction $(R-T-t_Q,\ R-T-t_{P'})$ and the shell of thickness $(R-T-t_{P'},\ R-T)$ where $t_{P'}$ is the thickness of the root or the anti-root under the computation point P or P', respectively (Fig. 4.6). Then the formula for the potential of the isostatic compensation masses can be given by a formula similar to Eq. (4.42) with Eq. (4.43):

$$V_I\big|_{\mathbf{r}=\mathbf{r}_P} = \frac{4\pi G\Delta\rho}{3r_P}\left[(R-T)^3-(R-T-t_P)^3\right] + \frac{G\Delta\rho}{2}\iint\limits_{\sigma}\left[F_0(r,\psi,\xi)\big|_{\mathbf{r}=\mathbf{r}_P}\right]_{R-T-t_P}^{R-T-t_Q}d\sigma, \tag{4.84}$$

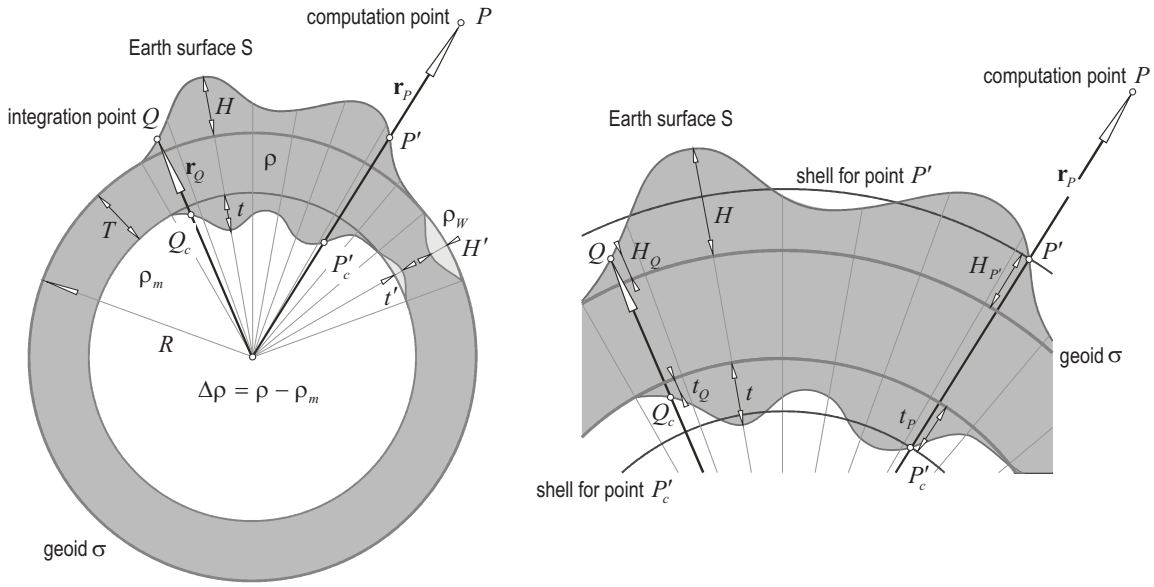

Fig. 4.6: Spherical Airy-Heiskanen topographic-isostatic model

where $\Delta\rho = \rho_m - \rho_{cr}$ is the difference between the density of the mantle and the density of the isostatic compensation masses and $F_0(r, \psi, \xi)$ is given by Eq. (4.43). The first term of Eq. (4.84) represents the effect of the spherical Bouguer shell of the compensating masses for point P'_c.

The first and second derivatives of the potential of the isostatic compensation masses necessary for airborne vector gravimetry and gradiometry at aeroplane or satellite altitude can be determined using the same formulae as applied for the determination of the effects of the topographic masses. Only the integration limits have to be selected properly as illustrated in Fig. 4.6. The radial derivative $(V_I)_z$ (z -direction, see Fig. 4.5) reads

$$\left.\frac{\partial V_I}{\partial z}\right|_{\mathbf{r}=\mathbf{r}_P} = -\frac{4\pi G\Delta\rho}{3r_P^2}\left[(R-T)^3 - (R-T-t_P)^3\right] + G\Delta\rho \iint\limits_{\sigma} \left[F_1(r,\psi,\xi)|_{\mathbf{r}=\mathbf{r}_P}\right]_{R-T-t_P}^{R-T-t_Q} d\sigma, \qquad (4.85)$$

where $F_1(r, \psi, \xi)$ is given by Eq. (4.49). The effects of the compensating masses on the other components of the first and second derivatives can be determined analogously.

The combined effect of the topographic-isostatic masses on the different gravity functionals is the difference between the effect of the topographic masses and the effect of the isostatic compensation masses. It reads e.g.,

$$V_{TI}|_{\mathbf{r}=\mathbf{r}_P} = V_t|_{\mathbf{r}=\mathbf{r}_P} - V_I|_{\mathbf{r}=\mathbf{r}_P}\,. \qquad (4.86)$$

In the previous formulae in spherical approximation the topographic effects are calculated by setting H_{eq} for H. If the density is laterally variable, the thickness of the rock equivalent heights H_{eq} can be determined by the condition that the mass density of an equivalent rock layer is equal to the mass density of the constant crust (see chapter 3).

All the equations derived for the Airy-Heiskanen model can be used also for the Vening-Meinesz model with the only difference that the roots and anti-roots are determined according to the equations given in chapter 3 (see, e.g., Abd-Elmotaal 1995a; Vening Meinesz 1939, 1941).

Pratt-Hayford model In case of the Pratt-Hayford model the effect of the topographic masses is calculated in two parts: one for the land areas and the other for the ocean areas. The same has to be done for the

effects of the isostatic compensation masses. The second derivative of the effect of the topographic masses in the radial direction (see Fig. 4.7) reads:

$$\left.\frac{\partial^2 V_t^L}{\partial z^2}\right|_{\mathbf{r}=\mathbf{r}_P} = G \iint_\sigma \left[F_3(r,\psi,\xi)|_{\mathbf{r}=\mathbf{r}_P} \right]_R^{r_Q} \rho_L d\sigma, \tag{4.87}$$

with the density ρ_L in land areas (see chapter 3) and the function $F_3(r,\psi,\xi)$ as given by Eq. (4.62). If the density of the topographic masses is known then it can be used instead of ρ_L. This formula holds for land areas, i.e., in those cases where the heights H are positive. In case of ocean areas (with the water density ρ_w), that means for negative heights H', the effects of the topographic masses can be given by

$$\left.\frac{\partial^2 V_t^O}{\partial z^2}\right|_{\mathbf{r}=\mathbf{r}_P} = G(\rho_{cr}-\rho_w) \iint_\sigma \left[F_3(r,\psi,\xi)|_{\mathbf{r}=\mathbf{r}_P} \right]_R^{r_Q} d\sigma. \tag{4.88}$$

The effect of the compensation masses for land areas is given by

$$\left.\frac{\partial^2 V_c^L}{\partial z^2}\right|_{\mathbf{r}=\mathbf{r}_P} = G \iint_\sigma \left[F_3(r,\psi,\xi)|_{\mathbf{r}=\mathbf{r}_P} \right]_{R-D}^{R} (\rho_{cr}-\rho_L) d\sigma, \tag{4.89}$$

and for ocean areas by

$$\left.\frac{\partial^2 V_c^O}{\partial z^2}\right|_{\mathbf{r}=\mathbf{r}_P} = G \iint_\sigma \left[F_3(r,\psi,\xi)|_{\mathbf{r}=\mathbf{r}_P} \right]_{R-D}^{r_Q} (\rho_{cr}-\rho_O) d\sigma, \tag{4.90}$$

where ρ_O is the density in the ocean area.

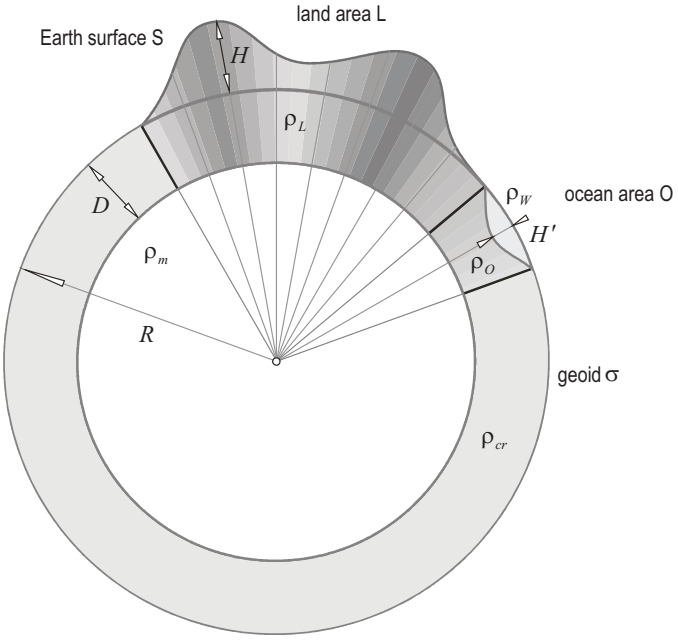

Fig. 4.7: Spherical Pratt-Hayford topographic-isostatic model

The first and second derivatives of the potential of the topographic-isostatic masses can be determined using corresponding formulae as used in section 4.1.2.1, but the different cases corresponding to the four integrals of Eq. (4.87) to Eq. (4.90) have to be distinguished. The concept of a rock equivalent topography will not be applied in this study. The effect of the tesseroid at the computation point must be calculated separately using the prism formulae.

Combined Airy-Pratt model The effects of the topographic-isostatic masses in land areas are calculated according to the Airy-Heiskanen model and the effects of the topographic-compensation masses in ocean areas according to the Pratt-Hayford model.

4.1.2.3 Effect of the condensation masses

In Helmert's methods of condensation, the compensation masses are condensed on a mass layer at a depth D_1 below the geoidal sphere (*Helmert's first method of condensation*) or on the geoid (*Helmert's second method of condensation*) which provides a simpler integral kernel. The potential of the condensed masses at the computation point P can be given by (Heiskanen and Moritz 1967):

$$V_c|_{\mathbf{r}=\mathbf{r}_P} = G \iint_\sigma \left. \frac{k_Q}{l_c} \right|_{\mathbf{r}=\mathbf{r}_P} R_c^2 d\sigma, \tag{4.91}$$

with the spatial distance

$$l_c(r, \psi, R_c) = \sqrt{r^2 + R_c^2 - 2rR_c \cos\psi}, \tag{4.92}$$

the density of the surface layer k_Q, and the radius of the condensation sphere R_c. In case of Helmert's first condensation method or generalized Helmert model of condensation it holds $R_c = R - D_1$, and in case of Helmert's second condensation method $R_c = R$ (see Fig. 4.8). In order to relate the potential of the

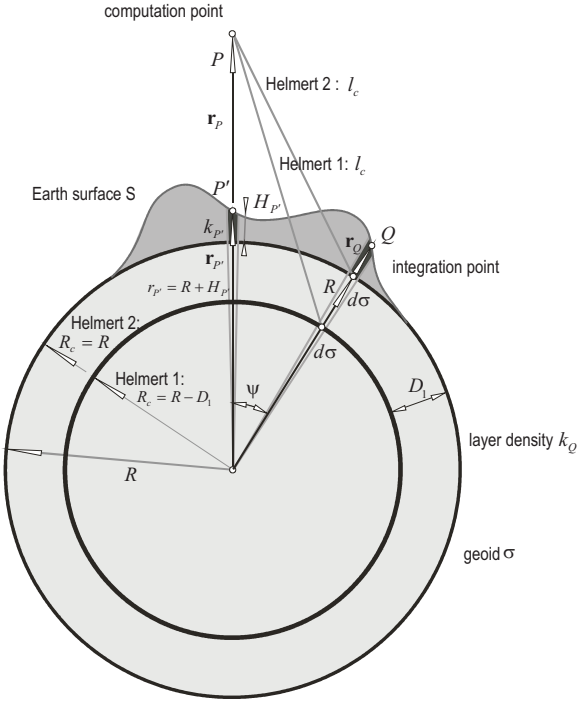

Fig. 4.8: Geometry of Helmert's condensation models

condensed masses to the potential of the topography the layer density k_Q has to be given as a function of the topographical heights. It holds in spherical approximation (see chapter 3):

$$k_Q = \rho_{cr} \frac{r_Q^3 - R^3}{3R_c^2}. \tag{4.93}$$

By adding and subtracting the density corresponding to the point P', the integral in Eq. (4.91) can be written in the following form (Heck 2003):

$$\begin{aligned} V_c|_{\mathbf{r}=\mathbf{r}_P} &= \left.\frac{4\pi G k_{P'} R_c^2}{r}\right|_{\mathbf{r}=\mathbf{r}_P} + G R_c^2 \iint\limits_{\sigma} \left.\frac{k_Q - k_{P'}}{l_c(r,\psi,R_c)}\right|_{\mathbf{r}=\mathbf{r}_P} d\sigma \\ &= \left.\frac{4\pi G \rho (r_{P'}^3 - R^3)}{3r}\right|_{\mathbf{r}=\mathbf{r}_P} + G R_c^2 \iint\limits_{\sigma} \left.\frac{k_Q - k_{P'}}{l_c(r,\psi,R_c)}\right|_{\mathbf{r}=\mathbf{r}_P} d\sigma. \end{aligned} \tag{4.94}$$

The first term of Eq. (4.94) represents the effect of the condensation layer with the layer density $k_{P'}$. The first derivative of the potential of the condensation masses at P, $(V_c)_z$, with the layer density $k_{P'}$ can be determined by differentiation of Eq. (4.94) with respect to r as follows:

$$\left.\frac{\partial V_c}{\partial z}\right|_{\mathbf{r}=\mathbf{r}_P} = \left.\frac{\partial V_c}{\partial r}\right|_{\mathbf{r}=\mathbf{r}_P} = -\left.\frac{4\pi G k_{P'} R_c^2}{r^2}\right|_{\mathbf{r}=\mathbf{r}_P} - G \iint\limits_{\sigma} \left.\frac{(k_Q - k_{p'})}{l_c^3(r,\psi,R_c)}(r - R_c\cos\psi)\right|_{\mathbf{r}=\mathbf{r}_P} R_c^2 d\sigma. \tag{4.95}$$

Inserting the relation

$$\left.\frac{r - R_c\cos\psi}{l_c^3(r,\psi,R_c)}\right|_{\mathbf{r}=\mathbf{r}_P} = \frac{1}{2r}\left.\left(\frac{1}{l_c(r,\psi,R_c)} + \frac{r^2 - R_c^2}{l_c^3(r,\psi,R_c)}\right)\right|_{\mathbf{r}=\mathbf{r}_P}, \tag{4.96}$$

the formula can be rewritten in the form:

$$\begin{aligned} \left.\frac{\partial V_c}{\partial z}\right|_{\mathbf{r}=\mathbf{r}_P} =& -\left.\frac{4\pi G \rho_{cr}(r_{P'}^3 - R^3)}{3r^2}\right|_{\mathbf{r}=\mathbf{r}_P} - \\ &- \frac{G\rho_{cr}}{r_P} \iint\limits_{\sigma} \left(\frac{r_Q^3 - r_{p'}^3}{6}\right) \left.\left(\frac{r^2 - R_c^2}{l_c^3(r,\psi,R_c)} + \frac{1}{l_c(r,\psi,R_c)}\right)\right|_{\mathbf{r}=\mathbf{r}_P} d\sigma. \end{aligned} \tag{4.97}$$

Following a procedure as applied for the determination of Eq. (4.50) and Eq. (4.57), the first derivatives of the condensation masses with respect to x and y, $(V_c)_x$ and $(V_c)_y$, are given by:

$$\left.\frac{\partial V_c}{\partial x}\right|_{\mathbf{r}=\mathbf{r}_P} = -\frac{G\rho_{cr}}{r_P} \iint\limits_{\sigma} \left(\frac{r_Q^3 - r_{p'}^3}{3}\right) \left.\frac{R_c r\sin\psi}{l_c^3(r,\psi,R_c)} \frac{\partial\psi}{\partial\varphi}\right|_{\mathbf{r}=\mathbf{r}_P} d\sigma, \tag{4.98}$$

$$\left.\frac{\partial V_c}{\partial y}\right|_{\mathbf{r}=\mathbf{r}_P} = -\frac{G\rho_{cr}}{r_P\cos\varphi} \iint\limits_{\sigma} \left(\frac{r_Q^3 - r_{p'}^3}{3}\right) \left.\frac{R_c r\sin\psi}{l_c^3(r,\psi,R_c)} \frac{\partial\psi}{\partial\lambda}\right|_{\mathbf{r}=\mathbf{r}_P} d\sigma. \tag{4.99}$$

where $\partial\psi/\partial\varphi$ and $\partial\psi/\partial\lambda$ are given by Eq. (4.53) and Eq. (4.58), respectively.

The second derivatives of the potential of the condensation masses in radial direction, $(V_c)_{zz}$, can be determined by differentiating Eq. (4.97) with respect to r and using Eq. (4.96), so that it follows:

$$\begin{aligned} \left.\frac{\partial^2 V_c}{\partial z^2}\right|_{\mathbf{r}=\mathbf{r}_P} =& \left.\frac{8\pi G \rho_{cr}(r_{P'}^3 - R^3)}{3r^3}\right|_{\mathbf{r}=\mathbf{r}_P} + \\ &+ \frac{G\rho_{cr}}{r_P^2} \iint\limits_{\sigma} \left(\frac{r_Q^3 - r_{p'}^3}{4}\right) \left.\left(\frac{(r^2 - R_c^2)^2}{l_c^5(r,\psi,R_c)} - \frac{4r^2}{3l_c^3(r,\psi,R_c)} + 2\frac{(r^2 - R_c^2)}{l_c^3(r,\psi,R_c)} + \frac{1}{l_c(r,\psi,R_c)}\right)\right|_{\mathbf{r}=\mathbf{r}_P} d\sigma. \end{aligned} \tag{4.100}$$

The second derivatives of the potential of the condensation masses in x direction, $(V_c)_{xx}$, can be determined according to Eq. (4.63) with the first term of this equation as given by Eq. (4.97) and the second term as given by:

$$\begin{aligned}\frac{1}{r^2}\frac{\partial^2 V_t}{\partial\varphi^2}\bigg|_{\mathbf{r}=\mathbf{r}_P} =& \frac{G\rho_{cr}}{r_P^2}\iint\limits_{\sigma}\left(\frac{r_Q^3-r_{p'}^3}{3}\right)\Bigg[-R_c\sin\psi r l_c^{-3}(r,\psi,R_c)\frac{\partial^2\psi}{\partial\varphi^2}+\\ &+\left(-R_c r\cos\psi l_c^{-3}(r,\psi,R_c)+3R_c^2r^2\sin^2\psi l_c^{-5}(r,\psi,R_c)\right)\left(\frac{\partial\psi}{\partial\varphi}\right)^2\Bigg]\Bigg|_{\mathbf{r}=\mathbf{r}_P}d\sigma,\end{aligned} \tag{4.101}$$

based on Eq. (4.64) and Eq. (4.98), where $\partial V_t/\partial\psi$ and $\partial^2 V_t/\partial\psi^2$ are given by Eq. (4.55) and Eq. (4.66), respectively. The formula used for calculating the second derivatives with respect to y, $(V_c)_{yy}$, is given by Eq. (4.69) with the first term given in Eq. (4.97) and the third term in Eq. (4.98). The second term of this equation can be derived based on Eq. (4.70) and Eq. (4.99) as follows:

$$\begin{aligned}&\frac{1}{r^2\cos^2\varphi}\frac{\partial^2 V_c}{\partial\lambda^2}\bigg|_{\mathbf{r}=\mathbf{r}_P}=\frac{1}{r^2\cos^2\varphi}\frac{\partial^2 V_c}{\partial\psi^2}\left(\frac{\partial\psi}{\partial\lambda}\right)^2\bigg|_{\mathbf{r}=\mathbf{r}_P}+\frac{1}{r^2\cos^2\varphi}\frac{\partial V_c}{\partial\psi}\frac{\partial^2\psi}{\partial\lambda^2}\bigg|_{\mathbf{r}=\mathbf{r}_P}\\ &=\frac{G\rho_{cr}}{r_P^2\cos^2\varphi}\iint\limits_{\sigma}\frac{r_Q^3-r_{p'}^3}{3}\left[-R_c r\cos\psi l_c^{-3}(r,\psi,R_c)+3R_c^2r^2\sin^2\psi l_c^{-5}(r,\psi,R_c)\right]\left(\frac{\partial\psi}{\partial\lambda}\right)^2\bigg|_{\mathbf{r}=\mathbf{r}_P}d\sigma-\\ &-\frac{G\rho_{cr}}{r_P^2\cos^2\varphi}\iint\limits_{\sigma}\frac{\left(r_Q^3-r_{P'}^3\right)}{3}R_c r\sin\psi l_c^{-3}(r,\psi,R_c)\frac{\partial^2\psi}{\partial\lambda^2}\bigg|_{\mathbf{r}=\mathbf{r}_P}d\sigma,\end{aligned} \tag{4.102}$$

where $\partial\psi/\partial\lambda$ and $\partial^2\psi/\partial\lambda^2$ due to Eq. (4.58) and Eq. (4.71), respectively. The mixed second derivatives of the potential with respect to xz and xy, $(V_c)_{xz}$ and $(V_c)_{xy}$, read as follows:

$$\frac{\partial^2 V_c}{\partial x\partial z}\bigg|_{\mathbf{r}=\mathbf{r}_P}=-\frac{1}{r}\frac{\partial V_c}{\partial\varphi}\bigg|_{\mathbf{r}=\mathbf{r}_P}+\frac{1}{r}\frac{\partial^2 V_c}{\partial\varphi\partial r}\bigg|_{\mathbf{r}=\mathbf{r}_P}, \tag{4.103}$$

$$\frac{\partial^2 V_c}{\partial x\partial y}\bigg|_{\mathbf{r}=\mathbf{r}_P}=\frac{\tan\varphi}{r}\frac{\partial V_c}{\partial y}\bigg|_{\mathbf{r}=\mathbf{r}_P}+\frac{1}{r^2\cos\varphi}\frac{\partial^2 V_c}{\partial\varphi\partial\lambda}\bigg|_{\mathbf{r}=\mathbf{r}_P}. \tag{4.104}$$

The first terms of Eq. (4.103) and Eq. (4.104) are calculated using Eq. (4.98) and Eq. (4.99), respectively. The second term of Eq. (4.103) can be determined using the following equation:

$$\begin{aligned}\frac{1}{r}\frac{\partial^2 V_c}{\partial\varphi\partial r}\bigg|_{\mathbf{r}=\mathbf{r}_P}=&\frac{G\rho}{r_P}\iint\limits_{\sigma}\left(\frac{r_Q^3-r_{p'}^3}{3}\right)\left[-R_c\sin\psi\, l^{-3}(r,\psi,R_c)+\right.\\ &\left.+3R_c r\sin n\psi(r-R_c\cos\psi)l^{-5}(r,\psi,R_c)\right]\frac{\partial\psi}{\partial\varphi}\bigg|_{\mathbf{r}=\mathbf{r}_P}d\sigma.\end{aligned} \tag{4.105}$$

The second term of Eq. (4.104) is given by

$$\begin{aligned}\frac{1}{r^2\cos\varphi}\frac{\partial^2 V_c}{\partial\varphi\partial\lambda}\bigg|_{\mathbf{r}=\mathbf{r}_P}=&\frac{1}{r_P^2\cos\varphi}\iint\limits_{\sigma}\frac{\left(r_Q^3-r_{P'}^3\right)}{3}\left(\left[-R_c r\cos\psi\, l^{-3}(r,\psi,R_c)+3R_c^2r^2\sin^2\psi l^{-5}(r,\psi,R_c)\right]\cdot\right.\\ &\left.\cdot\frac{\partial\psi}{\partial\lambda}\frac{\partial\psi}{\partial\varphi}-\frac{R_c r\sin\psi}{l_c^3(r,\psi,R_c)}\frac{\partial^2\psi}{\partial\varphi\partial\lambda}\right)\bigg|_{\mathbf{r}=\mathbf{r}_p}d\sigma,\end{aligned} \tag{4.106}$$

where $\partial\psi/\partial\varphi$, $\partial\psi/\partial\lambda$ and $\partial^2\psi/\partial\varphi\partial\lambda$ are given by Eq. (4.53), Eq. (4.58) and Eq. (4.81), respectively. Finally, the effect of the condensation masses in yz- direction, $(V_c)_{yz}$, is calculated as follows:

$$\frac{\partial^2 V_c}{\partial y\partial z}\bigg|_{\mathbf{r}=\mathbf{r}_P}=-\frac{1}{r}\frac{\partial V_c}{\partial y}\bigg|_{\mathbf{r}=\mathbf{r}_P}+\frac{1}{r\cos\varphi}\frac{\partial^2 V_c}{\partial\lambda\partial r}\bigg|_{\mathbf{r}=\mathbf{r}_P}, \tag{4.107}$$

with the first term given by Eq. (4.99). The second term can be determined based on Eq. (4.78) as follows:

$$\frac{1}{r\cos\varphi}\frac{\partial^2 V_c}{\partial\lambda\partial r}\Big|_{\mathbf{r}=\mathbf{r}_P} = -\frac{G\rho_{cr}}{r_P}\iint_\sigma \frac{r_Q^3 - r_{P'}^3}{3}\left[-R_c\sin\psi\, l^{-3}(r,\psi,R_c) + \right.$$
$$\left. +3R_c r\,\sin\psi(r - R_c\cos\psi)l^{-5}(r,\psi,R_c)\right]\sin\alpha_Q\big|_{\mathbf{r}=\mathbf{r}_P}\, d\sigma. \tag{4.108}$$

4.2 Spherical harmonic expansion

In this section, an algorithm for the computation of the spherical harmonic expansion of the topographic-isostatic masses from a digital terrain model (DTM) is presented. The method is based on a series expansion of the inverse distance function – the kernel function of the Newtonian potential. The isostatic compensation of the topography for different topographic-isostatic models is taken into account. This method is appropriate especially for satellite applications. For airborne gravimetry and for gravimetry at the Earth surface a method is presented for the calculation of far-zone effects of the topographic-isostatic masses.

4.2.1 Effects of topographic-isostatic masses in satellite applications

4.2.1.1 The effect of topographic masses

For determining the effect of topographic masses, again we start with the formula for the gravitational potential of the Earth at any point P on or outside the Earth's surface as it is given by Newton's law of gravitation,

$$V^t\big|_{\mathbf{r}=\mathbf{r}_P} = G\iiint_v \frac{\rho(Q)}{l}\Big|_{\mathbf{r}=\mathbf{r}_P} dv. \tag{4.109}$$

The distance between the computation point P and the source point Q, $l|_{\mathbf{r}=\mathbf{r}_P}$, is given by Eq. (4.38). The gravitational potential is harmonic outside the masses and its spherical harmonic expansion is convergent outside a sphere enclosing the total mass of the Earth (see chapter 2). The series expansion for the inverse distance $l|_{\mathbf{r}=\mathbf{r}_P}$ in spherical coordinates can be written as follows (Heiskanen and Moritz 1967, Eq. 1.81):

$$\left[l|_{\mathbf{r}=\mathbf{r}_P}\right]^{-1} = \left\{\begin{array}{lll} \displaystyle\sum_{n=0}^{\infty}\frac{\xi^n}{r_P^{n+1}}P_n(\cos\psi_{PQ}) & \text{for} & r_P > \xi \\ \displaystyle\sum_{n=0}^{\infty}\frac{r_P^n}{\xi^{n+1}}P_n(\cos\psi_{PQ}) & \text{for} & r_P < \xi \end{array}\right\}, \tag{4.110}$$

where $P_n(\cos\psi_{PQ})$ are the Legendre polynomials of degree n and ψ_{PQ} is the spherical distance between the geocentric direction of points P and Q which can be computed by the spherical angle cosine theorem,

$$\cos\psi_{PQ} = \cos\varphi\cos\varphi_Q + \sin\varphi\sin\varphi_Q\cos(\lambda - \lambda_Q). \tag{4.111}$$

Firstly, we refer to a computation point outside the sphere enclosing the total masses of the Earth (for calculating the effect of topographic and isostatic masses at aeroplane or at satellite altitude). Therefore, only the first term of Eq. (4.110) is taken into consideration. The second term has been described in Engels and Grafarend (1993). Applying the addition theorem of the spherical harmonic functions to separate the coordinate dependencies related to point P from those related to point Q gives

$$P_n(\cos\psi_{PQ}) = \frac{1}{2n+1}\sum_{m=0}^{n} P_{nm}(\cos\theta)P_{nm}(\cos\theta_Q)\cdot$$
$$\cdot\left[\cos m\lambda\cos m\lambda_Q + \sin m\lambda\sin m\lambda_Q\right], \tag{4.112}$$

where P_{nm} are the fully normalized associated Legendre functions of degree n and order m. Then the inverse distance can be written as follows (Rummel et al. 1988):

$$\left[l|_{\mathbf{r}=\mathbf{r}_P}\right]^{-1} = \frac{1}{r_P}\sum_{n,m,\alpha}(\xi/r_P)^n \frac{1}{2n+1} Y^{\alpha}_{nm}(p)Y^{\alpha}_{nm}(Q), \tag{4.113}$$

with the surface spherical harmonics

$$\begin{aligned} Y^{\alpha=0}_{nm} &= P^m_n(\cos\theta)\cos m\lambda, \\ Y^{\alpha=1}_{nm} &= P^m_n(\cos\theta)\sin m\lambda. \end{aligned} \tag{4.114}$$

By substituting Eq. (4.113) with Eq. (4.114) into Eq. (4.109), the gravitational potential can be written as follows (Tsoulis 1999a):

$$\begin{aligned} V^t|_{\mathbf{r}=\mathbf{r}_P} =& G\iiint_v \tilde{\rho}(Q)\frac{1}{r_p}\sum_{n=0}^{\infty}\left(\frac{\xi}{r_p}\right)^n \frac{1}{2n+1}\sum_{m=0}^{n}\sum_{\alpha=0}^{1} Y^{\alpha}_{nm}(P)Y^{\alpha}_{nm}(Q)dv, \\ =& \frac{GM}{R}\sum_{n=0}^{\infty}\frac{R^{n+1}}{r_P^{n+1}}\sum_{m=0}^{n}\sum_{\alpha=0}^{1} Y^{\alpha}_{nm}(P)\bar{C}^{\alpha,T}_{nm}, \end{aligned} \tag{4.115}$$

with the mass of the Earth M, the mean Earth radius R, the fully normalized spherical harmonic coefficients $\bar{C}^{\alpha}_{nm}$ and the density function

$$\tilde{\rho}(Q) = \left\{\begin{array}{ll} \rho(Q) & \text{in land areas} \\ \rho_w - \rho_{cr} & \text{in ocean areas} \end{array}\right\}. \tag{4.116}$$

Then the potential coefficients of the topographic masses can be given by (Rummel et al. 1988):

$$\bar{C}^{\alpha,T}_{nm} = \frac{1}{M(2n+1)}\iiint_v \left(\frac{\xi}{R}\right)^n \tilde{\rho}(\xi)Y^{\alpha}_{nm}(\xi)dv, \tag{4.117}$$

with the total mass of the Earth in spherical approximation,

$$M = 4\pi\bar{\rho}R^3/3, \tag{4.118}$$

where $\bar{\rho}$ is the mean density of the Earth . After introducing the volume of the integration element in spherical coordinates $dv = \xi^2 d\xi d\sigma$, the spherical harmonic coefficients of the potential of the topographic masses can be written in the following form:

$$\bar{C}^{\alpha,T}_{nm} = \frac{3}{\bar{\rho}R(2n+1)}\frac{1}{4\pi}\iint_{\sigma} A^T(Q)Y^{\alpha}_{nm}d\sigma, \tag{4.119}$$

where the surface topography part $A^T(Q)$ in case of topographic masses above the geoid is given by

$$A^T(Q) = \int_{\xi=r_g}^{r_s}\tilde{\rho}(Q)\left(\frac{\xi}{R}\right)^{n+2}d\xi. \tag{4.120}$$

The quantities r_g and r_s are the radius of the geoid and the surface of the Earth, respectively. After integration Eq. (4.120) results in:

$$\begin{aligned} A^T(Q) =& \left[\frac{R}{n+3}\tilde{\rho}(Q)\left(\frac{\xi}{R}\right)^{n+3}\right]_{r_g}^{r_s} = \tilde{\rho}(Q)\frac{R}{n+3}\left[\left(\frac{r_s}{R}\right)^{n+3} - \left(\frac{r_g}{R}\right)^{n+3}\right] \\ =& \tilde{\rho}(Q)\frac{R}{n+3}\left[\left(1+\frac{r_s-R}{R}\right)^{n+3} - \left(1+\frac{r_g-R}{R}\right)^{n+3}\right]. \end{aligned} \tag{4.121}$$

After some algebraic operations Eq. (4.121) can be written in the following form:

$$A^T(Q) = \tilde{\rho}(Q)R\left(\left[\left(\frac{r_s-R}{R}\right)-\left(\frac{r_g-R}{R}\right)\right]+\frac{n+2}{2}\left[\left(\frac{r_s-R}{R}\right)^2-\left(\frac{r_g-R}{R}\right)^2\right]+\right.$$
$$\left.+\frac{(n+2)(n+1)}{6}\left[\left(\frac{r_s-R}{R}\right)^3-\left(\frac{r_g-R}{R}\right)^3\right]+\frac{1}{n+3}\sum_{k=4}^{n+3}\binom{n+3}{k}\left[\left(\frac{r_s-R}{R}\right)^k-\left(\frac{r_g-R}{R}\right)^k\right]\right). \tag{4.122}$$

Inserting Eq.(4.122) into Eq.(4.119) gives the potential coefficients of the topographic masses as follows:

$$\bar{C}^{\alpha,T}_{nm} = \frac{3}{(2n+1)\bar{\rho}}\left\{R1^{\alpha}_{nm}+\frac{n+2}{2}R2^{\alpha}_{nm}+\frac{(n+1)(n+2)}{6}R3^{\alpha}_{nm}+\frac{1}{n+3}\sum_{k=4}^{n+3}\binom{n+3}{k}Rk^{\alpha}_{nm}\right\}, \tag{4.123}$$

with the coefficients

$$R1^{\alpha}_{nm} = \frac{1}{4\pi}\iint_{\sigma}\left[\left(\frac{r_s-R}{R}\right)-\left(\frac{r_g-R}{R}\right)\right]\tilde{\rho}(Q)Y^{\alpha}_{nm}d\sigma = \frac{1}{4\pi}\iint_{\sigma}\left[\left(\frac{H_Q-N_Q}{R}\right)\right]\tilde{\rho}(Q)Y^{\alpha}_{nm}d\sigma, \tag{4.124}$$

$$Rk^{\alpha}_{nm} = \frac{1}{4\pi}\iint_{\sigma}\left[\left(\frac{r_s-R}{R}\right)^k-\left(\frac{r_g-R}{R}\right)^k\right]\tilde{\rho}(Q)Y^{\alpha}_{nm}d\sigma\frac{1}{4\pi}\iint_{\sigma}\left[\left(\frac{H^k_Q-N^k_Q}{R^k}\right)\right]\tilde{\rho}(Q)Y^{\alpha}_{nm}d\sigma, \tag{4.125}$$

where N is the geoid heights.

If the geoid is approximated by a sphere with a radius equal to the mean Earth radius, the surface topography part (Eq. 4.120) will be transformed to:

$$A^T(Q) = \int_{\xi=R}^{\xi=R+H_Q}\tilde{\rho}(Q)\left(\frac{\xi}{R}\right)^{n+2}d\xi, \tag{4.126}$$

with the topographic or bathymetric height H or H', respectively. If the topography columns consist of several layers with constant densities in each layer (see chapter 3), then the surface topography part is written as:

$$A^T(Q) = \sum_{i=0}^{l}\int_{\xi=R}^{\xi=R+H_i}(\tilde{\rho}_i(Q)-\tilde{\rho}_{i+1}(Q))\left(\frac{\xi}{R}\right)^{n+2}d\xi = \sum_{i=0}^{l}\int_{\xi=R}^{\xi=R+H_i}\delta\tilde{\rho}_i(Q_i)\left(\frac{\xi}{R}\right)^{n+2}d\xi, \tag{4.127}$$

where $\tilde{\rho}_i(Q)$ is the density of every topographic layer; ρ_0, ρ_{l+1} are defined in chapter 3. After performing the integration with respect to ξ, Eq. (4.127) results in

$$A^T(Q) = R\sum_{i=0}^{l}(\tilde{\rho}_i(Q)-\tilde{\rho}_{i+1}(Q))\left[\frac{H_i}{R}+\frac{(n+2)}{2}\left(\frac{H_i}{R}\right)^2+\frac{(n+2)(n+1)}{6}\left(\frac{H_i}{R}\right)^3+\right.$$
$$\left.+\frac{1}{n+3}\sum_{k=4}^{n+3}\binom{n+3}{k}\left(\frac{H_i}{R}\right)^k\right]. \tag{4.128}$$

Insertion of Eq. (4.128) into Eq. (4.119) gives the potential coefficients of the topographic masses in spherical approximation,

$$\bar{C}^{\alpha,T}_{nm} = \frac{3}{(2n+1)\bar{\rho}}\left\{ha1^{\alpha}_{nm}+\frac{n+2}{2}ha2^{\alpha}_{nm}+\frac{(n+1)(n+2)}{6}ha3^{\alpha}_{nm}+\frac{1}{n+3}\sum_{k=4}^{n+3}\binom{n+3}{k}hak^{\alpha}_{nm}\right\}, \tag{4.129}$$

with the coefficients

$$hak_{nm}^{\alpha} = \frac{1}{4\pi} \iint_{\sigma} \sum_{i=0}^{l} (\tilde{\rho}_i(Q) - \tilde{\rho}_{i+1}(Q)) \left(\frac{H_i}{R}\right)^k Y_{nm}^{\alpha} d\sigma. \tag{4.130}$$

If digital density models (DDM) in 2-D are available only (i.e., the density of the topographic masses is considered to be laterally variable only), then the spherical harmonic potential coefficients of the topographic masses can be simplified as,

$$\bar{C}_{nm}^{\alpha,T} = \frac{3}{(2n+1)\bar{\rho}} \left[h1 d_{nm}^{\alpha} + \frac{n+2}{2} h2 d_{nm}^{\alpha} + \frac{(n+1)(n+2)}{6} h3 d_{nm}^{\alpha} + \frac{1}{n+3} \sum_{k=4}^{n+3} \binom{n+3}{k} \cdot hk d_{nm}^{\alpha} \right], \tag{4.131}$$

with the coefficients

$$hk d_{nm}^{\alpha} = \frac{1}{4\pi} \iint_{\sigma} \left(\frac{H_Q}{R}\right)^k \tilde{\rho}(Q) Y_{nm}^{\alpha} d\sigma. \tag{4.132}$$

To reduce CPU time, in practical application, the topographic heights and bathymetric depths of global DTMs can be replaced by equivalent rock topography heights (see chapter 3). This simplification entails no loss of accuracy because the error introduced by the rock equivalent procedure are smaller than 1% (Classens 2003). After using the rock equivalent topography procedure, Eq. (4.129) can be transformed to (Rummel et al. 1988)

$$\bar{C}_{nm}^{\alpha,T} = \frac{3}{(2n+1)} \frac{\rho_{cr}}{\bar{\rho}} \left\{ h1_{nm}^{\alpha} + \frac{n+2}{2} h2_{nm}^{\alpha} + \frac{(n+1)(n+2)}{6} h3_{nm}^{\alpha} + \frac{1}{n+3} \sum_{k=4}^{n+3} \binom{n+3}{k} \cdot hk_{nm}^{\alpha} \right\}, \tag{4.133}$$

with the expressions

$$hk_{nm}^{\alpha} = \frac{1}{4\pi} \iint_{\sigma} \left(\frac{H_{eq}}{R}\right)^k Y_{nm}^{\alpha} d\sigma. \tag{4.134}$$

For the effects of the topographic masses at satellite altitude, only the first three terms of Eq. (4.134) are necessary and the maximum degree can be restricted to n_{max} =360 (see, e.g., Sun 2002; Sun and Sjöberg 2001). For computing the topographic effects at aeroplane altitudes if the heights of the aeroplane are higher than the maximum height of the topography, the series expansion given in Eq. (4.129) and Eq. (4.133) has to be extended to higher terms (see, e.g., Sun 2002; Sun and Sjöberg 2001). Finally, for determining the indirect effect the computation point is taken to be at the geoid. Then convegent expansion of the potential of the topographic masses for othometric height (in case of land areas) as a series of spherical harmonic reads (Nahavandchi and Sjöberg 1998):

$$V_t = G\rho_{cr} R^2 \sum_{n=0}^{\infty} \iint_{\sigma} \left[\frac{H_Q}{R} + \frac{(1-n)}{2} \left(\frac{H_Q}{R}\right)^2 + \frac{n(n-1)}{6} \left(\frac{H_Q}{R}\right)^3 \right] p_n(\cos\psi_{PQ}) d\sigma. \tag{4.135}$$

After employing the defination of Eq.(4.112), the potential of the topographic masses in case of land areas at the geoid is given by:

$$V_t = 4\pi G\rho_{cr} R^2 \sum_{n=0}^{\infty} \frac{1}{2n+1} \left[\sum_{m=0}^{n} \sum_{\alpha=0}^{1} h1_{nm}^{\alpha} Y_{nm}^{\alpha} - \frac{(n-1)}{2} h2_{nm}^{\alpha} Y_{nm}^{\alpha} + \frac{n(n-1)}{6} h3_{nm}^{\alpha} Y_{nm}^{\alpha} \right], \tag{4.136}$$

where the expressions $h1_{nm}$, $h2_{nm}$ and $h2_{nm}$ are computed using heights above the geoid only. The potential of the topographic masses (in case ocean areas) is computed using the potential coefficients, Eq. (4.133), with the coefficients $h1_{nm}$, $h2_{nm}$ and $h2_{nm}$ computed from bathymetric depths.

4.2.1.2 Effect of the isostatic masses

The topographic-isostatic models due to Airy-Heiskanen, Vening-Meinesz, Pratt-Hayford and the combined Airy-Pratt model as well as Helmert's first and second condensation methods will be formulated in terms of spherical harmonic expansions in the following.

Airy-Heiskanen model The spherical harmonic coefficients of the isostatic masses can be derived similar to those of the topographic masses according to Eq. (4.119) (e.g. Rummel et al. 1988):

$$\bar{C}_{nm}^{\alpha,C} = \frac{3}{\bar{\rho}R(2n+1)}\frac{1}{4\pi}\iint\limits_{\sigma} A^C(Q)Y_{nm}^{\alpha}d\sigma, \tag{4.137}$$

where the isostatic compensation masses are covered by

$$A^C(Q) = \int\limits_{R-T-t_Q}^{R-T} \Delta\rho\left(\frac{\xi}{R}\right)^{n+2} d\xi, \tag{4.138}$$

with the thickness of the crust T and the difference in density between the crust and the mantle $\Delta\rho = \rho_m - \rho_{cr}$. After performing the integration, the isostatic compensation part is given by:

$$A^C(Q) = \Delta\rho\frac{R}{n+3}\left[\left(\frac{R-T)}{R}\right)^{n+3} - \left(\frac{R-T-t_Q}{R}\right)^{n+3}\right]. \tag{4.139}$$

Eq. (4.139) can be written in the following form:

$$\begin{aligned} A^C(Q) = \frac{\Delta\rho R}{n+3}\Bigg[\left(\frac{R-T)}{R}\right)^{n+3} - \left(\frac{R-T}{R}\right)^{n+3}\Bigg(1-(n+3)\frac{t_Q}{(R-T)} + \frac{(n+2)(n+3)}{2}\cdot \\ \cdot\left(\frac{t_Q}{R-T}\right)^2 - \frac{(n+3)(n+2)(n+1)}{6}\left(\frac{t_Q}{R-T}\right)^3 + \frac{1}{(n+3)}\sum_{k=4}^{n+3}\binom{n+3}{k}\left(\frac{-t_Q}{R-T}\right)^k\Bigg)\Bigg], \end{aligned} \tag{4.140}$$

and after some algebraic rearrangements,

$$\begin{aligned} A^C(Q) =& \Delta\rho R\left(\frac{R-T)}{R}\right)^{n+2}\Bigg[\frac{t_Q}{R} - \frac{R(n+2)}{2(R-T)}\left(\frac{t_Q}{R}\right)^2 + \frac{R^2(n+2)(n+1)}{6(R-T)^2}\left(\frac{t_Q}{R}\right)^3 - \\ & - \frac{1}{(n+3)}\sum_{k=4}^{n+3}\binom{n+3}{k}\left(\frac{-t_Q}{R}\right)^k\left(\frac{R}{R-T}\right)^{k-1}\Bigg]. \end{aligned} \tag{4.141}$$

The potential coefficients of the isostatic masses read analogously to Eq. (4.133)

$$\begin{aligned} \bar{C}_{nm}^{\alpha,C} =& \frac{3\Delta\rho}{(2n+1)\bar{\rho}}\left(\frac{R-T)}{R}\right)^{n+2}\Bigg[t1_{nm}^{\alpha} - \frac{R(n+2)}{2(R-T)}t2_{nm}^{\alpha} + \frac{R^2(n+2)(n+1)}{6(R-T)^2}t3_{nm} - \\ & - \frac{1}{(n+3)}\sum_{k=4}^{n+3}\binom{n+3}{k}\left(\frac{R}{R-T}\right)^{k-1}(-1)^k\cdot tk_{nm}^{\alpha}\Bigg], \end{aligned} \tag{4.142}$$

with the terms

$$tk_{nm}^{\alpha} := \frac{1}{4\pi}\iint\limits_{\sigma}\left(\frac{t_Q}{R}\right)^k Y_{nm}^{\alpha}d\sigma. \tag{4.143}$$

The roots and anti-roots are determined based on the formulae as given in chapter 3.

If the density of the topographic masses is considered to be constant and the equivalent rock topography procedures (see chapter 3) are introduced, Eq. (4.142) can be written in the form (after expanding the equivalent roots, Eq. (3.18), to the third order in equivalent heights)

$$\begin{aligned}\bar{C}_{nm}^{\alpha,C} =& \frac{3}{(2n+1)}\frac{\rho_{cr}}{\bar{\rho}}\left(\frac{R-T)}{R}\right)^n \left\{h1_{nm}^{\alpha} + \left[(\eta+1) - \frac{\eta(n+2)}{2}\right] h2_{nm}^{\alpha} + \right. \\ &\left. + \left[\frac{\eta^2(n+2)(n+1)}{6} - (n+2)\left(\eta+\eta^2\right) + \left(\frac{1}{3} + 2\eta + \frac{5}{3}\eta^2\right)\right] h3_{nm}^{\alpha}\right\},\end{aligned} \tag{4.144}$$

with

$$\eta = \left(\frac{R}{R-T}\right)^3 \frac{\rho_{cr}}{\Delta\rho}, \tag{4.145}$$

where the coefficient $h1_{nm}^{\alpha}$, $h2_{nm}^{\alpha}$ and $h3_{nm}^{\alpha}$ are computed using Eq. (4.134).

Pratt-Hayford model The spherical harmonic terms for the Pratt-Hayford model can be derived similar to those for the Airy-Heiskanen model. In this case the potential coefficients are given by (Tsoulis 2001):

$$\bar{C}_{nm}^{\alpha,\Delta} = \frac{3}{\bar{\rho}R(2n+1)}\frac{1}{4\pi}\iint_{\sigma}\left[A^T(Q) - A^C(Q)\right]Y_{nm}^{\alpha}d\sigma, \tag{4.146}$$

where the topography part (consisting of layers with known density) can be represented as:

$$A^T(Q) = \left\{\begin{array}{l} \displaystyle\sum_{i=0}^{l}\int_{R}^{R+H_i}\left[\rho_i(Q) - \rho_{i+1}(Q)\right]\left(\frac{\xi}{R}\right)^{n+2}d\xi \\ \displaystyle\int_{\xi=R-H'_Q}^{R}\left(\frac{\xi}{R}\right)^{n+2}(\rho_w - \rho_{cr})d\xi \end{array}\right\}, \tag{4.147}$$

and the compensating part as:

$$A^C(Q) = \left\{\begin{array}{l} \displaystyle\int_{\xi=R-D}^{R}\left(\frac{\xi}{R}\right)^{n+2}\Delta\rho_L(Q)d\xi \\ \displaystyle\int_{\xi=R-D}^{R-H'_Q}\left(\frac{\xi}{R}\right)^{n+2}\Delta\rho_O(Q)d\xi \end{array}\right\}. \tag{4.148}$$

The integral of Eq. (4.147) for the topographical masses (in case of land area) corresponds to those of the Airy-Heiskanen model according to (Eq. 4.126). For the ocean areas it can be formulated as follows:

$$A_O^T = \left[\rho_w - \rho_{cr}\right]\frac{R}{n+3}\left[\left(\frac{\xi}{R}\right)^{n+3}\right]_{R-H'_Q}^{R} = \left[\rho_w - \rho_{cr}\right]\frac{R}{n+3}\left[1 - \left(\frac{R-H'_Q}{R}\right)^{n+3}\right]. \tag{4.149}$$

Expanding the terms in Eq. (4.149) into a binomial series up to k^{th} order gives

$$A_O^T = \left[\rho_w - \rho_{cr}\right]R\left[\frac{H'_Q}{R} - \frac{(n+2)}{2}\left(\frac{H'_Q}{R}\right)^2 + \frac{(n+1)(n+2)}{6}\left(\frac{H'_Q}{R}\right)^3 - \frac{1}{n+3}\sum_{k=4}^{n+3}\binom{n+3}{k}\cdot\left(\frac{-H'_Q}{R}\right)^k\right]. \tag{4.150}$$

Then, the contribution of the oceanic part to the potential coefficients can be given analogously to Eq. (4.133) by:

$$\begin{aligned}\bar{C}^{\alpha,T,O}_{nm} =& \frac{3}{2n+1}\frac{(\rho_w-\rho_{cr})}{\bar{\rho}}\left\{h'1^{\alpha}_{nm}-\frac{n+2}{2}h'2^{\alpha}_{nm}+\frac{(n+1)(n+2)}{6}h'3^{\alpha}_{nm}-\right.\\ &\left.-\frac{1}{n+3}\sum_{k=4}^{n+3}\binom{n+3}{k}\cdot(-1)^k\,h'k^{\alpha}_{nm}\right\},\end{aligned} \tag{4.151}$$

with the coefficients

$$h'k^{\alpha}_{nm}=\frac{1}{4\pi}\iint_{\sigma}\left(\frac{H'_Q}{R}\right)^k Y^{\alpha}_{nm}d\sigma. \tag{4.152}$$

For calculating the effect of the compensating masses in case of the land part (upper term of Eq. 4.148), the density deficiency is calculated as follows:

$$\Delta\rho^L(Q)=\rho_{cr}-\rho_L(Q). \tag{4.153}$$

Inserting this relation into the first term of Eq. (4.148) and integrating over r_Q yields:

$$A^C_L=\Delta\rho^L(Q)\frac{R}{n+3}\left[1-\left(\frac{R-D}{R}\right)^{n+3}\right]. \tag{4.154}$$

Similarly, the density surplus for the suboceanic columns is given by:

$$\Delta\rho^O(Q)=\rho_{cr}-\rho_O(Q), \tag{4.155}$$

where ρ_O and ρ_L are calculated using the formulae in chapter 3. Inserting Eq. (4.155) in the lower term of Eq. (4.148) and integrating over ξ gives the contribution for the oceanic areas:

$$\begin{aligned}A^C_O =& \Delta\rho^O(Q)R\left[-\left(\frac{H'_Q}{R}\right)+\frac{n+2}{2}\left(\frac{H'_Q}{R}\right)^2-\frac{(n+2)(n+1)}{6}\left(\frac{H'_Q}{R}\right)^3+\right.\\ &\left.+\frac{1}{n+3}\sum_{k=4}^{n+3}\binom{n+3}{k}\cdot\left(\frac{-H'_Q}{R}\right)^k\right]+\Delta\rho^{ocean}\frac{R}{n+3}\left[1-\left(\frac{R-D}{R}\right)^{n+3}\right].\end{aligned} \tag{4.156}$$

Finally, the potential coefficients of the compensating masses for land areas read

$$\bar{C}^{\alpha,C,L}_{nm}=\frac{3}{\bar{\rho}(2n+1)(n+3)}\left[1-\left(\frac{R-D}{R}\right)^{n+3}\right]h^{\alpha}_{dh}, \tag{4.157}$$

and for ocean areas

$$\begin{aligned}\bar{C}^{\alpha,C,O}_{nm} =& \frac{3}{\bar{\rho}(2n+1)}\left\{-h''1^{\alpha}_{nm}+\frac{n+2}{2}h''2^{\alpha}_{nm}-\frac{(n+1)(n+2)}{6}h''3^{\alpha}_{nm}+\right.\\ &\left.+\frac{1}{n+3}\sum_{k=4}^{n+3}\binom{n+3}{k}\cdot(-1)^k\,h''k^{\alpha}_{nm}\right\}+\frac{3}{(2n+1)(n+3)\bar{\rho}}\left[1-\left(\frac{R-D}{R}\right)^{n+3}\right]h''^{\alpha}_{dh},\end{aligned} \tag{4.158}$$

with the terms

$$h^{\alpha}_{dh}=\frac{1}{4\pi}\iint_{\sigma}\Delta\rho^L(Q)Y^{\alpha}_{nm}d\sigma, \tag{4.159}$$

$$h''1^{\alpha}_{nm} = \frac{1}{4\pi}\iint_{\sigma} \Delta\rho^{O}(Q)\frac{H'_Q}{R}Y^{\alpha}_{nm}d\sigma, \tag{4.160}$$

$$h''2^{\alpha}_{nm} = \frac{1}{4\pi}\iint_{\sigma} \Delta\rho^{O}(Q)\left(\frac{H'_Q}{R}\right)^2 Y^{\alpha}_{nm}d\sigma, \tag{4.161}$$

$$h''3^{\alpha}_{nm} = \frac{1}{4\pi}\iint_{\sigma} \Delta\rho^{O}(Q)\left(\frac{H'_Q}{R}\right)^3 Y^{\alpha}_{nm}d\sigma, \tag{4.162}$$

$$h''k^{\alpha}_{nm} = \frac{1}{4\pi}\iint_{\sigma} \Delta\rho^{O}\left(\frac{H'}{R}\right)^k Y^{\alpha}_{nm}d\sigma, \tag{4.163}$$

$$h''^{\alpha}_{dh} = \frac{1}{4\pi}\iint_{\sigma} \Delta\rho^{O}(Q)Y^{\alpha}_{nm}d\sigma. \tag{4.164}$$

If the density of the topographic masses is assumed to be unknown, Eqs. (4.147) and (4.148) can be simplified to

$$A^{T}(Q) = \left\{ \begin{array}{l} \displaystyle\int_{R}^{R+H_Q} \rho_L(Q)\left(\frac{\xi}{R}\right)^{n+2}d\xi \\ \displaystyle\int_{\xi=R-H'_Q}^{R} \left(\frac{\xi}{R}\right)^{n+2}(\rho_w-\rho_{cr})d\xi \end{array} \right\}, \tag{4.165}$$

and the compensation term is given by

$$A^{C}(Q) = \left\{ \begin{array}{l} \displaystyle\int_{\xi=R-D}^{R} \left(\frac{\xi}{R}\right)^{n+2}\Delta\rho_L(Q)d\xi \\ \displaystyle\int_{\xi=R-D}^{R-H'_Q} \left(\frac{\xi}{R}\right)^{n+2}\Delta\rho_O d\xi \end{array} \right\}. \tag{4.166}$$

In this case the potential coefficients of the topographic masses (in case of land area) is given by:

$$\bar{C}^{\alpha,T,L}_{nm} = \frac{3}{(2n+1)\bar{\rho}}\left\{h1L^{\alpha}_{nm} + \frac{n+2}{2}h2L^{\alpha}_{nm} + \frac{(n+1)(n+2)}{6}h3L^{\alpha}_{nm} + \frac{1}{n+3}\sum_{k=4}^{n+3}\binom{n+3}{k}\cdot hkL^{\alpha}_{nm}\right\}, \tag{4.167}$$

with the expressions

$$hkL^{\alpha}_{nm} = \frac{1}{4\pi}\iint_{\sigma}\left(\frac{H_Q}{R}\right)^k \rho_L Y^{\alpha}_{nm}d\sigma. \tag{4.168}$$

After calculating all the potential coefficients of the topographic and compensating masses, the potential coefficients for the Pratt-Hayford model can be determined as follows:

$$\bar{C}^{\alpha,\Delta}_{nm} = \bar{C}^{\alpha,T,L}_{nm} + \bar{C}^{\alpha,T,O}_{nm} - \bar{C}^{\alpha,C,L}_{nm} - \bar{C}^{\alpha,C,O}_{nm}. \tag{4.169}$$

The depths of oceans are adapted from global bathymetry models as absolute values; the concept of equivalent rock topography is not applied in determining the Eq. (4.169). All the previous equations can also be used

for calculating the Pratt-Hayford model in planar approximation. Differences occur only in determining the variable density (chapter 3). An alternative method can be developed in case of the unknown density of the topography for computing the Pratt-Hayford compensation model: In this method the potential coefficients of the topographic masses are considered to be equal the potential coefficients for the Airy-Heiskanen model and the potential coefficients of the compensating masses are calculated in one step according to the following equation:

$$\bar{C}_{nm}^{\alpha,\Delta} = \frac{3}{\bar{\rho}R(2n+1)}\frac{1}{4\pi}\iint_{\sigma}\left[A^T(Q) - A^C(Q)\right]Y_{nm}^{\alpha}d\sigma, \tag{4.170}$$

with the topography and compensation constituents

$$A^T(Q) = \left\{ \begin{array}{l} \int\limits_{R}^{R+H_Q} \rho_{cr}\left(\frac{\xi}{R}\right)^{n+2}d\xi \\ \\ \int\limits_{\xi=R-H'_Q}^{R} \left(\frac{\xi}{R}\right)^{n+2}(\rho_w - \rho_{cr})d\xi \end{array} \right\}, \tag{4.171}$$

$$A^C(Q) = \int\limits_{\xi=R-D}^{R+H_Q}\left(\frac{\xi}{R}\right)^{n+2}\Delta\rho(Q)d\xi, \tag{4.172}$$

where $\Delta\rho(Q)$ is the difference between the density of the integration element and the constant crust density in case of the land and ocean areas and H is the orthometric height in case of the topographic and bathymetric depths in ocean areas. Eq. (4.171) is the same as the equation derived for the Airy-Heiskanen model for calculating the effects of the topographic masses. After integration and insertion of the integral limits, Eq. (4.172) can be written as:

$$\begin{aligned} A^C(Q) =& \Delta\rho(Q)R\left[\left(\frac{HQ}{R}\right) + \frac{n+2}{2}\left(\frac{H_Q}{R}\right)^2 + \frac{(n+2)(n+1)}{6}\left(\frac{H_Q}{R}\right)^3 + \right. \\ &\left. + \frac{1}{n+3}\sum_{k=4}^{n+3}\binom{n+3}{k}\cdot\left(\frac{H_Q}{R}\right)^k\right] + \Delta\rho(Q)\frac{R}{n+3}\left[1 - \left(\frac{R-D}{R}\right)^{n+3}\right]. \end{aligned} \tag{4.173}$$

Finally, the potential coefficients of the compensating masses for land and ocean areas are given by:

$$\begin{aligned} \bar{C}_{nm}^{\alpha,C} =& \frac{3}{\bar{\rho}(2n+1)}\left\{hb_{nm}^{\alpha} + \frac{n+2}{2}h2b_{nm}^{\alpha} + \frac{(n+1)(n+2)}{6}h3b_{nm}^{\alpha} + \right. \\ &\left. + \frac{1}{n+3}\sum_{k=4}^{n+3}\binom{n+3}{k}\cdot hkb_{nm}^{\alpha}\right\} + \frac{3}{(2n+1)(n+3)\bar{\rho}}\left[1 - \left(\frac{R-D}{R}\right)^{n+3}\right]h_{dh}^{\alpha}, \end{aligned} \tag{4.174}$$

with the coefficients

$$hkb_{nm}^{\alpha} = \frac{1}{4\pi}\iint_{\sigma}\Delta\rho(Q)\left(\frac{H_Q}{R}\right)^k Y_{nm}^{\alpha}d\sigma. \tag{4.175}$$

Combined Airy-Pratt model In this model the potential coefficients of the topographic and isostatic compensation masses for continental areas are computed according to the Airy-Heiskanen model and the

potential coefficients of the topographic-isostatic compensation masses for ocean areas according to the Pratt-Hayford model. The spherical harmonic coefficients read as follows,

$$\bar{c}_{nm}^{\alpha,\Delta} = \underbrace{\bar{c}_{nm}^{\alpha,T,L} - \bar{c}_{nm}^{\alpha,C,L}}_{Airy-Heiskanen\ model} + \underbrace{\bar{c}_{nm}^{\alpha,T,O} - \bar{c}_{nm}^{\alpha,C,O}}_{Pratt-Hayford\ model} . \tag{4.176}$$

In this investigation, the concept of rock equivalent topographic heights will not be applied in the case of the Pratt-Hayford and the combined Airy-Pratt models.

Vening-Meinesz isostatic model In case of the Vening-Meinesz model, the isostatic compensation part of the topography is filtered for small scale signals, i.e. for high frequencies. This can be taken into account by using degree-dependent low-pass spectral smoothing filter coefficients β_n for the compensation part. Inserting these filter coefficients into Eq. (4.144) results in the following equation for the spherical harmonic compensation coefficients

$$\bar{c}_{nm}^{\beta,\alpha,C} = \beta_n(n_b,k)\bar{c}_{nm}^{\alpha,C}. \tag{4.177}$$

The spectral amplitude filter coefficients β_n are defined as follows:

$$\beta_n(n_b,k) = \sqrt{\frac{1}{1+(n/n_b)^{2k}}}, \tag{4.178}$$

with the order k of the filter and the band degree n_b at which the power (or the amplitude) is halved (cf. Haagmans 2000). The parameter k defines the steepness of the low-pass filter. For $k = 0$ the coefficients are not filtered at all and for $k = \infty$ all the coefficients below n_b are preserved and the coefficients above n_b are set equal to zero. The choice of n_b can be based upon the spatial scale for which the Airy-Heiskanen model is no longer valid. Haagmans (2000) and Pail (2000) states that the compensation model is not likely to be valid for topographic signals at spatial scales smaller than 200 km while Sjöberg (1998b) gives a value of 500 km. The value of Haagmans corresponds more or less to the non-validity of the compensation model for frequencies above degree 200. In this study, the parameters chosen by Haagmans (2000) are used as $k = 3$ and $n_b = 150$.

4.2.1.3 Helmert's condensation methods

The potential due to the topographic masses in case of Helmert's condensation methods is identical to that of the Airy-Heiskanen model Eq. (4.129). The potential of the condensed masses can be given by the following equation (Heck 2003):

$$V^c|_{\mathbf{r}=\mathbf{r}_P} = G\iint_\sigma \frac{k_Q}{l_c}\bigg|_{\mathbf{r}=\mathbf{r}_P} R_c^2 d\sigma, \tag{4.179}$$

where R_c is the radius of the condensed masses and k_Q is the surface density at the integration point, Q. The surface density can be calculated using the formulae as given in chapter 3. The reciprocal of the distance can be written as spherical harmonic expansion as follows:

$$l_c^{-1} = (r^2 + R_c^2 - 2rR_c\cos\psi)^{-\frac{1}{2}} = \frac{1}{r}\sum_{n=0}^{\infty}\left(\frac{R_c}{r}\right)^n P_n(\cos\psi). \tag{4.180}$$

Inserting Eq. (4.180) into Eq. (4.179) with k_Q as defined in chapter 3 yields:

$$V^c|_{\mathbf{r}=\mathbf{r}_P} = GR_c^2\sum_{n=0}^{\infty}\left(\frac{R}{r_P}\right)^{n+1}\left(\frac{R_c}{R}\right)^n \iint_\sigma \sum_{i=0}^{l}\frac{(\rho_i-\rho_{i+1})}{R_c^2}R^3\left[\left(\frac{H_i}{R}\right)+\left(\frac{H_i}{R}\right)^2+\frac{1}{3}\left(\frac{H_i}{R}\right)^3\right]P_n(\cos\psi)d\sigma.$$

(4.181)

Following the procedures that led to Eq. (4.129), the potential coefficients for the condensed masses are determined as follows:

$$\bar{C}^{\alpha,C}_{nm} = \frac{3}{(2n+1)\bar{\rho}}\left[\left(\frac{R_c}{R}\right)^n ha^{\alpha}_{nm} + \left(\frac{R_c}{R}\right)^n ha2^{\alpha}_{nm} + \left(\frac{R_c}{R}\right)^n ha3^{\alpha}_{nm}\right]. \tag{4.182}$$

The coefficients hak^{α}_{nm} are computed from Eq. (4.130).

Finally, the differences between the potential coefficients of the topographic and condensed masses read

$$\begin{aligned} c^{\alpha,I}_{nm} =& \frac{3}{(2n+1)\bar{\rho}}\left\{\left[1-\left(\frac{R_c}{R}\right)^n\right] ha1^{\alpha}_{nm} + \left[\frac{n+2}{2}-\left(\frac{R_c}{R}\right)^n\right] ha2^{\alpha}_{nm} + \right. \\ &\left. + \frac{1}{3}\left[\frac{(n+2)(n+1)}{2}-\left(\frac{R_c}{R}\right)^n\right] ha3^{\alpha}_{nm} + \frac{1}{n+3}\sum_{k=4}^{n+3}\binom{n+3}{k}\cdot hak^{\alpha}_{nm}\right\}. \end{aligned} \tag{4.183}$$

The quantity R_c is the radius of the (approximate) condensation sphere. In case of *Helmert's first or generalized condensation method* it holds $R_c = R - D_1$, and in case of *Helmert's second condensation method* $R_c = R$.

If the density of the topographic masses is considered to be constant or the rock equivalent topography is used, the potential coefficients of the topographic and condensed masses will be given by:

$$\begin{aligned} c^{\alpha,I}_{nm} =& \frac{3\rho_{cr}}{(2n+1)\bar{\rho}}\left\{\left[1-\left(\frac{R_c}{R}\right)^n\right] h1^{\alpha}_{nm} + \left([\frac{n+2}{2}-\left(\frac{R_c}{R}\right)^n\right] h2^{\alpha}_{nm} + \right. \\ &\left. + \frac{1}{3}\left[\frac{(n+2)(n+1)}{2}-\left(\frac{R_c}{R}\right)^n\right] h3^{\alpha}_{nm} + \frac{1}{n+3}\sum_{k=4}^{n+3}\binom{n+3}{k}\cdot hk^{\alpha}_{nm}\right\}, \end{aligned} \tag{4.184}$$

where the coefficients $h1^{\alpha}_{nm}$, $h2^{\alpha}_{nm}$, $h3^{\alpha}_{nm}$ and hk^{α}_{nm} are computed according to Eq. (4.134).

4.2.2 Spherical harmonic expansion for calculating the far-zone topographical effects

Let us start with the potential of the topographic masses as given by Newton's integral

$$V^t\big|_{\mathbf{r}=\mathbf{r}_P} = G\rho_{cr}\iint_{\sigma}\left[\int_R^{r_Q}\frac{\xi^2}{l}\Big|_{\mathbf{r}=\mathbf{r}_P} d\xi\right] d\sigma. \tag{4.185}$$

The integration domain is divided into two parts $\sigma = \sigma_0 \cup \sigma_{Fz}$ where σ_0 is the near zone and σ_{Fz} is the far-zone. Then the integral in Eq. (4.185) can be written as the sum of the two parts as follows:

$$\begin{aligned} V^t\big|_{\mathbf{r}=\mathbf{r}_P} &= G\rho_{cr}\iint_{\sigma_0}\left[\int_R^{R+H_Q}\frac{\xi^2}{l}\Big|_{\mathbf{r}=\mathbf{r}_P} d\xi\right] d\sigma + G\rho_{cr}\iint_{\sigma_{Fz}}\left[\int_R^{R+H_Q}\frac{\xi^2}{l}\Big|_{\mathbf{r}=\mathbf{r}_P} d\xi\right] d\sigma \\ &=: V^{t_0}\big|_{\mathbf{r}=\mathbf{r}_P} + V^{t_{Fz}}\big|_{\mathbf{r}=\mathbf{r}_P}. \end{aligned} \tag{4.186}$$

Here we will study the term $V^{t_{Fz}}|_{\mathbf{r}=\mathbf{r}_P}$ or quantities related to this term. The quantity $V^{t_{Fz}}|_{\mathbf{r}=\mathbf{r}_P}$ is expressed by a series expansion in terms of Laplace's surface spherical harmonics. Then the truncation coefficients due to Molodenskii will be derived to get an impression of the far-zone effects.

4.2.2.1 The direct topographical effects on gravity

Helmert's second method of condensation The topographical masses are condensed on the geoid as a single layer. The direct topographical effect DTE on gravity was given by Martinec and Vaníček (1994b) in spherical approximation. DTE can be obtained from the difference between the first derivatives of the potential of the topographic and the condensed masses as follows:

$$\begin{aligned} DTE(r,\varphi,\lambda)|_{\mathbf{r}=\mathbf{r}_P} &= \left.\frac{\partial V}{\partial r}\right|_{\mathbf{r}=\mathbf{r}_P} \\ &= G\rho_{cr}\iint_{\sigma}\frac{\partial}{\partial r}\int_{\xi=R}^{R+H_Q} l^{-1}(r,\psi\,,\xi)|_{\mathbf{r}=\mathbf{r}_P}\,\xi^2 d\xi d\sigma - G\rho_{cr}\iint_{\sigma}\left(\int_{\xi=R}^{R+H_Q}\xi^2 d\xi\right)\frac{\partial}{\partial r}l^{-1}(r,\psi,\,R)|_{\mathbf{r}=\mathbf{r}_P}\,d\sigma. \end{aligned} \tag{4.187}$$

The reciprocal distance between the computation and the integration point is given by

$$l^{-1}(r,\psi,\xi) = (r^2+\xi^2-2r\xi\cos\psi)^{-1/2}, \tag{4.188}$$

with the spherical distance ψ expressed as:

$$\cos\psi = \cos\varphi\cos\varphi_Q + \sin\varphi\sin\varphi_Q\cos(\lambda-\lambda_Q). \tag{4.189}$$

The contribution of the integral of Eq. (4.187) can be developed in the following form (Novák et al. 2001):

$$\begin{aligned} DTE|_{\mathbf{r}=\mathbf{r}_P} =& A^b + G\rho_{cr}\iint_{\sigma}\int_{\xi=R+H_{P'}}^{R+H_Q}\frac{\partial}{\partial r}l^{-1}(r,\psi,\xi)\;|_{\mathbf{r}=\mathbf{r}_P}\xi^2 d\xi d\sigma - \\ &- A^{cb} - G\rho_{cr}\iint_{\sigma}\int_{\xi=R+H_{P'}}^{R+H_Q}\frac{\partial}{\partial r}\,l^{-1}(r,\psi,R)\big|_{\mathbf{r}=\mathbf{r}_P}\,\xi^2 d\xi d\sigma. \end{aligned} \tag{4.190}$$

A^b and A^{cb} are the gravitational effects of the topographical Bouguer shell and the corresponding Bouguer layer. The terms A^b and A^{cb} are equal if mass conservation is anticipated (Wichiencharoen 1982). In this case both terms cancel eact other. The difference between the other two terms is called the direct terrain effect DTE^{ter} in the following. The far-zone contribution can be determined in an economic approximative way. This section treats only the far-zone contribution of the topographic-condensation masses which is given by Eq. (4.191) as derived in Appendix A.1.1:

$$\begin{aligned} DTE^{ter}_{FZ}\big|_{\mathbf{r}=\mathbf{r}_P} =& 2\pi G\rho_{cr}\left(\sum_{n=0}^{N_{\max}} t_n(\eta,\psi,\psi_0)H_n(\varphi,\lambda) + \frac{1}{r_P}\sum_{n=0}^{N_{\max}} u_n(\eta,\psi,\psi_0)H_n^2(\varphi,\lambda) - \right. \\ &- \frac{2H_P}{r_P}\sum_{n=0}^{N_{\max}} u_n(\eta,\psi,\psi_0)H_n(\varphi,\lambda) - \sum_{n=0}^{N_{\max}} w_n(H_P,\psi,\psi_0)H_n(\varphi,\lambda) - \\ &\left. - \frac{2(H_{P'}-H_P)}{r_P}\sum_{n=0}^{N_{\max}} v_n(\eta,\psi,\psi_0)H_n(\varphi,\lambda) - \frac{1}{R}\sum_{n=0}^{N_{\max}} w_n(H_P,\psi,\psi_0)H_n^2(\varphi,\lambda)\right) + [C_1 - C_2]\,, \end{aligned} \tag{4.191}$$

where $t_n(\eta,\psi,\psi_0)$, $u_n(\eta,\psi,\psi_0)$, $v_n(\eta,\psi,\psi_0)$ and $w_n(H_P,\psi,\psi_0)$ are Molodenskii's truncation coefficients as defined in Appendix A.1.1 by Eqs. (A.20), (A.25), (A.26) and (A.28), respectively. C_1 and C_2 are given by Eqs. (A.27) and (A.37), respectively.

The Laplace surface spherical harmonics of the height function $H_n(\varphi,\lambda)$ and the squared height function $H_n^2(\varphi,\lambda)$ are given by:

$$H_n(\varphi,\lambda) = \sum_{m=-n}^{n} H_{n,m}Y_{n,m}(\varphi,\lambda), \qquad H_n^2(\varphi,\lambda) = \sum_{m=-n}^{n} H_{n,m}^2 Y_{n,m}(\varphi,\lambda), \tag{4.192}$$

where the coefficients $H_{n,m}$ and $H^2_{n,m}$ can be computed based on a global DTM and $Y_{n,m}(\varphi,\lambda)$ are the surface spherical harmonics of degree n and order m (Heiskanen and Moritz 1967). The numerical computation of the coefficients for the height function and the squared height function will be given in chapter 5.

Helmert's first or generalized method of condensation The topographic masses are condensed on an internal surface at a depth of D_1 below the geoid and parallel to it. To determine the far-zone contribution of the direct terrain effect, Eq. (4.190) has to be modified as follows:

$$\begin{aligned} DTE^{ter}\big|_{\mathbf{r}=\mathbf{r}_P} =& G\rho_{cr} \iint_{\sigma} \frac{\partial}{\partial r} \int_{\xi=R+H_{P'}}^{R+H_Q} l^{-1}(r,\psi,\xi)\,|_{\mathbf{r}=\mathbf{r}_P} \xi^2 d\xi d\sigma - \\ & - G\rho_{cr} \iint_{\sigma} \int_{\xi=R+H_{P'}}^{R+H_Q} \frac{\partial}{\partial r}\, l^{-1}(r,\psi,R-D_1)\big|_{\mathbf{r}=\mathbf{r}_P}\, \xi^2 d\xi d\sigma, \end{aligned} \tag{4.193}$$

where again the attraction of the Bouguer shell and the condensation layer are considered as identical, $A^b \triangleq A^{cb}$. The far-zone direct terrain effect for this method is calculated using Eq. (4.191), where $w_n(H_P,\psi,\psi_0)$ has to be modified as shown in Appendix A.1.2 by the Eqs. (A.36) with (A.38).

Airy-Heiskanen model The mountains of constant density ρ_{cr} float on a mantle of constant density ρ_m with roots reflecting the heights of the mountains. The roots or anti-roots in this model for the linear approximation are given by (Rummel et al. 1988, Lambeck 1988 ; see Fig. 4.6):

$$t = CH, \tag{4.194}$$

with a constant C in case of mountains,

$$C := \left(\frac{R}{R-T}\right)^2 \frac{\rho_{cr}}{\rho_m - \rho_{cr}}, \tag{4.195}$$

and in case of the oceans,

$$C := \left(\frac{R}{R-T}\right)^2 \frac{\rho_{cr} - \rho_w}{\rho_m - \rho_{cr}}, \tag{4.196}$$

where R is the Earth radius, ρ_w is the water density and T is the Airy-Heiskanen depth for zero elevation.

The direct topographical effect for the Airy-Heiskanen model can be given analogously to Eq. (4.190):

$$\begin{aligned} DTE^{ter}\big|_{\mathbf{r}=\mathbf{r}_P} =& G\rho_{cr} \iint_{\sigma} \int_{\xi=R}^{R+H_Q} \frac{\partial}{\partial r} l^{-1}(r,\psi\,,\xi)|_{\mathbf{r}=\mathbf{r}_P}\, \xi^2 d\xi d\sigma - \\ & - G\Delta\rho \iint_{\sigma} \int_{\xi=R-T-t_Q}^{R-T} \frac{\partial}{\partial r} l^{-1}(r,\psi,\xi)|_{\mathbf{r}=\mathbf{r}_P} \xi^2 d\xi d\sigma \\ =& A^b + G\rho \iint_{\sigma} \int_{\xi=R+H_{P'}}^{R+H_Q} \frac{\partial}{\partial r} l^{-1}(r,\psi\,,\xi)|_{\mathbf{r}=\mathbf{r}_P} \xi^2 d\xi d\sigma - \\ & - A^{bi} + G\Delta\rho \iint_{\sigma} \int_{\xi=R-T-t_P}^{R-T-t_Q} \frac{\partial}{\partial r} l^{-1}(r,\psi\,,\xi)|_{\mathbf{r}=\mathbf{r}_P}\, \xi^2 d\xi d\sigma, \end{aligned} \tag{4.197}$$

where t_P is the root under the computation point and t_Q is the thickness of the variable root (Fig. 4.6). A^b and A^{bi} are the effects of the Bouguer shells. These terms are identical if mass conservation is anticipated. In this case both terms cancel each other. Also, the difference between the remaining terms is called in the following the direct terrain effect DTE^{ter}.

The first term on the right hand side of Eq. (4.197) has been derived in (Eq. A24). The second term is determined following the procedures used for the first term of Eq. (4.190). Finally, the direct far-zone terrain effect for this model is given by:

$$\begin{aligned} DTE^{ter}_{FZ}\big|_{\mathbf{r}=\mathbf{r}_P} =& 2\pi G\rho_{cr}\left(\sum_{n=0}^{N_{\max}} t_n(\eta,\psi,\psi_0)H_n(\varphi,\lambda)+\frac{1}{r_P}\sum_{n=0}^{N_{\max}} u_n(\eta,\psi,\psi_0)H_n^2(\varphi,\lambda)-\right.\\ &-\frac{2H_P}{r_P}\sum_{n=0}^{N_{\max}} u_n(\eta,\psi,\psi_0)H_n(\varphi,\lambda)-\frac{2(H_{P'}-H_P)}{r_P}\sum_{n=0}^{N_{\max}} v_n(\eta,\psi,\psi_0)H_n(\varphi,\lambda)\Big)+\\ &+2\pi G\Delta\rho\left[-\sum_{n=0}^{N_{\max}} q_n(\eta,\psi,\psi_0)H_n(\varphi,\lambda)C+\frac{1}{r_P}\sum_{n=0}^{N_{\max}} r_n(\eta,\psi,\psi_0)H_n^2(\varphi,\lambda)C^2+\right.\\ &+\frac{2(H_P+T)}{r_P}\sum_{n=0}^{N_{\max}} r_n(\eta,\psi,\psi_0)H_n(\varphi,\lambda)C-\\ &\left.-\frac{2(T+t_P+H_P)}{r_P}\sum_{n=0}^{N_{\max}} s_n(\eta,\psi,\psi_0)H_n(\varphi,\lambda)C\right]+C_1+C_3, \end{aligned} \tag{4.198}$$

where the coefficients $q_n(\eta,\psi,\psi_0)$, $r_n(\eta,\psi,\psi_0)$ and $s_n(\eta,\psi,\psi_0)$ are calculated based on Eq. (A20), Eq. (A.25) and Eq. (A.26), respectively, with the parameter η given in Eq. (A.41). C_1 and C_3 are defined in Eq. (A.27) and Eq. (A.42), respectively. If the roots and anti-roots are taken according to Eq. (3.18), the DTE^{ter}_{FZ} is given by:

$$\begin{aligned} DTE^{ter}_{FZ}\big|_{\mathbf{r}=\mathbf{r}_P} =& 2\pi G\rho_{cr}\left(\sum_{n=0}^{N_{\max}} t_n(\eta,\psi,\psi_0)H_n(\varphi,\lambda)+\frac{1}{r_P}\sum_{n=0}^{N_{\max}} u_n(\eta,\psi,\psi_0)H_n^2(\varphi,\lambda)-\right.\\ &-\frac{2H_P}{r_P}\sum_{n=0}^{N_{\max}} u_n(\eta,\psi,\psi_0)H_n(\varphi,\lambda)-\frac{2(H_{P'}-H_P)}{r_P}\sum_{n=0}^{N_{\max}} v_n(\eta,\psi,\psi_0)H_n(\varphi,\lambda)\Big)+\\ &+2\pi G\Delta\rho\left[-\sum_{n=0}^{N_{\max}} q_n(\eta,\psi,\psi_0)t_n(\varphi,\lambda)+\frac{1}{r_P}\sum_{n=0}^{N_{\max}} r_n(\eta,\psi,\psi_0)t_n^2(\varphi,\lambda)+\right.\\ &+\frac{2(H_P+T)}{r_P}\sum_{n=0}^{N_{\max}} r_n(\eta,\psi,\psi_0)t_n(\varphi,\lambda)-\\ &\left.-\frac{2(T+t_P+H_P)}{r_P}\sum_{n=0}^{N_{\max}} s_n(\eta,\psi,\psi_0)t_n(\varphi,\lambda)\right]+C_1+C_3', \end{aligned} \tag{4.199}$$

with Laplace surface spherical harmonics of the root function $t_n(\varphi,\lambda)$ and the squared root function $t_n^2(\varphi,\lambda)$ are given by:

$$t_n(\varphi,\lambda)=\sum_{m=-n}^{n} t_{n,m}Y_{n,m}(\varphi,\lambda),\qquad t_n^2(\varphi,\lambda)=\sum_{m=-n}^{n} t_{n,m}^2Y_{n,m}(\varphi,\lambda), \tag{4.200}$$

where the coefficients $t_{n,m}$ and $t_{n,m}^2$ are computed according to Eq. (4.143) and the parameters C_3' is given by

$$\begin{aligned} C_3' =& 2\pi G\Delta\rho_{cr}\left[q_0(\eta,\psi,\psi_0)t_P-\frac{1}{r_P}r_0(\eta,\psi,\psi_0)t_P^2-\right.\\ &\left.-\frac{2(H_P+T)}{r_P}r_0(\eta,\psi,\psi_0)t_P+\frac{2(T+t_P+H_P)}{r_P}s_0(\eta,\psi,\psi_0)\,t_P\right]. \end{aligned} \tag{4.201}$$

4.2.2.2 The primary indirect topographical effect on geoidal heights

The primary indirect topographical effect *PITE* on the geoid is given by Bruns's theorem (Bruns 1878). The potentials of the Bouguer shell and the Bouguer layer of the condensed masses are studied by Vaníček et al. (2001),

$$\delta V = \delta V^{shell} + \delta V^{ter}. \tag{4.202}$$

It reads in terms of the primary indirect effect according to Eq. (4.202)

$$PITE = PITE^{shell} + PITE^{ter} := \frac{\delta V}{\gamma_0} = \frac{\delta V^{shell}}{\gamma_0} + \frac{\delta V^{ter}}{\gamma_0}, \tag{4.203}$$

where δV^{shell} is the difference between the gravitational potential of topographic Bouguer shell and the condensed Bouguer layer.

Helmert's second method of condensation We focus on the term $PITE^{ter}$ which is called the primary indirect terrain effect on the geoid in case of Helmert's second method of condensation. The $PITE^{ter}$ is given by (Martinec and Vaníček 1994a):

$$\begin{aligned} PITE^{ter}\big|_{\mathbf{r}=\mathbf{r}_{P_0}} = \frac{\partial V^{ter}}{\gamma_0} = \frac{G}{\gamma_0}\rho_{cr} \iint\limits_{\sigma} \int\limits_{\xi=R+H_{P'}}^{R+H_Q} l^{-1}(r,\psi,\xi)\,|_{\mathbf{r}=\mathbf{r}_{P_0}} \xi^2 d\xi d\sigma - \\ -\frac{G}{\gamma_0}\rho_{cr} \iint\limits_{\sigma} \int\limits_{\xi=R+H_{P'}}^{R+H_Q} l^{-1}(r,\psi,R)\,|_{\mathbf{r}=\mathbf{r}_{P_0}} \xi^2 d\xi d\sigma. \end{aligned} \tag{4.204}$$

The inner integral of the first term of Eq. (4.204) can be written as follows (Gradshteyn and Ryzhik 1980):

$$\begin{aligned} \int\limits_{R+H_{P'}}^{R+H_Q} l^{-1}(r,\psi,\xi)|_{\mathbf{r}=\mathbf{r}_{P_0}}\, \xi^2 d\xi =& \frac{1}{2}(\xi + 3r_{P_0})l(r_{P_0},\psi,\xi) + \\ &+ \frac{r_{P_0}^2}{2}(3\cos^2\psi - 1)\ln|\xi - r_{P_0}\cos\psi + l(r_{P_0},\psi,\xi)|\Big|_{R+H_{P'}}^{R+H_Q}, \end{aligned} \tag{4.205}$$

with $r_{P_0} = R$.

Using the following parameters

$$\zeta = \frac{\xi}{R} - 1, \quad \zeta_Q = \frac{\xi_Q}{R} - 1, \quad \xi = R + H_{P'}, \quad \eta = \frac{\xi}{R}, \quad \eta_Q = \frac{\xi_Q}{R}, \quad \xi_Q = R + H_Q, \tag{4.206}$$

Eq. (4.205) is written as

$$\begin{aligned} \int\limits_{R+H_{P'}}^{R+H_Q} l^{-1}(r,\psi,\xi)|_{\mathbf{r}=\mathbf{r}_{P_0}}\, \xi^2 d\xi =& \frac{R^2}{2}(\eta_Q + 3\cos\psi)(1 + \eta_Q^2 - 2\eta_Q\cos\psi)^{\frac{1}{2}} + \\ &+ \frac{R^2}{2}(3\cos^2\psi - 1)\ln\left|\frac{\eta_Q - \cos\psi + (1 + \eta_Q^2 - 2\eta_Q\cos\psi)^{\frac{1}{2}}}{\eta - \cos\psi + (1 + \eta^2 - 2\eta\cos\psi)^{\frac{1}{2}}}\right| - \\ &- \frac{R^2}{2}(\eta + 3\cos\psi)(1 + \eta^2 - 2\eta\cos\psi)^{\frac{1}{2}}. \end{aligned} \tag{4.207}$$

The distance function and the logarithmic function in Eq. (4.207) can be developed based on Eq. (A.4) and Eq. (A.9), respectively. The substitutions of Eq. (A.4) and Eq. (A.9) in Eq. (4.207) result in

$$\int_{R+H_{P'}}^{R+H_Q} l^{-1}(r,\psi\,,\xi)|_{\mathbf{r}=\mathbf{r}_{P_0}}\,\xi^2 d\xi = R^2(\zeta_Q-\zeta)N_1(\eta,\psi) + R^2(\zeta_Q^2-\zeta^2)N_2(\eta,\psi) - \\ - R^2(\zeta_Q-\zeta)^2 N_3(\eta,\psi), \tag{4.208}$$

with the integral kernels (Novák et al. 2001)

$$N_1(\eta,\psi) = \frac{3}{4}(2-2\cos\psi)^{\frac{1}{2}}(1+\cos\psi) + \frac{(3\cos^2\psi-1)\left[2+(2-2\cos\psi)^{\frac{1}{2}}\right]}{4\left[\eta-\cos\psi+(1+\eta^2-2\eta\cos\psi)^{\frac{1}{2}}\right]}, \tag{4.209}$$

$$N_2(\eta,\psi) = \frac{5+3\cos^2\psi}{8(2-2\cos\psi)^{\frac{1}{2}}} + \frac{(3\cos^2\psi-1)(1+\cos\psi)}{8(2-2\cos\psi)^{\frac{1}{2}}\left[\eta-\cos\psi+(1+\eta^2-2\eta\cos\psi)^{\frac{1}{2}}\right]}, \tag{4.210}$$

$$N_3(\eta,\psi) = \frac{(3\cos^2\psi-1)\left[3-\cos\psi+2(2-\cos\psi)^{\frac{1}{2}}\right]}{8\left[\eta-\cos\psi+(1+\eta^2-2\eta\cos\psi)^{\frac{1}{2}}\right]^2}. \tag{4.211}$$

Applying the procedure introduced by Molodenskii as shown in detail in Appendix A.1.1, the far-zone primary indirect topographic effect on the geoid heights of the topographic masses for Helmert's second condensation method is given by:

$$\frac{G}{\gamma_0}\rho_{cr}\iint_{\sigma}\int_{\xi=R+H_{P'}}^{R+H_Q} l^{-1}(R,\psi,\xi)\,|_{\mathbf{r}=\mathbf{r}_P}\xi^2 d\xi d\sigma = 2\pi\frac{G}{\gamma_0}\rho_{cr}\left[R\sum_{n=0}^{N_{\max}} a_n^{(1)}(\eta,\psi,\psi_0)H_n(\varphi,\lambda) + \right. \\ \left. + \sum_{n=0}^{N_{\max}} c_n^{(1)}(\eta,\psi,\psi_0)H_n^2(\varphi,\lambda) + 2H_{P'}\sum_{n=0}^{N_{\max}} b_n^{(1)}(\eta,\psi,\psi_0)H_n(\varphi,\lambda) + C_4\right. \tag{4.212}$$

and for the condensed masses analogously to Eq. (A.33)

$$-\frac{G}{\gamma_0}\rho_{cr}\iint_{\sigma}\int_{\xi=R+H_{P'}}^{R+H_Q} l^{-1}(R,\psi,R)\,\xi^2 d\xi\big|_{\mathbf{r}=\mathbf{r}_{P_0}} d\sigma = -2\pi\frac{G}{\gamma_0}\rho_{cr}\left[R\sum_{n=0}^{N_{\max}} e_n^{(1)}(\eta,\psi,\psi_0)H_n(\varphi,\lambda) + \right. \\ \left. + \sum_{n=0}^{N_{\max}} e_n^{(1)}(\psi,\psi_0)H_n^2(\varphi,\lambda)\right] + C_5. \tag{4.213}$$

The truncation coefficients of Eq. (4.212) and Eq. (4.213) are given by:

$$a_n^{(1)}(\eta,\psi,\psi_0) = \int_{\psi=\psi_0}^{\pi} N_1(\eta,\psi)P_n(\cos\psi)\sin\psi d\psi, \tag{4.214}$$

$$c_n^{(1)}(\eta,\psi,\psi_0) = \int_{\psi=\psi_0}^{\pi} \left[N_2(\eta,\psi)-N_3(\eta,\psi)\right]P_n(\cos\psi)\sin\psi d\psi, \tag{4.215}$$

$$b_n^{(1)}(\eta,\psi,\psi_0) = \int_{\psi=\psi_0}^{\pi} N_3(\eta,\psi)P_n(\cos\psi)\sin\psi d\psi, \tag{4.216}$$

$$e_n^{(1)}(\psi,\psi_0) = R \int_{\psi=\psi_0}^{\pi} l^{-1}(R,\psi,R) P_n(\cos\psi)\sin\psi d\psi, \tag{4.217}$$

with the parameter

$$\eta = \frac{R+H_{P'}}{R}. \tag{4.218}$$

The terms C_4 and C_5 are given by:

$$C_4 = \frac{2\pi G\rho}{\gamma_0}\left[-H_{P'}Ra_0^{(1)}(\eta,\psi,\psi_0) - H_{P'}^2 c_0^{(1)}(\eta,\psi,\psi_0)\ -2H_{P'}^2 b_0^{(1)}(\eta,\psi,\psi_0)\right], \tag{4.219}$$

$$C_5 = \frac{2\pi G\rho}{\gamma_0}\left[e_0(\psi,\psi_0)RH_{P'} + e_0\ (\psi,\psi_0)H_{P'}^2\right]. \tag{4.220}$$

Helmert's first or generalized method of condensation The coefficients $e_n^{(1)}(\psi,\psi_0)$ of Eq. (4.217) have to be replaced by:

$$e_n^{(1)}(\psi,\psi_0,D_1) = R \int_{\psi=\psi_0}^{\pi} l^{-1}(R,\psi,R-D_1) P_n(\cos\psi)\sin\psi d\psi. \tag{4.221}$$

Airy-Heiskanen model The far-zone primary indirect terrain effect for the topographic-isostatic masses is given by:

$$\begin{aligned} PITE^{ter}\big|_{\mathbf{r}=\mathbf{r}_{P_0}} =& \frac{G}{\gamma_0}\rho_{cr}\iint_{\sigma}\int_{\xi=R+H_{P'}}^{R+H_Q} l^{-1}(R,\psi,\xi)|_{\mathbf{r}=\mathbf{r}_{P_0}}\,\xi^2 d\xi d\sigma - \\ &- \frac{G}{\gamma_0}\Delta\rho\iint_{\sigma}\int_{\xi=R-T-t_P}^{R-T-t_Q} l^{-1}(R,\psi,\xi)|_{\mathbf{r}=\mathbf{r}_{P_0}}\,\xi^2 d\xi d\sigma. \end{aligned} \tag{4.222}$$

The first term of Eq. (4.222) represents the effect of the topographic masses and is given by Eq. (4.212). The second term can be derived using the same procedure as used in Eq. (4.205), resulting in

$$\begin{aligned} \int_{R-T-t_p}^{R-T-t_Q} l^{-1}(r,\psi\ ,\xi)|_{\mathbf{r}=\mathbf{r}_{P_0}}\,\xi^2 d\xi =& R^2(\zeta_Q-\zeta)N_1(\eta,\psi) + R^2(\zeta_Q^2-\zeta^2)N_2(\eta,\psi) - \\ &- R^2(\zeta_Q-\zeta)^2 N_3(\eta,\psi), \end{aligned} \tag{4.223}$$

with the parameters

$$\zeta = \frac{\xi}{R} - 1, \quad \zeta_Q = \frac{\xi_Q}{R} - 1, \quad \xi = R-T-t_p, \quad \eta = \frac{\xi}{R}, \quad \eta_Q = \frac{\xi_Q}{R}, \quad \xi_Q = R-T-t_Q. \tag{4.224}$$

$N_1(\eta,\psi), N_2(\eta,\psi)$ and $N_3(\eta,\psi)$ are given by Eq. (4.209) to Eq. (4.211) with the parameter η as defined in Eq. (4.222).

Inserting the integration limits and the parameters, as shown in Eq. (4.224), Eq. (4.223) can be transformed into the following practical computation formula:

$$\begin{aligned} \int_{R-T-t_P}^{R-T-t_Q} l^{-1}(r,\psi,\xi)\,\xi^2 d\xi\Big|_{\mathbf{r}=\mathbf{r}_{P_0}} =& -RC\,(H_Q - H_{P'})\,N_1(\eta,\psi) + \\ &+ 2TC\,(H_Q - H_{P'})\,[N_2(\eta,\psi) - N_3(\eta,\psi)] + C^2\left(H_Q^2 - H_{P'}^2\right)\cdot \\ &\cdot [N_2(\eta,\psi) - N_3(\eta,\psi)] + 2C\,[T+t_P]\,N_3(\eta,\psi)(H_Q - H_{P'}). \end{aligned} \tag{4.225}$$

Applying the procedure introduced by Molodenskii as shown in Appendix A.1.1, the second term of Eq. (4.219) is given by:

$$\begin{aligned}\frac{G}{\gamma_0}\Delta\rho \iint\limits_{\sigma\to\sigma_{FZ}} \int\limits_{\xi=R-T-t_p}^{R-T-t_Q} l^{-1}(R,\psi,\xi)\xi^2 d\xi d\sigma = 2\pi\frac{G}{\gamma_0}\Delta\rho \Bigg[-RC\sum_{n=0}^{N_{\max}} o_n^{(1)}(\eta,\psi,\psi_0)H_n(\varphi,\lambda) + \\ + C^2\sum_{n=0}^{N_{\max}} f_n^{(1)}(\eta,\psi,\psi_0)H_n^2(\varphi,\lambda) + 2TC\sum_{n=0}^{N_{\max}} f_n^{(1)}(\eta,\psi,\psi_0)H_n(\varphi,\lambda) + \\ + 2(T+t_P)C\sum_{n=0}^{N_{\max}} g_n^{(1)}(\eta,\psi,\psi_0)H_n(\varphi,\lambda)\Bigg] + C_6,\end{aligned} \tag{4.226}$$

with T and C as defined in Eqs. (4.194) to (4.196). The truncation coefficients of Eq. (4.226) are given by:

$$o_n^{(1)}(\eta,\psi,\psi_0) = \int\limits_{\psi=\psi_0}^{\pi} N_1(\eta,\psi)P_n(\cos\psi)\sin\psi d\psi, \tag{4.227}$$

$$f_n^{(1)}(\eta,\psi,\psi_0) = \int\limits_{\psi=\psi_0}^{\pi} \left[N_2(\eta,\psi) - N_3(\eta,\psi)\right] P_n(\cos\psi)\sin\psi d\psi, \tag{4.228}$$

$$g_n^{(1)}(\eta,\psi,\psi_0) = \int\limits_{\psi=\psi_0}^{\pi} N_3(\eta,\psi)P_n(\cos\psi)\sin\psi d\psi, \tag{4.229}$$

and the parameter C_6 is defined as

$$\begin{aligned}C_6 =& 2\pi\frac{G}{\gamma_0}\Delta\rho\Big[RCH_{P'}o_0^{(1)}(\eta,\psi,\psi_0) - C^2 f_0^{(1)}(\eta,\psi,\psi_0)H_{P'}^2 - \\ & -2TCf_0^{(1)}(\eta,\psi,\psi_0)H_{P'} - 2(T+t_P)Cg_0^{(1)}(\eta,\psi,\psi_0)H_{P'}\Big].\end{aligned} \tag{4.230}$$

If the roots and anti-roots are taken according to Eq. (3.18), the second term of Eq. (4.219) is given by:

$$\begin{aligned}\frac{G}{\gamma_0}\Delta\rho \iint\limits_{\sigma\to\sigma_{FZ}} \int\limits_{\xi=R-T-t_p}^{R-T-t_Q} l^{-1}(R,\psi,\xi)\xi^2 d\xi d\sigma = 2\pi\frac{G}{\gamma_0}\Delta\rho \Bigg[-R\sum_{n=0}^{N_{\max}} o_n^{(1)}(\eta,\psi,\psi_0)t_n(\varphi,\lambda) + \\ + \sum_{n=0}^{N_{\max}} f_n^{(1)}(\eta,\psi,\psi_0)t_n^2(\varphi,\lambda) + 2T\sum_{n=0}^{N_{\max}} f_n^{(1)}(\eta,\psi,\psi_0)t_n(\varphi,\lambda) + \\ + 2(T+t_P)\sum_{n=0}^{N_{\max}} g_n^{(1)}(\eta,\psi,\psi_0)H_t(\varphi,\lambda)\Bigg] + C_6',\end{aligned} \tag{4.231}$$

with

$$\begin{aligned}C_6' =& 2\pi\frac{G}{\gamma_0}\Delta\rho\Big[Rt_P o_0^{(1)}(\eta,\psi,\psi_0) - f_0^{(1)}(\eta,\psi,\psi_0)t_P^2 - \\ & -2Tf_0^{(1)}(\eta,\psi,\psi_0)t_P - 2(T+t_P)g_0^{(1)}(\eta,\psi,\psi_0)t_P\Big].\end{aligned} \tag{4.232}$$

Then, the $PITE_{Fz}^{ter}$ is the sum of Eq. (4.212) and Eq. (4.226) or Eq. (4.231).

4.2.2.3 The secondary indirect topographical effect on gravity

For the Stokes problem the spherical form of the secondary indirect topographical effect on gravity was formulated by Vaníček et al. (1999) as a rescaled value of the residual topographical potential evaluated at a radius equal to the radius of the Earth's surface. The scale is set to $2/r$. The different topographic-isostatic models will be discussed in the following.

Helmert's second method of condensation The difference between the gravitational potential of the topographical shell and its condensed counterpart is zero in case of mass conservation. Then, the secondary indirect terrain effect can be computed using the following expression (Vaníček et al. 1999):

$$\begin{aligned} SITE^{ter}\big|_{\mathbf{r}=\mathbf{r}_{P'}} =& \frac{2G}{r_{P'}}\rho_{cr}\iint_{\sigma}\int_{\xi=R+H_{P'}}^{R+H_Q} l^{-1}(r,\psi\,,\xi)\big|_{\mathbf{r}=\mathbf{r}_{P'}}\,\xi^2 d\xi d\sigma - \\ & - \frac{2G}{r_{P'}}\rho_{cr}\iint_{\sigma}\int_{\xi=R+H_{P'}}^{R+H_Q} l^{-1}(r,\psi,\,R)\big|_{\mathbf{r}=\mathbf{r}_{P'}}\,\xi^2 d\xi d\sigma. \end{aligned} \tag{4.233}$$

Applying the same procedure as used in Eq. (4.205), the first term of Eq. (4.233) results in

$$\begin{aligned} \iint_{\sigma}\int_{\xi=R+H_{P'}}^{R+H_Q} l^{-1}(r,\psi\,,\xi)\big|_{\mathbf{r}=\mathbf{r}_{P'}}\,\xi^2 d\xi d\sigma =& r_{P'}^2(\zeta_Q-\zeta)M_1(\psi) + r_{P'}^2(\zeta_Q^2-\zeta^2)M_2(\psi) - \\ & - r_{P'}^2(\zeta_Q-\zeta)^2 M_3(\psi), \end{aligned} \tag{4.234}$$

with the terms

$$\zeta = \frac{\xi}{r_{P'}} - 1, \quad \zeta_Q = \frac{\xi_Q}{r_{P'}} - 1, \quad \xi = R + H_{P'}, \quad \eta = 1.0, \quad \eta_Q = \frac{\xi_Q}{r_{P'}}, \quad \xi_Q = R + H_Q. \tag{4.235}$$

Inserting the integration limits and the parameters as shown in Eq. (4.235), Eq. (4.234) can be transformed to the following practical computation formula:

$$\begin{aligned} \iint_{\sigma}\int_{\xi=R+H_{P'}}^{R+H_Q} l^{-1}(r,\psi\,,\xi)\big|_{\mathbf{r}=\mathbf{r}_{P'}}\,\xi^2 d\xi d\sigma =& \, r_{P'}(H_Q - H_{P'})M_1(\psi) + \\ & + (H_Q^2 + H_{P'}^2)\left[M_2(\psi) - M_3(\psi)\right] - 2H_{P'}H_Q\left[M_2(\psi) - M_3(\psi)\right], \end{aligned} \tag{4.236}$$

with

$$M_1(\psi) = \frac{3}{4}(2-2\cos\psi)^{\frac{1}{2}}(1+\cos\psi) + \frac{(3\cos^2\psi - 1)\left[2 + (2-2\cos\psi)^{\frac{1}{2}}\right]}{4\left[1 - \cos\psi + (2-2\cos\psi)^{\frac{1}{2}}\right]}, \tag{4.237}$$

$$M_2(\psi) = \frac{5 + 3\cos^2\psi}{8(2-2\cos\psi)^{\frac{1}{2}}} + \frac{(3\cos^2\psi - 1)(1+\cos\psi)}{8(2-2\cos\psi)^{\frac{1}{2}}\left[1 - \cos\psi + (2-2\cos\psi)^{\frac{1}{2}}\right]}, \tag{4.238}$$

$$M_3(\psi) = \frac{(3\cos^2\psi - 1)\left[3 - \cos\psi + 2(2-\cos\psi)^{\frac{1}{2}}\right]}{8\left[1 - \cos\psi + (2-2\cos\psi)^{\frac{1}{2}}\right]^2}. \tag{4.239}$$

Again, applying the procedure introduced by Molodenskii as shown in Appendix A.1.1, the second term of Eq. (4.233) is given by:

$$\frac{2G}{r_{P'}}\rho_{cr}\iint\limits_{\sigma}\int\limits_{\xi=R+H_{P'}}^{R+H_Q} l^{-1}(r,\psi\,,\xi)|_{\mathbf{r}=\mathbf{r}_{P'}}\,\xi^2 d\xi d\sigma = 4\pi G\rho_{cr}\left[\sum_{n=0}^{N_{\max}} a_n^{(2)}(\psi,\psi_0)H_n(\varphi,\lambda) - \right.$$
$$\left. -\frac{2H_{P'}}{r_{P'}}\sum_{n=0}^{N_{\max}} b_n^{(2)}(\psi,\psi_0)H_n(\varphi,\lambda) + \frac{1}{r_{P'}}\sum_{n=0}^{N_{\max}} b_n^{(2)}(\psi,\psi_0)H_n^2(\varphi,\lambda)\right] + C_7, \tag{4.240}$$

with

$$a_n^{(2)}(\psi,\psi_0) = \int\limits_{\psi=\psi_0}^{\pi} M_1(\psi)P_n(\cos\psi)\sin\psi d\psi, \tag{4.241}$$

$$b_n^{(2)}(\psi,\psi_0) = \int\limits_{\psi=\psi_0}^{\pi} \left[M_2(\psi) - M_3(\psi)\right] P_n(\cos\psi)\sin\psi d\psi, \tag{4.242}$$

and

$$C_7 = 4\pi G\rho\left[-H_{P'}a_0^{(2)}(\psi,\psi_0) + H_{P'}^2 b_0^{(2)}(\psi,\psi_0)/r_{P'}\right]. \tag{4.243}$$

The second term of Eq. (4.233) is developed based on the procedure used in Eq. (A33) resulting in:

$$-\frac{2G}{r_{P'}}\rho_{cr}\iint\limits_{\sigma}\int\limits_{\xi=R+H_{P'}}^{R+H_Q} l^{-1}(r,\psi,\,R)|_{\mathbf{r}=\mathbf{r}_{P'}}\,\xi^2 d\xi d\sigma = \frac{-4\pi G\rho_{cr}}{r_{P'}}\left[\sum_{n=0}^{N_{\max}} d_n^{(2)}(H_{P'},\psi,\psi_0)H_n(\varphi,\lambda) + \right.$$
$$\left. +\frac{1}{R}\sum_{n=0}^{N_{\max}} d_n^{(2)}(H_{P'},\psi,\psi_0)H_n^2(\varphi,\lambda)\right] + C_8, \tag{4.244}$$

where the Molodenskii truncation coefficient $d_n^{(2)}(H_{P'},\psi,\psi_0)$ is given by:

$$d_n^{(2)}(H_{P'},\psi,\psi_0) = R^2\int\limits_{\psi=\psi_0}^{\pi} M_4(H_{P'},\psi)P_n(\cos\psi)\sin\psi d\psi, \tag{4.245}$$

with the integral kernel

$$M_4(H_{P'},\psi) = \frac{1}{l(R+H_{P'},\psi,R)}. \tag{4.246}$$

The parameter C_8 is defined as:

$$C_8 = \frac{4\pi G\rho}{r_{P'}}\left[d_0^{(2)}H_{P'} + \frac{1}{R}d_0^{(2)}H_{P'}^2\right]. \tag{4.247}$$

Helmert's first or generalized method of condensation The following coefficient $M_4(H_{P'},\psi,D_1)$ has to be used instead of Eq. (4.246):

$$M_4(H_{P'},\psi,D_1) = \frac{1}{l(R+H_{P'},\psi,R-D_1)}. \tag{4.248}$$

Airy-Heiskanen model For this model, the far-zone contribution of the topographic-isostatic terrain masses can be determined as follows (Novàk et al. 2001):

$$\begin{aligned} SITE^{ter}\big|_{\mathbf{r}=\mathbf{r}_{P'}} =& \frac{2G}{R}\rho_{cr}\iint_{\sigma}\int_{\xi=R+H_{p'}}^{R+H_Q} l^{-1}(r,\psi,\xi)|_{\mathbf{r}=\mathbf{r}_{P'}}\,\xi^2 d\xi d\sigma + \\ &+ \frac{2G}{R}\Delta\rho\iint_{\sigma}\int_{\xi=R-T-t_P}^{R-T-t_Q} l^{-1}(r,\psi,\xi)|_{\mathbf{r}=\mathbf{r}_{P'}}\xi^2 d\xi d\sigma. \end{aligned} \tag{4.249}$$

The first term of Eq. (4.249) is given by Eq. (4.240). Following the same procedures as used for the determination of the direct topographic-isostatic effect, the inner integral of the second term of Eq. (4.249) can be written as:

$$\begin{aligned} \int_{\xi=R-T-t_P}^{R-T-t_Q} l^{-1}(r_P,\psi,\xi)|_{\mathbf{r}=\mathbf{r}_{P'}}\xi^2 d\xi =& -r_{P'}\left(H_Q - H_{P'}\right)N_1(\eta,\psi)C + 2(H_{P'}+T)\left(H_Q - H_{P'}\right)\cdot \\ &\cdot C\left[N_2(\eta,\psi) - N_3(\eta,\psi)\right] + \left(H_Q^2 - H_{P'}^2\right)\left[N_2(\eta,\psi) - N_3(\eta,\psi)\right]C^2 + \\ &+ 2C\left(H_Q - H_{P'}\right)N_3(\eta,\psi)(T + t_P + H_{P'}). \end{aligned} \tag{4.250}$$

The integral kernels $N_1(\eta,\psi)$, $N_2(\eta,\psi)$ and $N_3(\eta,\psi)$ are determined based on Eq. (4.209) to Eq. (4.211), with the parameter $\eta = R - T - t_p/r_{P'}$.

Again, applying the technique introduced by Molodenskii Eq. (4.250) is written as

$$\begin{aligned} \frac{2G\Delta\rho}{r_{P'}}\int_{\xi=R-T-t_P}^{R-T-t_Q} l^{-1}(r_P,\psi,\xi)|_{\mathbf{r}=\mathbf{r}_{P'}}\xi^2 d\xi =& \frac{4\pi G\Delta\rho}{r_{P'}}\left[-r_{P'}\sum_{n=0}^{N_{\max}} o_n^{(2)}(\eta,\psi,\psi_0)H_n(\varphi,\lambda)C + \right. \\ &+ 2(T+H_{P'})\sum_{n=0}^{N_{\max}} f_n^{(2)}(\eta,\psi,\psi_0)H_n(\varphi,\lambda)C + \sum_{n=0}^{N_{\max}} f_n^{(2)}(\eta,\psi,\psi_0)H_n^2(\varphi,\lambda)C^2 + \\ &\left. +2\sum_{n=0}^{N_{\max}} g_n^{(2)}(\eta,\psi,\psi_0)H_n(\varphi,\lambda)(T+t_P+H_{P'})C\right] + C_9. \end{aligned} \tag{4.251}$$

The truncation coefficients $o_n^{(2)}(\eta,\psi,\psi_0)$, $f_n^{(2)}(\eta,\psi,\psi_0)$ and $g_n^{(2)}(\eta,\psi,\psi_0)$ are calculated based on Eqs. (4.227) to (4.229) but with the parameter $\eta = R - T - t_p/r_{P'}$ and T and C as defined in Eqs. (4.194) to (4.196). The parameter C_9 is determined by:

$$\begin{aligned} C_9 =& \frac{4\pi G\Delta\rho}{r_{P'}}\left[Cr_{P'}o_0^{(2)}(\eta,\psi,\psi_0)H_{P'} - 2C(T+H_{P'})\,f_0^{(2)}(\eta,\psi,\psi_0)H_{P'} - \right. \\ &\left. -C^2 f_0^{(2)}(\eta,\psi,\psi_0)H_{P'}^2 - 2(T + CH_{P'} + H_{P'})CH_{P'}g_0^{(n)}(\eta,\psi,\psi_0)\right]. \end{aligned} \tag{4.252}$$

Also, in case of not using the linear approximation of roots and anti-roots, the second term of Eq. (4.251) is given by:

$$\begin{aligned} \frac{2G\Delta\rho}{r_{P'}}\int_{\xi=R-T-t_P}^{R-T-t_Q} l^{-1}(r_P,\psi,\xi)|_{\mathbf{r}=\mathbf{r}_{P'}}\xi^2 d\xi =& \frac{4\pi G\Delta\rho}{r_{P'}}\left[-r_{P'}\sum_{n=0}^{N_{\max}} o_n^{(2)}(\eta,\psi,\psi_0)t_n(\varphi,\lambda) + \right. \\ &+ 2(T+H_{P'})\sum_{n=0}^{N_{\max}} f_n^{(2)}(\eta,\psi,\psi_0)t_n(\varphi,\lambda)C + \sum_{n=0}^{N_{\max}} f_n^{(2)}(\eta,\psi,\psi_0)t_n^2(\varphi,\lambda) + \\ &\left. +2\sum_{n=0}^{N_{\max}} g_n^{(2)}(\eta,\psi,\psi_0)t_n(\varphi,\lambda)(T+t_P+H_{P'})\right] + C_9', \end{aligned} \tag{4.253}$$

with

$$C_9' = \frac{4\pi G\Delta\rho}{r_{P'}}\Big[r_{P'}o_0^{(2)}(\eta,\psi,\psi_0)t_P - 2(T+H_{P'})\,f_0^{(2)}(\eta,\psi,\psi_0)t_P - \\ -f_0^{(2)}(\eta,\psi,\psi_0)t_P^2 - 2(T+t_P+H_{P'})t_{P'}g_0^{(n)}(\eta,\psi,\psi_0)\Big]. \tag{4.254}$$

The $SITE_{Fz}^{ter}$ of the topographic and isostatic masses is the sum of Eq. (4.244) and Eq. (4.251) or Eq. (4.253).

4.3 Space localizing base functions

The spherical harmonic expansions treated in section 4.2 can be used for calculating topographic-isostatic effects of long and medium and a small part from short wavelength features of the topographic masses at the surface of the Earth or at aeroplane altitudes. This is especially the case also for the reduction of observables at satellite altitudes (SST and SGG observables). Spherical harmonic expansions are also a proper representation for the computation of topographic-isostatic far-zone effects. For the near-zone effects at low altitudes a representation by space-localizing base functions is preferable. They are useful especially in the case of computing the effects of residual topographical masses at the surface of the Earth or at low altitudes as for airborne gravimetry. In this investigation only the formulae for Helmert's methods of condensation are investigated.

4.3.1 Direct topographical effects on gravity

We start from Eq. (4.41) for the determination of the potential of the topographic masses:

$$V^t\big|_{\mathbf{r}=\mathbf{r}_P} = G\rho_{cr}\iint_\sigma \int_R^{R+H_Q} \frac{1}{l(r,\psi,\xi)}\bigg|_{\mathbf{r}=\mathbf{r}_P} \xi^2 d\xi d\sigma. \tag{4.255}$$

Inserting the first term of Eq. (4.110) into Eq. (4.255) and interchanging the summation and the integration results in:

$$V_t\big|_{\mathbf{r}=\mathbf{r}_P} = G\rho_{cr}R^2\left[\sum_{n=0}^{\infty}\left(\frac{R}{r_P}\right)^{n+1}\sum_{k=1}^{n+3}\frac{1}{k}\binom{n+2}{k-1}^k \iint_\sigma P_n(\cos\psi_{PQ})\left(\frac{H_Q}{R}\right)^k d\sigma\right]. \tag{4.256}$$

Similarly, the potential of the condensation masses can be given as:

$$V_c(r_P,\varphi,\lambda) = GR_c^2\iint_\sigma \frac{\kappa_Q}{l(r_P,\psi,R_c)}d\sigma, \tag{4.257}$$

where κ_Q is the single layer density, R_c the radius of the condensed masses and D_1 the Helmert's condensation depth which is equal to zero in case of Helmert's second method of condensation.

If the mass of the topography is considered identical to the mass of the condensed topography (mass-preservation condition), then the single mass layer density in spherical approximation reads as follows:

$$\kappa_Q = \frac{\rho_{cr}}{R^2}\int_R^{R+H_Q}\xi^2 d\xi, \tag{4.258}$$

$$\kappa_Q = \rho_{cr}R\left[\frac{H_Q^1}{R} + \left(\frac{H_Q}{R}\right)^2 + \frac{1}{3}\left(\frac{H_Q}{R}\right)^3\right]. \tag{4.259}$$

Inserting Eq. (4.259) into Eq. (4.257) and following the same procedure as used for the determination of the potential of the topographic masses results in

$$V_t(r_P,\varphi,\lambda) = G\rho_{cr}\frac{R^3}{r_P}\sum_{n=0}^{\infty}\left(\frac{R_c}{r_P}\right)^n \iint_\sigma P_n(\cos\psi_{PQ})\left(\frac{H_Q}{R}+\frac{H_Q^2}{R^2}+\frac{1}{3}\frac{H_Q^3}{R^3}\right)d\sigma. \tag{4.260}$$

Then the residual potential is given by:

$$\begin{aligned}\delta V|_{\mathbf{r}=\mathbf{r}_P} =& G\rho_{cr}R^2\sum_{n=0}^{\infty}\left(\frac{R}{r_P}\right)^{n+1}\left\{\left[1-\left(\frac{R_c}{R}\right)^n\right]\iint_\sigma \frac{1}{R}H_Q^1 P_n(\cos\psi_{PQ})d\sigma+\right.\\ &+\left[\frac{n+2}{2}-\left(\frac{R_c}{R}\right)^n\right]\iint_\sigma \frac{1}{R^2}H_Q^2 P_n(\cos\psi_{PQ})d\sigma+\\ &\left.+\left[\frac{(n+2)(n+1)}{6}-\frac{1}{3}\left(\frac{R_c}{R}\right)^n\right]\iint_\sigma \frac{1}{R^3}H_Q^3 P_n(\cos\psi_{PQ})d\sigma\right\}.\end{aligned} \tag{4.261}$$

Applying the partial radial derivative to Eq. (4.261), we obtain the direct topographical effect as follows:

$$\begin{aligned}DTE|_{\mathbf{r}=\mathbf{r}_P} =& -G\rho_{cr}R\sum_{n=0}^{\infty}\left(\frac{R}{r_P}\right)^{n+2}(n+1)\left\{\left[1-\left(\frac{R_c}{R}\right)^n\right]\frac{1}{R}\iint_\sigma H_Q^1 P_n(\cos\psi_{PQ})d\sigma+\right.\\ &+\left[\frac{n+2}{2}-\left(\frac{R_c}{R}\right)^n\right]\frac{1}{R^2}\iint_\sigma H_Q^2 P_n(\cos\psi_{PQ})d\sigma+\\ &\left.+\left[\frac{(n+2)(n+1)}{6}-\frac{1}{3}\left(\frac{R_c}{R}\right)^n\right]\frac{1}{R^2}\iint_\sigma H_Q^3 P_n(\cos\psi_{PQ})d\sigma\right\}.\end{aligned} \tag{4.262}$$

The topographical heights shall now be represented by the following approximation:

$$H_Q^k = \sum_{i=1}^{I} a_i^k \Phi^k(r_Q, r_{S_i}), \qquad k = 1,2,3,... \tag{4.263}$$

where a_i^k $(k=1,2,3)$ are the unknown base function parameters, r_Q represents the field point and the points r_{s_i} indicate the locations of the i nodal points. As base functions isotropic base functions can be used such as spline functions $\Phi^k(r_Q, r_{S_i})$. A general form of the spline function can be given by:

$$\Phi^k(r_Q, r_{S_i}) = \sum_{n=0}^{N_{\max}} C_n^k P_n(\cos\psi_{QS_i}). \tag{4.264}$$

The coefficients C_n^k define the shape of the spline function; in this particular case degree variances of the heights are used. The quadratic and cubic heights will also be modelled by spline functions. With this definition, the base functions can be interpreted as isotropic and homogenous harmonic spline functions (Freeden et al. 1998). The nodal points can be generated by a uniform subdivision of an icosahedron or selected according to a Gauss-Legendre grid.

Inserting Eq. (4.264) into Eq. (4.263) results in:

$$H_Q^k = \sum_{i=1}^{I} a_i^k \sum_{n=0}^{N\max} C_n^k P_N(\cos\psi_{QS_i}). \tag{4.265}$$

Applying the addition theorem of spherical harmonics

$$P_n(P,Q) = \frac{1}{2n+1}\sum_{m=-n}^{n} Y_{nm}(P)\, Y_{nm}(Q), \tag{4.266}$$

and taking into account the orthogonality relations

$$\iint_{\sigma} Y_{\bar{n}\bar{m}}(Q)\, Y_{nm}(Q)\, d\sigma = 4\pi\delta_{n\bar{n}}\delta_{m\bar{m}}, \tag{4.267}$$

the double integral in Eq. (4.262) can be expressed (e.g., for $k = 1$) as:

$$\begin{aligned}&\sum_{n=0}^{\infty}\left(\frac{R}{r_P}\right)^{n+2}(n+1)\left[1-\left(\frac{R_c}{R}\right)^{n}\right]\frac{1}{R}\iint_{\sigma} H_Q^1 P_n(\cos\psi_{PQ})d\sigma = \\ &\sum_{n=0}^{\infty}\left(\frac{R}{r_P}\right)^{n+2}(n+1)C_n^1\frac{4\pi}{(2n+1)}\left[1-\left(\frac{R_c}{R}\right)^{n}\right]\sum_{i=1}^{I}a_i^1 P_n(\cos\psi_{PS_i}).\end{aligned} \tag{4.268}$$

Eq. (4.268) (for $k = 1, 2, 3$) into Eq. (4.262), the *direct topographical effect* of the residual terrain in terms of spherical splines as base functions is finally given by:

$$\begin{aligned}DTE^{res}|_{\mathbf{r}=\mathbf{r}_P} = &-4\pi G\rho_{cr}R\sum_{n=l}^{N_{\max}}\left(\frac{R}{r_p}\right)^{n+2}\frac{(n+1)}{(2n+1)}\left\{\left[1-\left(\frac{R_c}{R}\right)^{n}\right]\frac{1}{R}\sum_{i=1}^{I}a_i^1C_n^1P_n(\cos\psi_{PS_i})+\right.\\ &+\left[\frac{n+2}{2}-\left(\frac{R_c}{R}\right)^{n}\right]\frac{1}{R^2}\sum_{i=1}^{I}a_i^2C_n^2P_n(\cos\psi_{PS_i})+\\ &\left.+\left[\frac{(n+2)(n+1)}{6}-\frac{1}{3}\left(\frac{R_c}{R}\right)^{n}\right]\frac{1}{R^3}\sum_{i=1}^{I}a_i^3C_n^3P_n(\cos\psi_{PS_i})\right\}.\end{aligned} \tag{4.269}$$

In case of *Helmert's second method of condensation*, Eq. (4.269) will be reduced to

$$\begin{aligned}DTE^{l}\big|_{\mathbf{r}=\mathbf{r}_P} = &-2\pi G\rho_{cr}R\sum_{n=l}^{N_{\max}}\left(\frac{R}{r_P}\right)^{n+2}\frac{n(n+1)}{(2n+1)}\left\{\frac{1}{R^2}\sum_{i=1}^{I}a_i^2C_n^2\ P_n(\cos\psi_{PS_i})+\right.\\ &\left.+\ \frac{(n+3)}{3R^3}\sum_{i=1}^{I}a_i^3C_n^3P_n(\cos\psi_{PS_i})\right\},\end{aligned} \tag{4.270}$$

where l is the minimum degree of the spherical harmonic expansion and is taken to be 0 in case of satellite applications.

4.3.2 Primary indirect topographical effect

The residual potential on the geoid is known as the *primary indirect topographical effect on the potential*. The primary indirect topographical effect on the geoid is given by Bruns's theorem (1878). The potential of the topographic masses on the geoid is given by:

$$V_t(R,\varphi,\lambda) = G\rho_{cr}\iiint_{v}\frac{1}{l(R,\psi,\xi)}dv = G\rho_{cr}\iint_{\sigma}\int_{R}^{R+H_Q}\frac{\xi^2}{l(R,\psi,\xi)}d\xi d\sigma. \tag{4.271}$$

In this case, the Newton integral kernel $l(R,\lambda,\phi)^{-1}$ can be expanded into a convergent series as follows:

$$l^{-1} = \frac{1}{\xi}\sum_{n=0}^{\infty}\left(\frac{R}{\xi}\right)^{n}P_n(\cos\psi_{pQ}). \tag{4.272}$$

Substituting from Eq. (4.272) into Eq. (4.271), results in

$$V_t(R,\varphi,\lambda) = G\rho_{cr}\sum_{n=0}^{\infty} R^n \iint_{\sigma} \int_{R}^{R+H_Q} \xi^{-n+1} d\xi d\sigma. \tag{4.273}$$

Integrating the term in the brackets and expanding the result into a series up to the third order, then the potential of the topographic masses can be given for computation points located at the geoid:

$$V_t(R,\varphi,\lambda) = G\rho_{cr}R^2\sum_{n=0}^{\infty} \iint_{\sigma} \left[\frac{H_Q}{R} + \frac{(1-n)}{2}\left(\frac{H_Q}{R}\right)^2 + \frac{n(n-1)}{6}\left(\frac{H_Q}{R}\right)^3\right] p_n(\cos\psi_{PQ}) d\sigma. \tag{4.274}$$

The corresponding potential of the condensed masses at the geoid is given by:

$$V_c(R,\varphi,\lambda) = GR^2 \iint_{\sigma} \kappa_Q l^{-1}(R,\psi,R_c) d\sigma. \tag{4.275}$$

The Newtonian integration kernel can be expanded again into a convergent series:

$$l^{-1}(R,\psi,R_c) = \frac{1}{R}\sum_{n=0}^{\infty}\left(\frac{R_c}{R}\right)^n P_n(\cos\psi_{pQ}). \tag{4.276}$$

Substituting κ_Q from Eq. (4.258) and $l^{-1}(R,\psi,R)$ from Eq. (4.276) into Eq. (4.275) results in

$$V_{ct}(R,\varphi,\lambda) = G\rho_{cr}R^2\sum_{n=0}^{\infty}\left(\frac{R_c}{R}\right)^n \iint_{\sigma}\left[\frac{H_Q}{R} + \left(\frac{H_Q}{R}\right)^2 + \frac{1}{3}\left(\frac{H_Q}{R}\right)^3\right] p_n(\cos\psi_{PQ}) d\sigma. \tag{4.277}$$

Differencing Eqs. (4.274) and (4.277) yields the residual potential on the geoid,

$$\begin{aligned}\delta V(R,\varphi,\lambda) =& G\rho_{cr}R^2\sum_{n=0}^{\infty}\left\{\left[1-\left(\frac{R_c}{R}\right)^n\right]\frac{1}{R}\iint_{\sigma} H_Q^1 P_n(\cos\psi_{PQ})d\sigma + \right.\\ &+\left[\frac{1-n}{2}-\left(\frac{R_c}{R}\right)^n\right]\frac{1}{R^2}\iint_{\sigma} H_Q^2 P_n(\cos\psi_{PQ})d\sigma + \\ &\left.+\left[\frac{(n-1)n}{6}-\frac{1}{3}\left(\frac{R_c}{R}\right)^n\right]\frac{1}{R^3}\iint_{\sigma} H_Q^3 P_n(\cos\psi_{PQ})d\sigma\right\}.\end{aligned} \tag{4.278}$$

Following the same procedure as used for the direct topographical effect, the band-limited *primary indirect topographical effect (for orthometric height) on the geoid heights* can be given as:

$$\begin{aligned}PITE^{res} =& \frac{4\pi G\rho_{cr}R^2}{\gamma}\sum_{n=l}^{N_{max}}\left\{\frac{1}{2n+1}\left[1-\left(\frac{R_c}{R}\right)^n\right]\frac{1}{R}\sum_{i=1}^{I} a_i^1 C_n^1 P_n(\cos\psi_{PS_i}) + \right.\\ &+\left[\frac{(1-n)}{2}-\left(\frac{R_c}{R}\right)^n\right]\frac{1}{R^2}\sum_{i=1}^{I} a_i^2 C_n^2 P_n(\cos\psi_{PS_i}) + \\ &\left.+\left[\frac{(n-1)n}{2}-\frac{1}{3}\left(\frac{R_c}{R}\right)^n\right]\frac{1}{R^3}\sum_{i=1}^{I} a_i^3 C_n^3 P_n(\cos\psi_{PS_i})\right\},\end{aligned} \tag{4.279}$$

where l stands for the minimum degree and n for the maximum degree. Again in case of *Helmert's second method of condensation*, Eq. (4.279) is given by,

$$\begin{aligned}PITE^{res} =& \frac{2\pi G\rho_{cr}R^2}{\gamma}\sum_{n=l}^{N_{max}}\frac{(n+1)}{(2n+1)}\left\{\frac{-1}{R^2}\sum_{i=1}^{I} a_i^2 C_n^2 P_n(\cos\psi_{PS_i}) + \right.\\ &\left.+\frac{(n-2)}{3}\frac{1}{R^3}\sum_{i=1}^{I} a_i^3 C_n^3 P_n(\cos\psi_{PS_i})\right\}.\end{aligned} \tag{4.280}$$

5. Numerical analysis

In this chapter, the effects of the topographic-isostatic masses for various geodetic observables are investigated numerically. In the first section, the test areas are presented. They are selected such that typical features of the topographic-isostatic effects can be demonstrated. In the second section, computational aspects are discussed. It includes the investigation of discretization effects for the numerical integration method and the calculation procedure of the spherical harmonic coefficients as well as the near and far-zone aspects. In the third section, the effects of topographic-isostatic masses are investigated at the surface of the Earth and at altitude for airborne gravimetry/gradiometry. The near and far-zone effects of the topography are considered in this section. The effects of topographic-isostatic masses in the observables of the Satellite-to-Satellite Tracking (SST) technique and the Satellite Gravity Gradiometry (SGG) are determined in the last section. Throughout the numerical computations the density of the topography and the crust is taken to be 2670 kg/m^3, the density of the mantle 3270 kg/m^3, the mean density of the Earth 5498 kg/m^3 and the density of sea water 1030 kg/m^3. Also, the depths of the Airy-Heiskanen and Vening Meinesz model are taken to be constant and equal to 30 km.

5.1 Test regions

Four different computation areas have been selected to demonstrate typical features of the effects of the topographic-isostatic masses. For airborne gravimetry and gravimetry at the surface of the Earth, the Canadian Rocky Mountains are chosen. In case of airborne gradiometry, the Himalaya region is selected. To give an impression about the effects of the topographic-isostatic masses at satellite altitude, the Asian region is selected. Finally, the total surface of the Earth has been taken to show the effects of topographic-isostatic masses in its global distribution. All test areas will be summarized in the following.

5.1.1 Canadian Rocky Mountains

This area covers the longitude from 241^0 to 244^0 and the latitude from 49^0 to 52^0 (see Fig. 5.1). The digital terrain model GEBCO (General Bathymetric Chart of the Oceans) with one arc-minute resolution (www.ngdc.noaa.gov/mgg/gebco) has been used for the test computations. The topographic heights of this area range from 336 to 3112 m. This area with rough topography has been used for determining the effects of topographic-isostatic masses at the surface of the Earth and at aeroplane altitude.

5.1.2 Himalaya

The Himalaya region is bounded by the meridians of 75^0 and 105^0 eastern longitude and the parallels of 25^0 and 40^0 northern latitude (see Fig. 5.2). Also, the digital terrain model GEBCO with one arc-minute resolution has been used for the numerical computations. The topographic heights range from 0 m to 8424.56 m.

5.1.3 Asia

The Asian area has been taken to be extended from 40^0 to 150^0 in longitude and from -20^0 to 80^0 in latitude (see Fig. 5.3). The digital terrain model ETOPO5 with five arc-minute resolution has been used for the numerical calculation (NOAA 1988). The topographic heights and bathymetric depths range from approximately -7000 m to 9 000 m.

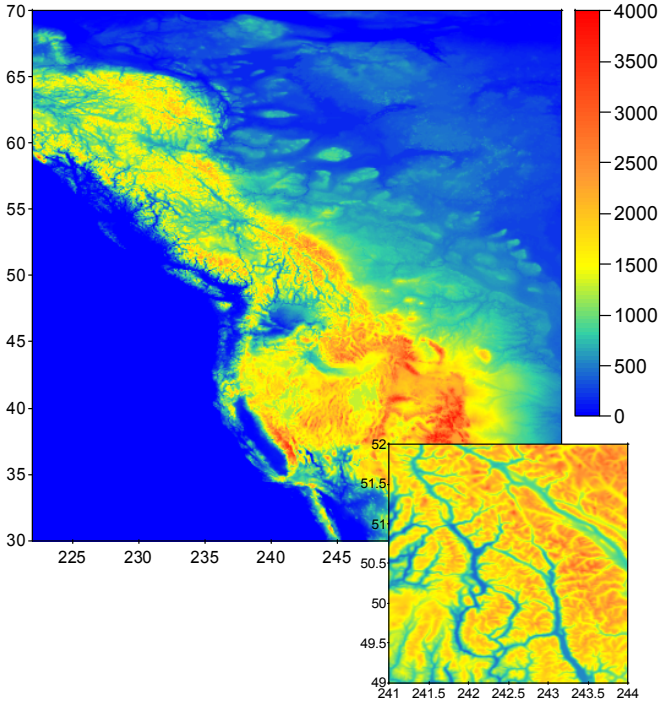

Fig. 5.1: GEBCO topography for Canadian Rocky Mountains (units in meter)

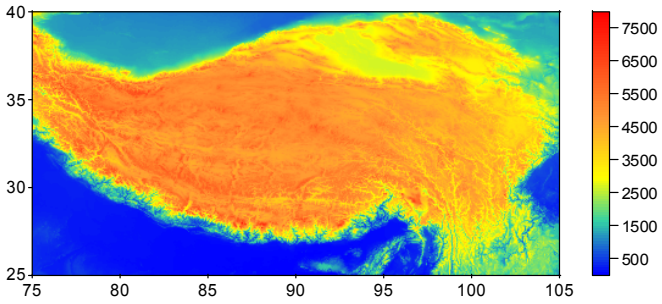

Fig. 5.2: GEBCO topography for Himalaya (units in meter)

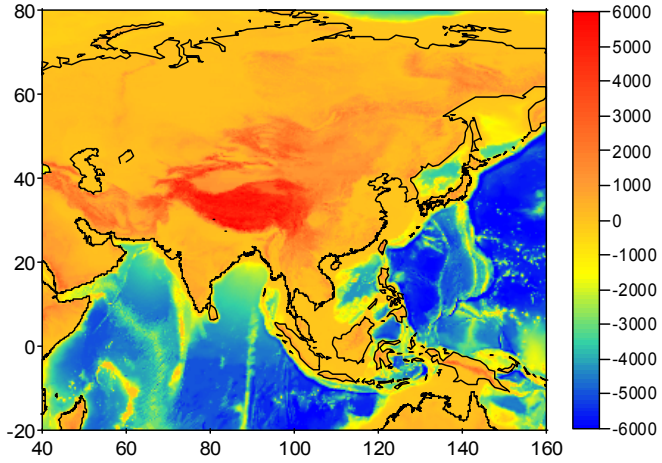

Fig. 5.3: ETOPO5 topography for Asia (units in meter)

5.1.4 Earth

To give an impression about the distribution of the effects of the topographic-isostatic masses, the total surface of the Earth has been taken in the test computations (see Fig. 5.4). Also, the digital terrain model ETOPO5 with five arc-minute resolution has been used for the numerical calculation (NOAA 1988). The topographic heights and bathymetric depths range from approximately -8000 to 9 000 m.

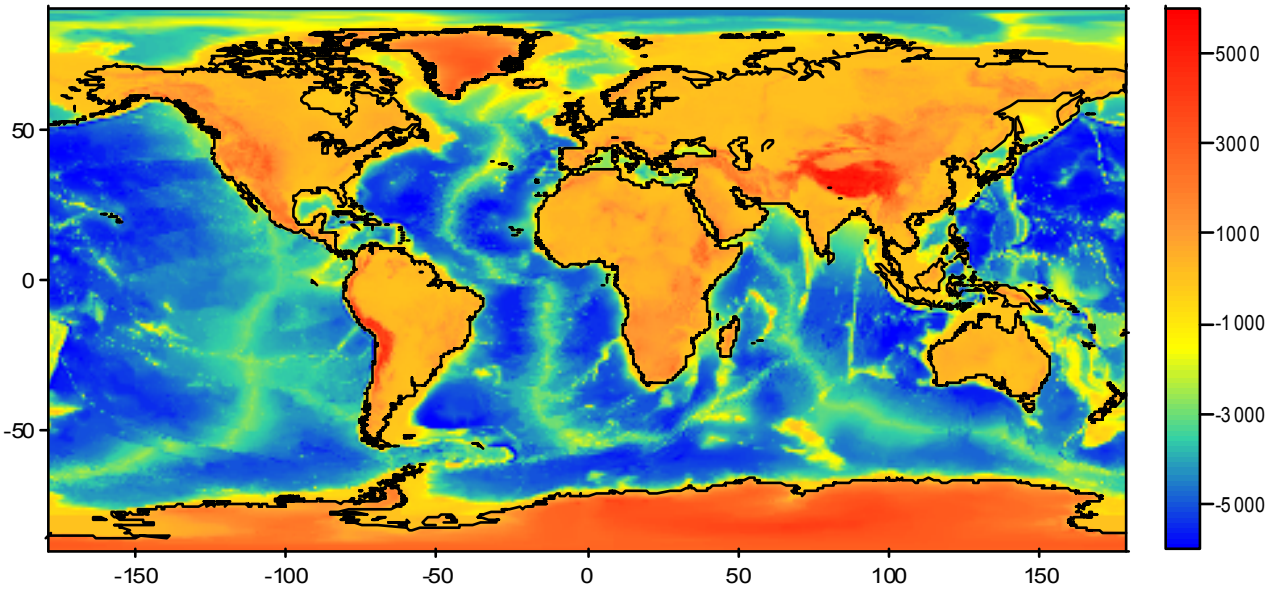

Fig. 5.4: ETOPO5 topography for the Earth (units in meter)

5.2 Computation aspects

5.2.1 Discretization effects

The integral formulae given in section 4.1.2 have been evaluated numerically such that the rigorous spherical volume elements of the integrals defined by the geographical coordinate lines and the topography within these compartments are approximated by mass lines in the center of these compartments. To avoid singularities at the surface of the Earth, the locations of the computation points were selected at the intersection points of the geographical coordinate lines (longitudes and latitudes). The discretization errors of these approximations were investigated in the following for the potential, the first and the second derivatives of the potential for different altitudes of the computation point and different resolutions of the topographic masses.

As a test example the spherical Bouguer shell has been chosen where the different gravitational functionals of this shell can be determined analytically. For the thickness of the shell a value of $\Delta R = 2500\ m$ has been selected; the radius of the inner sphere coincides with the spherical approximation of the Earth, $R_1 = R = 6371\ km$, and for the radius of the outer sphere follows $R_2 = R + \Delta R$. It shall be pointed out that this test example represents an extreme situation in reality which may occur only in few cases, because in the usual applications the numerical computations are restricted to the terrain corrections while the effects of the spherical shell are computed analytically. The true values can be calculated analytically in arbitrary altitudes by the following equations (see chapter 4 for the general formulae). It reads for the potential

$$V_t|_{\mathbf{r}=\mathbf{r}_P} = \frac{4\pi G\rho}{3r_P}(R_2^3 - R_1^3), \tag{5.1}$$

and for the first radial derivative,

$$\left.\frac{\partial V_t}{\partial r}\right|_{\mathbf{r}=\mathbf{r}_P} = -\frac{4\pi G\rho}{3r_p^2}(R_2^3 - R_1^3), \tag{5.2}$$

as well as for the second radial derivative,

$$\left.\frac{\partial^2 V_t}{\partial r^2}\right|_{\mathbf{r}=\mathbf{r}_P} = \frac{8\pi G\rho}{3r_P^3}(R_2^3 - R_1^3). \tag{5.3}$$

The second horizontal components in x and y direction are identical and half of this expression with a negative sign to fulfill the Laplace differential equation.

Figure 5.5 shows the differences between the numerical integration and the analytical computation of the gravitational potential for various altitudes of the computation point above the the Bouguer shell and different resolutions of the spherical volume elements, approximated by the mass-line elements. Figure 5.6 shows these differences for the first radial derivative of the potential (in units of $mGal$). It is obvious that in case of high accuracy demands and low flight altitudes it is necessary to use very high resolution of the DTM and alternative precise approximation of the volume elements instead of the mass-lines. In the vicinity of the computation points it might be sufficient to apply a rigorous planar representation such as the prism formulae proposed, e.g., by Nagy (1966). The requirements are much less critical in case of increasing altitudes. Figure 5.7 and Fig. 5.8 show the approximation errors of the second radial derivatives of the potential and for the (identical) horizontal components x and y, respectively, again for various altitudes of the computation point above the shell up to 10000 m and different resolutions.

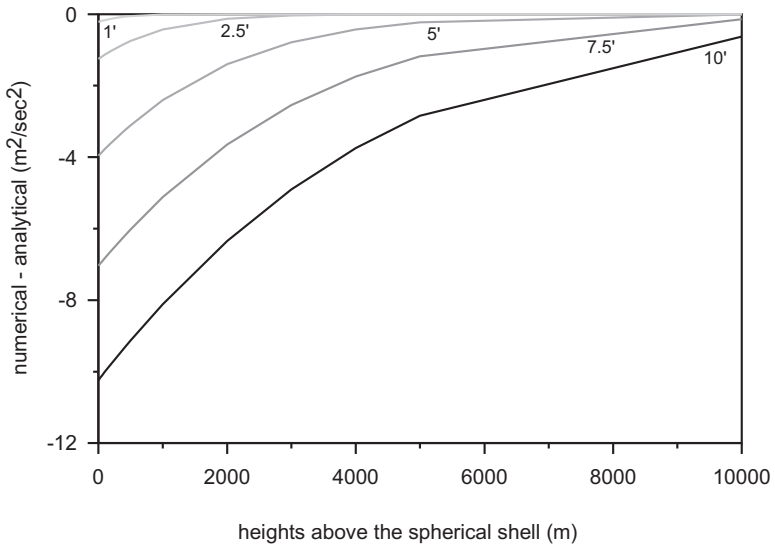

Fig. 5.5: Differences between the numerical integration and the analytical computation of the potential of a Bouguer shell with a thickness of 2500 m (units in m^2/s^2)

The integral formulae become more and more critical if the computation point approaches the outer shell surface. In this case a poor resolution causes large errors in the vicinity of the computation point. Table 5.1 illustrates the situation for computation points close to the spherical shell (the altitudes vary between 10 m and 50 m) based on increasing detailed resolutions of the DTM from $5''$ down to $0.125''$. It is obvious that an extremely fine resolution is necessary for precise computations of the topographic-isostatic effects of the second derivatives of the potential in case of computation points close to the Earth's surface. These instabilities are caused by the jump relations of the second derivatives dependent on the jumps of the density function of the volume masses. Because of the jump relation of the, e.g., second radial derivative of our spherical shell with an outer limit of

$$\left.\frac{\partial^2 V_{t+}}{\partial r^2}\right|_{r=R_2} = \frac{8\pi G\rho}{3R_2^3}(R_2^3 - R_1^3), \tag{5.4}$$

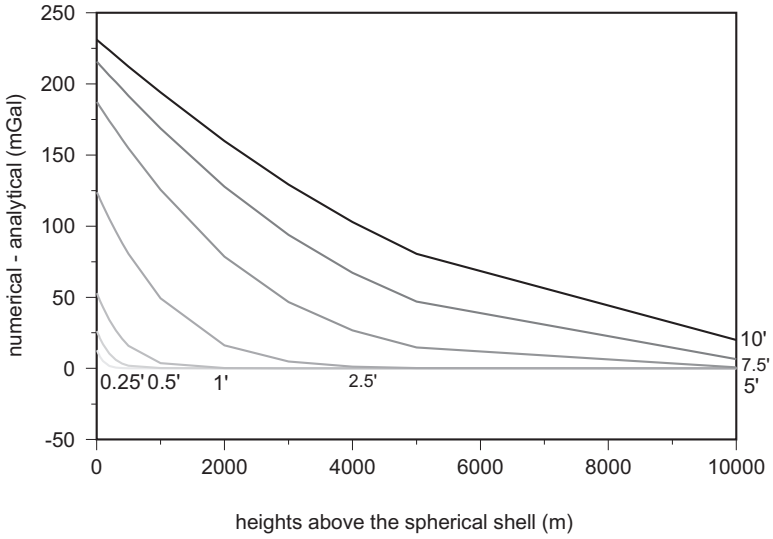

Fig. 5.6: Differences between the numerical integration and the analytical computation of the first radial derivative of the potential of a Bouguer shell with a thickness of 2500 m (units in $mGal$)

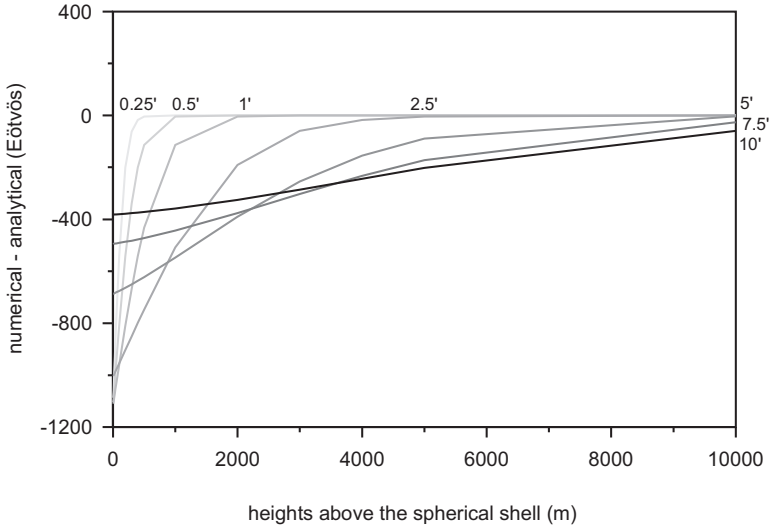

Fig. 5.7: Differences between the numerical integration and the analytical computation of the second radial derivative of the potential of a Bouguer shell with a thickness of 2500 m (units in Eötvös)

Table 5.1: Differences between the numerical integration and the analytical computation of the potential of a Bouguer shell with a thickness 2500 m (units in m^2/s^2)

resolution height (m)	5"∗5"	2"∗2"	1"∗1"	0.25"∗0.25"	0.125"∗0.125"
10	-930.33	-668.72	-338.73	-1.16	< 1E-3
20	-751.64	-338.61	-62.25	< 1E-4	< 1E-4
30	-560.66	-151.30	-10.90	< 1E-4	< 1E-4
40	-452.40	-62.24	-1.15	< 1E-4	< 1E-4
50	-338.62	-22.56	-0.04	< 1E-4	< 1E-4

and an inner limit of

$$\left.\frac{\partial^2 V_{t-}}{\partial r^2}\right|_{r=R_2} = -\frac{4\pi G\rho}{3R_2^3}\left(R_2^3 + 2R_1^3\right). \tag{5.5}$$

We cannot expect a reasonable result in case of computation points close to or at the outer spherical surface of the shell.

The numerical values for the present example read for the outer limit of the radial component 1.75 Eötvös and for the inner limit −2236 Eötvös. The results of the numerical integration for computation points at the surface of the shell turn out to be (approximately) the arithmetic mean of the inner and the outer values, approximately −1118 Eötvös (Fig. 5.9). This is only the case if the resolution is selected adequately high - in case of a coarse grid the approximation errors cannot be interpreted anymore. The situation cannot be explained in such a simple way as in case of the local horizontal directions x and y which are perpendicular to the radial direction. No jump occurs in these cases, so that it holds at the outer shell boundary, e.g., for the derivation with respect to x,

$$\left.\frac{\partial^2 V_{t+}}{\partial x^2}\right|_{r=R_2} = \left.\frac{\partial^2 V_{t-}}{\partial x^2}\right|_{r=R_2}. \tag{5.6}$$

Therefore, in these cases there would be no reason for an unstable behavior as in case of the radial component. Here we have to keep in mind that the formulae for the computation of the second derivatives are derived such that the Laplace equation is fulfilled in the space outside the masses as demonstrated in Figs. 5.7 and 5.8, even if the computation point is arbitrarily close to the surface of the shell. This is the case despite the fact that the formulae are only approximate. A numerical consequence is that the second horizontal derivatives will never converge to the correct value at the outer boundary even in case of a very fine resolution of the digital terrain model (Fig. 5.9).

In the vicinity of the computation point a rigorous tesseroid formula in three dimensions (Kuhn 2000a) is necessary or to choose a sufficient fine grid of the DTM, where a planar approximation based on the prism formulae technique of Nagy (1966) might be sufficient. It should be pointed out that the Laplace equation is fulfilled as long as the computation point is located outside the masses as demonstrated in Figs. 5.7 and 5.8, even if the computation point is arbitrarily close to the surface of the shell. The situation is less critical in practical applications as it may seem from the aforementioned facts; in these cases a Bouguer plate or a Bouguer shell is used, whose effects can be determined analytically, and the (in general small) terrain corrections can be determined by numerical integration based on a DTM with a sufficient fine resolution or any rigorous (planar) formula. A detailed investigation of these error effects has to be performed in a forthcoming study.

5.2.2 Surface spherical harmonic expansion of the topography

There are many methods for calculating the surface spherical harmonic expansions of the topography such as quadrature methods, least squares, Paul integral, integral through Legendre polynomials (see, e.g., Tsoulis 1999a; Sneeuw 1994; Sneeuw and Bun 1996). In this investigation only a simple quadrature and the Gauss-Legendre quadrature methods have been used.

5.2.2.1 Resolution aspects

The spherical harmonic expansion of the topography is a very efficient technique for calculating the topographic-isostatic mass effects, but it is limited to an upper spherical harmonic degree of about 2700 which corresponds to a 4 arc-minute resolution. Beyond this degree numerical computation problems concerning the stability of the recursive computation of the associated Legendre's functions occur (see, e.g., Holmes and Featherstone 2002) and increasing the computational time. For this reason, the spherical harmonic expansion of the topography can be used for calculating the long and medium wavelength effects of the topography. These long and medium wavelengths are important for calculating the effects at satellite altitude or for calculating the far-zone effects of the topographic masses for the points at the Earth's surface and at certain altitudes for airborne gravimetry.

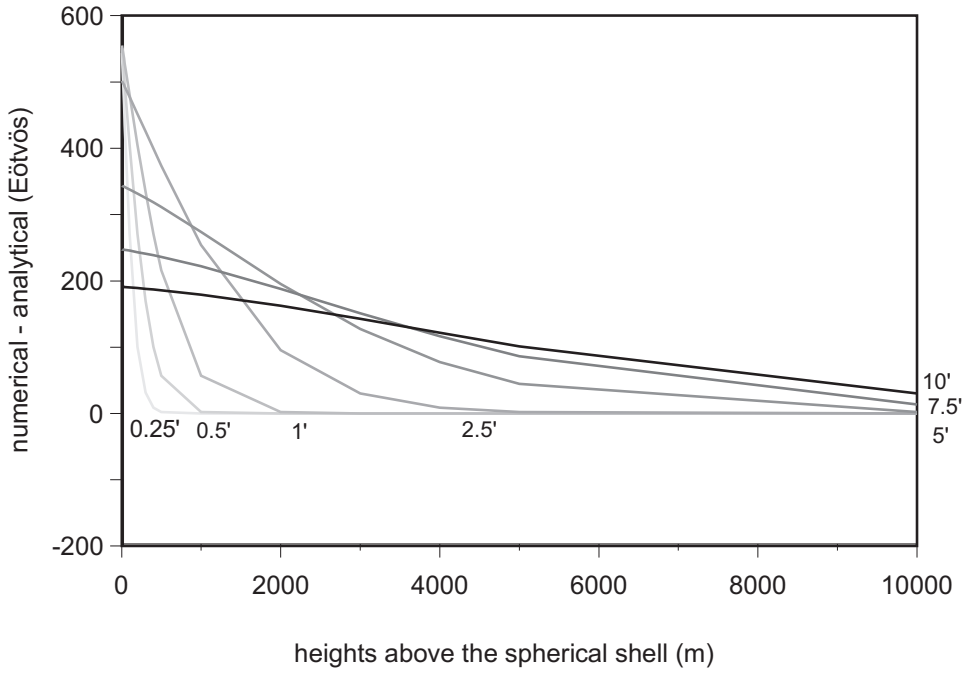

Fig. 5.8: Differences between the numerical integration and the analytical computation of the second horizontal (xx and yy) derivative of the potential of a Bouguer shell with a thickness 2500 m (units in Eötvös)

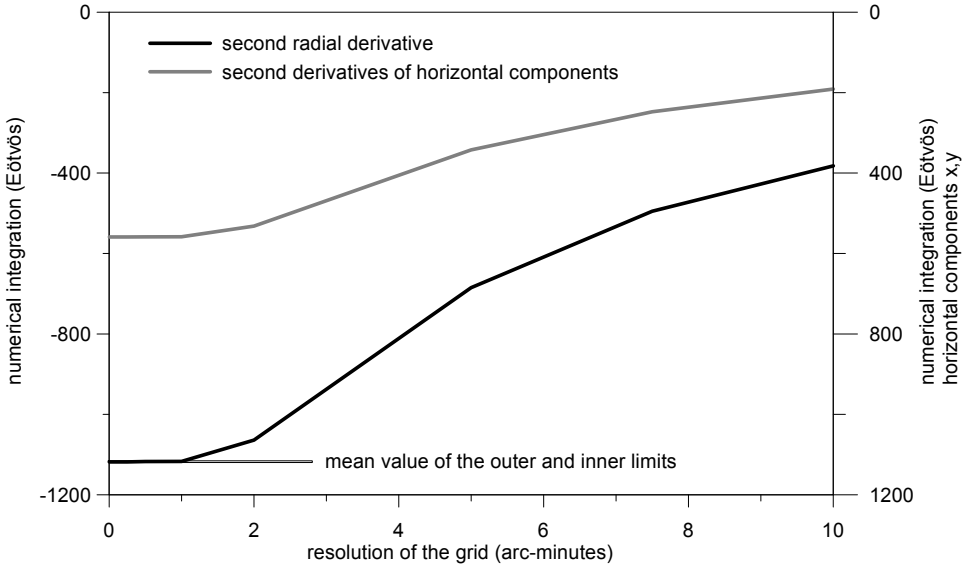

Fig. 5.9: Second derivatives of the potential of a Bouguer shell with a thickness of 2500 m (Eötvös) determined by numerical integration using different discretizations

5.2.2.2 Numerical computation of the surface spherical harmonics

It is known that a square integrable function on the sphere can be developed into harmonic coefficients using the global spherical harmonic analysis (GSHA). In our study, the integrable function is the topography above the geoid. The computation of the spherical harmonics using quadrature method will be discussed in the following.

Simple quadrature method The spherical harmonic coefficients of the topography can be calculated by replacing the double integral by a double summation all over the world. For an efficient computation, the two step analysis approach proposed by Neumann (1838) and Gauss (1839) has been applied. The double integration or summation is splitted into a longitude and a latitude dependent part. For example, Eq. (4.134) reads as follows (e.g. in case of k=1):

$$hk_{nm}^{\alpha} = \frac{1}{4\pi} \iint\limits_{\sigma} \left(\frac{H_{eq}(\varphi,\lambda)}{R} \right) Y_{nm}^{\alpha} d\sigma. \tag{5.7}$$

This equation can be splitted into two equations as follows:

$$\left\{ \begin{matrix} a_m(\varphi) \\ b_m(\varphi) \end{matrix} \right\} = \frac{1}{(1+\delta_{m0})\pi} \int\limits_{\lambda=0}^{2\pi} \left(\frac{H_{eq}(\varphi,\lambda)}{R} \right) \left\{ \begin{matrix} \cos m\lambda \\ \sin m\lambda \end{matrix} \right\} d\lambda, \tag{5.8}$$

$$\left\{ \begin{matrix} h_{nm}^{c} \\ h_{nm}^{s} \end{matrix} \right\} = \frac{1}{4}(1+\delta_{m0}) \int\limits_{\varphi=0}^{\pi} \left\{ \begin{matrix} a_m(\varphi) \\ b_m(\varphi) \end{matrix} \right\} P_{nm}(\sin\varphi)\cos\varphi d\varphi. \tag{5.9}$$

The reason for the greater efficiency of the two-step formulation is twofold. Firstly, Eq. (5.8) can be treated by Fourier transformations over single parallels. Secondly, the equations may be evaluated for separate orders m. In reality one has to deal with discretized function values, either point values or area means. In our study, we approximate the function of heights by point values. The aliasing problem will be ignored, i.e. it is assumed that the function does not contain information above degree N. Since the distribution of parallels has not been decided yet and since the problem of non-orthogonality of the discretized Legendre function has not been resolved, the determination of coefficients is still bending. In order to solve this problem of non-orthogonality, Neumann's method has been used.

Neumann's method A special case of exact quadrature is achieved by restricting the φ-grid. Neumann (1887) showed that if one chooses the latitude circles to coincide with the zeros of the Legendre polynomials of degree $N+1$, i.e.

$$P_{N_{max+1}}(\sin\varphi_i) = 0, \qquad i = 1, 2, ..., N_{max}, \tag{5.10}$$

the number of parallels can be reduced to $N = N_{max} + 1$. The specific φ- or ϑ-grid leads to the Gauss-Legendre quadrature method (Lanczos 1956; Krylov 1962; Stroud and Secrest 1966; Colombo 1981). The specific grid is referred as Gauss grid (Payne 1971). Neumann's method can be summarized as follows: An exact GSHA is performed up to degree N_{max} making use of a Gauss-Neumann grid (see Fig. 5.10 blue), defined by:

$$\begin{aligned} &P_{N_{max+1}}(sin\varphi_i) = 0, && i = 1, 2, ..., N_{max}+1, \\ &\lambda_j = j\Delta\lambda, && j = 1, 2, ..., 2N_{max}-1, \\ &\Delta\lambda = \frac{\pi}{N_{max}}. \end{aligned} \tag{5.11}$$

For the computations of weights in Neumann's method, the existing literature on Gauss quadrature methods can be used. If the Lengendre polynomials of $P_{N_{max+1}}(\sin\varphi)$ are available, the weights may be calculated for instance from:

$$w_i = \frac{2}{(1-(\sin\varphi_i)^2)(P'_{N_{max+1}}(\sin\varphi_i))^2}, \tag{5.12}$$

where $P'_{N_{max+1}}(sin\varphi)$ is the first derivative of the Legendre polynomial of degree $N+1$, when N is the maximum degree to be determined. Further numerical aspects of finding nodes and weights can be found in Press et al. (1986) and Prey (1922). The Neumann method requires the data points to be located at a specific grid, called Gauss-Legendre Grid. Using cubic spline interpolation for the DTM, the topographic heights can be determined at the nodes of this grid. This quadrature method has the advantage of maintaining the orthogonality relations of the Legendre function despite the discretization procedure.

Simple quadrature versus Neumann method In order to compare the quadrature methods sketched above, the spherical harmonic coefficients of topography have been calculated up to degree and order 2160 using ETOPO5 (rock equivalent heights). In case of the simple quadrature, the weights $\cos\varphi \mathrm{d}\varphi \mathrm{d}\lambda$ were used (see Fig. 5.10 red). From the two sets of coefficients, the heights of the topography were reconstructed by the global spherical harmonic synthesis (GSHS) as follows:

$$H(\varphi,\lambda) = R\sum_{n=0}^{N_{max}}\sum_{m=0}^{n}(h^c_{nm}\cos m\lambda + h^s_{nm}\sin m\lambda)P_{nm}(\sin\varphi). \tag{5.13}$$

The reconstructed heights for a small region are shown in Fig. 5.11. It has been found that the difference between the computed heights from the two sets of coefficients and the heights from ETOPO5 are approximately the same. This means that, in case of the the simple quadrature method, the effect of non-orthogonality can be ignored if the grid size is very small. This would be expected because for very fine grids the discrete Legendre function behaves as a continuous function.

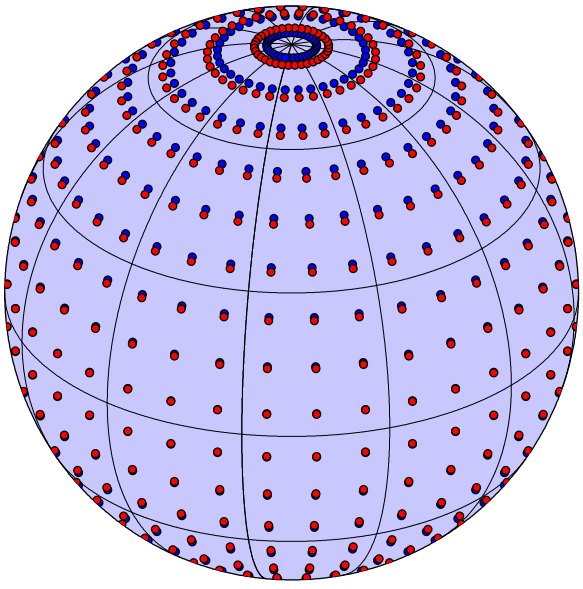

Fig. 5.10: Geographical grid (red) and Gauss-Legendre grid (blue)

After comparing the simple quadrature method with the Gauss-Legendre quadrature method, the spherical harmonic coefficients for square and cubic heights have been calculated also up to degree 2160.

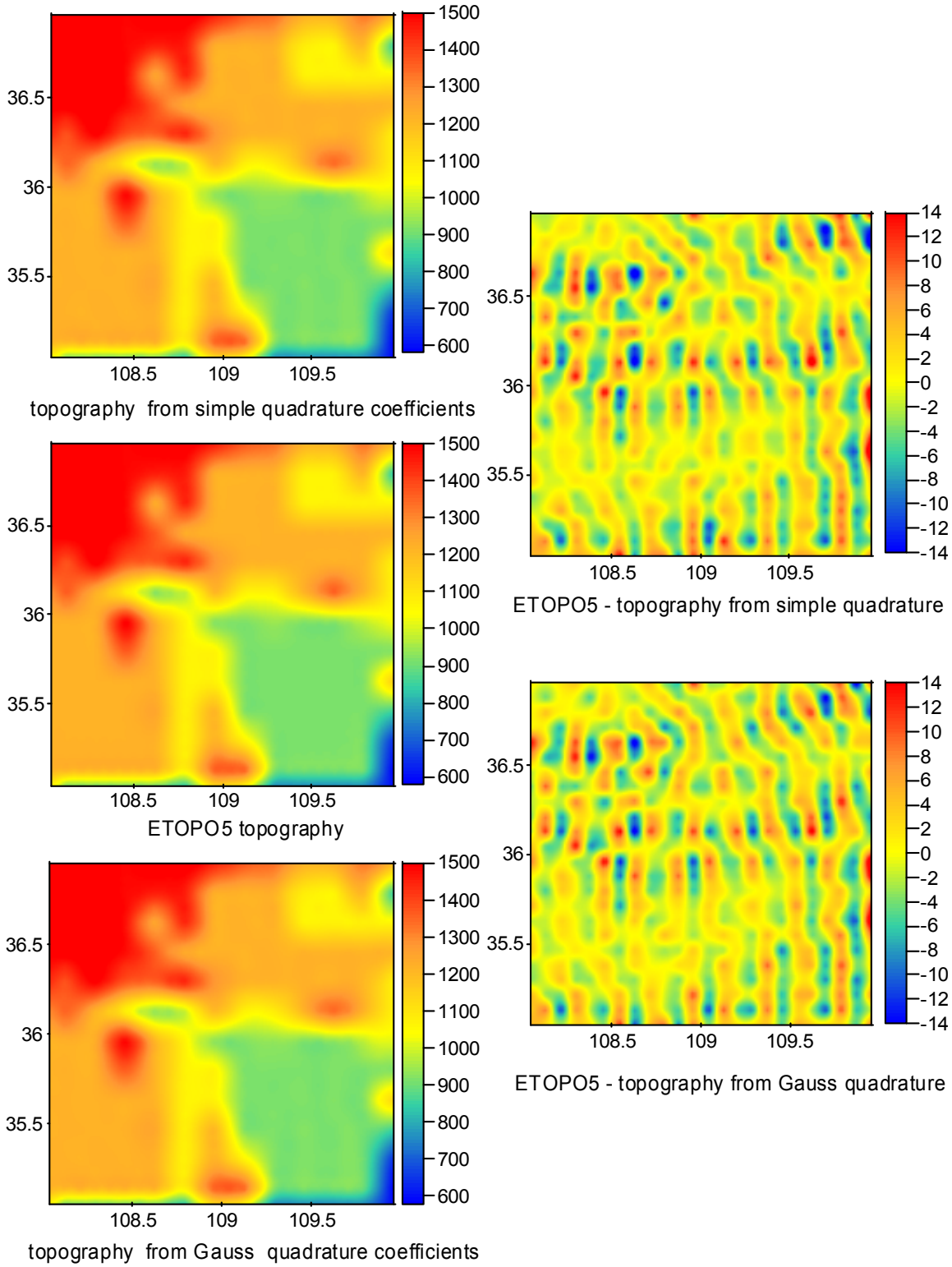

Fig. 5.11: Comparison between simple quadrature and Gauss Legendre quadrature methods (units in meter)

5.2.2.3 Degree variances of different topographic-isostatic models

To visualize the spectral behavior of the topography the spectrum of the potential coefficients has been computed. The degree variance of a set of coefficients for degree n can be computed as follows (Rapp 1982):

$$\sigma_n^2 = \sum_{m=0}^{n} (c_{nm}^2 + s_{nm}^2). \tag{5.14}$$

Firstly, to get an idea about the contribution of the first, second and third order terms of Eq. (4.134) to the harmonic coefficients of the uncompensated topographic potential, the separate degree variance for h_{nm}^{α}, $h2_{nm}^{\alpha}$ and $h3_{nm}^{\alpha}$ have been computed and shown in Fig. 5.12. The $h2_{nm}^{\alpha}$, $h3_{nm}^{\alpha}$ and h_{nm}^{α} are properly multiplied by the respective factors as given in Eq. (4.133)

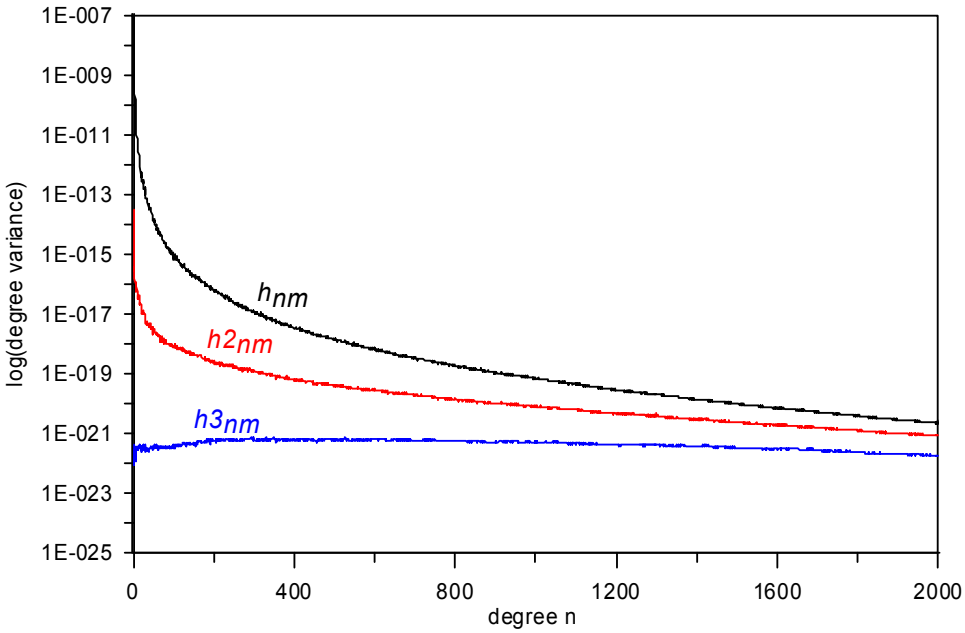

Fig. 5.12: Separate contributions of h_{nm}^{α}, $h2_{nm}^{\alpha}$ and $h3_{nm}^{\alpha}$ to the computation of the uncompensated potential coefficients

The results shown in Fig. 5.12 agree with those reported in Rummel et al. (1988) and Tsoulis (2001). The power spectrum of $(h/R)^2$ and $(h/R)^3$ are approximately 10^{-6} and 10^{-13} of the power spectrum of (h/R) for the degrees n=0 to 180. After this degree and up to n = 1000, the power spectrum of $(h/R)^2$ and $(h/R)^3$ are approximately 10^{-3} and $10^{-6}$of the power spectrum of (h/R). For higher degrees the power spectra of the quadratic and cubic terms are approximately 10^{-1} and 10^{-3} of the linear terms. From the above results, it can be concluded that at satellite altitude only the linear and quadratic terms of heights are necessary for calculating the gravitational effects of the topographic-isostatic masses. On the other hand, at least the first, second and third terms of height must be taken into account for calculating the gravitational effect at aeroplane altitudes as the spherical harmonic coefficients are taken to higher degrees.

Secondly, to compare the different topographic isostatic models, the degree variances of all topographic-isostatic models, uncompensated topography and of the coefficients of the gravitational model EGM96 (Lemoine et al. 1998) are shown in Fig. 5.13. It is shown from Fig. 5.13 that:

1. the degree variances of the potential coefficients for the uncompensated topography (Bouguer model) are significantly higher than those obtained from the EGM96 coefficients. This means that the topography must be considered in isostatic equilbrium.

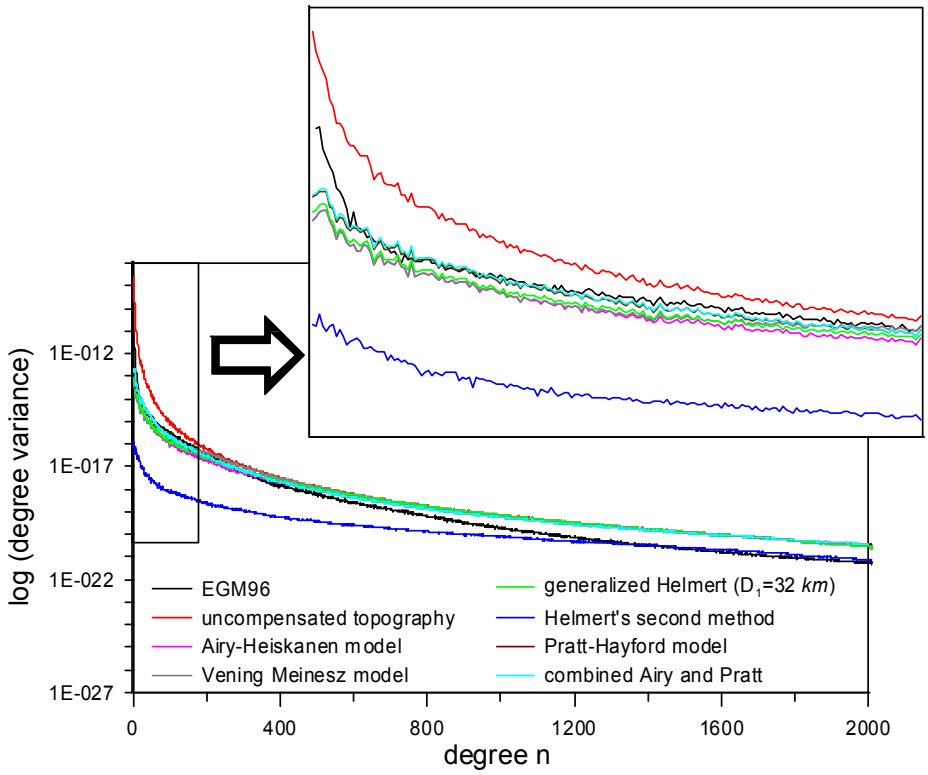

Fig. 5.13: Degree variances of different topographic-isostatic models

2. the degree variances of the potential coefficients of the Airy-Heiskanen model and the generalized Helmert's model of condensation with a condensation depth=32 km are approximately the same.
3. the degree variances of the Pratt-Hayford model are approximately the same as for the combined Airy and Pratt model. This means that the effects of the topographic heights are significantly smaller than the effects of bathymetric heights.
4. the degree variances of the Pratt-Hayford model agree quit well with the degree variance of the EGM96 coefficients.
5. the degree variances of the Vening Meinesz model are larger than the degree variances of the Airy-Heiskanen model for high degrees. This is caused by smoothing the roots and anti-roots in case of the Vening Meinesz model.

5.2.3 Near-zone and far-zone aspects

The effects of topographic-isostatic masses must be calculated globally which is very expensive in terms of computation time. To overcome this problem, the surface integration domain is divided into two integration sub-domains: a spherical cap around the computation point with a small radius, called near-zone contribution (σ_0), and the rest of the Earth, called far-zone contribution (σ_{Fz}). A fine resolution DTM must be used in the near zone while in the far-zone a coarser DTM is sufficient in most cases (Grüninger 1990). Near-zone topographic effects on the gravity and geoid heights can be calculated using rectangular prisms (Nagy 1966; Nagy et al. 2000, 2002), which lead to a particularly simple formula, or by using tesseroid formulae in case of the spherical approximation of the geoid (Smith et al. 2001; Kuhn and Seitz 2005; Makhloof and Ilk 2006). To arrive at economic computation formulae, the far-zone effects are represented by a global spherical harmonic expansion of the topography. This can be performed by a Molodenskii-type spectral approach as shown in chapter 4.

5.3 Effects of topographic-isostatic masses at the surface of the Earth and at aeroplane altitudes

In this section the near and far-zone effects of the topography will be discussed at the surface of the Earth and at aeroplane altitude. The potential of the topographic-isoatatic masses in terms of the indirect topographical effect has been computed. Also, the first derivatives of the potential in terms of the direct topographical effect have been determined. Moreover, the second derivatives of the potential of the topographic-isotatic masses at aeroplane altitude have been studied numerically.

5.3.1 Near-zone topography effects

To give an impression of the size and distribution of the topographic-isostatic mass effects on the gravitational functionals at the Earth's surface and at aeroplane altitudes, the Airy-Heiskanen model and Helmert's methods of condensation have been used. To reduce the discretization errors, the direct and indirect topographical effects have been splitted into two effects: (1) the effects of the Bouguer shells and (2) the effects of the terrain refinements. As the effects of the Bouguer shells of topographic and isostatic masses cancel each other in case of the direct topographical effect, only the terrain effects have been computed. In case of the primary indirect topographical effect, the terrain effects in addition to the effects of the Bouguer shells have been determined.

5.3.1.1 Direct terrain effect on gravity

In order to take the short wavelengths of the topography into account, the near-zone cap has been taken to be $\psi_0 = 3^0$. For the generalized Helmert model of condensation the depth of the condensation masses has been varied between 21 km to 40 km. These tests have been performed to show the coincidence of Helmert's models with an an appropriate condensation depth with the Airy-Heiskanen isostatic model. The computation points has an altitude of 4 km above the sea level. Examples of Helmert's generalized models with condensation depths (21, 25, 30, 32, 35 and 40 km) together with the Airy-Heiskanen model are given in Table 5.2.

Table 5.2: Near-zone terrain effects at an altitude of 4 km for Helmert's first and generalized model of condensation with different depths in comparison with Airy-Heiskanen (units in $mGal$)

topographic-isostatic model	RMS	Mean	Min	Max
Helmert's first method (21 km)	23.78	-4.23	-67.90	56.99
generalized Helmert model (25 km)	24.13	-4.76	-69.47	57.12
generalized Helmert model (30 km)	24.32	-5.45	-70.60	56.60
generalized Helmert model (32 km)	24.32	-5.58	-70.86	56.25
Airy-Heiskanen model	24.32	-6.04	-70.46	55.79
generalized Helmert model (35 km)	24.31	-5.89	-71.09	55.61
generalized Helmert model (40 km)	24.20	-6.38	-71.13	54.35

The coincidence of the generalized Helmert model of condensation with the Airy-Heiskanen model depends on the condensation depths of Helmert's model (Table 5.2). This means that, with a proper selection of Helmert's condensation depth D_1, the condensation method can be adjusted to be more realistic. To illustrate the size of the direct terrain effect dependent on the height of the calculation points, the direct terrain effects at the altitudes of 4 km, 6 km, 8 km, 10 km are shown in Table 5.3

Finally, to give an impression about the distribution of the near-zone terrain effects, the direct terrain effect for Helmert's second method of condensation, Helmert's generalized model with a condensation depth of 32 km and Airy-Heiskanen method are shown in Fig. 5.14.

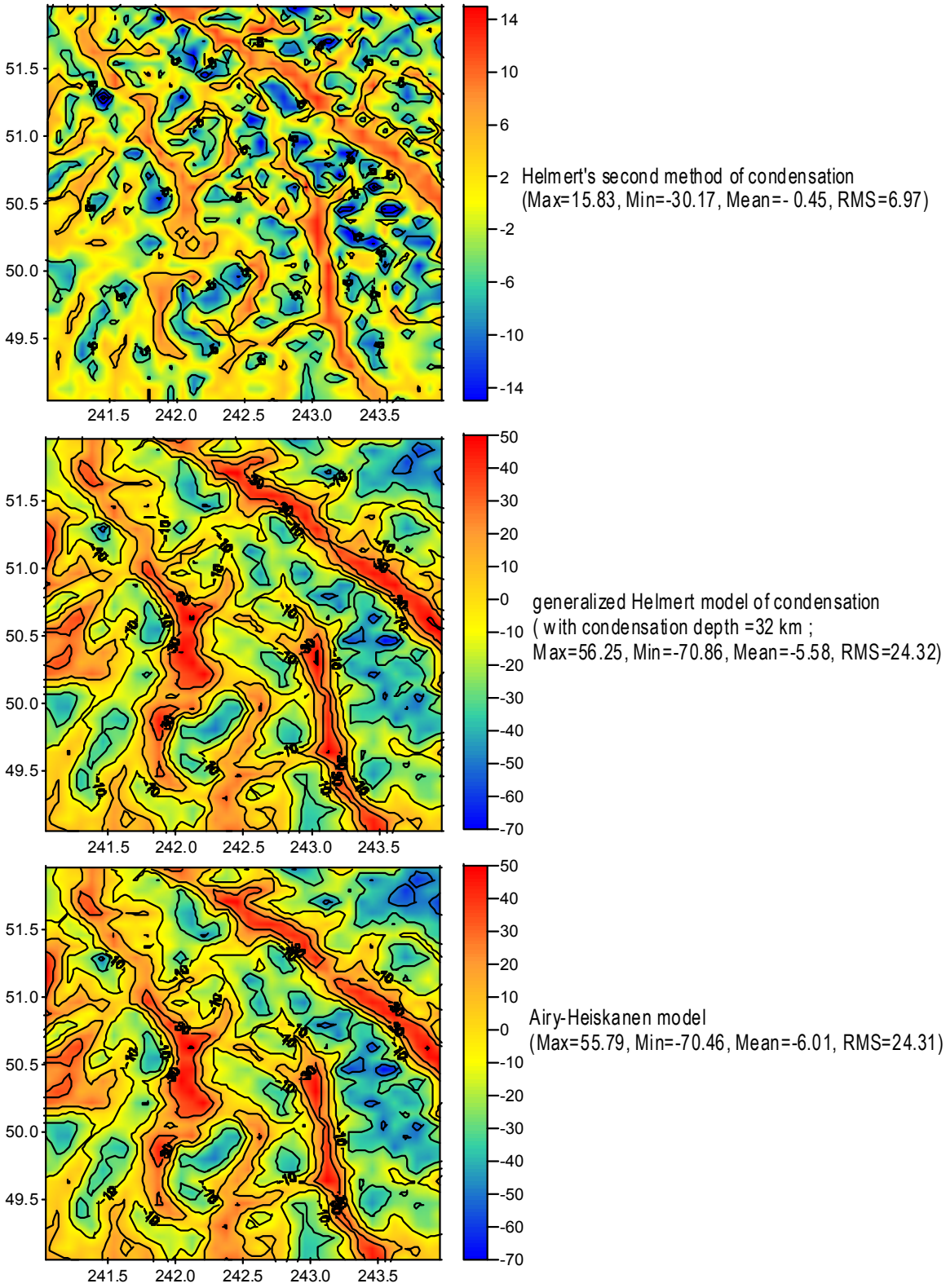

Fig. 5.14: Near-zone direct terrain effect on gravity of the area inside a cap size of $\psi_0 = 3^0$ for different topographic-isostatic models at an altitude of 4 km (units in $mGal$)

5.3.1.2 Indirect topographical effect on geoid and gravity

It is shown in Eq. (4.202) that the primary indirect topographical effects includes two parts: the effects of the Bouguer shells of the topographic and isostatic masses and the terrain effects. The effects of the Bouguer shell of the topographic masses and the Bouguer layer of the condensation masses in case of Helmert's methods of condensation can be determined by the following equation:

$$PITE^{Bouguer} = \frac{2\pi G\rho_{cr}\left[(R+H_{P'})^2 - R^2\right]}{\gamma_0} - \frac{4\pi G\rho_{cr}}{3(R+H_{P'})\gamma_0}\left[(R+H_{P'})^3 - R^3)\right], \tag{5.15}$$

where $H_{P'}$ is the orthometric height of the topography at the computation point. It can be seen that Eq. (5.15) is independent of the condensation depth of Helmert's first or generalized model of condensation. This is due to the fact that the potentials of the Bouguer layers of the condensation masses in case of Helmert's first and second method of condensation are equal. Also, the potential of the Bouguer shell of the compensating masses in case of the Airy-Heiskanen model are equal to the potential of the Bouguer layer in case of Helmert's model. This is based on the mass conservation principle of the topographic and isostatic or condensation masses. The effects of the Bouguer shells for the Canadian Rocky Mountains are shown in Fig. 5.15.

Also, the near-zone primary indirect terrain effects are shown in Fig. 5.16. The plot shows that the primary

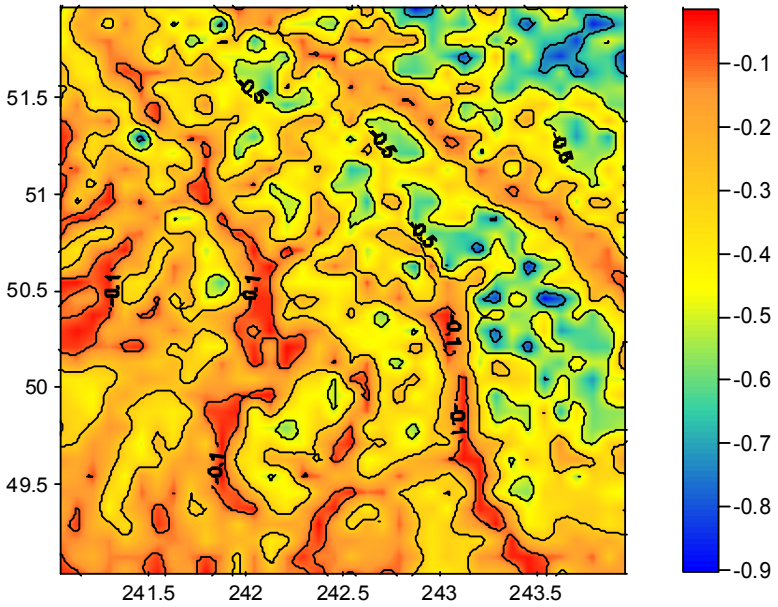

Fig. 5.15: Primary indirect effects of Bouguer shells of the topographic masses (units in $mGal$)

indirect terrain effects in case of the generalized Helmert model of condensation and the Airy-Heiskanen model are large compared to the effects of the Bouguer shells and depend significantly on the heights of the topography. These effects must be taken into account for calculating the 1 cm geoid in case of local geoid determination. On the other hand the near zone primary indirect terrain effects in case of Helmert's second method of condensation are small but these value must be taken into account in case of 1 cm geoid determination. Finally, the near zone secondary indirect terrain effects for the same area are shown in Fig. 5.17. Again the near-zone secondary indirect terrain effects for Helmert's first and the generalized methods as well as Airy-Heiskanen method reach significant values compared to the accuracy of the observation data.

5.3.1.3 Terrain effect on airborne gradiometry

Airborne gravity gradiometry is not yet popular but may represent a potential technique for the future, e.g., it is imaginable that HALO (High Altitude and LOng Range Research Aircraft) could be equipped with

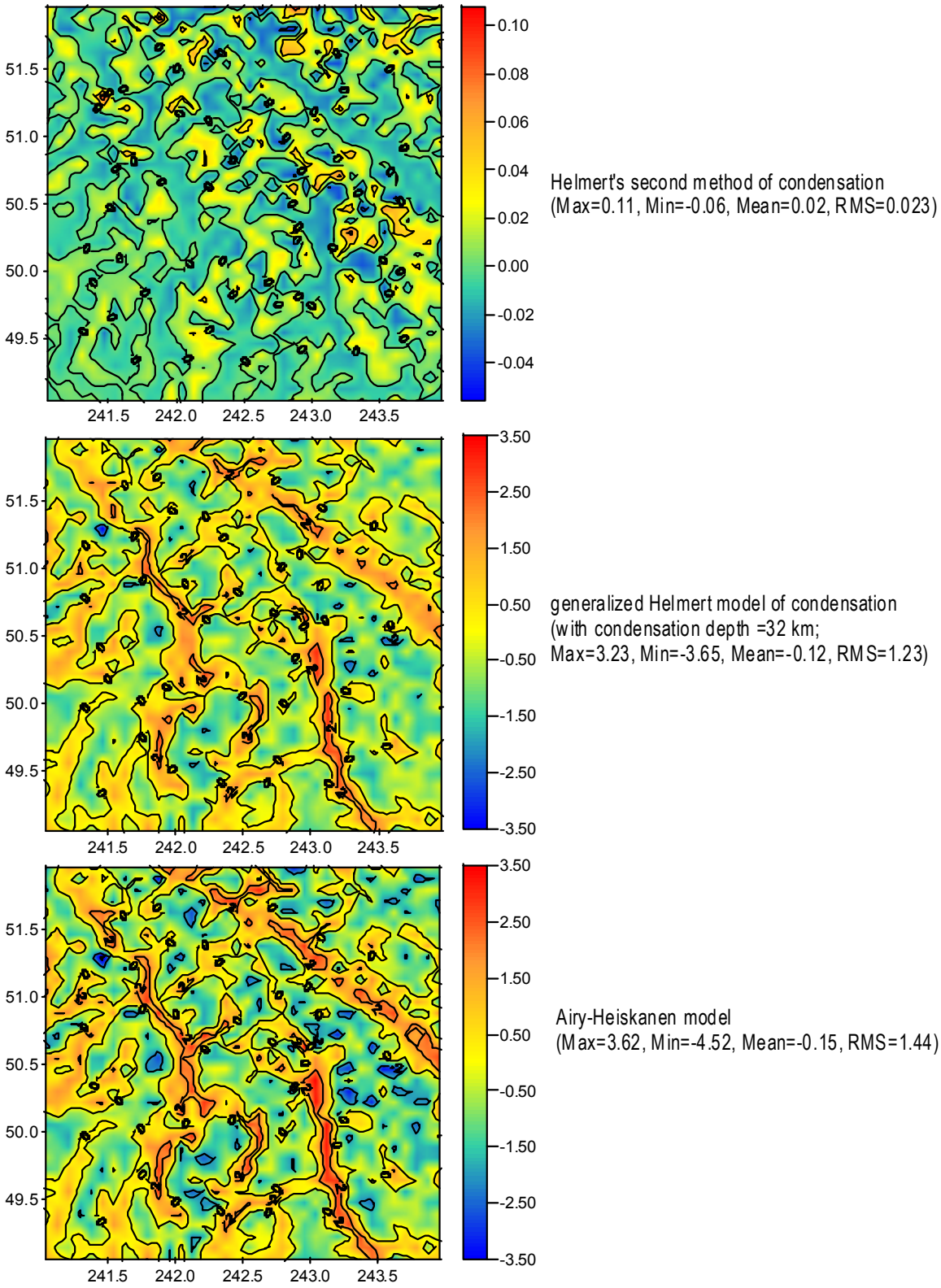

Fig. 5.16: Near-zone primary indirect terrain effect on geoid heights of the area inside a cap size of $\psi_0 = 3^0$ for different topographic-compensation models (units in meter)

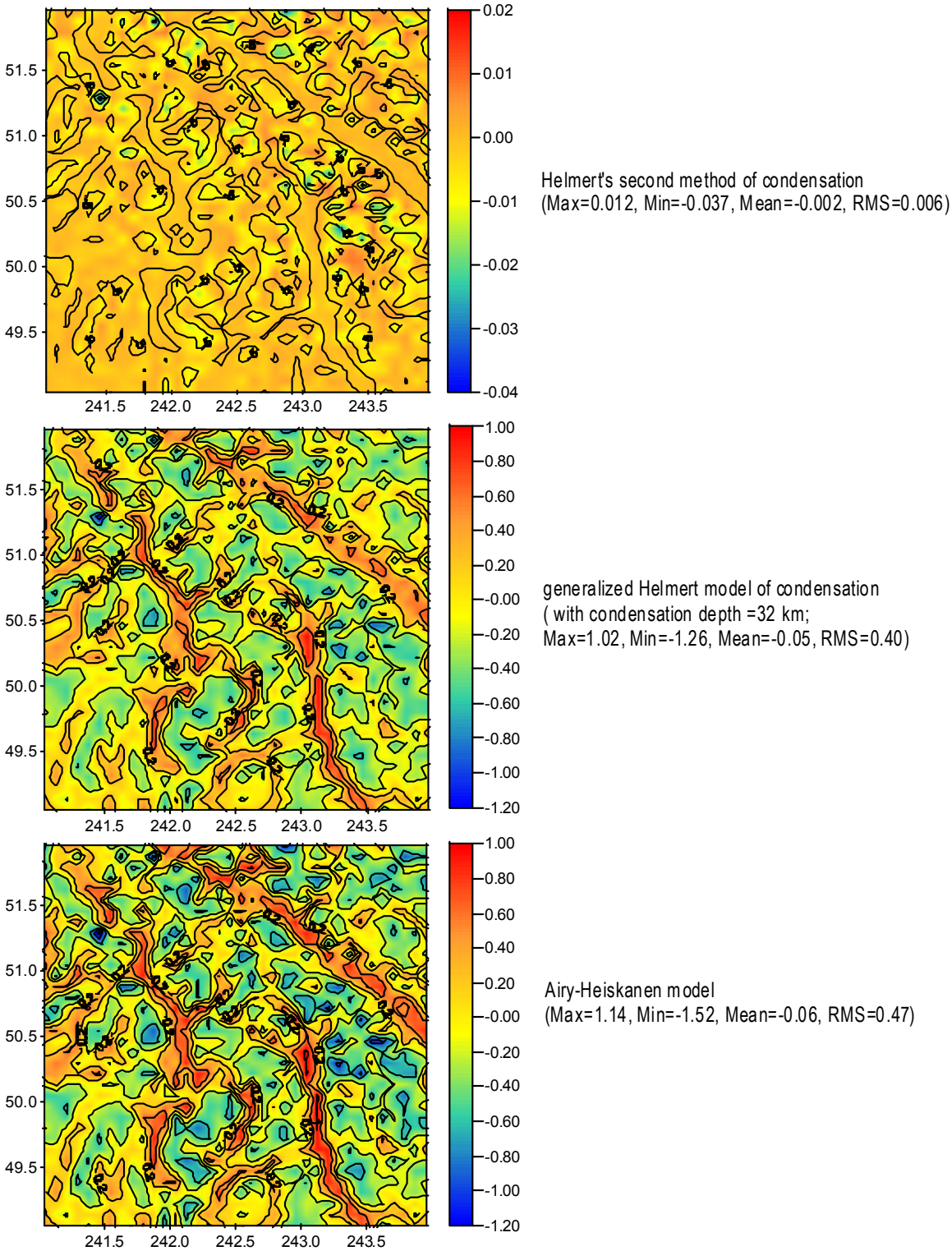

Fig. 5.17: Near-zone secondary indirect terrain effect on gravity of the area inside a cap size of $\psi_0 = 3^0$ for different topographic-isostatic models at the surface of the Earth (units in $mGal$)

a gravity gradiometer. Therefore, it is interesting to investigate the topographic-isostatic effects of gravity gradients in an aeroplane altitude. The near-zone terrain effects of the topographic-isostatic masses on the gravitational tensor component V_{zz} at an altitude of 10 km based on the Airy-Heiskanen model is shown in Fig. 5.18 for the Himalaya region.

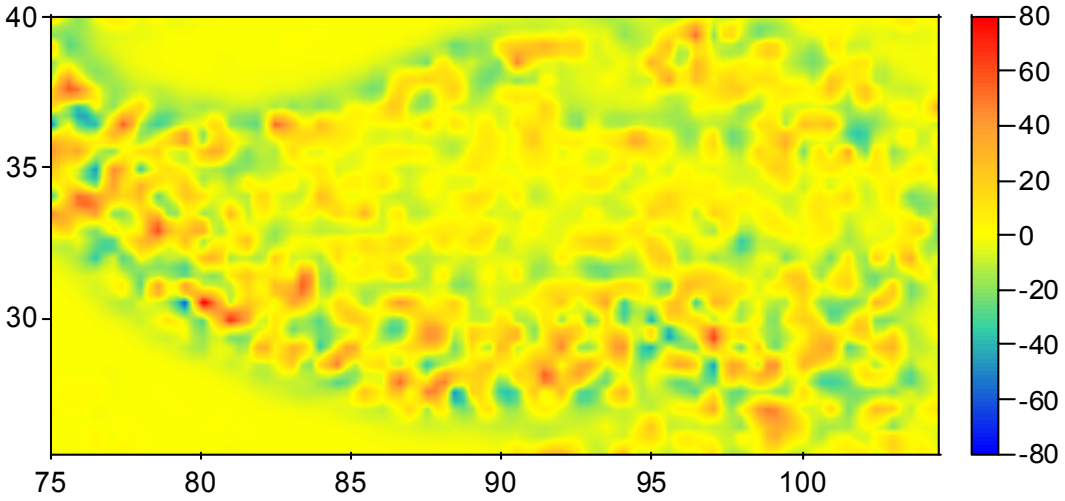

Fig. 5.18: Effects of the near-zone terrain masses on the tensor component V_{zz} at an altitude of 10 km for the Airy-Heiskanen model for the Himalaya region (units in Eötvös)

5.3.2 Far-zone topography effects

The computational area is taken as the same used for the near-zone terrain effects (Fig. 5.1). The calculations are performed for a far-zone cap size of $\psi_0 \geq 3^0$. In this case the series expansions fulfill the convergence criterion given in Eq. (A.6). In addition, various other cases of far zones have been investigated. The upper degree of the spherical harmonic expansion of the topography is taken to be $Nmax = 360$ as the effects above this degree are neglected (will be seen later). Again, for the generalized Helmert model of condensation the depth of the condensation masses has been varied between 21 km to 40 km. These tests have been performed to show that a varying condensation depth approximates the Airy-Heiskanen isostatic model quite well. Examples of condensation depths (21, 25, 30, 32, 35 and 40 km) are given in Table 5.4.

5.3.2.1 Direct terrain effect on gravity

To illustrate the size of the direct terrain effect against the cap size of the far-zone, the RMS-values (root mean square of point values) of these effects for the three models are shown in Fig. 5.19 for computation points at an altitude of 4 km. It is shown that a far-zone cap size of $\psi_0 \geq 3^0$ gives small RMS-values in case of Helmert's second method of condensation compared to the accuracy of the observation. Table 5.5 shows the far-zone effects in case of cap-size radii of 3^0, 10^0 and 20^0 in case of Helmert's second method of condensation. The situation is different in case of the generalized Helmert model of condensation and the Airy-Heiskanen model where these effects are much larger. Table 5.6 gives an overview of the far-zone effects depending on the cap-size radius (3^0, 10^0, 20^0,.....,90^0). It is interesting to note that these effects depend only marginally on the altitude of the computation points.

The accuracy of the spherical harmonic formulae derived in this case has been tested using the integration method with tesseroid formulae (Makhloof and Ilk 2006). Figure 5.20 shows the direct terrain far-zone effects along the 50^0 latitude, determined by the formulae based on a spherical harmonic expansion up to degree $N_{max} = 360$ and based on a numerical quadrature method using tesseroid formulae with a corresponding grid

Table 5.3: Near-zone direct terrain effects for different altitudes for Helmert's methods of condensation and Airy-Heiskanen model (units in *mGal*)

Model	statistics	H= 4 km	H= 6 km	H= 8 km	H= 10 km
Helmert's second method	RMS	6.97	3.93	2.63	1.91
	Max	15.83	9.42	6.46	4.54
	Min	-30.17	-13.17	-8.24	-5.81
	Mean	-0.45	-0.35	-0.31	-0.28
generalized Helmert (D_1=32 km)	RMS	24.32	18.07	14.42	12.02
	Max	56.25	37.62	30.24	25.30
	Min	-70.86	-49.49	-45.33	-41.62
	Mean	-5.58	-5.19	-4.92	-4.69
Airy-Heiskanen model	RMS	24.31	18.21	14.67	12.37
	Max	55.79	37.07	30.49	25.64
	Min	-70.46	-51.87	-48.46	-44.50
	Mean	-6.01	-5.65	-5.36	-5.11

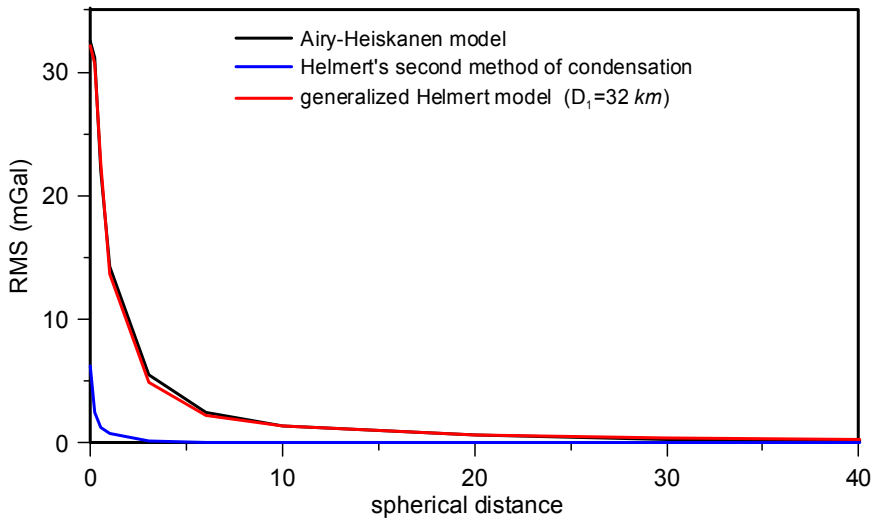

Fig. 5.19: RMS of direct topographical effects at an altitude of 4 km against the cap radius for different topographic-isostatic models

Table 5.4: Far-zone terrain effects at an altitude of 4 km for Helmert's first and generalized model of condensation with different depths in comparison with Airy-Heiskanen (units in *mGal*)

topographic-isostatic model	RMS	Mean	Min	Max
Helmert's first method (21 km)	3.25	-8.49	-16.21	-0.31
generalized Helmert model (25 km)	3.82	-10.08	-19.13	-0.43
generalized Helmert model (30 km)	4.53	-12.07	-22.77	-0.58
generalized Helmert model (32 km)	4.82	-12.86	-24.23	-0.65
Airy-Heiskanen model	5.58	-13.05	-26.88	0.44
generalized Helmert model (35 km)	5.25	-14.05	-26.41	-0.74
generalized Helmert model (40 km)	5.95	-16.03	-30.03	-0.91

Table 5.5: Far-zone direct terrain effects for different cap size radii and different altitudes in case of Helmert's second method of condensation (units in $mGal$)

cap radius	statistics	Earth surface	H= 4 km	H= 6 km	H= 10 km
3^0	RMS	0.238	0.237	0.237	0.234
	Max	0.301	0.301	0.301	0.300
	Min	-0.844	-0.843	-0.840	-0.828
	Mean	-0.131	-0.129	-0.128	-0.122
10^0	RMS	0.071	0.071	0.070	0.070
	Max	0.164	0.164	0.165	0.166
	Min	-0.177	-0.176	-0.175	-0.171
	Mean	0.035	0.036	0.037	0.039
20^0	RMS	0.033	0.033	0.034	0.034
	Max	0.103	0.103	0.103	0.103
	Min	-0.059	-0.059	-0.058	-0.056
	Mean	0.042	0.042	0.042	0.044

Table 5.6: Far-zone direct terrain effects for different cap size radii and different altitudes in case of the generalized Helmert model of condensation ($D_1 = 32$ km; units in $mGal$)

cap radius	statistics	Earth surface	H= 4 km	H= 6 km	H= 10 km
3^0	RMS	4.835	4.820	4.812	4.803
	Max	-0.631	-0.640	-0.650	-0.660
	Min	-24.285	-24.230	-24.220	-24.149
	Mean	-12.900	-12.860	-12.850	-12.828
10^0	RMS	1.418	1.418	1.417	1.415
	Max	-3.620	-3.615	-3.614	-3.609
	Min	-10.596	-10.590	-10.580	-10.560
	Mean	-7.344	-7.338	-7.330	-7.323
20^0	RMS	0.716	0.716	0.715	0.714
	Max	2.647	-2.645	-2.643	-2.639
	Min	-6.181	-6.181	-6.178	-6.170
	Mean	-4.514	-4.513	-4.511	-4.505
40^0	RMS	0.336	0.335	0.335	0.335
	Max	-1.414	-1.413	-1.412	-1.410
	Min	-3.068	-3.067	-3.065	-3.061
	Mean	-2.277	-2.76	-2.275	-2.272
50^0	RMS	0.251	0.251	0.251	0.250
	Max	-1.008	-1.007	-1.006	-1.005
	Min	-2.242	-2.241	-2.240	-2.238
	Mean	-1.653	-1.652	-1.651	-1.649
90^0	RMS	0.093	0.093	0.093	0.093
	Max	-0.330	-0.329	-0.329	-0.329
	Min	-0.785	-0.785	-0.784	-0.784
	Mean	-0.565	-0.564	-0.564	-0.564

size of $5' * 5'$. There are identical results in case of Helmert's condensation methods and some small differences in case of the Airy-Heiskanen method. These differences most probably are caused by the restriction of the Taylor expansions of Eq. (A.4) and Eq. (A.9) to the second term only. For this reason it would be necessary to develop the series including the cubic term of Taylor expansions for distance and logarithmic functions to remove these differences. Another interesting aspect of this method is the choice of the maximum expansion degree of the spherical harmonic series representing the topography. Figure 5.21 gives an impression of the size of different spectral bands of the spherical harmonic expansion. It seems that an upper degree of 100 is sufficient even for high accuracy airborne gravimetry (1-2 $mGal$) for all topographic-compensation models investigated here. At the Earth's surface a high degree of $N_{max} = 360$ is necessary to consider the effects of the topographic-compensating masses in case of Helmert's first or generalized methods of condensation and the Airy-Heiskanen isostatic model. In case of Helmert's second method of condensation, an upper degree of 50 may fulfill the accuracy demand of Earth's surface gravimetry.

To give an impression of the distribution of the far-zone terrain effects depending on the topography within the near zone, the direct terrain effect for Helmert's methods of condensation and the Airy-Heiskanen model at an altitude of 4 km are plotted in Fig. 5.22.

5.3.2.2 Indirect terrain effect on geoid and gravity

Finally, the indirect terrain effects for the same test region are shown in Figs. 5.24 and 5.25. Figure 5.24 shows the far-zone primary indirect terrain effects on the geoid heights for the different topographic-compensating models. The effects are rather large for the generalized Helmert model ($D_1 = 32\ km$) and for the Airy-Heiskanen model, except those for Helmert's second condensation method. The situation is similar for the far-zone secondary indirect terrain effects on gravity at the surface of the Earth as Fig. 5.25 demonstrates.

5.3.2.3 Concluding remarks to the terrain effects of gravity and geoid heights

For the cap size of $\psi_0 = 3^0$ investigated here, the far-zone contributions for the primary topographic indirect effect are as large as up to 13 m while the direct topographic effect is in the size of up to 28 $mGal$. That means that the far-zone contributions to the primary indirect effects are of comparable magnitude as the near-zone contributions in contrast to the direct effect. This is caused by the fact that the potential is inverse to the distance between the computation point and mass elements while gravity is inverse to the squared distance which tapers off more quickly.

From Fig. 5.22 it can be concluded that the far-zone terrain effects at aeroplane altitude in case of Helmert's second method of condensation can be neglected for spherical cap size radii larger than 3^0 as the maximum values of these effects are smaller than the accuracy of the airborne gravity measurements (1-2 $mGal$). On the other hand, these effects must be taken into account for Helmert's first or generalized model of condensation and the Airy-Heiskanen model. Figure 5.23 shows that the far-zone effects at the surface of the Earth are more or less the same as at aeroplane attitudes higher than 4 km and for all topographic-isostatic models.

The results of the far-zone effects determined in the present investigation at the surface of the Earth were compared with those calculated from Novàk et al. (2001). Both soluations are shown in Fig. 5.26. There are some differences between the two methods. These differences are caused by a different handling of the topography height of the computation point. In case of Novàk et al. (2001) the heights of the computation points are computed from the spherical harmonic expansion up to the maximum degree used for calculating the far-zone effects. This is not sufficient for a precise determination of the far-zone effects. But we have to point out that this holds for a region with a rough topography. Therefore the differences between the two methods may be neglected for areas with a smooth topography or if the maximum degree of the spherical harmonic expansion of the topography has been extended to a high degree as for example $Nmax = 2160$.

The formulae based on the spherical harmonics as derived in this study are very efficient. The computation of the various topographic-isostatic effects at a grid with a grid size of $5' * 5'$ – these are 1296 point values

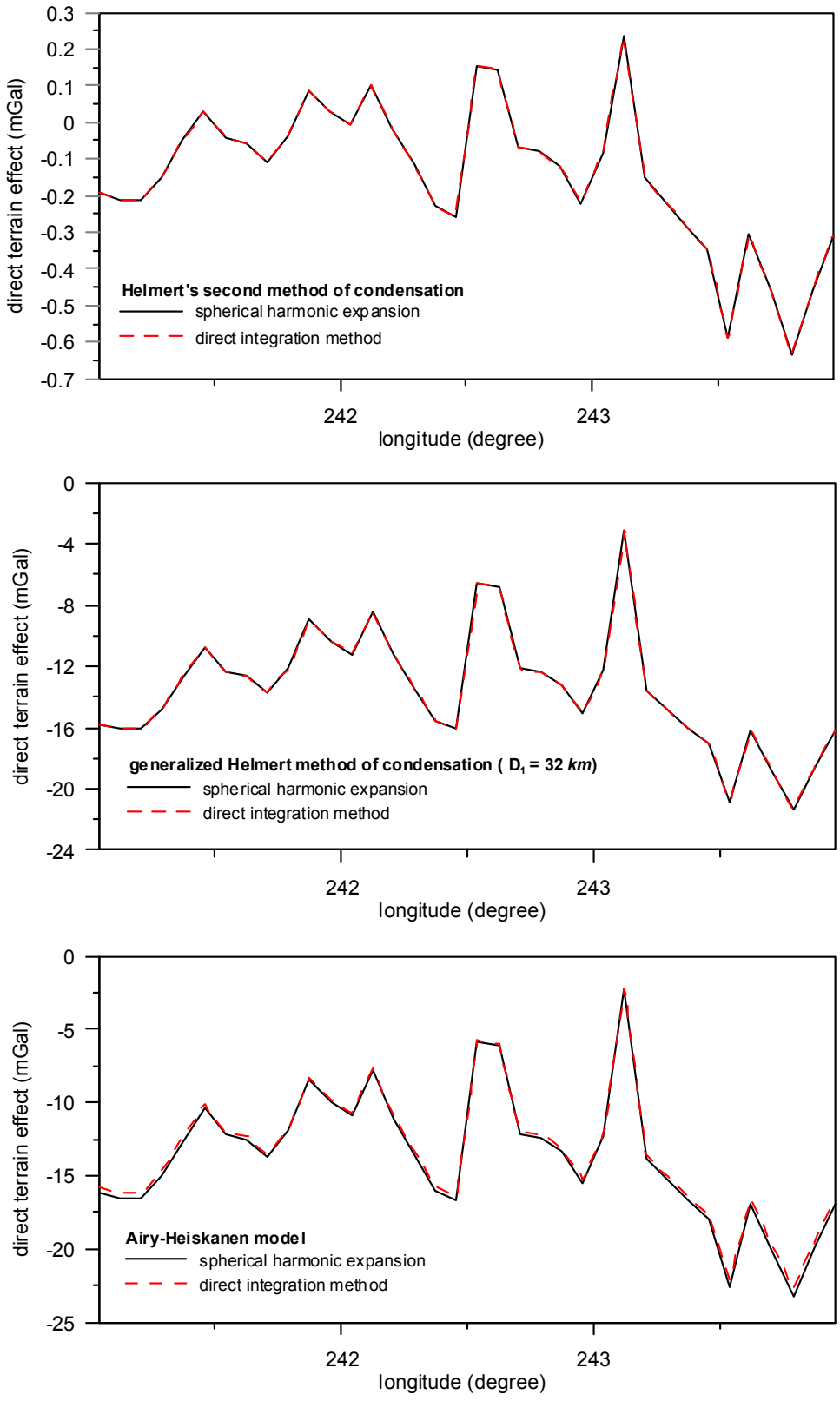

Fig. 5.20: Far-zone direct terrain effect along the 50^0 latitude for different topographic-isostatic models at an altitude of 4 km

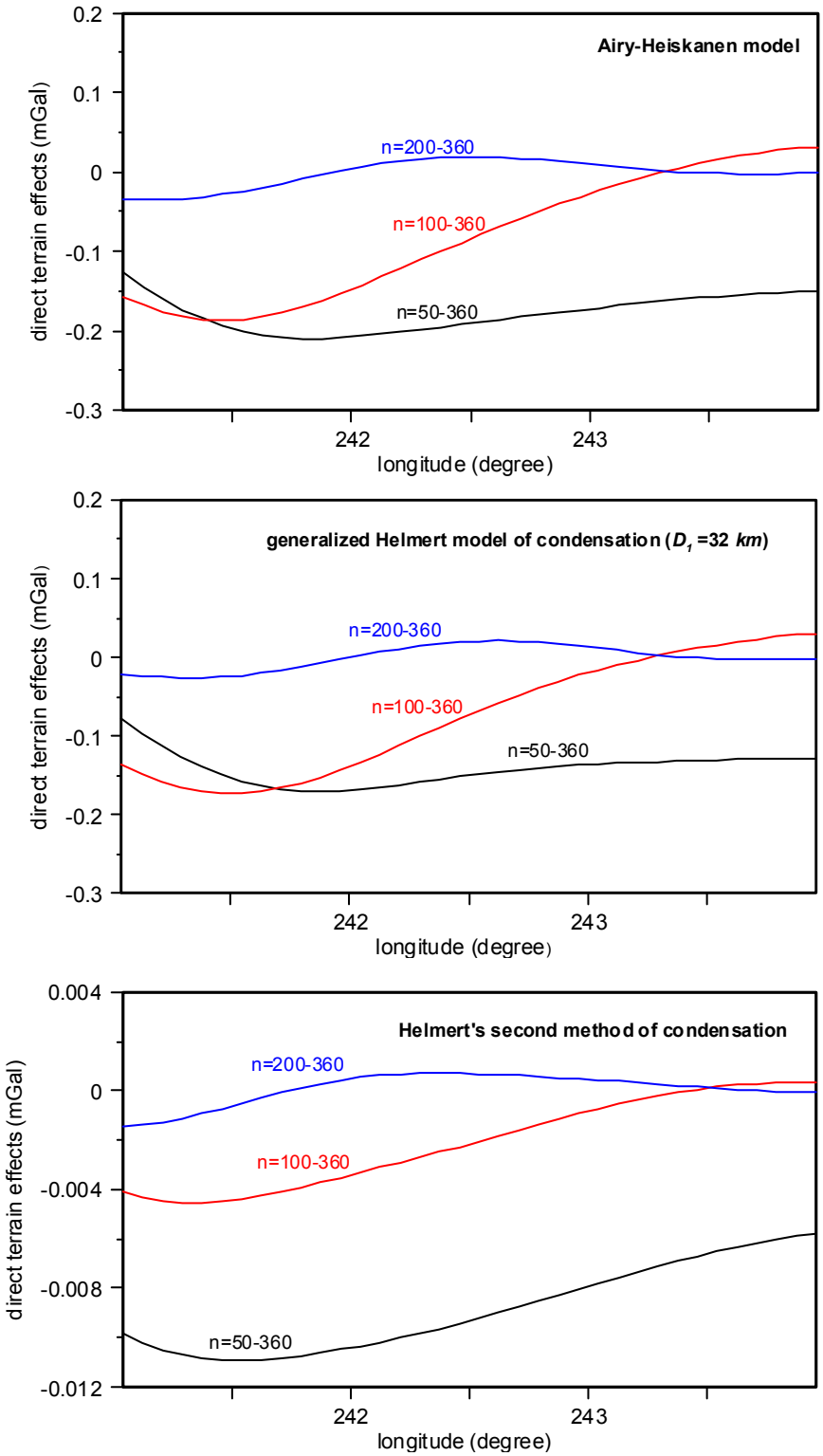

Fig. 5.21: Far-zone direct terrain effect along the 50^0 latitude for different spectral bands of the spherical harmonic expansion

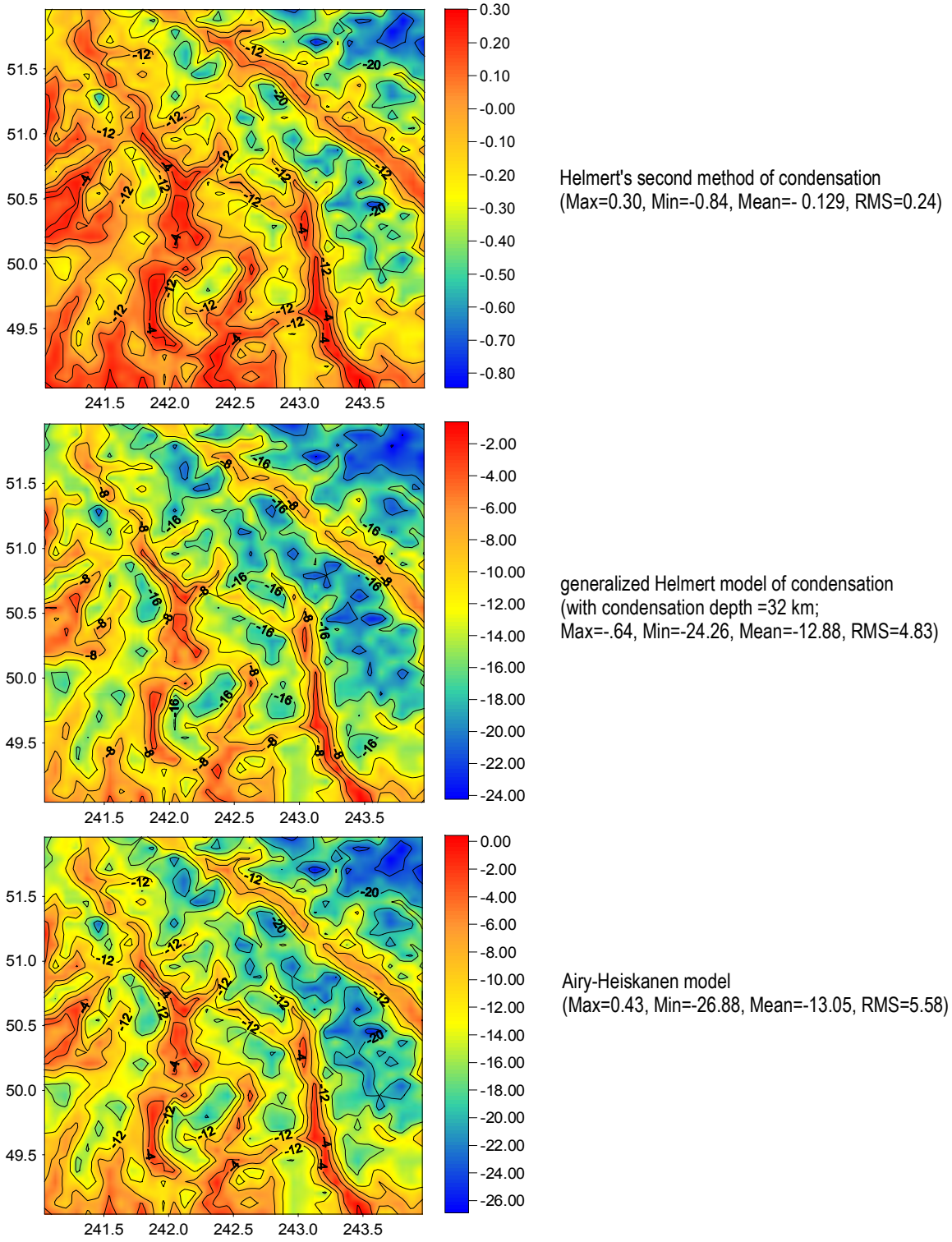

Fig. 5.22: Far-zone direct terrain effect on gravity of the area outside a cap size of $\psi_0 = 3^0$ for different topographic-isostatic models at an aeroplane altitude of $4km$ (units in $mGal$)

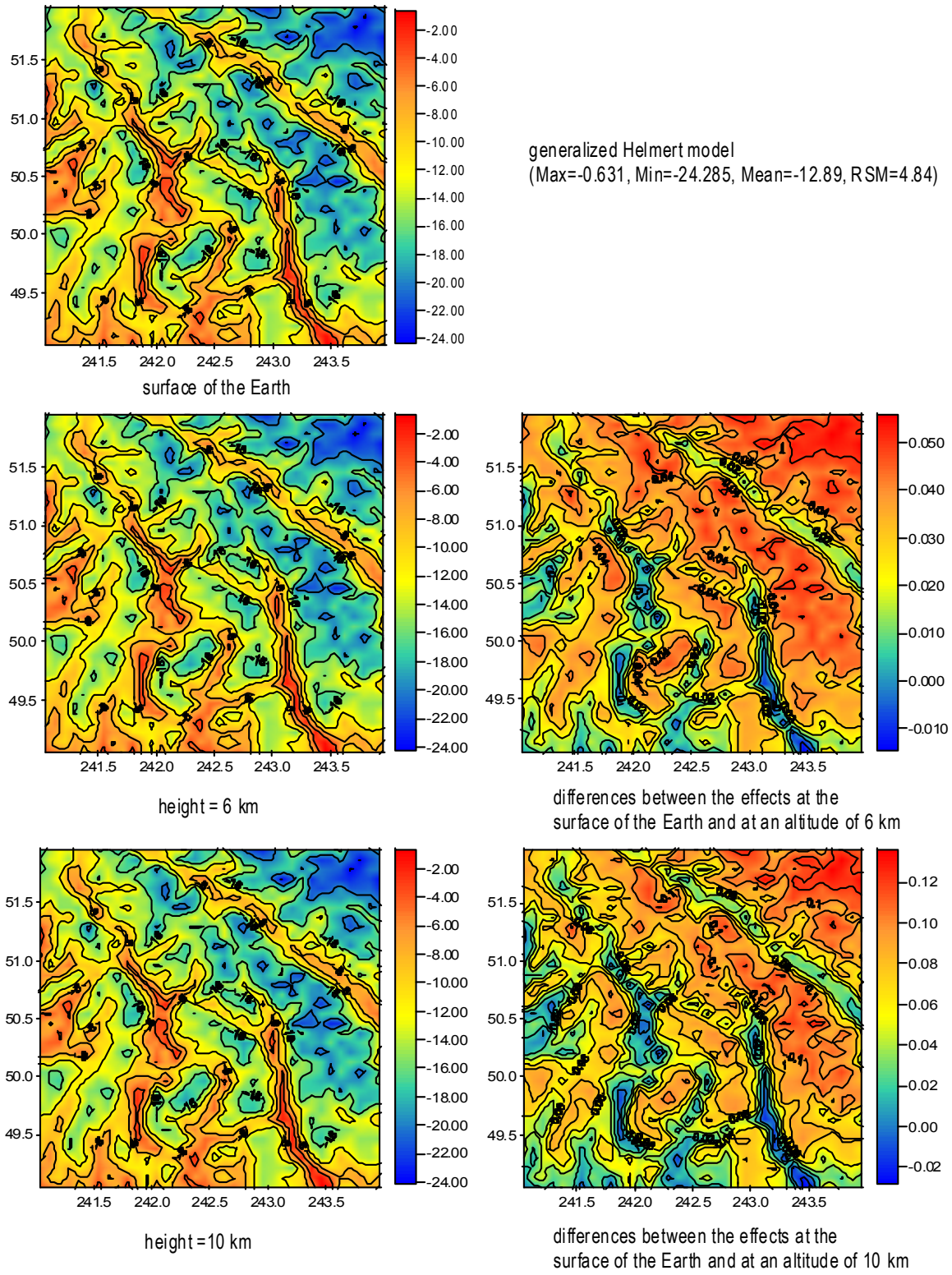

Fig. 5.23: Far-zone direct terrain effect on gravity of the area outside a cap size of $\psi_0 = 3^0$ in case of generalized Helmert method ($D_1 = 32\ km$) at different altitudes of the computation point (units in $mGal$)

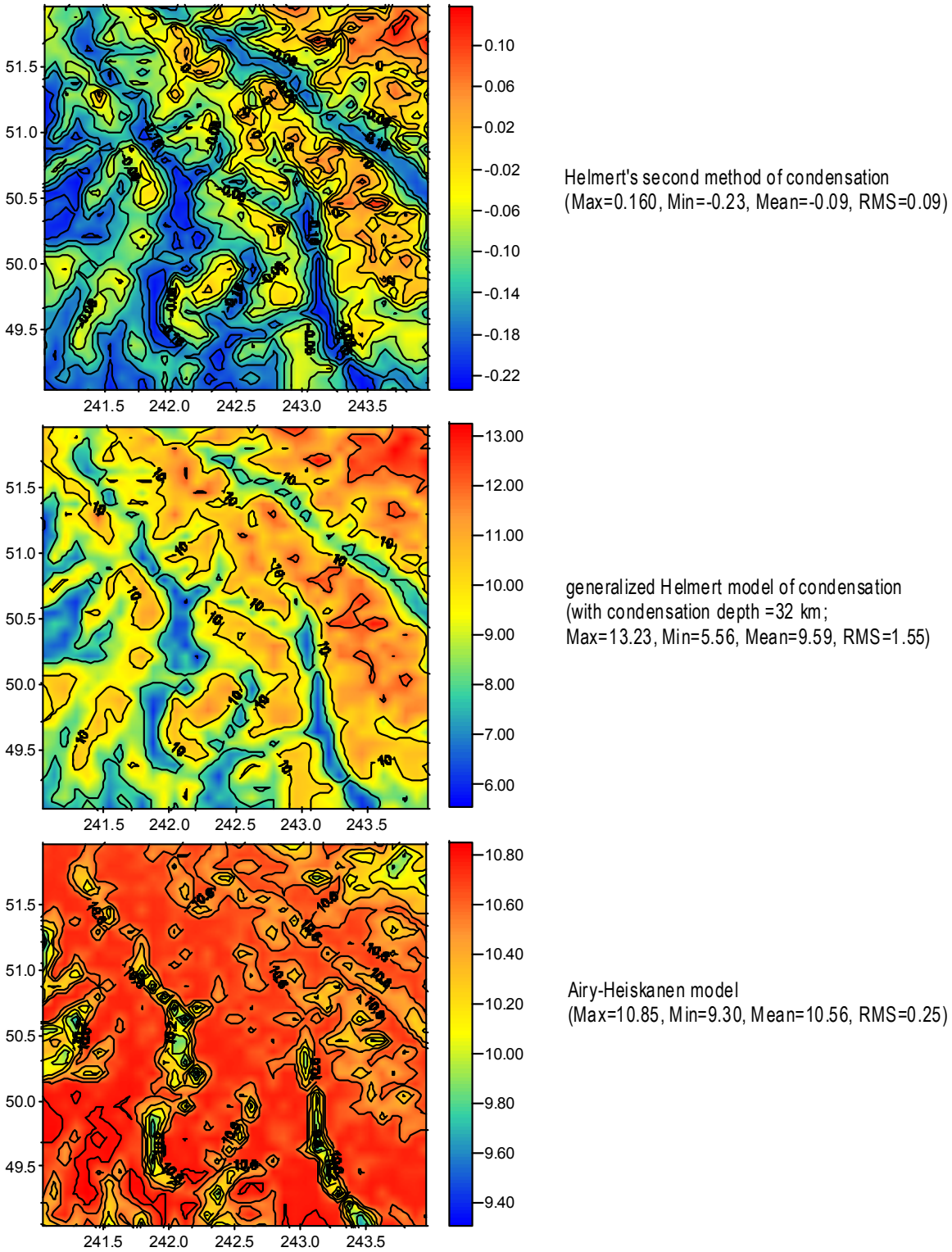

Fig. 5.24: Far-zone primary indirect terrain effect on geoid heights of the area outside a cap size of $\psi_0 = 3^0$ for different topographic-compensation models (units in meter)

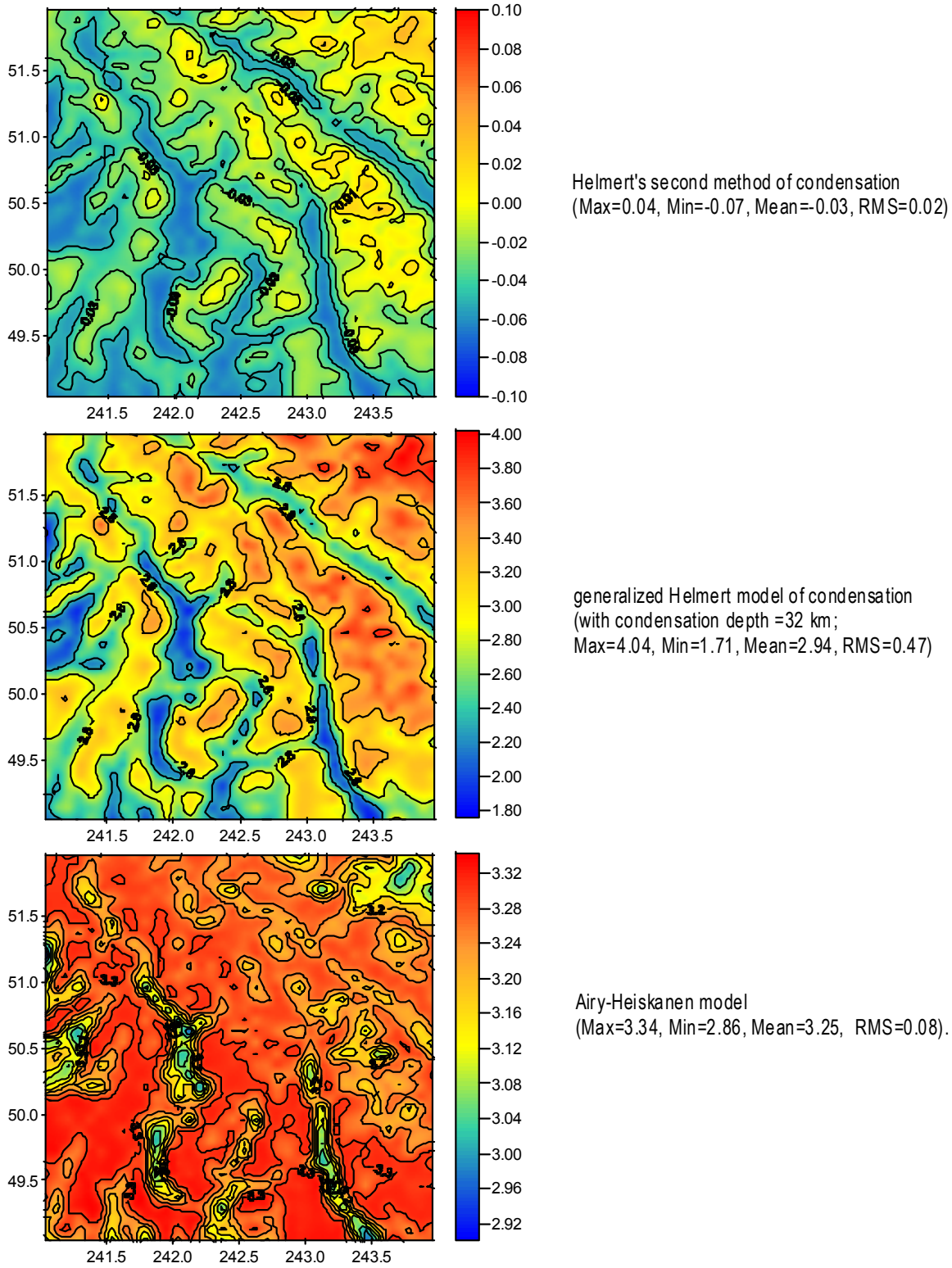

Fig. 5.25: Far-zone secondary indirect terrain effect on gravity of the area outside a cap size of $\psi_0 = 3^0$ for different topographic-isostatic models at the surface of the Earth (units in $mGal$)

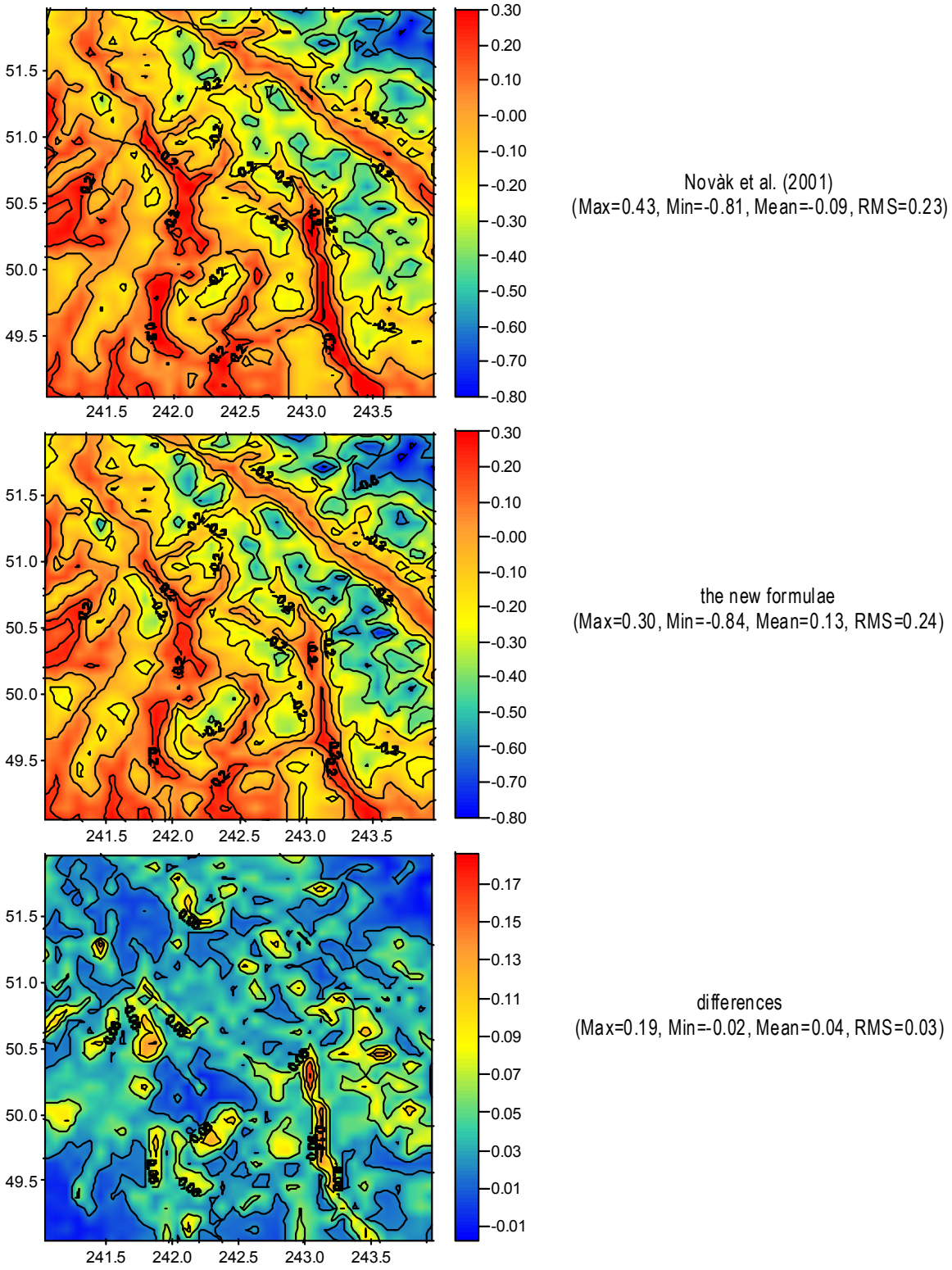

Fig. 5.26: Far-zone direct terrain effects in case of Helmert's second method of condensation at the surface of the Earth: (a) formulae in Novàk et al. (2001), (b) from Eq. (4.191), (c) differences between the two methods (units in *mGal*)

for our test area – and a spherical harmonic expansion of the topography of up to degree $N_{max} = 360$ takes 48 *sec* on a PC (1, 8 GHz processor frequency). The computation costs are reduced further in case of larger cap size radii, because in this case the upper degree of the spherical harmonic expansion can be reduced as well.

5.3.2.4 Far-zone terrain effect on airborne gradiometry

The far-zone terrain effects at aeroplane altitude for the Himalaya region on $z-$ component in a local coordinates system of the gravity tensor, V_{zz}, are shown in Fig. 5.27. The cap size has been taken to be 3^0. Figure 5.27 shows that the effects of far-zone terrain effects are very small and in the size of approximately one percent of the total effect. This is caused by the fact that the second derivatives of the potential is inverse to the cubic distance between the computation and integration points which tapers off very quickly.

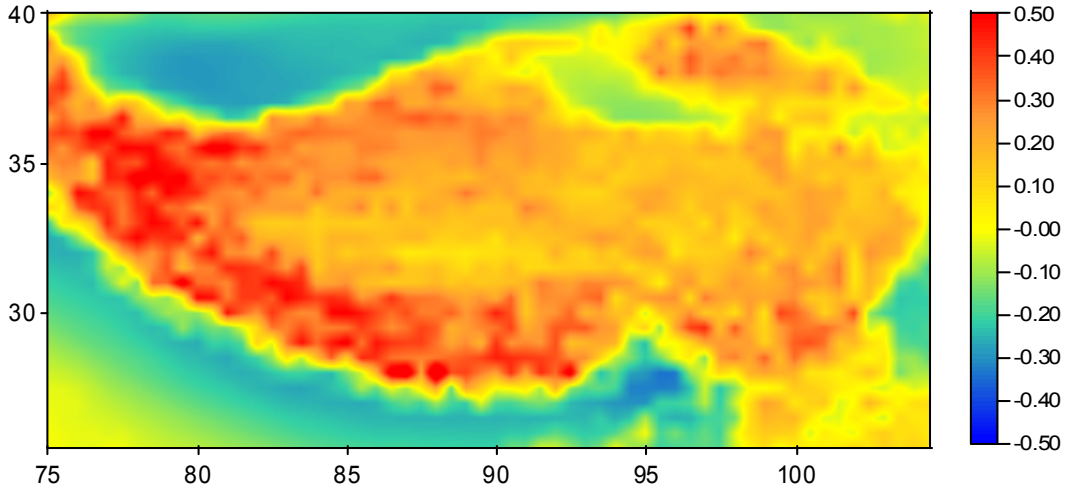

Fig. 5.27: Effects of the far-zone terrain on the tensor components V_{zz} of the area outside a cap size of $\psi_0 = 3^0$ at an altitude of 10 km for the Airy-Heiskanen model for the Himalaya region (units in Eötvös)

5.4 Effect of topographic-isostatic masses in satellite applications

As we stated in section 4.1.2 and section 4.2 the effects of topographic-isostatic masses at satellite altitude can be determined from the direct integration method or by a using spherical harmonic expansion. Therefore, this section starts with the determination of the effects of topographic masses on Satellite Gravity Gradiometry based on the two methods. The results have been compared and show the efficiency of the spherical harmonic approach is demonstrated. Then the effects of the topographic-isostatic masses for different models at GOCE altitude have been determined. Finally, the effects of the topographic-isostatic masses on POD (Precis orbit determination) and SST (Satellite-to-Satellite Tracking) observations are investigated.

5.4.1 Topographic-isostatic effects on gravity gradients

5.4.1.1 Computation formulae

To determine the effects of topographic-isostatic masses on the gravity gradients at GOCE altitude from spherical harmonic expansions of the topography, the formulae derived by Tscherning (1976) are used for the potential and its first and second derivations. The potential of the topographic-isostatic masses reads (ibid.):

$$V(r,\varphi,\lambda) = \frac{Gm}{R}\sum_{n=0}^{N_{max}}\left(\frac{R}{r}\right)^{n+1}\sum_{m=0}^{n}(c_{nm}\cos m\lambda + s_{nm}\sin m\lambda)P_{nm}(\sin\varphi), \tag{5.16}$$

its derivates with respect to (r, ϑ, λ) yields (ibid.):

$$V_r(r,\varphi,\lambda) = -\frac{Gm}{R^2}\sum_{n=0}^{N_{max}}(n+1)\left(\frac{R}{r}\right)^{n+2}\sum_{m=0}^{n}(c_{nm}\cos m\lambda + s_{nm}\sin m\lambda)P_{nm}(\sin\varphi), \tag{5.17}$$

$$V_\varphi(r,\varphi,\lambda) = \frac{Gm}{R}\sum_{n=0}^{N_{max}}\left(\frac{R}{r}\right)^{n+1}\sum_{m=0}^{n}(c_{nm}\cos m\lambda + s_{nm}\sin m\lambda)\frac{\partial P_{nm}(\sin\varphi)}{\partial\varphi}, \tag{5.18}$$

$$V_\lambda(r,\varphi,\lambda) = \frac{Gm}{R}\sum_{n=0}^{N_{max}}\left(\frac{R}{r}\right)^{n+1}\sum_{m=0}^{n}m(-c_{nm}\sin m\lambda + s_{nm}\cos m\lambda)P_{nm}(\sin\varphi). \tag{5.19}$$

The second derivatives can be determined by the formulae (ibid.)

$$V_{rr}(r,\varphi,\lambda) = \frac{Gm}{R^3}\sum_{n=0}^{N_{max}}(n+1)(n+2)\left(\frac{R}{r}\right)^{n+3}\sum_{m=0}^{n}P_{nm}(\sin\varphi)(c_{nm}\cos m\lambda + s_{nm}\sin m\lambda), \tag{5.20}$$

$$V_{r,\varphi}(r,\varphi,\lambda) = -\frac{Gm}{R^2}\sum_{n=0}^{N_{max}}(n+1)\left(\frac{R}{r}\right)^{n+2}\sum_{m=0}^{n}(c_{nm}\cos m\lambda + s_{nm}\sin m\lambda)\frac{\partial P_{nm}(\sin\varphi)}{\partial\varphi}, \tag{5.21}$$

$$V_{r,\lambda}(r,\varphi,\lambda) = \frac{Gm}{R^2}\sum_{n=0}^{N_{max}}(n+1)\left(\frac{R}{r}\right)^{n+2}\sum_{m=0}^{n}m(c_{nm}\sin m\lambda - s_{nm}\cos m\lambda)P_{nm}(\sin\varphi), \tag{5.22}$$

$$V_{\lambda,\lambda}(r,\varphi,\lambda) = -\frac{Gm}{R}\sum_{n=0}^{N_{max}}\left(\frac{R}{r}\right)^{n+1}\sum_{m=0}^{n}m^2(c_{nm}\cos m\lambda + s_{nm}\sin m\lambda)P_{nm}(\sin\varphi), \tag{5.23}$$

$$V_{\varphi,\varphi}(r,\varphi,\lambda) = \frac{Gm}{R}\sum_{n=0}^{N_{max}}\left(\frac{R}{r}\right)^{n+1}\sum_{m=0}^{n}(c_{nm}\cos m\lambda + s_{nm}\sin m\lambda)\frac{\partial^2 P_{nm}(\sin\varphi)}{\partial\varphi^2}, \tag{5.24}$$

$$V_{\varphi,\lambda}(r,\varphi,\lambda) = \frac{Gm}{R}\sum_{n=0}^{N_{max}}\left(\frac{R}{r}\right)^{n+1}\sum_{m=0}^{n}m(-c_{nm}\sin m\lambda + s_{nm}\cos m\lambda_p)\frac{\partial P_{nm}(\sin\varphi)}{\partial\varphi}. \tag{5.25}$$

In order to simplify the evaluation of the second derivatives of the gravitational potential, let us introduce a tangential coordinate system frame at a point with spherical coordinates (r, φ, λ) as shown in Fig. 4.5 as follows: the x-axis is directed to the north, the y- axis to the east, and the z-axis coincides with the radius vector. Then the first and second derivatives of the gravitational potential with respect to x,y and z may be related to the first and second derivatives with respect to r, φ, λ in the following equations:

$$V_x(r,\varphi,\lambda) = \frac{1}{r}V_\varphi, \tag{5.26}$$

$$V_y(r,\varphi,\lambda) = \frac{1}{r\cos\varphi}V_\lambda, \tag{5.27}$$

$$V_z(r,\varphi,\lambda) = V_r, \tag{5.28}$$

$$V_{xx}(r,\varphi,\lambda) = \frac{1}{r}V_r(r,\varphi,\lambda) + \frac{1}{r^2}V_{\varphi\varphi}(r,\varphi,\lambda), \tag{5.29}$$

$$V_{xy}(r,\varphi,\lambda) = V_{yx}(r,\varphi,\lambda) = \frac{1}{r^2\cos\varphi}(\tan\varphi V_\lambda(r,\varphi,\lambda) + V_{\varphi\lambda}(r,\varphi,\lambda)), \tag{5.30}$$

$$V_{xz}(r,\varphi,\lambda) = V_{zx}(r,\varphi,\lambda) = \frac{1}{r^2}(-V_\varphi(r,\varphi,\lambda) + rV_{r\varphi}(r,\varphi,\lambda)), \tag{5.31}$$

$$V_{yy}(r,\varphi,\lambda) = \frac{1}{r}V_r(r,\varphi,\lambda) - \frac{\tan\varphi}{r^2}V_\varphi(r,\varphi,\lambda) + \frac{1}{r^2\cos^2\varphi}V_{\lambda\lambda}(r,\varphi,\lambda), \tag{5.32}$$

$$V_{yz}(r,\varphi,\lambda) = V_{zy}(r,\varphi,\lambda) = \frac{1}{r\cos\varphi}(-\frac{1}{r}V_{\lambda}(r,\varphi,\lambda) + V_{r\lambda}(r,\varphi,\lambda)), \tag{5.33}$$

$$V_{zz}(r,\varphi,\lambda) = V_{rr}(r,\varphi,\lambda). \tag{5.34}$$

Finally, the first and second derivatives of the potential can be calculated using the following formulae:

$$V_x(r,\varphi,\lambda) = \frac{GM}{r^2}\sum_{n=0}^{N_{max}}\left(\frac{R}{r}\right)^n \sum_{m=0}^{n}(\cos m\lambda c_{nm} + \sin m\lambda s_{nm})\frac{\partial P_{nm}(\sin\varphi)}{\partial\varphi}, \tag{5.35}$$

$$V_y(r,\varphi,\lambda) = \frac{GM}{r^2\cos\varphi}\sum_{n=0}^{N_{max}}\left(\frac{R}{r}\right)^n \sum_{m=0}^{n} m(-c_{nm}\sin m\lambda + s_{nm}\cos m\lambda)P_{nm}(\sin\varphi), \tag{5.36}$$

$$V_z(r,\varphi,\lambda) = -\frac{Gm}{r^2}\sum_{n=0}^{N_{max}}(n+1)\left(\frac{R}{r}\right)^n \sum_{m=0}^{n}(c_{nm}\cos m\lambda + s_{nm}\sin m\lambda)P_{nm}(\sin\varphi), \tag{5.37}$$

$$V_{xx}(r,\varphi,\lambda) = \frac{GM}{r^3}\sum_{n=0}^{N_{max}}\left(\frac{R}{r}\right)^n \sum_{m=0}^{n}(\,c_{nm}\cos m\lambda + s_{nm}\sin m\lambda) \left[-(n+1)P_{nm}(\sin\varphi) + \frac{\partial^2 P_{nm}(\sin\varphi)}{\partial\varphi^2}\right], \tag{5.38}$$

$$V_{xy}(r,\varphi,\lambda) = \frac{GM}{r^3\cos\varphi}\sum_{n=0}^{N_{max}}\left(\frac{R}{r}\right)^n \sum_{m=0}^{n} m\,(\,-c_{nm}\sin m\lambda + s_{nm}\cos m\lambda) \left[\tan\varphi P_{nm}(\sin\varphi) + \frac{\partial P_{nm}(\sin\varphi)}{\partial\varphi}\right], \tag{5.39}$$

$$V_{xz}(r,\varphi,\lambda) = -\frac{GM}{r^3}\sum_{n=0}^{N_{max}}\left(\frac{R}{r}\right)^n (n+2)\sum_{m=0}^{n}(c_{nm}\cos m\lambda + s_{nm}\sin m\lambda)\frac{\partial P_{nm}(\sin\varphi)}{\partial\varphi}, \tag{5.40}$$

$$V_{yy}(r,\varphi,\lambda) = \frac{GM}{r^3}\sum_{n=0}^{N_{max}}\left(\frac{R}{r}\right)^n \sum_{m=0}^{n}(\,c_{nm}\cos m\lambda + s_{nm}\sin m\lambda) \left\{\left[-(n+1) - \frac{m^2}{\cos^2\varphi}\right]P_{nm}(\sin\varphi) - \tan\varphi\frac{\partial P_{nm}(\sin\varphi)}{\partial\varphi}\right\}, \tag{5.41}$$

$$V_{yz}(r,\varphi,\lambda) = \frac{Gm}{r^3\cos\varphi}\sum_{n=0}^{N_{max}}(n+2)\left(\frac{R}{r}\right)^n \sum_{m=0}^{n} m(c_{nm}\sin m\lambda - s_{nm}\cos m\lambda)P_{nm}(\sin\varphi), \tag{5.42}$$

$$V_{zz}(r,\varphi,\lambda) = \frac{GM}{r^3}\sum_{n=0}^{Nmax}(n+1)(n+2)\left(\frac{R}{r}\right)^n \sum_{m=0}^{n}(c_{nm}\cos m\lambda + s_{nm}\sin m\lambda)P_{nm}(\sin\varphi). \tag{5.43}$$

5.4.1.2 Integral formulae versus determination by spherical harmonic expansion

In order to get insight into the numerical differences between the numerical integration method and the spherical harmonic expansion of the topography, the effects of the topographic masses on the second derivatives of the gravitational masses at GOCE altitude caused by the global topography have been determined by both methods. In both cases the rock equivalent heights procedures with a resolution of 5 arc-minutes have been used. This fine grid size has been chosen to overcome the discretization errors in case of the numerical integration method and to minimize the problem of the non-orthogonality of the discrete Legendre polynomials in case of the spherical harmonic expansion. The evaluation has been performed for the Asia region. The differences between the numerical results of the discretized numerical integration and the spherical harmonic approach are shown in Table 5.7. The table shows that the differences between the two methods are very small and can be neglected if we keep in mind the accuracy of the observation from the GOCE satellite ($5 * 10^{-3}$ Eötvös). This means that it is better to use the spherical harmonic expansion for determining the effects at satellite altitude as it sharply saves CPU time.

Table 5.7: Statistics of the differences between the numerical integration method and the spherical harmonic expansion on the tensor component at an altitude of 250 km for Airy-Heiskanen model (units in Eötvös)

tensor components	Max	Min	RMS
xx	2.3E-5	-1.8E-4	2.8E-5
yy	1.1E-4	-2.37E-5	1.5E-5
zz	7.9E-5	-3.7E-6	1.7E-5

5.4.1.3 Computation of various topographic-isostatic models

The topographic-isostatic effects of the components of the gravitational tensor at a satellite altitude of 250 km are already considerably damped (Fig. 5.28) compared to the features in an aircraft altitude of 10 km (Fig. 5.27) for the same region. Nevertheless, the structure of the topographic-isostatic effects at a satellite altitude of 250 km shows still steep changes with a gradient of 0.70 Eötvös per 100 km in north-south direction (Fig. 5.29) and of 0.50 m Eötvös per 100 km in east-west direction (Fig. 5.30).

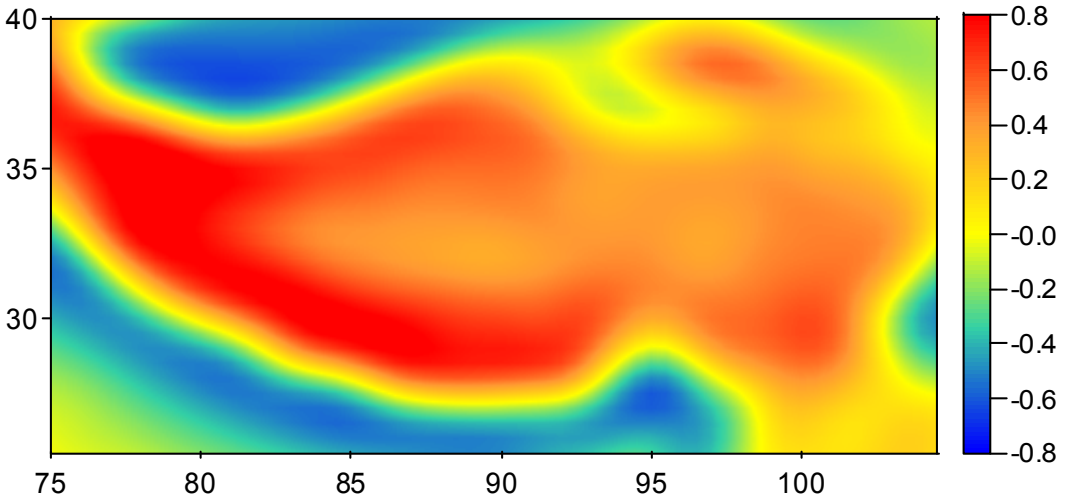

Fig. 5.28: Effects of the topographic-isostatic masses on the tensor component V_{zz} at an altitude of 250 km for the Airy-Heiskanen model for the Himalaya region; units in Eötvös)

If it is possible to remove this sort of roughness from the observations with a noise level of approximately $5 * 10^{-3}$ Eötvös expected for GOCE the downward continuation can be considerably simplified. The GOCE mission is designed to derive the static part of the gravity field with an extremely high precision. Therefore, it is very important to filter the observations by the topographic-isostatic gravity field effects to ease the requirements for the downward continuation. An additional regularization might be avoided in that case; but this depends on the envisaged resolution of the gravity field model and on the error level of the observations.

Figs. 5.31 to 5.33 give an impression of the size of the effects of the topographic-isostatic masses for the xx, yy and zz-components of the gravitational tensor, respectively. The effects of the topographic-isostatic masses for the Pratt-Hayford and the combined Airy-Pratt model are slightly larger than in case of the Airy-Heiskanen and Helmert's first condensation model, while Helmert's second condensation model produces only tiny effects. The results indicate that the effects of topographic-isostatic masses and the gradient of the different tensor components for different models are significant and it seems to be advantageous to take them into account for the gravity field recovery of the GOCE observations. This question will be investigated in a simulation experiment.

Again, the coincidence of the generalized Helmert model of condensation with the other isostatic models depends strongly on the condensation depths of Helmert's model (Table 5.8 and Fig. 5.34). E.g, the ge-

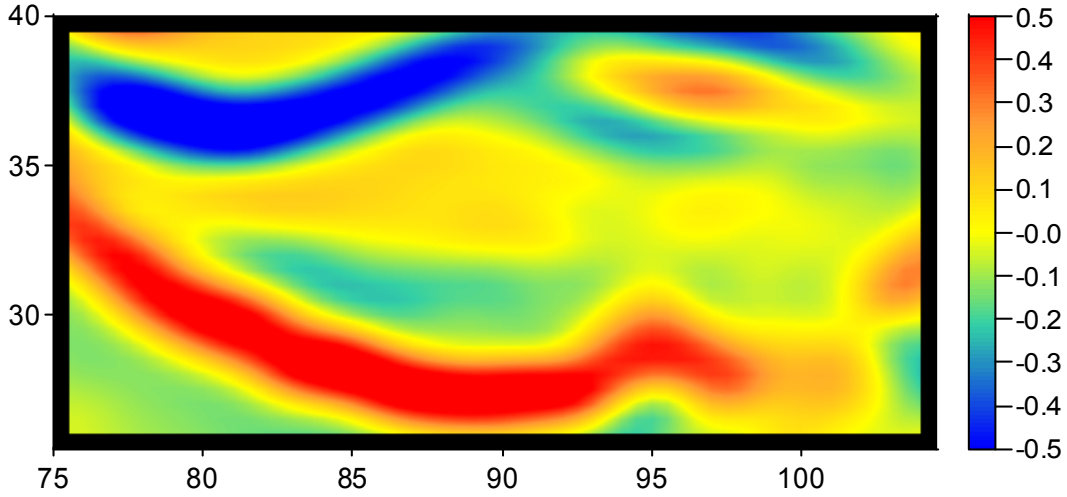

Fig. 5.29: Direction derivation of the tensor component V_{zz} in north-south direction at an altitude of 250 km (effect of the topographic-isostatic masses on the tensor component V_{zz} for the Airy-Heiskanen model for the Himalaya region; units in Eötvös/degree)

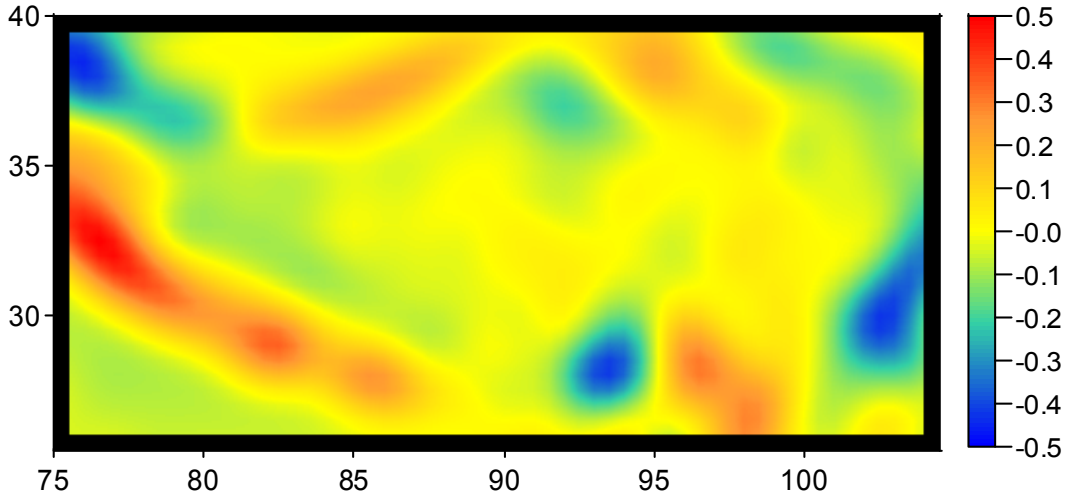

Fig. 5.30: Direction derivation of the tensor component V_{zz} in west-east direction at an altitude of 250 km (effect of the topographic-isostatic masses on the tensor component V_{zz} for the Airy-Heiskanen model for the Himalaya region; units in Eötvös/degree)

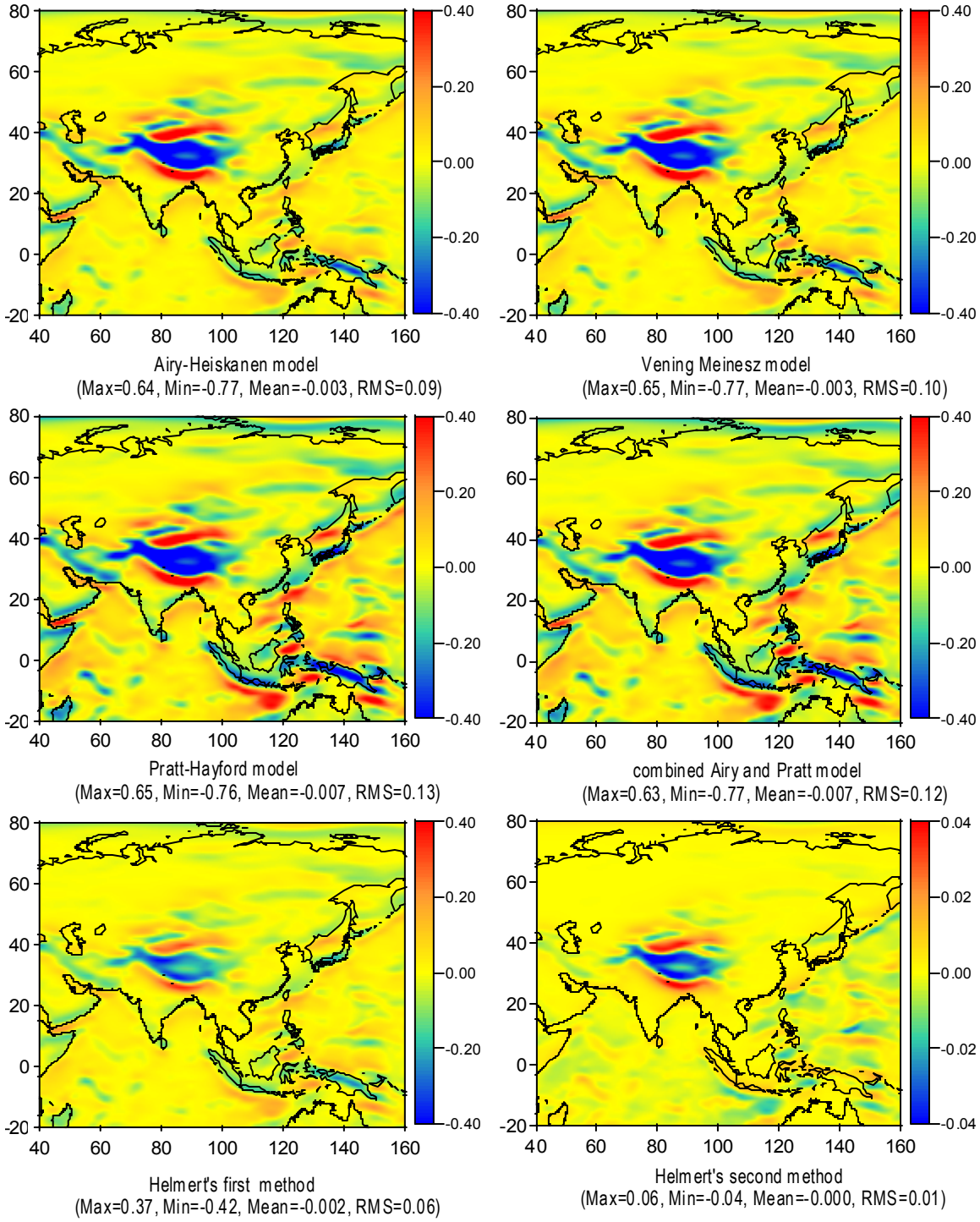

Fig. 5.31: Effects of the topographic-isostatic masses on the tensor component V_{xx} at an altitude of 250 km for different topographic-isostatic models (units in Eötvös)

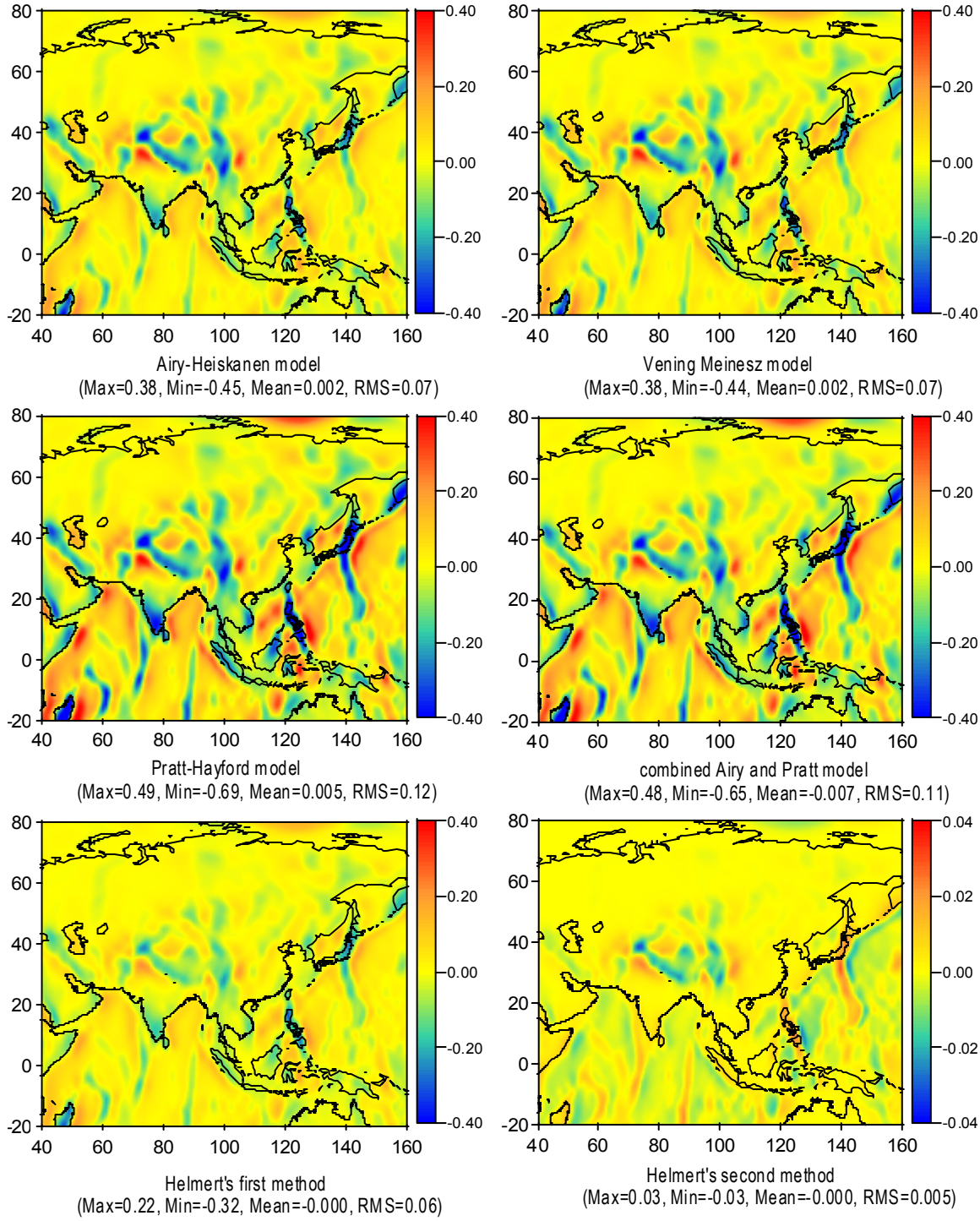

Fig. 5.32: Effects of the topographic-isostatic masses on the tensor component V_{yy}at an altitude of 250 km for Helmert's first method of condensation with different depths (units in Eötvös)

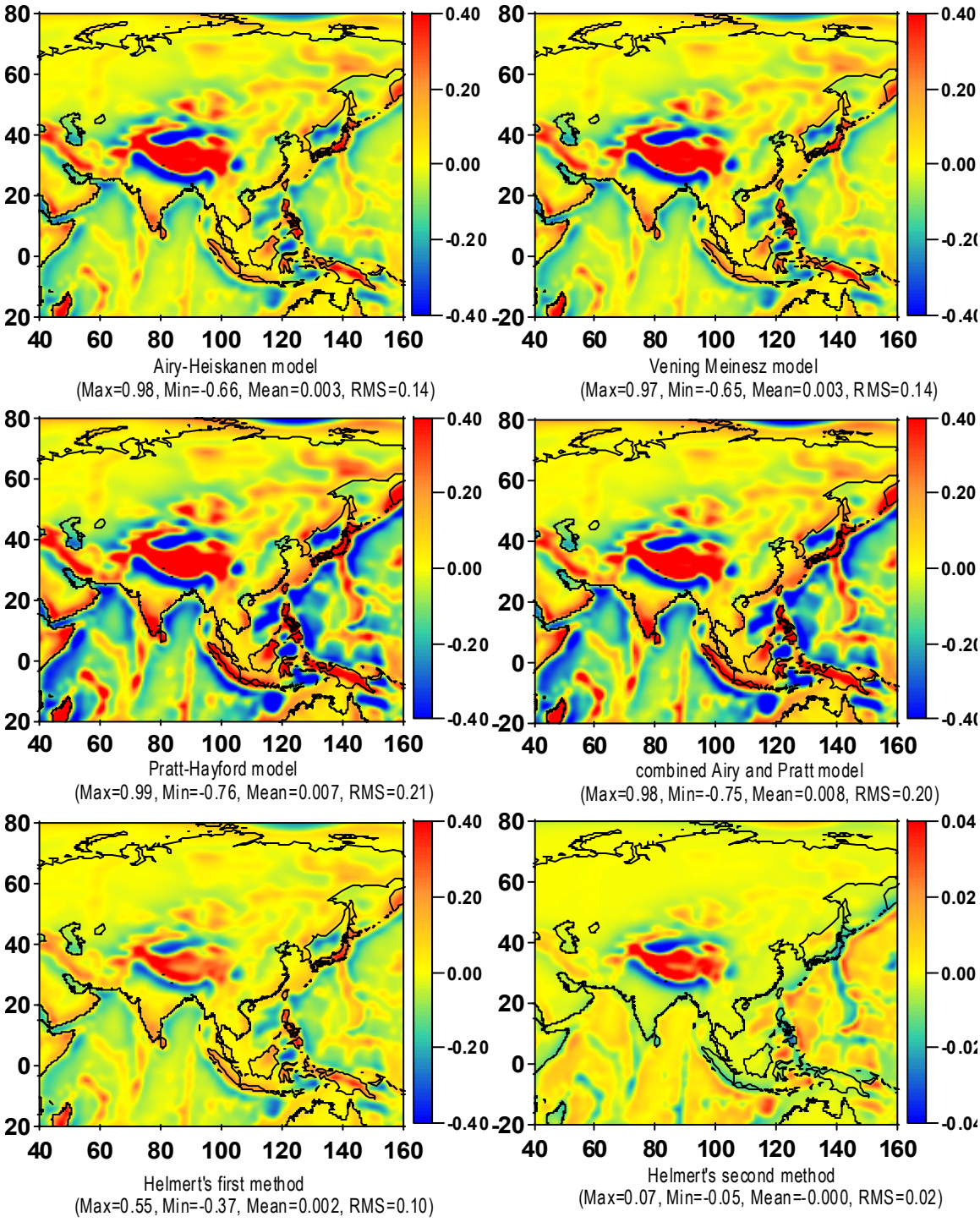

Fig. 5.33: Effects of the topographic-isostatic masses on the tensor component V_{zz} at an altitude of 250 km for different topographic-isostatic models (units in Eötvös)

neralized Helmert model of condensation with a condensation depth between 45 km and 50 km coincides well with the Pratt-Hayford model. In case of a condensation depth of 30 km for the generalized Helmert model the effects coincide approximately with the Airy-Heiskanen model. For the second radial derivatives the numerical results for different topographic-isostatic models are practically equivalent to those reported in Heck and Wild (2005) and Wild and Heck (2004b).

Finally, the effects of the topographic-isostatic masses in the global scale for different topographic-isostatic models are shown in Figs. 5.35 to 5.37. The plots show the distribution of these effects for the diagonal components of the gravity tensor. The condensation depth of the generalized Helmert model for this test computation has been taken to be 30 km. The effects are as large as 1 Eötvös and more. Compared to the observation accuracy of approximately $5 * 10^{-3}$ Eötvös, again these are significant gravity field effects according to the topography and its isostatic compensation in the gravity field signal.

Table 5.8: Effects of the topographic-isostatic masses on the tensor component at an altitude of 250 km for Helmert's first or generalized method of condensation with different depths in comparison with Airy-Heiskanen and Pratt-Hayford models (units in Eötvös)

topographic-isostatic model	RMS	Mean	Min	Max
Helmert's first method	0.10	0.002	-0.37	0.55
generalized Helmert model (25 km)	0.12	0.002	-0.43	0.63
Airy-Heiskanen	0.14	0.003	-0.65	0.97
Vening Meinesz	0.14	0.003	-0.66	0.98
generalized Helmert model (30 km)	0.14	0.003	-0.49	0.73
generalized Helmert model (35 km)	0.16	0.003	-0.56	0.83
generalized Helmert model (40 km)	0.18	0.004	-0.64	0.92
generalized Helmert model (45 km)	0.20	0.004	-0.71	1.01
Pratt-Hayford	0.21	0.007	-0.76	0.99
generalized Helmert model (50 km)	0.22	0.005	-0.78	1.10

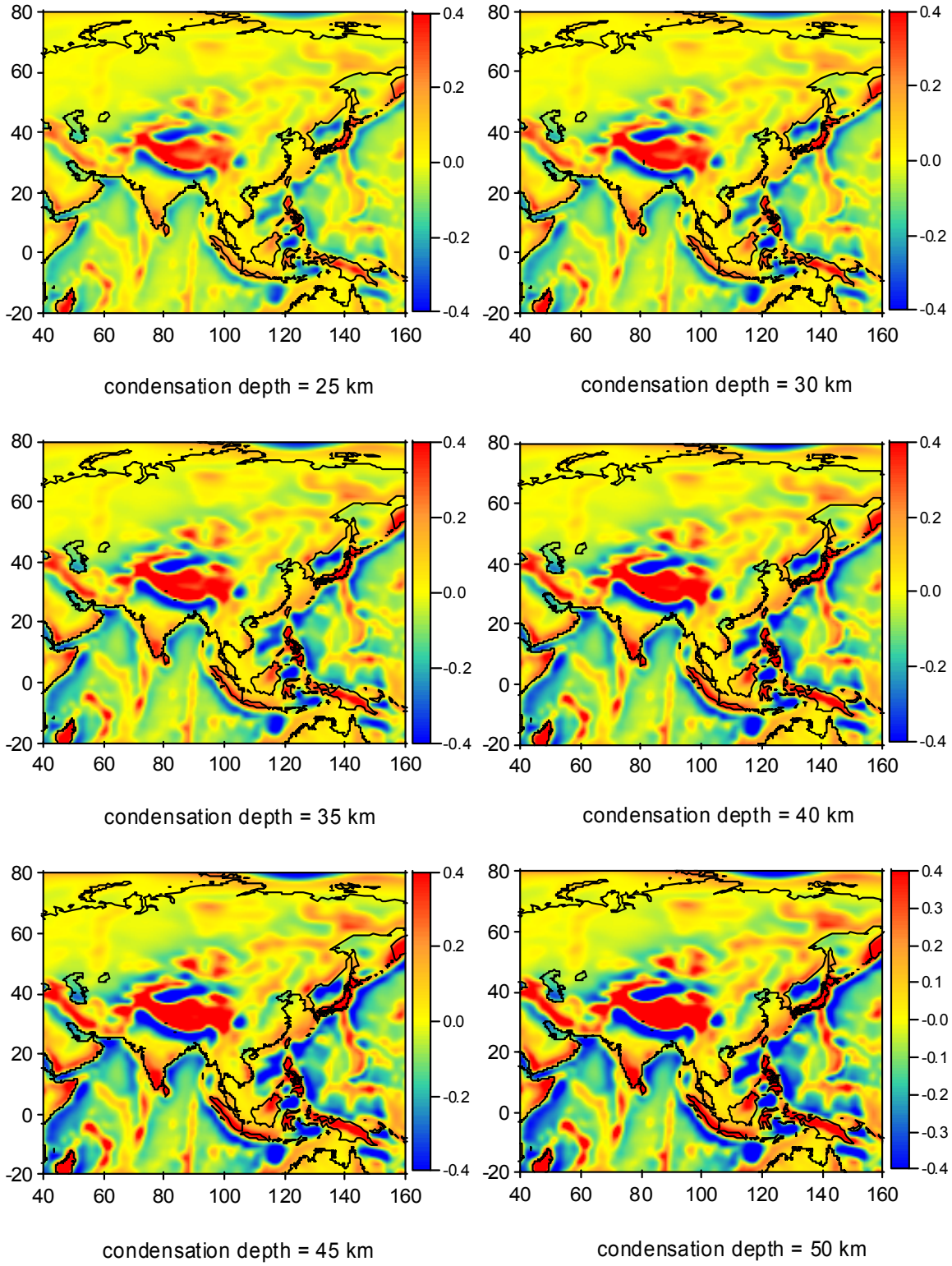

Fig. 5.34: Effects of the topographic-isostatic masses on the tensor component V_{zz} at an altitude of 250 km for generalized Helmert model of condensation with different depths (units in Eötvös)

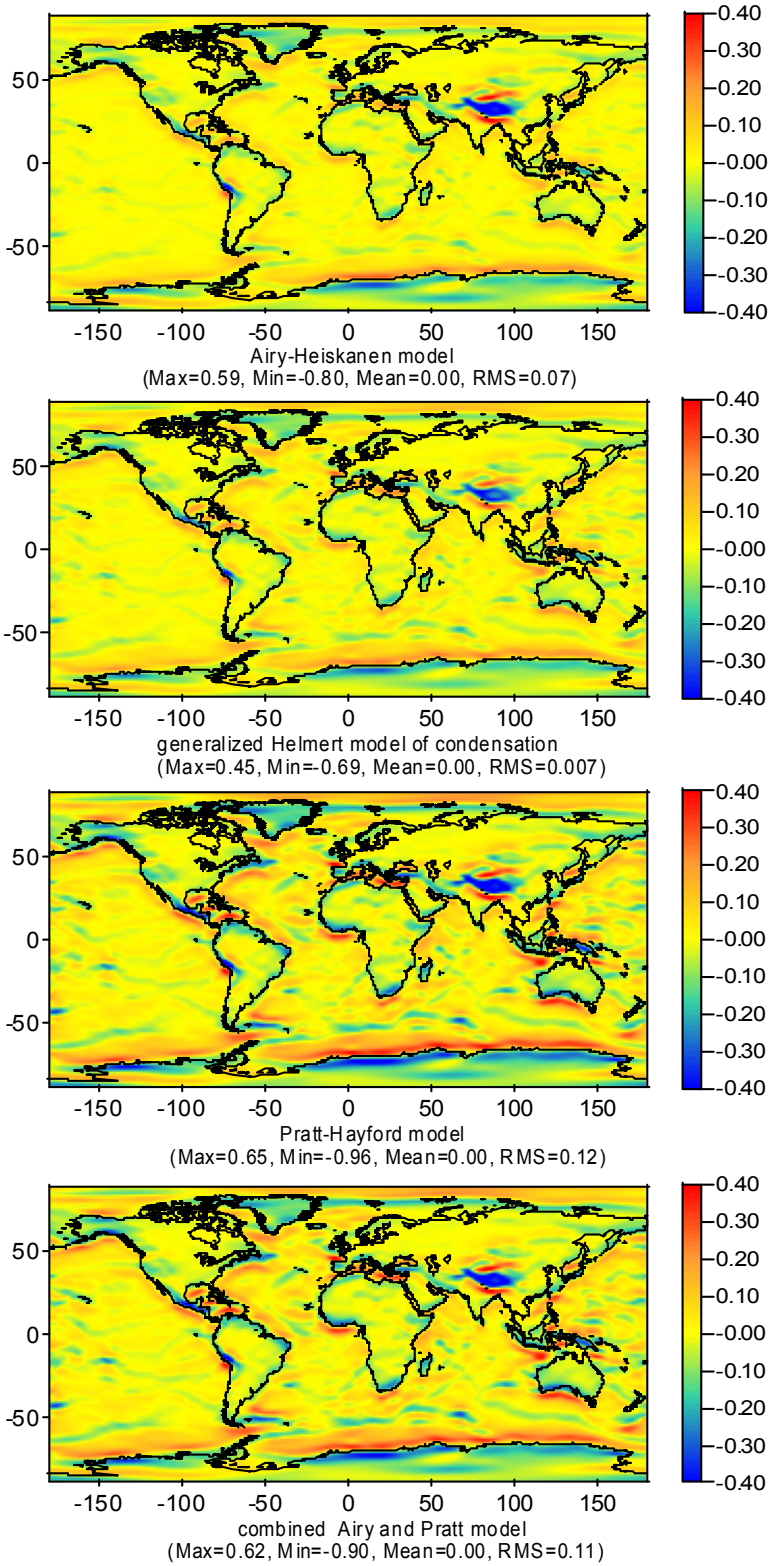

Fig. 5.35: Effects of the topographic-isostatic masses on the tensor component V_{xx} at an altitude of 250 km for different topographic-isostatic models (units in Eötvös)

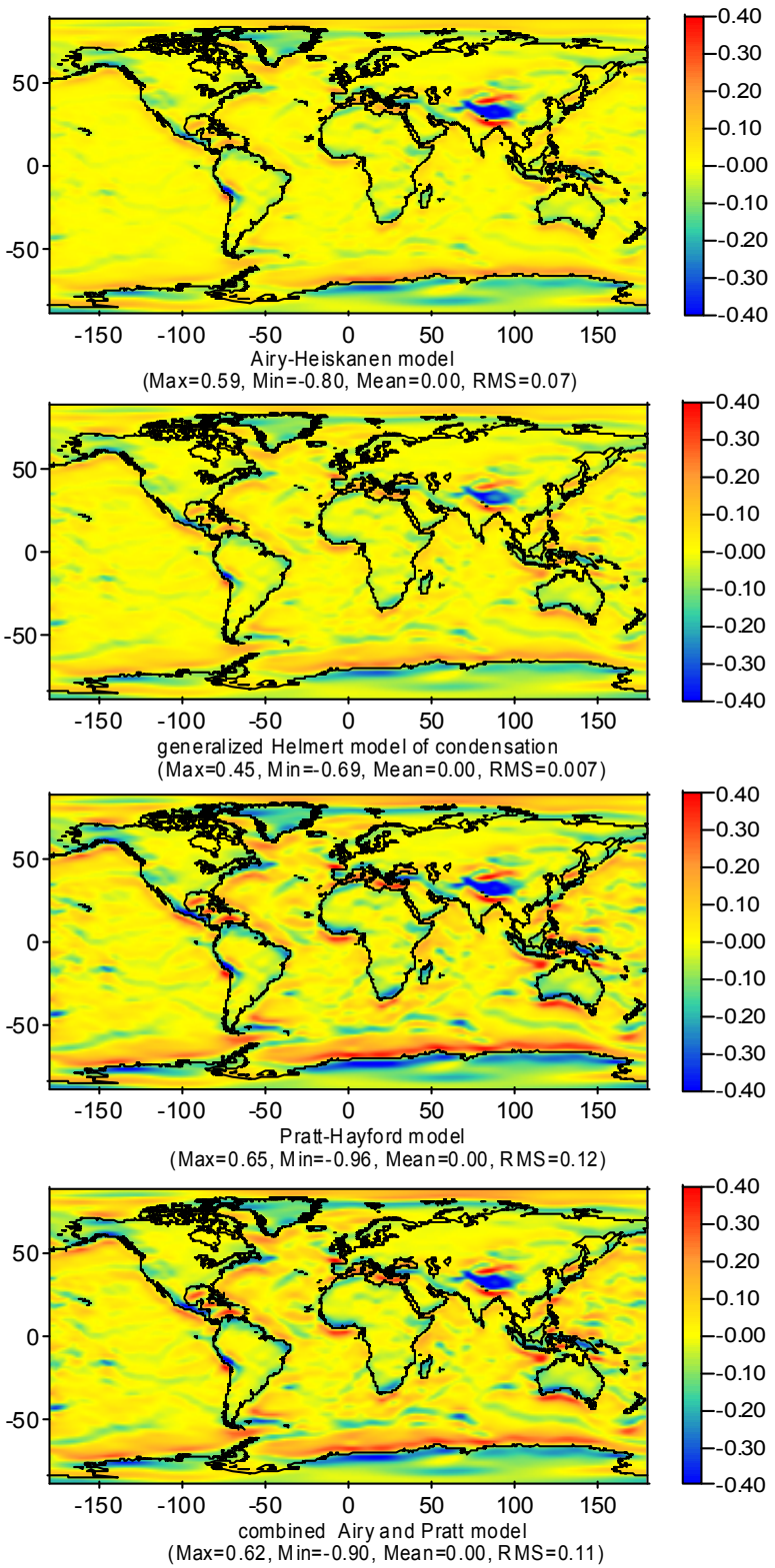

Fig. 5.36: Effects of the topographic-isostatic masses on the tensor component V_{yy} at an altitude of 250 km for different topographic-isostatic models (units in Eötvös)

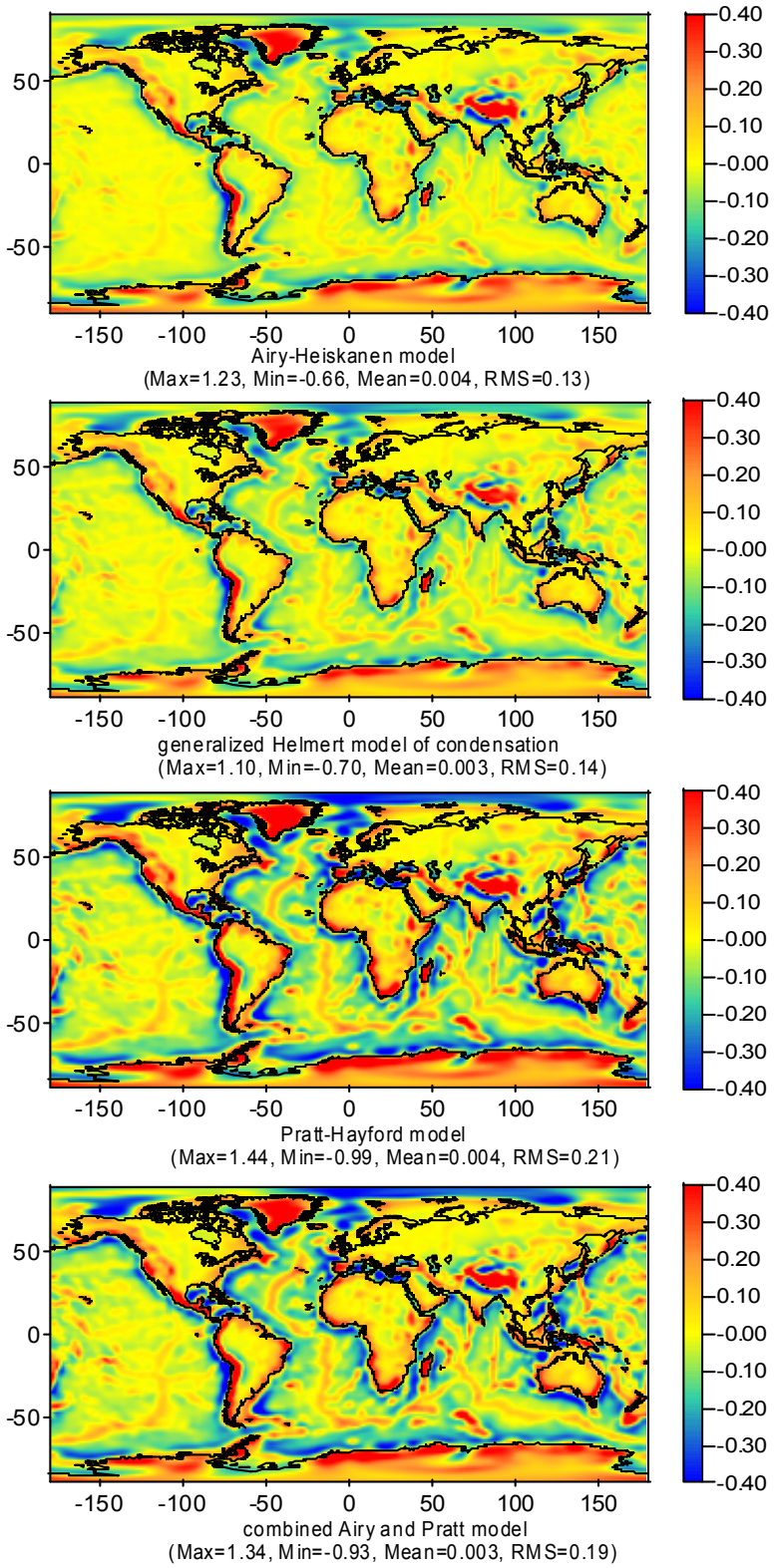

Fig. 5.37: Effects of the topographic-isostatic masses on the tensor component V_{zz} at an altitude of 250 km for different topographic-isostatic models (units in Eötvös)

5.4.2 Topographic-isostatic effects on SST observations

As sketched in chapter 2, the gravity field recovery from SST data is based on the analysis of short precisely determined kinematical orbits based mainly on GPS measurements in an altitude of $\sim 400\ km$.

5.4.2.1 Effects on the orbit

To get an impression of the size of the topographic-isostatic effects on the short arcs, a 30-minute-arc has been determined dynamically twice, the first version based on EGM96 potential coefficients (Lemoine et al. 1998) complete up to degree $N_{max} = 360$, the second version based on EGM96 minus the effects of the topographic-isostatic masses. Then both orbits have been compared applying a least squares fit of both orbits. The differences in the coordinates represent the effect of the topographic-isostatic gravity field effects in the short arcs. Figure 5.38 shows the effects of different topographic isostatic models. The Airy-Heiskanen model and the Vening Meinesz model as well as the generalized Helmert model of condensation show significant deviations up to two meters. The Pratt-Hayford model as well as the combined Pratt-Airy model show even larger deviations up to four meters while the gravity field effect of Helmert's second model is very small, only a couple of centimeters.

5.4.2.2 Effects on the relative motion of two satellites

To investigate the gravity field effects of the topographic-isostatic models on the ranges and range-rates of a twin-satellite scenario like GRACE the relative orbits of a 30-minute-arc have been determined dynamically twice again: The first version has been based on EGM96 potential coefficients complete up to degree $N_{max} = 360$, the second one based on EGM96 coefficients minus the effects of the topographic-isostatic models. Then both relative orbits have been compared applying a least squares fit of both relative orbits.

The differences in the ranges and range-rates represent the effect of the topographic-isostatic gravity field effects in the short relative arcs. Figure 5.39 shows the effects of the topographic-isostatic models in the ranges and Fig. 5.40 in the range-rates. Again the Airy-Heiskanen model and the Vening Meinesz model as well as the generalized Helmert model of condensation show significant deviations up to a couple of decimeters while the gravity field effect of Helmert's second model again is very small. Also, the Pratt-Hayford model and the combined Airy-Pratt model show significant deviations larger than the other models.

The situation is similar in case of the topographic-isostatic effects in the range-rates between the GRACE satellites. Again the Airy-Heiskanen model and the Vening Meinesz model as well as the Helmert's first or generalized condensation method show significant deviations up to ± 200 to $300 \mu m/s$ while the gravity field effect of Helmert's second model is very small. In addition, the effect of the Pratt-Hayford model and the combined Airy-Pratt model show significant deviations larger than those of the other models. Compared to the observation accuracy of approximately $0.2 \mu m/s$ these are significant effects in the gravity field signal.

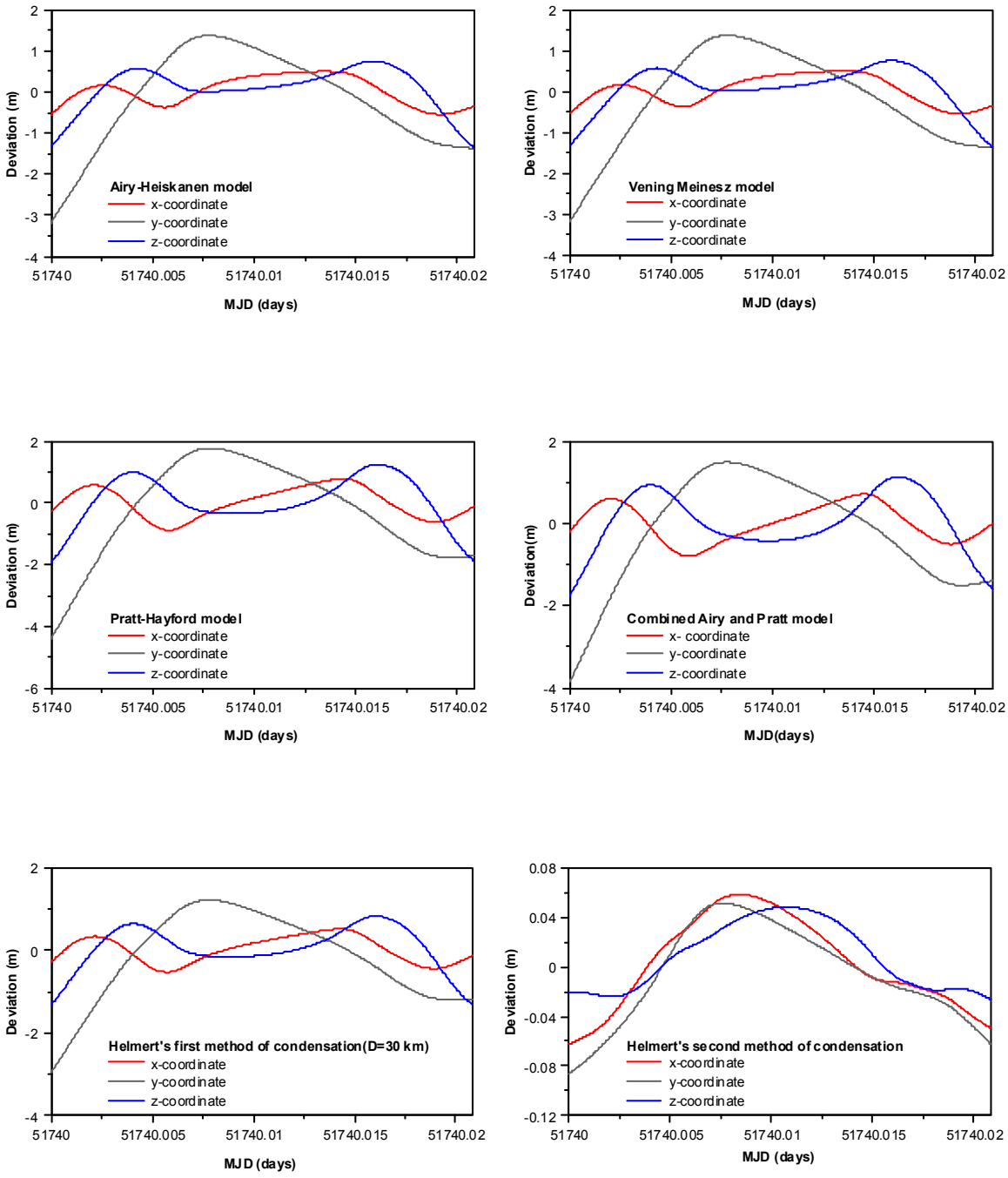

Fig. 5.38: Orbit deviations for different topographic isostatic models (altitude: ∼400 km)

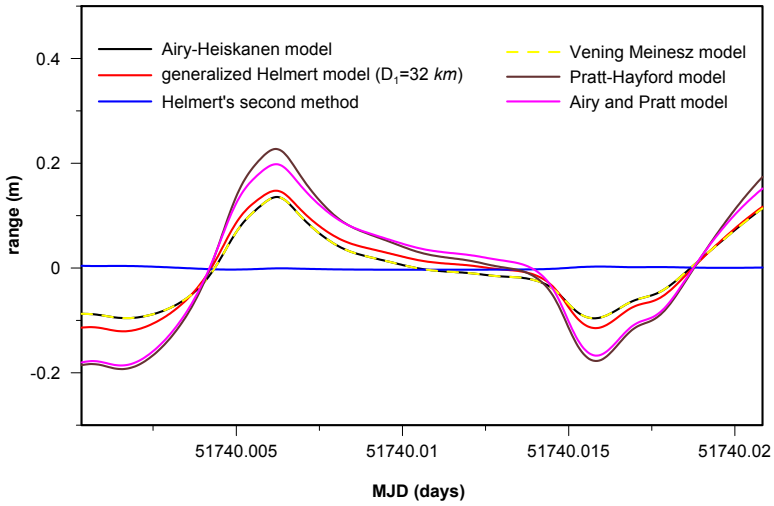

Fig. 5.39: SST ranges: EGM96 versus (EGM96-T/I-models) (altitude: $\sim$ 450 km)

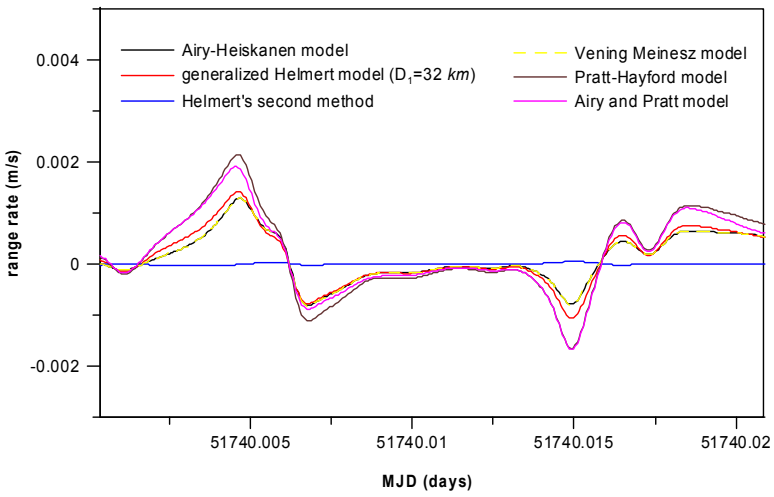

Fig. 5.40: SST range-rates: EGM96 versus (EGM96-T/I-models)(altitude: $\sim$ 450 km)

6. Discussion and conclusions

In this study the integral formulae for the calculation of the first and second derivatives of the gravitational potential of the topographic-isostatic masses were derived for various frequently applied topographic-isostatic models in spherical approximation by approximating the spherical volume elements by mass-lines located in the center of the compartments. To our knowledge, only the formula for the determination of the first derivative in the radial direction has been derived but not for the other two components. The situation is similar for the second derivatives of the potential; only an alternative equivalent formula for the radial component has been published in various papers (Heck and Wild 2005; Wild and Heck 2004a, b). The other second derivatives of the potential have not been studied till now to our knowledge. The formulae can be used to determine the topographic-isostatic effects at aircraft altitudes for airborne applications or at satellite altitudes to reduce the observation functionals of Satellite Gravity Gradiometry missions. The integral formulae presented here allow to use DTMs with an – in principle – arbitrary high resolution depending on the numerical integration method. Obviously such a high resolution is not necessary for satellite altitudes, because only a comparably coarse digital elevation model is required. In these cases it might be preferable to apply formulae which are based on the expansion of Newton's integral in spherical harmonics at least for global applications (see, e.g., Makhloof and Ilk 2004). If the potential coefficients are determined once for all, then the same results can be achieved with less CPU time and sufficient accuracy. The situation is different, if the topographic-isostatic effects are required at the surface of the Earth or at aeroplane altitudes. Then a higher resolution of the DTMs is indispensable and the computation of the corresponding spherical harmonic coefficients can be critical because of numerical problems (Holmes and Featherstone 2002). Also, the computational effort increases quadratically with data resolution. Therefore only a maximum degree of 2700 corresponding to a compartment size of $4''$ can be determined efficiently. Due to this limitation a spherical harmonic expansion of the topographic-isostatic masses cannot be used for exact determinations of the geoid (see Kuhn and Seitz 2005). At the surface of the Earth or at low altitudes the formulae for the second derivatives have to be applied with care because of instabilities and discretization errors caused by the jump relation of the second derivatives of the gravitational potential at the Earth's surface. There are various ways out of these problems: The cap around the computation point can be calculated using the rigorous tesseroid formula approach in three dimensions such as proposed by Kuhn (2000) or the prism formulae as proposed by Nagy (1966, 2000, 2002). Another possibility is to model the topography in a cap of sufficient spherical radius around the computation point with a higher resolution than in the distant regions. Discretization problems are less critical for the first derivatives or even for the potential. The errors depend on the resolution of the DTMs and the altitudes of the computation points as demonstrated in chapter 5.

For the determination of a 1 *cm* geoid from ground and airborne gravimetry, formulae for the far-zone direct and indirect terrain effects for Helmert's condensation methods and for the Airy-Heiskanen model are derived and transformed into the spectral domain following Molodenskii's approach. These formulae that are based on spherical harmonic expansions can be applied very economically for all models investigated here. From the point of view of computation costs it would be desirable to select the cap size radius as small as possible to reduce the work load for the near zone computations, e.g., for the direct terrain effects on gravity. A cap radius of at least 3^o is necessary for the Taylor expansion of the formulae for the far-zone effects (see chapters 4 and 5).

The gravity field effects of the topography and the isostatic compensation masses strongly depend on the applied topographic-isostatic models. For the gravity field recovery procedure it is important to know the size of these effects in the satellite observations which are used for the determination of gravity field parameters. The results of chapter 5 demonstrate that the Pratt-Hayford model shows the largest effects at satellite altitude, followed – as expected – by the combined Airy and Pratt model. The Airy-Heiskanen and the Vening Meinesz models as well as Helmert's first condensation model show similar slightly smaller effects, while Helmert's second condensation model produces only tiny effects compared to the other models. This means that these gravity field effects are remarkable large compared to the measurement accuracy. If the three-dimensional position coordinates of a satellite such as CHAMP derived by a kinematical orbit determination

procedure are used within the so-called Precise Orbit Determination (POD) gravity field recovery approach then the coordinates must be known with an accuracy of one to two centimeters. It becomes obvious that an effect in the orbit of up to a couple of meters (as shown in chapter 5) corresponding to a signal-to-noise ratio of approximately 1000 requires a careful computation of the topographic-isostatic effects. The situation is similar if low-low SST data of a GRACE-type twin satellite mission are used for the gravity field recovery. Again the ratio of the topographic-isostatic effect to the measurement noise is approximately 1000 for these observables. This holds approximately for all models except for Helmert's second condensation method. The topographic-isostatic effects might be also important for the gravity field mission GOCE where the gravity gradients are measured with high precsion, especially the diagonal elements. The size of the diagonal elements of the gravity gradients is largest for the radial component V_{zz} and approximately half of these values for the local horizontal components V_{xx} and V_{yy}. Also in this case the signal-to-noise ratio is approximately 1000 if we take into account the measurement accuracy of the Satellite Gravity Gradiometry mission GOCE in the size of 0.003 Eötvös. Therefore, also in this case a remove-restore procedure can significantly stabilize the downward continuation procedure and can help to improve the final results.

The far-zone direct terrain effects are rather high for Helmert's first or generalized condensation method as well as for the Airy-Heiskanen model and very small in case of Helmert's second condensation method. It is interesting to note that the altitude of the computation point has a minor influence on the size of the far-zone effects for all topographic-compensation models. The far-zone effects decrease slightly with increasing altitude and are more or less identical in case of cap radii of 10^o and larger. Therefore, the results hold for ground gravity measurements and for airborne gravimetry. The far-zone effects increase with the condensation depth selected for the generalized Helmert model (and are very small for the second Helmert method). A corresponding behaviour show the numerical tests for the far-zone primary and secondary indirect terrain effects. An important question is the selection of the cap radius for the determination of far-zone topographic-compensation effects. For Helmert's second method of condensation the far-zone terrain effects in case of a cap radius of 3^o and larger have a minor influence on airborne gravity measurements in relation to a measurement accuracy of 1 to 2 $mGal$ and can be omitted completely. The situation is different in case of ground gravity measurements with a much higher measurement accuracy of 0.02 $mGal$. In this case the far-zone effects have to be considered in case, e.g. of a cap radius of 3^o. The maximum harmonic degree of 50 should be sufficient for the determination of the far-zone effects in this case. The situation is different in case of Helmert's generalized condensation models (including Helmert's first model) and in case of the Airy-Heiskanen model. Even in case of the minor accuracy of airborne gravimetry the far-zone effects have to be considered for cap radii of 3^o and also larger ones. The maximum degree of the spherical harmonic expansion can be restricted to 50 in case of airborne gravimetry and up to degree 200 and higher for ground gravity measurements, depending on the accuracy demands. If we keep in mind that the accuracy of the airborne gravimetry is 1-2 $mgal$ and the band limted geoid is determined, then it is better to use space localizing space function than the integral formulae for determinig the topographic-compensating masses effects.

Now the question arises which model should preferably be used for the filtering of satellite born observations such as low-low SST data, airbore gravimetry, three-dimensional position coordinates or measured gravity gradients as preparation for the subsequent downward continuation procedure? While Helmert's second condensation method might be useful for geoid computations, its usefulness for the processing of satellite in-situ observations cannot be answered in such a simple generally valid way. Indeed the task of filtering topographic-isostatic effects in the satellite observations is helpful only if these quantities show a significant size in the observations. Obviously, this fact depends on the validity of the topographic-isostatic hypothesis in specific geographic regions. This can be decided only after a careful analysis of the specific gravity field features within the various geographical regions of the Earth to find out which model describes the reality in these regions in the best possible way. It is well-known that the Earth is isostatically compensated by an amount of approximately 90%, but it is difficult to decide which model fits best. Although seismic measurement results indicate the validity of an Airy-Heiskanen type of topographic-isostatic compensation, in some parts of the Earth the isostatic compensation seems to follow the Pratt-Hayford model (Heiskanen and Moritz 1967). If the specific topographic-isostatic model holds more or less uniformly for a larger region then this model can be used to filter the satellite observations before the application of the regional gravity field recovery procedure. The situation is more complicated in case of regionally varying deviations of the

reality from a specific model; further investigations are necessary to consider this case. The numerical results indicate that the effects of topographic and isostatic masses for Helmert's first method of condensation with a condensation depth of 30 km coincides approximately with the effects of the Airy-Heiskanen model. The change of the condensation level by using a sort of generalized Helmert model (Heck 2003) could be used to fit the topographic-isostatic model to the reality. An interesting side effect would be the reduction of the computation costs due to the efficiency of this model.

Because of the varying effects of the topographic-isostatic models depending on the type of observables such as gravity vectors or tensor components the frequently expressed argument that a high resolution gravity field model might be sufficient to reduce observations at aeroplane or satellite altitude is not valid. Therefore, additional investigations are necessary to demonstrate the benefit of a remove-restore procedure taking into account individually selected topographic-isostatic models for the processing of airborne measurements and SGG observables. Therefore, an integration of this processing steps into the global but especially the regional gravity field recovery procedure as developed at the Institute of Theoretical Geodesy, University of Bonn, and various other aspects mentioned here have to be investigated. In addition, further investigations are necessary to demonstrate the benefit of a remove-restore procedure taking into account topographic-compensation effects for the processing of POD and low-low SST observables. Also, further investigations are necessary to take the cubic terms of the Taylor expansion into account in the case of the Airy-Heiskanen model. Also, further investigation can be performed to apply the Molodenskii's approach for determing the far-zone effects for other topographic-isostatic models such as the Pratt-Hayford model. Finally, the geophysical models in coincidence with modern models of plate tectonics must be investigated with respect to its topographic-isostatic effects.

Acknowledgement

This research was carried out in the framework of the exchange grant by the Egyptian government in the Institute of Theoretical Geodesy, University of Bonn. I have received a great support during my research, therefore I would like to address my special thanks to the following persons: I would like to express my deep and sincere appreciation to my research advisor Prof. Dr. Karl Heinz Ilk for offering me the opportunity to carry out my research in his institute, for his guidance, helpful advice and supervision. I am indebted to his constant encouragement and fruitful and interesting discussions throughout this work. Most importantly, his ever willingness and dedication to solve my personal and numerical problems worth more mention. He has critically read this thesis and his valuable comments and suggestions are gratefully appreciated. I would like to express my deep thanks to Prof. Dr. Bertold Witte for his evaluation of my thesis. I wish to express my deep gratitude to Prof. Dr. Hussein Abd-Elmotaal, Faculty of Engineering, Minia University, for his encouragement. I am deeply indepted to the secretaries of the Institute of Theoretical Geodesy, Mrs. Schleifenbaum and Mrs. Losch, for their generous continous help and to all members of the Institute for their help during my stay in Bonn. To my friend Anno Löcher (Institute of Theoretical Geodesy, Bonn University) for his help during programming, his help during writing in Latex and for reading the thesis. I would like to thank the Egyptian Ministry of Higher Education, the Faculty of Engineering, Minia University, Egypt for providing me with a Ph.D. scholarship. To my colleagues of the Civil Engineering Department, Faculty of Engineering, Minia University, Egypt, for their continuous encouragement. My special thanks and appreciations are also due to my wife for her continuous encouragements and for providing me with an excellent environment and atmosphere for doing my research work. To my children who are in Egypt and who are here with me in Bonn. Lastly, very special thanks to my father, my mother, my sisters for their heartily feelings and continuous prayers. To all of you, thank you very much.

Atef Abdel-Hakeem Makhloof
Bonn, Germany

References

Abd-Elmotaal H (1991): Gravity anomalies based on the Vening Meinesz isostatic model and their statistical behavior. Mitteilung der Geodätischen Institute der Technischen Universität Graz, Folge 72

Abd-Elmotaal H (1995a): Theoretical background of the Vening Meinesz isostatic model. In: H. Sünkel and I. Marson (eds.): Gravity and Geoid. Joint Symposium of the International Gravity Commission and the International Geoid Commission, Symposium No. 113, pp. 268-277. Springer Verlag, Berlin, Heidelberg, New York

Abd-Elmotaal H (1995b): Attraction of the topographic masses, Bulletin Géodésique, 69(4): 304-307

Abd-Elmotaal H (1999): Comparison among different geoid solutions for the Egyptian south-western desert using FFT technique. Bolletino di Geofisica Teorica ed Applicata 40(3-4): 563-569

Anderson EG (1976): The effect of topography on solutions of Stokes' problem. Unisurv Report S14, University of New South Wales, Kensington, Australia

Banks RJ, Parker RL, Huestis SP (1977): Isostatic compensation on a continental scale: local versus regional mechanisms. The geophysical journal of the Royal Astronomical Society 51: 431-452

Blakely RJ (1995): Potential theory in gravity and magnetic applications. Cambridge University Press, Cambridge, UK

Bracewell R (1978): The Fourier transform and its applications. 2nd edn., McGraw-Hill, New York

Bruns H (1878): Die Figur der Erde. Publication des Königl.-Preuss. Geodätischen Institutes, Berlin

Claessens S (2003): A synthetic Earth model; analysis, implementation; validation and application. Delft University Press, Delft, The Netherlands

Colombo OL (1981): Numerical methods for harmonic analysis on the sphere. Reports of the Department of Geodetic Science and Surveying No. 310, Ohio State University, Columbus, Ohio

Courant R, Hilbert D (1953): Methods of the mathematical physics. Volume 1, Interscience Publishers, New York, London

Dutton CE (1889): On some of the greater problems of physical geology. Bulletin of the Philosophical Society of Washington, 11: 51-64

Eicker A, Mayer-Gürr T, Ilk KH (2004): Global gravity field solutions based on a simulation scenario of GRACE SST data and regional refinements by GOCE SGG observations. In: Jekeli C, Bastos L, Fernandes J (eds.): Gravity, Geoid and Space Missions. International Association of Geodesy Symposia, Vol. 129, Springer, Berlin, Heidelberg, New York, pp. 66-71

Engels J, Grafarend E (1993): The gravitational field of topographic-isostatic masses and the hypothesis of mass condensation. Surveys in Geophysics 140: 495-524

European Space Agency (1999): Gravity Field and Steady-State Ocean Circulation Explorer Mission (GOCE), Report for mission selection, in: The four canditate Earth explorer core missions, SP-1233, Nordwijk, The Netherlands

Featherstone WE (1992): A GPS controlled gravimetric determination of the geoid of the British Isles. D.Phil. thesis, University of Oxford, England

Featherstone WE, Kirby JF, Kearsley AHW, Gilliland JR, Johnston GM, Steed J, Forsberg R, Sideris MG (2001): The AUSGeoid98 geoid model of Australia: data treatment, computations and comparisons with GPS-levelling data. Journal of Geodesy 75(5-6): 313-330

Forsberg R (1984): A study of terrain reduction, density anomalies and geophysical inversion method in gravity field modelling. Reports of the Department of Geodetic Science and Surveying No. 335, Ohio State University, Columbus, Ohio

Forsberg R (1985): Gravity field terrain effect computation by FFT. Bulletin Géodésique 59: 342-360

Forsberg R, Sideris MG (1993): Geoid determination by multi-band spherical FFT approach. Manuscripta Geodaetica 18: 82-90

Forsberg R, Tscherning CC (1997): Topographic effects in gravity field modelling for BVP. In: Sansó F, Rummel R (eds.) Geodetic boundary value problems in view of the one centimetre geoid. Lecture Notes in Earth Sciences, Vol. 65. Springer, Berlin, Heidelberg, New York, pp 241-272

Freeden W, Windheuser U (1996): Spherical wavelet transform and its discretization. Advances in Computational Mathematics 5: 51-94

Freeden W, Gervens T, Schreiner M (1998): Constructive approximation on the sphere. Oxford University Press, Oxford, England

Gauss CF (1839): Allgemeine Theorie des Erdmagnetismus. In: Gauss CF and Weber W: Resultate aus den Beobachtungen des Magnetischen Vereins im Jahre 1838., Göttingen und Leipzig

Gradshteyn IS, Ryzhik IM (1980): Tables of Integrals, Series, and Products. Academic Press, New York

Grüninger W (1990): Zur Topographisch-Isostatischen Reduktion der Schwere. Ph.D. thesis, Technical University Karlsruhe

Haagmans R (2000): A synthetic Earth for use in geodesy. Journal of Geodesy 74(7-8): 503-511

Harrison JG, Dickinson M (1989): Fourier transforms method in local gravity field modelling. Bulletin Géodésique 63: 49-166

Heck B (1992): A revision of Helmert's second method of condensation in geoid and quasi-geoid determination. In: Montag H, Reigber C (eds.): Geodesy and Physics of the Earth. International Association of Geodesy Symposia, Vol. 112, Springer, Berlin, Heidelberg, New York, pp. 246-251

Heck B (2003): On Helmert's methods of condensation, Journal of Geodesy 77(3-4): 155-170

Heck B and Wild F (2005): Topographic-isostatic reductions in Satellite Gravity Gradiometry based on a generalized condensation model. In: Sansó F (ed.): A Window on the Future of Geodesy, International Association of Geodesy Symposia, Vol. 128, Springer, Berlin, Heidelberg, New York, pp. 294-299

Heck B and Seitz F (2006): A comparison of the tesseroid, prism and point-mass approaches for mass reductions in gravity field modelling. Journal of Geodesy 81(2):121-136

Heiskanen WA, Vening Meinesz FA (1958): The Earth and its gravity field. McGraw-Hill, New York

Heiskanen WA, Moritz H (1967): Physical Geodesy. W.H. Freeman and Company, San Francisco and London

Helmert FR (1884): Die mathematischen und physikalischen Theorien der höheren Geodäsie. Band II, Teubner, Leipzig. Reprint: Minerva, Frankfurt a. M. 1962

Hertz H (1884): Über das Gleichgewicht schwimmender elastischer Platten, Annalen der Physik und Chemie 22: 449-455

Holmes SA and Featherstone WE (2002): A unified approach to the Clenshaw summation and the recursive computation of very high degree and order normalized associated Legendre functions. Journal of Geodesy 76(5): 279-299

Hotine M (1969): Mathematical Geodesy. U. S. Government Printing Office, Washington, D.C.

Huang J, Vaníček P, Pagiatakis SD, Brink W (2001): Effect of topographical density on geoid in the Canadian Rocky Mountains. Journal of Geodesy 74(11-12): 805-815

Jeffreys H (1976): The Earth: its origin, history and physical constitution, 6th edn., Cambridge University Press, Cambridge, UK

Kertz W (1969): Einführung in die Geophysik. Band I: Erdkörper. Bibliographisches Institut, Mannheim

Kiamehr R and Sjöberg LE (2005): Effect of the SRTM global DEM on the determination of a high-resolution geoid model: a case study in Iran. Journal of Geodesy 79(9): 540-551

Kirby JF, Featherstone WE (1999): Terrain correcting the Australian gravity observations using the national digital elevation model and the Fast Fourier Transform, Australian Journal of Earth Science 46: 555-562

Klees R (1992): Lösung des fixen geodätischen Randwertproblems mit Hilfe der Randelementemethode. Deutsche Geodätische Kommission, Reihe C, Nr. 382, München

Klose U, Ilk KH (1993): A solution to the singularity problem occurring in the terrain correction formula. Manuscripta Geodaetica 18: 263-279

Koch KR (1965): Die topographische Schwere- und Lotabweichungsreduktion für Aufpunkte in geneigtem Gelände. Allgemeine Vermessungsnachrichten 11: 438-441

Koch KR, Kusche J (2003): Regularization of geopotential determination from satellite data by variance components estimation, Journal of Geodesy 76(5): 259-268

Krylov VI (1962): Approximate calculation of integrals. MacMillan, New York

Kuhn M (2000a): Geoidbestimmung unter Verwendung verschiedener Dichtehypothesen. Deutsche Geodätische Kommission, Reihe C, Nr. 520, München

Kuhn M (2000b): Density modelling for geoid determination. In: Sideris MG (ed.): Gravity, Geoid and Geodynamics 2000. International Association of Geodesy Symposia, Vol. 123, Springer, Berlin, Heidelberg, New York, pp. 271-276

Kuhn M (2002): On the indirect effect of Helmert's condensation methods. International Geoid Service 13: 50-52

Kuhn M (2003): Geoid determination with density hypotheses from isostatic models and geological information. Journal of Geodesy 77(1-2): 50-65

Kuhn M, Seitz K (2005): Comparison of Newton's integral in the space and frequency domains. In: Sansó F (ed.): A Window on the Future of Geodesy, International Association of Geodesy Symposia, Vol. 128, Springer, Berlin, Heidelberg, New York, pp. 386-391

Lambeck K (1988): Geophysical geodesy, the slow deformations of the Earth. Clarendon Press, Oxford, UK

Lanczos C (1956): Applied analysis. Prentice Hall, Englewood Cliffs, N.J.

Landau LD, Lifshitz EM (1959): Theory of elasticity. 3rd edn., Pergamon Press, Oxford, UK

Lehmann R (1994): Zur Bestimmung des Erdschwerefeldes unter Verwendung des Maximum-Entropie-Prinzipes. Deutsche Geodätische Kommission, Reihe C, Nr. 425, München

Lemoine FG, Kenyon SC, Factor JK, Trimmer RG, Pavlis NK, Chinn DS, Cox CM, Klosko SM, Luthcke SB, Torrence MH, Wang YM, Williamson RG, Pavlis EC, Rapp RH, Olson TR (1998): The development of the joint NASA GSFC and the National Imagery and Mapping Agency (NIMA) geopotential model EGM96. NASA/TP-1998-206861, Goddard Space Flight Center, Greenbelt, Maryland

Li YC, Sideris MG (1994): Improved gravimetric terrain corrections. Geophysical Journal International 119: 740-752

MacMillan WD (1930): Theoretical Mechanics, vol 2: the Theory of the potential. McGraw-Hill, New York (reprinted by Dover Publications, New York 1958)

Mader K (1951): Das Newtonsche Raumpotential prismatischer Körper und seine Ableitung bis zur dritten Ordnung. Sonderheft 11 der Österreichischen Zeitschrift für Vermessungswesen, Wien

Makhloof AA, Ilk KH (2004): The use of topographic-isostatic gravity field information in Satellite-to-Satellite tracking and Satellite Gravity Gradiometry. Poster presented at the IAG International Symposium Gravity, Geoid and Space Missions, Porto

Makhloof AA, Ilk KH (2006): Effects of topographic-isostatic masses on gravitational functionals at the surface of the Earth, at airborne and satellite altitudes, submitted to Journal of Geodesy

Márkus G (1978): Theorie und Berechnung rotationssymmetrischer Bauwerke. 3. Auflage, Werner-Verlag, Düsseldorf

Martinec Z (1993): Effect of lateral density variation of topographical masses in view of improving geoid model accuracy over Canada. Final Report under DSS Contract No. 23244-2-4356/01-SS, Geodetic Survey of Canada, Ottawa

Martinec Z (1998): Boundary-value problems for gravimetric determination of a precise geoid. Lecture Notes in Earth Sciences, Vol. 73, Springer, Berlin, Heidelberg, New York

Martinec Z, Vaníček P (1994a): The indirect effect of Stokes-Helmert's technique for a spherical approximation of the geoid. Manuscripta Geodetica 18: 213-219

Martinec Z, Vaníček P (1994b): Direct topographical effect of Helmert's condensation for a spherical geoid. Manuscripta Geodaetica 19: 257-268

Martinec Z, Matyska C, Grafarend EW, Vaníček P (1993): On Helmert's second condensation method. Manuscripta Geodetica 18: 417-421

Martinec Z, Vaníček P, Mainville A, Véronneau M (1996): Evaluation of the topographic effects in precise geoid computation from densely sampled heights. Journal of Geodesy 70(11): 746-754

Matyska C (1994): Topographic masses and mass heterogeneities in the upper mantle. In: Schutz BE, Anderson A, Froidevaux C, Parke M (eds.): Gravimetry and Space Techniques Applied to Geodynamics and Ocean Dynamics, Geophysical Monograph 82, pp. 125-132

Mayer-Gürr T (2006): Gravitationsfeldbestimmung aus der Analyse kurzer Bahnbögen am Beispiel der Satellitenmissionen CHAMP und GRACE. Ph.D. thesis, University Bonn

Mayer-Gürr T, Ilk KH, Eicker A, Feuchtinger M (2005): ITG-CHAMP01: A CHAMP gravity field model from short kinematical arcs of a one-year observation period, Journal of Geodesy 78: 462-480

Mayer-Gürr T, Eicker A, Ilk KH (2006): Gravity field recovery from GRACE-SST data of short arcs. In: Flury J, Rummel R, Reigber C, Rothacher M, Boedecker G, Schreiber U (eds.): Observation of the Earth System from Space. Springer, Berlin, Heidelberg, New York, pp. 131-148

Molodenskii MS, Fremeev VF, Yurkina MI (1962): Methods for the study of the external gravitational field and figure of the Earth. Office of Technical Services, Department of Commerce, Washington, D.C.

Moritz H (1965): The boundary value problem of physical geodesy. Publication of the Isostatic Institute of the IAG, No. 50, Helsinki

Moritz H (1968): Linear solution of the geodetic boundary-value problem. Deutsche Geodätische Kommission, Reihe A, Heft 58, München

Moritz H (1980): Advanced physical geodesy. Herbert Wichmann Verlag, Karlsruhe

Nahavandchi H, Sjöberg LE (1998): Terrain corrections to power H^3 in gravimetric geoid determination, Journal of Geodesy 72(3): 124-135

Nagy D (1966): The gravitational attraction of a right rectangular prism. Geophysics 31: 362-371

Nagy D, Papp G, Benedek J (2000): The gravitational potential and its derivatives for the prism. Journal of Geodesy 74(7-8): 552-560

Nagy D, Papp G, Benedek J (2002): Correction to The gravitational potential and its derivatives for the prism", Journal of Geodesy 76(8): 475

Neumann F (1838): Über eine neue Eigenschaft der Laplaceschen Y^n und ihre Anwendung zur analytischen Darstellung derjenigen Phänomene, welche Functionen der geographischen Länge und Breite sind, Schumachers Astronomische Nachrichten, 15: 313-325 (reprinted in: Mathematische Annalen 14(4): 567-576)

Neumann F (1887): Vorlesungen über die Theorie des Potentials und der Kugelfunctionen. Teubner, Leipzig

NOAA (1988): Data Announcement 88-MGG-02, Digital relief of the surface of the Earth. National Geophysical Data Center, Boulder, Colorado

Novák P (2000): Evaluation of gravity data for Stokes-Helmert solution to the geodetic boundary-value vroblem. Ph.D. thesis, University of New Brunswick, Fredericton, Canada

Novák P, Grafarend EW (2005): The ellipsoidal representation of the topographical potential and its vertical gradient. Journal of Geodesy 78(11-12): 691-706

Novák P, Vaníček P, Huang G (1998): Topography in the Stokes-Helmert solution of the geodetic boundary-value problem. Contract Report to Geodetic Survey Division, Ottawa

Novák P, Kern M, Schwarz KP (2000): On the determination of the relative geoid from airborne gravimetry. Poster presented at the IAG International Symposium Gravity, Geoid, and Geodynamics, Banff (paper can be submitted by request to interested parties)

Novák P, Vaníček P, Martinec Z, Véronneau M (2001): Effect of the spherical terrain on gravity and the geoid. Journal of Geodesy 75(9-10): 491-504

Pagiatakis SD, Armenakis C (1998): Gravimetric geoid modelling with GPS. International Geoid Service Bulletin 8: 105-112

Pail R (2000): Synthetic global gravity model for planetary bodies and applications in Satellite Gravity Gradiometry. Ph.D. thesis, Technical University Graz, Austria

Papp G and Wang ZT (1996): Truncation effects in using spherical harmonic expansions for forward local gravity field modelling. Acta Geodaetica et Geophysica Hungarica 31(1-2): 47-66

Parker RL (1995): Improved Fourier terrain correction, Part I. Geophysics 60: 1007-1017

Parker RL (1996): Improved Fourier terrain correction, Part II. Geophysics 61: 365-372

Paul MK (1974): The gravity effect of a homogeneous polyhedron for three-dimensional interpretation. Pure and Applied Geophysics 112(3): 553-561

Payne MH (1971): Truncation effects in geopotential modelling. Analytical Mechanics Associates, Seabrook, Maryland

Petrović, S. (1996): Determination of the potential of homogeneous polyhedral bodies using line integrals. Journal of Geodesy 71(1): 44-52

Press WH, Flannery BP, Teukolsky SA, Vetterling WT (1986): Numerical Recipes, Cambridge University Press, Cambridge, UK

Prey A (1922): Darstellung der Höhen- und Tiefenverhältinse der Erde durch eine Entwicklung nach Kugelfunktionen bis zur 16. Ordnung. Abhandlungen der Gesellschaft der Wissenschaften in Göttingen, Mathematisch-Physikalische Klasse, Neue Folge XI(1): 1-29

Rapp RH (1982): Degree variances of the Earth's potential, topography and its isostatic compensation. Bulletin Géodésique 56: 84-94

Reigber C, Schwintzer P, Lühr H (1999): The CHAMP geopotential mission. Bolletino di Geofisica Teorica ed Applicata 40: 285-289

Reigber C, Balmino G, Schwintzer P, Biancale R, Bode A, Lemoine JM, König R, Loyer S, Neumayer H, Marty JC, Barthelmes F, Perosanz F, Zhu SY (2002): A high quality global gravity field model from CHAMP GPS tracking data and accelerometry (EIGEN-1S). Geophysical Research Letters 29(14), 10.1029/2002GL015064.

Rummel R, Rapp RH, Sünkel H, Tscherning CC (1988): Comparisons of global topographic-isostatic models to the Earth's observed gravity field. Reports of the Department of Geodetic Science and Surveying No. 388, Ohio State University, Columbus, Ohio

Sandwell DT, Smith WHF (1997): Marine gravity anomaly from Geosat and ERS 1 satellite altimetry. Journal of Geophysical Research 102(B5): 10039-10054

Schwarz KP, Sideris MG, Forsberg R (1990): The use of FFT technique in physical geodesy. Geophysical Journal International 100: 485-514

Sjöberg LE (1994): On the total terrain effects in geoid and quasi-geoid determinations using Helmert second condensation method. Division of Geodesy Report 36, Royal Institute of Technology, Stockholm, Sweden

Sjöberg LE (1995): On the quasi-geoid to geoid separation. Manuscripta Geodaetica 20: 182-192

Sjöberg LE (1996a): The terrain effect in geoid computation from satellite derived geopotential models. Bollettino di geodesia e scienze affini 55(4): 385-392

Sjöberg LE (1996b): On the error of analytical continuation in physical geodesy. Journal of Geodesy 70(11): 724-730

Sjöberg LE (1998a): The exterior Airy-Heiskanen topographic-isostatic gravity potential, anomaly and the effect of analytical continuation in Stokes' formula. Journal of Geodesy 72(11): 654-662

Sjöberg LE (1998b): On the Pratt and Airy models of isostatic geoid undulations. Journal of Geodynamics 26(1): 137-147

Sjöberg LE, Nahavandchi H (1999): On the indirect effect in the Stokes-Helmert method of geoid determination, Journal of Geodesy 73(2): 87-93

Sideris MG (1985): Computation of gravimetric terrain corrections using Fast Fourier Transform techniques. UCSE Report No. 20007, University of Calgary, Calgary, Canada

Smith DA (2000): The gravitational attraction of any polygonally shaped vertical prism with inclined top and bottom faces. Journal of Geodesy 74(5): 414-420

Smith DA (2002): Computing components of the gravity field induced by distant topographic masses and condensed masses over the entire Earth using the 1D-FFT approach. Journal of Geodesy 76: 150-168

Smith DA, Milbert DG (1999): The GEOID96 high resolution geoid height model for the United States. Journal of Geodesy 73(5): 219-236

Smith DA, Robertson DS, Milbert DG (2001): Gravitational attraction of local crustal masses in spherical coordinates. Journal of Geodesy 74(11-12): 783-795

Sneeuw N (1994): Global spherical harmonic analysis by least squares and numerical quadrature methods in historical perspective. Geophysical Journal International 118: 707-716

Sneeuw N, Bun R (1996): Global spherical harmonic computation by two-dimensional Fourier methods. Journal of Geodesy 70(4): 224-232

Somigliana C (1929): Teoria Generale del Campo Gravitazionale dell' Elissoide di Rotazione. Memoire della Società Astronomica Italiana, Vol. 4, Milano, Italy

Stroud AH, Secrest D (1966): Gaussian quadrature formulas. Prentice Hall, Englewood Cliffs, N. J.

Sun W (2002): A formula for gravimetric terrain corrections using powers of topographic height. Journal of Geodesy 76(8): 399-406

Sun W, Sjöberg LE (2001): Convergence and optimal truncation of binomial expansions used in isostatic compensations and terrain corrections. Journal of Geodesy 74(9): 627-636

Sünkel H (1985): An isostatic Earth model. Reports of the Department of Geodetic Science and Surveying No. 367, Ohio State University, Columbus, Ohio

Sünkel H (1986): Global topographic isostatic models. In: Sünkel H (ed.): Mathematical and numerical techniques in physical geodesy. Lecture Notes in Earth Sciences, Vol. 7, Springer, Berlin, Heidelberg, New York

Talwani M, Ewing M(1960): Rapid computation of gravitational attraction of three-dimensional bodies of arbitrary shape. Geophysics 25: 203-225

Tapley BD, Bettadpur S, Watkins M, Reigber Ch (2004): The gravity recovery and climate experiment: mission overview and early results. Geophysical Research Letters 31, 10.1029/2004GL019920

Tenzer T, Vaníček P, Novák P (2003): Far-zone contributions to topographical effects in the Stokes-Helmert method of the geoid determination. Studia Geophysica et geodaetica 47: 467-480

Tenzer T, Vaníček P, Santos M, Featherstone WE, Kuhn M (2005): The rigorous determination of orthometric heights. Journal of Geodesy 79(1-3): 82-92

Tscherning CC (1976): Computation of the second-order derivatives of the normal potential based on the representation by a Legendre series. Manuscripta Geodaetica 1: 71-92

Tsoulis D (1999a): Spherical harmonic computations with topographic-isostatic coefficients. Schriftenreihe des Instituts für Astronomische und Physikalische Geodäsie und der Forschungseinrichtung Satellitengeodäsie, Vol. 3, München

Tsoulis D (1999): Analytical and numerical methods in gravity field modelling of ideal and real masses. Deutsche Geodätische Kommission, Reihe C, Nr. 510, München

Tsoulis D (2001): A comparison between the Airy-Heiskanen and the Pratt-Hayford isostatic models for the computation of potential harmonic coefficients. Journal of Geodesy 74(9): 637-643

Tsoulis D, Tziavos IN (2003): A comparison of some existing methods for the computation of terrain corrections in local gravity field modelling. In: Tziavos IN (ed.): Gravity and Geoid 2002, Ziti-Publishing Thessaloniki, pp. 156-160

Tsoulis D, Wziontek H, Petrović S (2003): A bilinear approximation of the surface relief in terrain correction computations. Journal of Geodesy 77(5-6): 338-344

Tziavos IN, Sideris MG, Sünkel H (1996): The effect of surface density variation on terrain modelling – a case study in Austria. In: Tziavos IN, Vermeer M (eds.): Techniques for Local Geoid Determination. Report of the Finnish Geodetic Institute 96:2, Masala, pp. 99-110

Vajda P, Vaníček P, Novák P, Meurers B (2004a): On evaluation of Newton integrals in geodetic coordinates: exact formulation and spherical approximation. Contributions to Geophysics and Geodesy 34(4): 289-314

Vajda P, Vaníček P, Meurers B (2004b): On the removal of the effect of topography on gravity disturbance in gravity data inversion or interpretation. Contributions to Geophysics and geodesy 34(4): 339-369

Vaníček P, Kleusberg A (1987): The Canadian geoid – Stokesian approach. Manuscripta Geodaetica 12(2): 86-98

Vaníček P, Huang J, Novák P, Pagiatakis S, Véronneau M, Martinec Z, Featherstone W (1999): Determination of boundary values for the Stokes-Helmert problem. Journal of Geodesy 73(4): 180-192

Vaníček P, Novák P, Martinec Z (2001): Geoid, topography, and the Bouguer plate or shell. Journal of Geodesy 75(4): 210-215

Vaníček P, Tenzer R, Sjöberg LE, Martinec Z, Featherstone WE (2004): New views of the spherical Bouguer gravity anomaly. Geophysical Journal International 159: 460-472

Vening Meinesz FA (1931): Une nouvelle méthode pour la réduction isostatique régionale de l'intensité de la pesanteur. Bulletin Géodésique 29: 35-51

Vening Meinesz FA (1939): Tables fundamentales pour la réduction isostatique régionale. Bulletin Géodésique 63:711-776

Vening Meinesz FA (1941): Tables for regional and local isostatic reduction (Airy system) for gravity values. Publication of the Netherlands Geodetic Commission, Delft, The Netherlands

Watts AB (2001): Isostasy and flexure of the lithosphere. Cambridge University Press, Cambridge, UK

Wichiencharoen C (1982): The direct effects on the computation of the geoid undulations. Reports of the Department of Geodetic Science and Surveying No. 336, Ohio State University, Columbus, Ohio

Wild F and Heck B (2004a): A comparison of different isostatic models applied to Satellite Gravity Gradiometry. In: Jekeli C, Bastos L, Fernandes J (eds.): Gravity, Geoid and Space Missions. International Association of Geodesy Symposia, Vol. 129, Springer, Berlin, Heidelberg, New York, pp. 230-235

Wild F and Heck B (2004b): Effects of topographic and isostatic masses in Satellite Gravity Gradiometry. In: GOCE, The Geoid and Oceanography. Proceedings of the Second International GOCE User Workshop Frascati/Italy, March 8-10, 2004, CD-ROM

A. Appendix

A.1 Truncation coefficients for the direct terrain effect

A.1.1 Helmert's second method of condensation

The direct terrain effect of the topographic and condensation masses can be derived based on Eq. (4.177) by setting $A^b \triangleq A^{cb}$,

$$\begin{aligned} DTE^{ter}\big|_{\mathbf{r}=\mathbf{r}_P} = G\rho_{cr} \iint_{\sigma} \int_{\xi=R+H_{P'}}^{R+H_Q} \frac{\partial}{\partial r} l^{-1}(r,\psi,\xi)\, \xi^2 d\xi\big|_{\mathbf{r}=\mathbf{r}_P} d\sigma - \\ - G\rho \iint_{\sigma} \int_{\xi=R+H_{P'}}^{R+H_Q} \xi^2 d\xi \frac{\partial}{\partial r}\, l^{-1}(r,\psi,R)\big|_{\mathbf{r}=\mathbf{r}_P}\, d\sigma. \end{aligned} \tag{A.1}$$

The inner integral of the first term can be performed based on (Gradshteyn and Ryzhik 1980) and rearranged to give:

$$\begin{aligned} \frac{\partial}{\partial r} \int_{\xi=R+H_{P'}}^{R+H_Q} l^{-1}(r,\psi,\xi)\, \xi^2 d\xi\big|_{\mathbf{r}=\mathbf{r}_P} = \left[(\xi^2 + 3r_P^2)\cos\psi + r_P\xi(1-6\cos^2\psi)\right] l^{-1}(r_P,\psi,\xi) + \\ + r_P(3\cos^2\psi - 1)\ln|\xi - r_P\cos\psi + l(r_P,\psi,\xi)|\big|_{R+H_{P'}}^{R+H_Q}, \end{aligned} \tag{A.2}$$

with $\mathbf{r}_P = (R+H_P, \varphi, \lambda)$, $\xi = R + H_{P'}$, $\xi_Q = R + H_Q$ and the height of the topography H_Q .

Using the following parameters

$$\zeta = \frac{H_{P'} - H_P}{r_P} \quad \text{and} \qquad \zeta_Q = \frac{H_Q - H_P}{r_P}, \tag{A.3}$$

the Newtonian Kernel l^{-1} and its inverse in Eq. (A.2) can be expanded into a binomial series as follows (Novàk et al. 2001):

$$\begin{aligned} l^{-1}(r_P,\psi,\xi) &= \frac{1}{r_P}(2-2\cos\psi)^{-1/2}\left[1+\zeta\left(1+\frac{\zeta}{2-2\cos\psi}\right)\right]^{-1/2} \\ &\approx \frac{1}{r_P}(2-2\cos\psi)^{-1/2}\left(1-\frac{\zeta}{2}+\frac{\zeta^2}{8}\frac{1-3\cos\psi}{1-\cos\psi}\right)+.... \end{aligned} \tag{A.4}$$

$$\begin{aligned} l(r_P,\psi,\xi) &= r_P(2-2\cos\psi)^{1/2}\left[1+\zeta\left(1+\frac{\zeta}{2-2\cos\psi}\right)\right]^{1/2} \\ &\approx r_P(2-2\cos\psi)^{1/2}\left(1+\frac{\zeta}{2}+\frac{\zeta^2}{8}\frac{1+\cos\psi}{1-\cos\psi}\right)+..... \end{aligned} \tag{A.5}$$

To give estimations for the quantities ζ and ζ_Q we consider the following example: the spherical cap shell is defined by a radius of $\psi \geq \psi_0 = 3^0$, the height of the computation point is considered to be 10 km above the geoid and the topography shall reach heights of maximum 9 km. In this case the quantities ζ and ζ_Q reach a maximum value of 0.00156. In this case it holds the relation

$$\left|\zeta\left(1+\frac{\zeta}{(2-2\cos\psi)}\right)\right| < 0.002 \ll 1. \tag{A.6}$$

Therefore, the truncation of the binomial series in Eq. (A.4) and (A.5) after the quadratic terms of ζ is fully justified.

After substituting of Eq. (A.4) and Eq. (A.5) into Eq. (A.2), the integral can be written as follows:

$$\begin{aligned}\frac{\partial}{\partial r}\int_{\xi=R+H_{P'}}^{R+H_Q} l^{-1}(r,\psi,\xi)\,\xi^2 d\xi\big|_{\mathbf{r}=\mathbf{r}_P} &= \left[(r_P(3+\eta_Q^2)\cos\psi+\eta_Q r_P(1-6\cos^2\psi)\right](2-2\cos\psi)^{-\frac{1}{2}}\cdot\\ &\cdot\left(1-\frac{\zeta_Q}{2}+\frac{\zeta_Q^2}{8}\frac{1-3\cos\psi}{1-\cos\psi}\right)-\left[r_P(3+\eta^2)\cos\psi+\eta r_P(1-6\cos^2\psi)\right](2-2\cos\psi)^{-\frac{1}{2}}\cdot\\ &\cdot\left(1-\frac{\zeta}{2}+\frac{\zeta^2}{8}\frac{1-3\cos\psi}{1-\cos\psi}\right)+r_P(3\cos^2\psi-1)\ln\left|\frac{\eta_Q-\cos\psi+(1+\eta_Q^2-2\eta_Q\cos\psi)^{\frac{1}{2}}}{\eta-\cos\psi+(1+\eta^2-2\eta\cos\psi)^{\frac{1}{2}}}\right|,\end{aligned} \tag{A.7}$$

with

$$\eta=\frac{\xi}{r_P},\quad \eta_Q=\frac{\xi_Q}{r_P}. \tag{A.8}$$

The logarithmic function in Eq. (A.7) can be developed into a binomial series as well and truncated after the quadratic terms as follows:

$$\begin{aligned}\ln\left|\frac{\eta_Q-\cos\psi+(1+\eta_Q^2-2\eta_Q\cos\psi)^{\frac{1}{2}}}{\eta-\cos\psi+(1+\eta^2-2\eta\cos\psi)^{\frac{1}{2}}}\right| &= \frac{\zeta_Q-\zeta+(2-2\cos\psi)^{\frac{1}{2}}\left(\frac{\zeta_Q-\zeta}{2}+\frac{\zeta_Q^2-\zeta^2}{8}\frac{1+\cos\psi}{1-\cos\psi}\right)}{\eta-\cos\psi+(1+\eta^2-2\eta\cos\psi)^{\frac{1}{2}}}-\\ &-\frac{1}{2}\left[\frac{\zeta_Q-\zeta+(2-2\cos\psi)^{\frac{1}{2}}\left(\frac{\zeta_Q-\zeta}{2}+\frac{\zeta_Q^2-\zeta^2}{8}\frac{1+\cos\psi}{1-\cos\psi}\right)}{\eta-\cos\psi+(1+\eta^2-2\eta\cos\psi)^{\frac{1}{2}}}\right]^2+.....\end{aligned} \tag{A.9}$$

Substituting Eq. (A.9) into Eq. (A.7) and rearranging of the terms results in:

$$\int_{\xi=R+H_{P'}}^{R+H_Q}\frac{\partial}{\partial r}l^{-1}(r,\psi,\xi)\big|_{\mathbf{r}=\mathbf{r}_P}\xi^2 d\xi = r_P\left[K_1(\eta,\psi)(\zeta_Q-\zeta)+K_2(\eta,\psi)\left(\zeta_Q^2-\zeta^2\right)+K_3(\eta,\psi)(\zeta_Q-\zeta)^2\right], \tag{A.10}$$

with the functions ζ and ζ_Q as defined in Eq. (A.3),

$$K_1(\eta,\psi)=\frac{1}{2}\frac{(1-6\cos^2\psi)}{(2-2\cos\psi)^{\frac{1}{2}}}+\frac{1}{2}\frac{(3\cos^2\psi-1)(2+(2-\cos\psi)^{\frac{1}{2}}))}{\eta-\cos\psi+(1+\eta^2-2\eta\cos\psi)^{\frac{1}{2}}}, \tag{A.11}$$

$$\begin{aligned}K_2(\eta,\psi=\frac{\cos\psi}{(2-2\cos\psi)^{\frac{1}{2}}}-\frac{1}{2}\frac{(1+2\cos\psi-6\cos^2\psi)}{(2-2\cos\psi)^{\frac{1}{2}}}+\frac{1}{8}\frac{(1-3\cos\psi)(1+4\cos\psi-6\cos^2\psi)}{(1-\cos\psi)(2-2\cos\psi)^{\frac{1}{2}}}+\\ +\frac{(1+\cos\psi)}{8(1-\cos\psi)}\frac{(3\cos^2-1)}{(2-2\cos\psi)^{-\frac{1}{2}}(\eta-\cos\psi+(1+\eta^2-2\eta\cos\psi)^{\frac{1}{2}})},\end{aligned} \tag{A.12}$$

$$K_3(\eta,\psi)=-\frac{1}{4}\frac{(3\cos^2\psi-1)\left[(3-\cos\psi)+2(2-2\cos\psi)^{\frac{1}{2}}\right]}{\left[(\eta-\cos\psi+(1+\eta^2-2\eta\cos\psi)^{\frac{1}{2}})\right]^2} \tag{A.13}$$

Eq. (A.10) can be rearranged to give:

$$\begin{aligned}\int_{\xi=R+H_{P'}}^{R+H_Q}\frac{\partial}{\partial r}l^{-1}(r,\psi,\xi)\big|_{\mathbf{r}=\mathbf{r}_P}\xi^2 d\xi = r_P\left[K_1(\eta,\psi)(\zeta_Q-\zeta)+K_2(\eta,\psi)(\zeta_Q^2-\zeta^2)+\right.\\ \left.+K_3(\eta,\psi)(\zeta_Q^2-\zeta^2)-2K_3(\eta,\psi)\zeta(\zeta_Q-\zeta)\right].\end{aligned} \tag{A.14}$$

The integration over the sphere σ in the first term of Eq. (A.1) can be performed by replacing the geocentric coordinates φ_Q and λ_Q by the spherical polar coordinates with the pole in the computation point, ψ and α. Then the first term in Eq. (A.1) can be written as

$$G\rho_{cr}\iint_{\sigma}\int_{\xi=R+H_{P'}}^{R+H_Q}\frac{\partial}{\partial r}l^{-1}(r,\psi,\xi)|_{\mathbf{r}=\mathbf{r}_P}\,\xi^2 d\xi d\sigma = G\rho\int_{\psi=0}^{\pi}\{(H_Q-H_{P'})\,K_1(\eta,\psi)+.$$
$$+\frac{1}{r_P}(H_Q^2-H_P^2)(K_2(\eta,\psi)+K_3(\eta,\psi))-\frac{2H_P}{r_P}\,(H_Q-H_P)\,[K_2(\eta,\psi)+K_3(\eta,\psi)]- \tag{A.15}$$
$$-\frac{2(H_{P'}-H_P)}{r_P}\,(H_Q-H_P)\,K_3(\eta,\psi)\Big\}\sin\psi\,d\psi\int_0^{2\pi}d\alpha.$$

By using the technique introduced by Molodenskii el al. (1960), the terms in Eq. (A.15) can be developed into a spectral form. If only the far zone has to be taken into account, then the kernels $K_i(\eta,\psi)$, i=1, 2, 3, in Eq. (A.15) have to be redefined as

$$\bar{K}_i(\eta,\psi)=\begin{cases}0 & 0\le\psi<\psi_0\\ K_i(\eta,\psi) & \psi_0\le\psi\le\pi\end{cases}\quad. \tag{A.16}$$

The function $\bar{K}_i(\eta,\psi)$, being piecewise continuous, may be expanded into a series of Legendre polynomials (zonal spherical harmonics). For example, it holds for the kernel

$$\bar{K}_1(\eta,\psi)=\sum_{n=0}^{\infty}\frac{2n+1}{2}t_n(\eta,\psi,\psi_0)P_n(\cos\psi), \tag{A.17}$$

with the Legendre polynomials P_n of degree n. The coefficients $t_n(\eta,\psi,\psi_0)$ are given by Heiskanen and Moritz (1967) in Sec. 1-13 by,

$$\frac{2n+1}{2}t_n(\eta,\psi,\psi_0)=\frac{2n+1}{4\pi}\int_0^{2\pi}\int_0^{\pi}\bar{K}_1(\eta,\psi)P_n(\cos\psi)\sin\psi d\psi d\alpha. \tag{A.18}$$

After integration with respect to α gives

$$t_n(\eta,\psi,\psi_0)=\int_{\psi=0}^{\pi}\bar{K}_1(\eta,\psi)P_n(\cos\psi)\sin\psi d\psi. \tag{A.19}$$

Introducing the definition of Eq. (A.16), $t_n(\eta,\psi,\psi_0)$ can be written as

$$t_n(\eta,\psi,\psi_0)=\int_{\psi=\psi_0}^{\pi}K_1(\eta,\psi)P_n(\cos\psi)\sin\psi d\psi. \tag{A.20}$$

Because of

$$H_Q(\psi,\alpha)=\sum_{n=0}^{\infty}H_nP_n(\cos\psi), \tag{A.21}$$

with

$$H_n=\frac{2n+1}{4\pi}\int_0^{2\pi}\int_{\psi=0}^{\pi}H_Q(\psi,\alpha)P_n(\cos\psi)\sin\psi d\psi d\alpha, \tag{A.22}$$

the first term of Eq. (A.15) can be expressed as:

$$\iint\limits_{\sigma} (H_Q - H_{P'})\, K_1(\eta,\psi) d\sigma = 2\pi \sum_{n=0}^{N_{\max}} t_n(\eta,\psi,\psi_0) H_n(\varphi,\lambda) - 2\pi t_0(\eta,\psi,\psi_0) H_{P'}, \tag{A.23}$$

where the truncation coefficients $t_n(\eta,\psi,\psi_0)$ are given by Eq. (A.20).

Applying this procedure (Eq. (A.16) to Eq. (A.23)) to the other terms in Eq. (A.15), we arrive at:

$$\begin{aligned} G\rho_{cr} \int\limits_{\sigma\to\sigma_{FZ}} \int\limits_{\xi=R+H_{P'}}^{R+H_Q} \frac{\partial}{\partial r} l^{-1}(r,\psi,\xi)|_{\mathbf{r}=\mathbf{r}_P}\, \xi^2 d\xi d\sigma = 2\pi G\rho_{cr} \Bigg[\sum_{n=0}^{N_{\max}} t_n(\eta,\psi,\psi_0) H_n(\varphi,\lambda) + \\ + \frac{1}{r_P} \sum_{n=0}^{N_{\max}} u_n(\eta,\psi,\psi_0) H_n^2(\varphi,\lambda) - \frac{2H_P}{r_P} \sum_{n=0}^{N_{\max}} u_n(\eta,\psi,\psi_0) H_n(\varphi,\lambda) - \\ - \frac{2(H_{P'} - H_P)}{r_P} \sum_{n=0}^{N_{\max}} v_n(\eta,\psi,\psi_0) H_n(\varphi,\lambda) \Bigg] + C_1, \end{aligned} \tag{A.24}$$

where the truncation coefficients $u_n(\eta,\psi,\psi_0)$ and $v_n(\eta,\psi,\psi_0)$ are given by:

$$u_n(\eta\psi,\psi_0) = \int\limits_{\psi=\psi_0}^{\pi} \left[K_2(\eta,\psi) + K_3(\eta,\psi)\right] P_n(\cos\psi)) \sin\psi d\psi, \tag{A.25}$$

$$v_n(\eta,\psi,\psi_0) = \int\limits_{\psi=\psi_0}^{\pi} K_3(\eta,\psi) P_n(\cos\psi) \sin\psi d\psi, \tag{A.26}$$

and C_1 reads

$$\begin{aligned} C_1 =& 2\pi G\rho_{cr} \left[-t_0(\eta,\psi,\psi_0) H_{P'} - u_0(\eta,\psi,\psi_0) H_{P'}^2/r_P + \right. \\ & \left. + 2u_0(\eta,\psi,\psi_0) H_P H_{P'}/r_P + 2v_0(\eta,\psi,\psi_0) H_{P'}(H_{P'} - H_P)/r_P \right]. \end{aligned} \tag{A.27}$$

The truncation coefficients, given in Eqs. (A.20), (A.25) and (A.26), can be calculated numerically by the Gauss-Legendre quadrature formula. It reads, e.g, in case of Eq. (A.20) if the integration ranges from 0 to π ($\psi_0 = 0^0$),

$$\begin{aligned} t_n(\eta,\psi,\psi_0) &= \int\limits_{\psi=\psi_0}^{\pi} K_1(\eta\psi)(P_n(\cos\psi)) \sin\psi d\psi \\ &\approx \sum_{i=1}^{i_{\max}} (P_n(\cos\psi_i)) K_1(\eta,\psi_i) w_i, \\ &= \sum_{i=1}^{i_{\max}} F(\eta,\psi_i) w_i. \end{aligned} \tag{A.28}$$

The factor w_i are the corresponding Gauss-Legendre quadrature weights,

$$w_i = \frac{2}{(1-x_i^2)(P'_{i_{\max}}(x_i))^2}, \tag{A.29}$$

where $x_i = \cos\psi_i$ and $P'_{i_{\max}}$ are the first derivatives of the Legendre polynomials with respect to x. The values ψ_i are the zeros of the Legendre polynomials used for a specific Gauss-Legendre quadrature formula.

In our case, the integration starts from $\psi_0 \neq 0^0$. Therefore, the zeros of the Legendre polynomials must be transformed as follows:

$$\psi_i' = a + b\psi_i, \tag{A.30}$$

with

$$a = \frac{\cos\psi_0 + \cos\pi}{2}, \qquad b = \frac{\cos\psi_0 - \cos\pi}{2}. \tag{A.31}$$

Then the truncation coefficients $t_n(\eta, \psi, \psi_0)$ are given by the quadratic formula

$$t_n(\eta, \psi, \psi_0) = b \sum_{i=1}^{i_{\max}} F(\eta, \psi_i')w_i. \tag{A.32}$$

The second integral of Eq. (A.1) can be treated analogously as before resulting in

$$\begin{aligned} G\rho_{cr} \iint_{\sigma} \int_{\xi=R+H_{P'}}^{R+H_Q} \xi^2 d\xi \frac{\partial}{\partial r} l^{-1}(r, \psi, R)|_{\mathbf{r}=\mathbf{r}_P}\, d\sigma &= G\rho_{cr} \iint_{\sigma} \left[\frac{\xi^3}{3}\right]_{R+H_{p'}}^{R+H_Q} K_4(R+H_P, \psi, R)\sin\psi\ d\psi d\alpha, \\ &= G\rho \iint_{\sigma} \left[\frac{1}{3}\left((R+H_Q)^3 - (R+H_{P'})^3\right)\right] K_4(R+H_P, \psi, R)\sin\psi d\psi d\alpha, \\ &= G\rho \iint_{\sigma} \frac{R^3}{3}\left[\frac{3(H_Q - H_{P'})}{R} + \frac{3(H_Q^2 - H_{P'}^2)}{R^2} + o\frac{H^3}{R^3}\right] K_4(R+H_P, \psi, R)\sin\psi\ d\psi d\alpha, \end{aligned} \tag{A.33}$$

where the integral kernel $K_4(R + H_P, \psi, R)$ is the radial derivative of the Newtonian kernel given by:

$$K_4(R+H_P, \psi, R) = \frac{R(\cos\psi - 1) - H_P}{l^3}. \tag{A.34}$$

By inserting Eq. (A.34) in Eq. (A.33), the second integral of Eq. (A.1) can be finally written as

$$\begin{aligned} G\rho_{cr} \int_{\sigma \to \sigma_{FZ}} \int_{\xi=R+H_{P'}}^{R+H_Q} \frac{\partial}{\partial r} l^{-1}(r, \psi, R)|_{\mathbf{r}=\mathbf{r}_P}\, \xi^2 d\xi d\sigma = 2\pi G\rho_{cr} \sum_{n=0}^{N_{\max}} w_n(H_P, \psi, \psi_0) H_n(\varphi, \lambda) + \\ + \frac{1}{R} \sum_{n=0}^{N_{\max}} w_n(H_P, \psi, \psi_0) H_n^2(\varphi, \lambda) + C_2, \end{aligned} \tag{A.35}$$

with

$$w_n(H_P, \psi, \psi_0) = R^2 \int_{\psi=\psi_0}^{\pi} K_4(R+H_P, \psi, R) P_n(\cos\psi)\sin\psi d\psi, \tag{A.36}$$

and

$$C_2 = 2\pi G\rho_{cr}\left[-w_0(H_P, \psi, \psi_0)H_{P'} - w_0\ (H_P, \psi, \psi_0)H_{P'}^2/r_P\right]. \tag{A.37}$$

A.1.2 Helmert's first or generalized method of condensation

The only difference between Helmert's first and second condensation method is a different calculation of the truncation coefficients $w_n(H_P, \psi, \psi_0)$. The integral kernel $K_4(R + H_P, \psi, R - D_1)$ in Helmert's first condensation method is given by:

$$K_4(R+H_P, \psi, R-D_1) =: \left.\frac{\partial\left(1/l(r, \psi, R-D_1)\right)}{\partial r}\right|_{\mathbf{r}=\mathbf{r}_P} = \frac{(R-D_1)\cos\psi - (R+H_P)}{l^3}. \tag{A.38}$$

A.1.3 Airy-Heiskanen model

In this model, the direct terrain effect of the topographic and isostatic masses is given by (Rummel et al. 1988):

$$\begin{aligned} DTE^{ter}\big|_{\mathbf{r}=\mathbf{r}_P} =& G\rho \iint_{\sigma} \int_{\xi=R+H_{P'}}^{R+H_Q} \frac{\partial}{\partial r} l^{-1}(r,\psi,\xi)\big|_{\mathbf{r}=\mathbf{r}_P} \xi^2 d\xi d\sigma + \\ &+ G\Delta\rho \iint_{\sigma} \int_{\xi=R-T-t_P}^{R-T-t_Q} \frac{\partial}{\partial r} l^{-1}(r,\psi,\xi)\big|_{\mathbf{r}=\mathbf{r}_P} \xi^2 d\xi d\sigma. \end{aligned} \tag{A.39}$$

The first integral of Eq. (A.39) is derived from Eq. (A.1) and given by Eq. (A.24). Following an analogous procedure as used for treating Eq. (A.1), the second integral can be derived resulting in

$$\begin{aligned} G\Delta\rho \int_{\sigma\to\sigma_{FZ}} \int_{\xi=R-T-t_P}^{R-T-t_Q} \frac{\partial}{\partial r} l^{-1}(r,\psi\,,\xi)\big|_{\mathbf{r}=\mathbf{r}_P} \xi^2 d\xi d\sigma = 2\pi G\Delta\rho \Bigg[&- \sum_{n=0}^{N_{\max}} q_n(\eta,\psi,\psi_0) H_n(\varphi,\lambda) C + \\ &+ \frac{1}{r_P} \sum_{n=0}^{N_{\max}} r_n(\eta,\psi,\psi_0) H_n^2(\varphi,\lambda) C^2 + \frac{2(H_P+T)}{r_P} \sum_{n=0}^{N_{\max}} r_n(\eta,\psi,\psi_0) H_n(\varphi,\lambda) C - \\ &- \frac{2(T+t_P+H_P)}{r_P} \sum_{n=0}^{N_{\max}} S_n(\eta,\psi,\psi_0) H_n(\varphi,\lambda) C \Bigg] + C_3. \end{aligned} \tag{A.40}$$

The coefficients $q_n(\eta,\psi,\psi_0)$, $r_n(\eta,\psi,\psi_0)$ and $s_n(\eta,\psi,\psi_0)$ are calculated based on Eqs. (A.20), (A.25) and (A.26), respectively, with the parameter

$$\eta = \frac{R-T-t_P}{r_P}. \tag{A.41}$$

The term C_3 is given by:

$$\begin{aligned} C_3 =& 2\pi G\Delta\rho_{cr} \left[C q_0(\eta,\psi,\psi_0) H_{P'} - \frac{1}{r_P} r_0(\eta,\psi,\psi_0) C^2 H_{P'}^2 - \right. \\ &\left. - \frac{2(H_P+T)}{r_P} r_0(\eta,\psi,\psi_0) C H_{P'} + \frac{2(T+t_P+H_P)}{r_P} s_0(\eta,\psi,\psi_0)\, C H_{P'} \right]. \end{aligned} \tag{A.42}$$

List of Figures

List of Tables

INFORMATION ABOUT THE AUTHOR

Atef Abdel-Hakeem Makhloof was born on 5 of January 1970 in El-Minia, Egypt. Between 1976 and 1982 he visited the primary school in Edmo and from 1982 to 1985 he visited the preparatory school in Demshir. From 1985 till 1988 he visited the Secondary school in Minia. After five years and in 1993 he got his B.Sc. in Civil Engineering from the Faculty of Engineering at Minia, Minia University. From 1993 to 1997 he got his M.Sc. in the field of civil engineering from the Faculty of Engineering at Minia, Minia University. From the period of 1997 to 2002 he worked as assistant lecturer in the Faculty of Engineering at Minia, Minia University. From the period of 2002 to 2006 he is a Ph.D student in the institute of the theoretical geodesy, Bonn University, Germany. The address of the author is

Civil Engineering departement
Faculty of Engineering
Minia university
Minia
Egypt
Email address: atef970@mailcity.com